



UNIVERSITY OF
LIVERPOOL

**Investigating the impact of, novel, therapeutic
delivery systems on immunological responses -
determination of short, and long-term, exposure
effects**

**Thesis submitted in accordance with the requirements of the
University of Liverpool for the degree of Doctor in Philosophy**

By Danielle Emma Brain

March 2023

This thesis is the result of my own work. The material contained within the thesis has not been presented, either wholly or in part, for any other degree or qualification.

Danielle Emma Brain

This research was carried out in the Department of Pharmacology and Therapeutics, Institute of Systems and Molecular Biology, University of Liverpool, UK.

Contents

Acknowledgements	4
Abbreviations	5
List of communications	13
Abstract	15
Chapter 1 General Introduction	16
Chapter 2 Pre-screen to assess sterility, common Acute Immunotoxicity, and the impact of differential culture on peripheral blood responses to POP materials	38
Chapter 3 Assessment of cell health, cell phenotypes and gene expression following continual exposure to FTC, 3TC and linear poly(FTC)	92
Chapter 4 Cytotoxicity and cell health assessment of TAF Carbamate Prodrugs	155
Chapter 5 Assessment of, potential, <i>in vivo</i> adverse reactions to POP implants; links to pharmacokinetic parameters	174
Chapter 6 General Discussion	202
References	224

Acknowledgements

First and foremost, I have to thank everyone in the group for their help and support throughout my PhD. From Meg, Helen and Jo for taking me under their wing when I first started. Chris for showing me how to use the equipment in the lab, help doing the r analysis and putting up with my endless questions. Beth, thanks for putting up with the many breakdowns and reasoning with me when I thought finishing this thesis wasn't going to be possible. Alex and Luke thanks for the support and laughs whilst getting this thesis written. Neill, I am grateful for your support as a supervisor both on the project and personally, a PhD really is a learning curve, but you have helped me to navigate it and come out of it as a better scientist and person. Thanks to my co-supervisors Andrew and Steve for your support throughout the project.

Thanks to Meg and the in vivo team from Andrews group for the in vivo work. Thanks to Sarah Northey and Francesca Sposito for their support with the Nanostring work and r analysis. Thanks to Dr Lorenzo Ressel and Emanuele Ricci at the Leahurst University of Liverpool Campus for carrying out the histology work. Thanks also go to Kartik, Faye and Anika for creating the materials tested in this thesis.

Thanks for all my hockey, climbing, canoe polo teammates and friends within GB, FOA Canoe club and Mossley Hill Hockey club for helping to keep me sane during the write up and my lab work. My hockey family deserves an extra mention for giving me a break from the thesis writing and supporting me during the write up.

Mum, Dad and Nicole thanks for the endless support and belief in me throughout the highs and lows of this PhD. It wasn't easy navigating a PhD straight from undergrad or through a pandemic, but you helped me to keep going.

Ed, thanks for taking up my share of the cooking and cleaning for the last few months of thesis writing and for your support to keep going and believing in me when I couldn't see the wood through the trees. Promise to do my share when you do your part 3.

Abbreviations

3TC	Lamivudine
A2M	Alpha-2-macroglobulin
AANAT	Aralkylamine N-acetyltransferase
ACAA2	Acetyl-CoA acyltransferase 2
ACN	Acetonitrile
ACOT12	Acyl-CoA thioesterase 12
ACY1	Aminoacylase
ADH1A	Alcohol dehydrogenase 1A (class I) alpha polypeptide
ADH6	Alcohol dehydrogenase 6 (class V)
ADORA2A	Adenosine A2a receptor
AIDS	Acquired Immune deficiency Syndrome
AKT3	AKT serine/threonine kinase 3
ALDOB	Aldolase, fructose-bisphosphate B
ALOX15	Arachidonate 15-lipoxygenase
ALT	Alanine aminotransferase
ANOVA	Analysis of Variance
AOC1	Amine oxidase copper containing 1
AOX1	Aldehyde oxidase 1
APC	Allophycocyanin
APOE	Apolipoprotein
ARG1	Arginase 1
ARV	Antiretroviral
ASS1	Argininosuccinate synthase 1

BHMT2	Betaine--homocysteine S-methyltransferase 2
BI	Binding Inhibitor
BIRC3	Baculoviral IAP repeat containing 3
BSA	Bovine Serum albumin
CA12	Carbonic anhydrase 12
CACNA1A	Calcium voltage-gated channel subunit alpha1 A
CACNG	Calcium voltage-gated channel auxiliary subunit gamma
CARD11	Caspase recruitment domain family member 11
CARPA	Complement activation-related pseudoallergy
CCL	C-C motif chemokine ligand
CCR5	C-C motif chemokine receptor 5
CD	Cluster of differentiation
CDS	Cytosolic DNA sensors
CEACAM3	Carcinoembryonic antigen related cell adhesion molecule 3
cGMAP	Cyclic guanosine monophosphate-adenosine monophosphate
CI	Calcium Ionophore A23187
CINC	Cytokine-Induced Neutrophil Chemoattractant
CMKLR1	Chemerin chemokine-like receptor 1
CO2	Carbon dioxide
COL6A1	Collagen type VI alpha 1 chain
COL6A3	Collagen type VI alpha 3 chain
CPA3	Carboxypeptidase A3
CRP	C-reactive protein
CSE	Control standard endotoxin
CSF3R	Colony stimulating factor 3 receptor

CVF	Cobra venom factor
CXCL	Chemokine (C-X-C motif)
CXCR	C-X-C chemokine receptor
CYP8B1	Cytochrome P450 family 8 subfamily B member 1
DAMP	Danger Associated molecular pattern
DC	Dendritic cell
DCIP	Dendritic cell inflammatory protein-1
DMSO	Dimethyl sulfoxide
DNA	Deoxynucleic Acid
DPBS	Dulbecco's Phosphate Buffered Saline
DUOX1	Dual oxidase 1
EC	Effective concentration
EGFR	Epidermal growth factor receptor
EIA	Enzyme Immunoassay
ELISA	Enzyme-linked immunosorbent assay
EOMES	Eomesodermin
FBP1	Fructose-bisphosphatase 1
FBS	Fetal Bovine Serum
FDA	US food and drug administration
FGF1	Fibroblast growth factor 1
FI	Fusion Inhibitor
FITC	Fluorescein isothiocyanate
FLT3	Fms related tyrosine kinase 3
FOLH1B	Folate hydrolase 1B
FOLR1	Folate receptor 1

FOXP3	Forkhead box P3
FTC	Emtricitabine
g	g-force
GLUT	Glucose transporter
GM-CSF	Granulocyte-macrophage colony-stimulating factor
gp	Glycoprotein
GRO	Growth-regulated oncogene
GZMB	Granzyme B
GZMH	Granzyme H
HAART	Highly Active Antiretroviral Therapy
HIV	Human Immunodeficiency virus
HLA-DQA1	Major histocompatibility complex, class II, DQ alpha 1
HLA-DR	Major histocompatibility complex, class II, DR alpha
HPD	4-hydroxyphenylpyruvate dioxygenase
HSD11B1	Hydroxysteroid 11-beta dehydrogenase 1
HSV	Herpes Simplex virus
ICAM	Intercellular adhesion molecule
ICOS	Inducible T-cell costimulator
IDO1	Indoleamine 2,3-dioxygenase 1
IFN	Interferon
IL	Interleukin
IL-2RA	IL-2 receptor subunit alpha
IL-4I1	IL-4 induced 1
INMT	indolethylamine N-methyltransferase
INSTI	Integrase strand transfer inhibitors

IRF1	Interferon regulatory factor 1
ITGA11	Integrin subunit alpha 11
ITGB5	Integrin subunit beta 5
IV	Intravenous
KLRK1	Killer cell lectin like receptor K1
KRT1	Keratin 1
KYNU	Kynureninase
LAG3	Lymphocyte activating 3
LAL	Limulus amebocyte lysate
LC	Langerhans cell
LCK	LCK proto-oncogene, Src family tyrosine kinase (),
LDH	Lactate dehydrogenase
LPS	Lipopolysaccharide
LTA	Lymphotoxin alpha
LTB	Lymphotoxin beta
LY86	Lymphocyte antigen 86
MAC	Membrane attack complex
MAPK8IP1	Mitogen-activated protein kinase 8 interacting protein 1
MC	Mast cell
MEM	Minimum Essential Medium
MIP	Macrophage inflammatory protein
MMP	Mitochondrial membrane potential
MoDC	Monocyte-derived dendritic cell
MPO	Myeloperoxidase
MRAS	Muscle RAS oncogene homolog

MS4A4A	Membrane spanning 4-domains A4A
MSU	Monosodium urate
MTT	Thiazolyl Blue Tetrazolium Bromide
MYCL	MYCL proto-oncogene, bHLH transcription factor
NAGLU	N-acetyl-alpha-glucosaminidase
NFKB2	NFκB subunit 2
NF-κB	Nuclear factor kappa-light-chain-enhancer of activated B cells
NHS	National Health Service
NICE	National Institute for Health and Care Excellence
NLRP3	NOD-, LRR- and pyrin domain containing protein 3
NNRTI	Non-Nucleoside Reverse Transcriptase Inhibitor
NOS2	Nitric oxide synthase 2
NOX3	NADPH oxidase 3
NPR2	Natriuretic peptide receptor 2
NQO1	NAD(P)H quinone dehydrogenase 1
NRTI	Nucleoside Reverse Transcriptase Inhibitor
OD	Optical density
ODN	Oligodeoxyribonucleotide
OGDHL	Oxoglutarate dehydrogenase like
OTC	Ornithine carbamoyltransferase
P2X7	P2X purinoceptor 7
PAMP	Pathogen-Associated Molecular Pattern
PBS	Phosphate Buffered Solution
PDGFB	Platelet derived growth factor subunit B
PDK4	Pyruvate dehydrogenase kinase 4

PE	Phycoerythrin
PEG	Polyethylene glycol
PGK1	Phosphoglycerate kinase 1
PHA-M	Phytohaemagglutinin-M
PI	Protease Inhibitor
PKLR	Pyruvate kinase L/R
PMA	Phorbol myristate acetate
PNOC	Prepronociceptin
POP	Polymer of Prodrug
PPARG	Peroxisome proliferator activated receptor gamma
PPARGC1A	PPARG coactivator 1 alpha
PRF1	Perforin 1
PRR	Pattern recognition receptors
PTGES	Prostaglandin E synthase
R848	Resiquimod
RGN	Regucalcin
RIMKLA	Ribosomal modification protein rimK like family member
ROS	Reactive oxygen species
RPMI	Roswell Park Memorial Institute
RT	Reverse Transcriptase
RUNX2	Runt related transcription factor 2
S	Stage
SDS	Serine dehydratase
SH2D1A	SH2 domain containing 1A
SLC16A6	Solute carrier family 16 member 6

SLC2A6	Solute carrier family 2 member 6
SLC2A8	Solute carrier family 2 member 8
SLC7A11	Solute carrier family 7 member 11
SOD2	Superoxide dismutase 2
TAF	Tenofovir alafenamide
THBS1	Thrombospondin 1
TIMP	Tissue inhibitors of metalloproteinases
TLR	Toll like receptor
TNF	Tumour necrosis factor
TNFRSF4	TNF receptor superfamily member 4
TPH1	Tryptophan hydroxylase 1
TRAF1	TNF receptor associated factor 1
TTPA	Alpha tocopherol transfer protein
VEGF	Vascular endothelial growth factor
ZNF682	Zinc finger protein 682

List of communications

Peer reviewed Publications

Brain D, Plant-Hately A, Heaton B, Arshad U, David C, Hedrich C, Owen A, Liptrott NJ. **Drug delivery systems as immunomodulators for therapy of infectious disease: Relevance to COVID-19.** Adv Drug Deliv Rev. 2021 Nov;178:113848. doi: 10.1016/j.addr.2021.113848. Epub 2021 Jun 25. PMID: 34182016; PMCID: PMC8233062.

Heaton BJ, Jensen RL, Line J, David CAW, **Brain DE**, Chadwick AE, Liptrott NJ. **Exposure of human immune cells, to the antiretrovirals efavirenz and lopinavir, leads to lower glucose uptake and altered bioenergetic cell profiles through interactions with SLC2A1.** Biomed Pharmacother. 2022 Jun;150:112999. doi: 10.1016/j.biopha.2022.112999. Epub 2022 Apr 20. PMID: 35461087.

Plant-Hately AJ, Eryilmaz B, David CAW, **Brain DE**, Heaton BJ, Perrie Y, Liptrott NJ. **Exposure of the Basophilic Cell Line KU812 to Liposomes Reveals Activation Profiles Associated with Potential Anaphylactic Responses Linked to Physico-Chemical Characteristics.** Pharmaceutics. 2022 Nov 15;14(11):2470. doi: 10.3390/pharmaceutics14112470. PMID: 36432660; PMCID: PMC9695975.

Publications in preparation

1st Author

Acute immunotoxicity of FTC containing POP materials.

Assessment of cell phenotype following repeat exposure to NRTIs: FTC, 3TC and linear poly(FTC).

Interindividual variability of complement responses to Doxil.

Co-author

TAF carbamate prodrug development.

In vivo PK and immunocompatibility assessment of FTC containing POP materials.

Conference Presentations

Danielle Brain, Christopher David, Ioana Martinas and Neill Liptrott. **Serum-derived exosomes affect responses to inflammatory stimuli – impact on A549 cell responses to TNF- α** . Non-animal approaches in science JRC Summer School 2019.

Danielle Brain, Christopher David, Ioana Martinas, Andrew Owen & Neill Liptrott. **Serum-derived exosomes affect responses to inflammatory stimuli – impact on A549 cell responses to TNF- α** . BSNM annual meeting 2019.

Danielle Brain, Christopher David, Ioana Martinas, Andrew Owen & Neill Liptrott. **Serum-derived exosomes impact response to inflammatory stimuli – influence on A549 cell responses to TNF- α** . BSI Congress 2019.

Danielle E. Brain, Christopher A.W. David, and Neill J. Liptrott. **Assessment of cell phenotype following repeat exposure to NRTIs: FTC and 3TC**. CLINAM 2022.

Abstract

Investigating the impact of, novel, therapeutic delivery systems on immunological responses - determination of short, and long-term, exposure effects by Danielle Brain

Long-acting therapeutics are being explored for their use in improving adherence to medication and enhancing overall treatment outcomes. Due to increased residence time at the site of administration e.g., subcutaneous, long-acting formulations may affect the responses of local immune cells, due to modifications in the long-acting formulations to improve administration and allow the drugs to be released over specific time periods. Therefore, adaptation of current safety assessments must be considered, to safely translate these formulations into clinical studies. Long-acting formulations of the Nucleotide Reverse Transcriptase Inhibitors (NRTIs): FTC, 3TC and TAF were developed for subcutaneous administration for the treatment of HIV, hereafter termed Polymer of Prodrug (POP) formulations. This thesis starts to explore the immunocompatibility of these POP formulations and their interactions with cells and components of the immune system. Complement analysis showed concentration dependent activation from the linear poly(FTC) formulation. Impact of repeated exposure of the NRTI drugs FTC, 3TC and the POP formulation linear poly(FTC) to cell lines was explored, responses were cell line and drug specific, the linear poly(FTC) formulation was only tested in the MUTZ-3 cell line and led to particularly interesting significant changes in marker expression. *In vivo* analysis of three FTC containing POP polymers were assessed for cytokine perturbations alongside the pharmacokinetic analysis, no significant perturbations were seen across the board for any of the three implants tested. Early analysis of TAF carbamate pro drugs was carried out to determine whether they could alter cell health and cytotoxicity, no significant perturbations were seen, suggesting that POP implants made from these prodrugs may be safe. The model systems used and developed in this thesis will help to characterise and assess the immunocompatibility of long-acting formulations in the future, particularly those administered subcutaneously.

Chapter 1

General introduction

1.1 HIV and antiretroviral therapy

Infection with Human Immunodeficiency virus (HIV) when left untreated leads to the development of Acquired Immune deficiency Syndrome (AIDS), characterised by, among other things, a dysregulated immune system associated with ongoing inflammation and susceptibility to co-infections. Without intervention, this can lead to the death of the person living with HIV. Antiretroviral (ARV) drugs suppress HIV infection in order to prevent the development of AIDS, and more recently have been used as pre-exposure prophylaxis. HIV infection is currently incurable and treatment requires chronic administration of ARV medication (Ruelas & Greene, 2013). There have however been three reports of a functional cure from bone marrow transplantation from donors with a homozygous C-C motif chemokine receptor 5 (CCR5) delta-32 mutation, however long term follow up is yet to reveal if the virus has been eradicated and the feasibility of this application as a global health intervention is unfeasible (Allers et al., 2011; Brown, 2015; Gupta et al., 2020; Reardon, 2023). In 2021 it was estimated that there are 38.4 million people living with HIV, but only 75% of these individuals were receiving ARV therapy and approximately 650,000 people died of HIV-related causes (World Health Organisation, 2022).

There are five main classes of ARVs: Entry Inhibitors (CCR5/ C-X-C chemokine receptor (CXCR) 4 Inhibitors), Fusion Inhibitors, Nucleoside reverse transcriptase inhibitors (NRTIs)/Non-nucleoside reverse transcriptase inhibitors (NNRTIs), integrase strand transfer inhibitors (INSTIs), and Protease Inhibitors, all illustrated in Figure 1.1 (Pau & George, 2014). CCR5 and CXCR4 are co-receptors which facilitate the uptake of HIV via the (Cluster of differentiation) CD4 T-cell receptor, inhibitors of these co-receptors prevent the glycoprotein (gp) 120 on the surface of HIV binding and inhibit viral entry into the cell (Grande et al., 2019). Fusion inhibitors bind the gp 41 on HIV preventing it from piercing the cell membrane and stopping the fusion of the virus with the cell (Jamjian & McNicholl, 2004). NRTIs exhibit competitive inhibition of the Reverse Transcriptase (RT) enzyme responsible for forming viral DNA from viral Ribonucleic acid (RNA), they mimic endogenous nucleotides except the 3'hydroxyl group on the pentose sugar is missing, meaning no further nucleotides can be added to the Deoxynucleic Acid (DNA) chain due to the absence of a phosphodiester bond, and termination of the chain occurs (Holec, Mandal, Prathipati, & Destache, 2017). NRTIs require modification by host enzymes and become either di- or tri-phosphorylated before they can compete for the RT active site (Holec et al., 2017). NNRTIs work in a similar way to NRTIs, but they exhibit non-competitive allosteric inhibition of the RT enzyme causing a conformational

change in the enzyme therefore preventing elongation of the DNA chain (de Béthune, 2010). Integrase strand transfer inhibitors (INSTIs) block the action of the integrase enzyme and therefore the incorporation of the double stranded pro-viral DNA into the host genome (Pandey & Grandgenett, 2008). Protease Inhibitors competitively inhibit the protease enzyme, which functions to carry out the proteolytic processing of the viral genome of the multi-protein complex at specific sites to form the gag and pol proteins (Lv, Chu, & Wang, 2015).

Highly active antiretroviral therapy combines the use of multiple drugs to control the viral replication, a triple therapy of three drugs is commonly used, commonly consisting of two NRTIs and one other ARV drug (de Béthune, 2010; G. Li, Wang, & De Clercq, 2022; Pau & George, 2014). Patients receiving ARV medication early and adhering to therapy can live a near normal life expectancy (Phanuphak & Gulick, 2020).

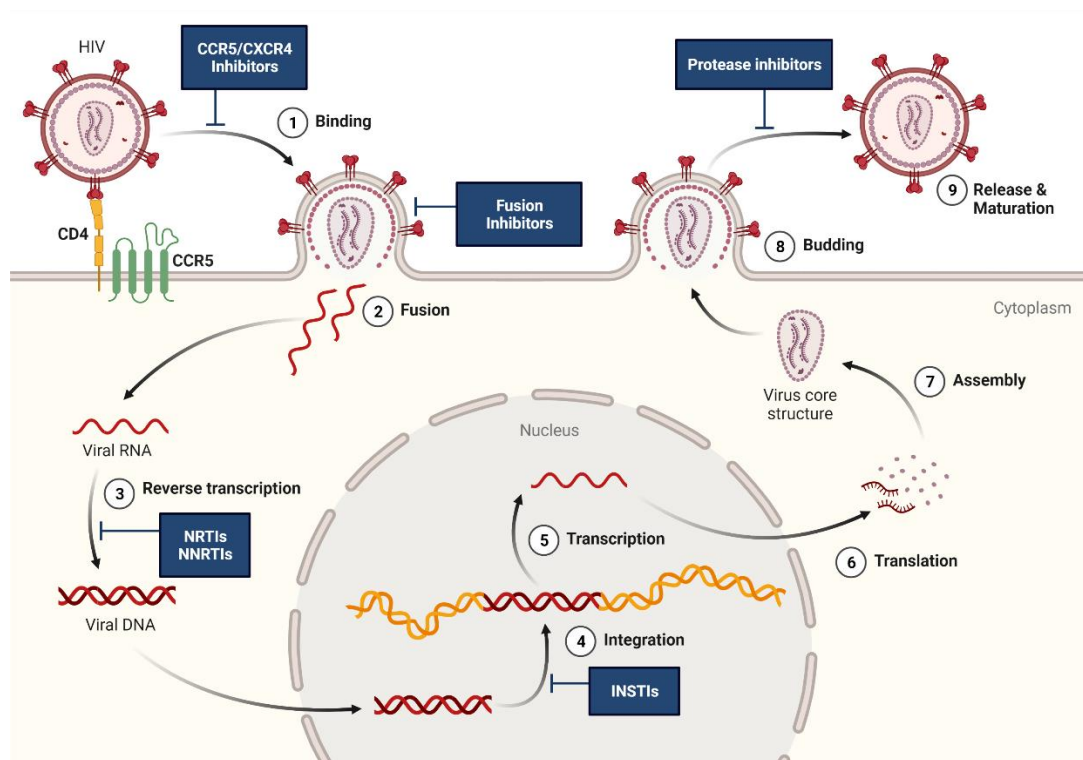


Figure 1.1: Illustration of the HIV replication cycle, with therapeutic intervention points labelled. **Binding Inhibitors** (CCR5 and CXCR4 inhibitors) act by preventing the binding of HIV to these co-receptors that are essential for the binding and subsequent internalisation. **Fusion inhibitors** work by preventing the internalisation of HIV. **NRTIs/NNRTIs** work by inhibiting the reverse transcriptase enzyme preventing the formation of viral DNA from viral RNA. **INSTIs** inhibit the integrase enzyme, preventing the insertion of the viral DNA into the

host's genome. **Protease inhibitors** inhibit the protease enzyme preventing the formation of essential viral proteins. Figure taken from BioRender.com (BioRender, 2020a).

1.2 Long-acting Delivery Systems

Long-acting drug delivery formulations are poised to address a number of issues with ARV therapy. Patient adherence to taking medications that must be taken every day can be low, as it can be easy to forget to take them now and again, as well as the limited consistency of medications in developing countries. If a long-acting formulation only needs to be administered every few weeks, months or years this should hopefully improve overall adherence to the medications, resulting in better treatment outcomes (Chandiwana et al., 2021). This will then lead to more stable and expected drug levels, which should reduce any potential side effects and lead to better monitoring of patients (Chue et al., 2005; Johnson, 2007; Nasrallah, 2007). Adherence is a major problem for the treatment of a number of diseases including HIV, poor adherence leads to reduced systemic drug levels and can lead to drug resistant viruses and subsequent treatment failure (Nachega et al., 2011). HIV and schizophrenia are diseases which have benefited from long-acting Nano-drugs in the form of intramuscular depots which can be injected and left to release over a period of time (Chue et al., 2005; Dolgin, 2014). These depots are used to deliver poorly water-soluble drugs and slowly disperse into the surrounding tissues and eventually into the lymphatics and the bloodstream. Another form of long-acting formulation is an implant; this has previously been used to release drugs such as Levonorgestrel and Etonogestrel as a form of contraception (Croxatto, Urbancsek, Massai, Coelingh Bennink, & van Beek, 1999; Sivin et al., 2001). Administration of other long-acting formulations can also be via intravenous (IV) or oral delivery, but for the purpose of this thesis, the focus will be on subcutaneous administration. Previously the subcutaneous administration route has been commonly used for the delivery of peptides or proteins and some implantable drug releasing rods.

While long-acting injectable or implantable formulations can provide a number of improvements to treatment, they also come with their own disadvantages. These include a prolonged period of potential side effects due to difficulty in removing the formulation, opposing patient views to needles, altered adverse effects, costly/require trained professionals to administer them and potential for local injection site reactions (Johnson, 2007; Nasrallah, 2007). The acute exposure to these long-acting formulations can be monitored *in vitro* similar to those formulations that are administered orally or IV. Where the challenges come is that oral formulations are cleared from the body within around 48 hours,

whereas long-acting formulations remain in the body for long periods from months to years. The wider distribution and increased exposure of these particles require multiple immune assessments, much greater than those used for oral or IV delivery. The adaptive immune response which is highly specific takes between 4-7 days to become initiated and involves the clonal expansion of T-cells and B-cells leading to immunological memory, this could be key when looking at the safety of long-acting medicines as oral or IV medicines have usually been cleared from the body at this point (Janeway CA Jr, 2001).

1.2.1 ARV long-acting delivery systems

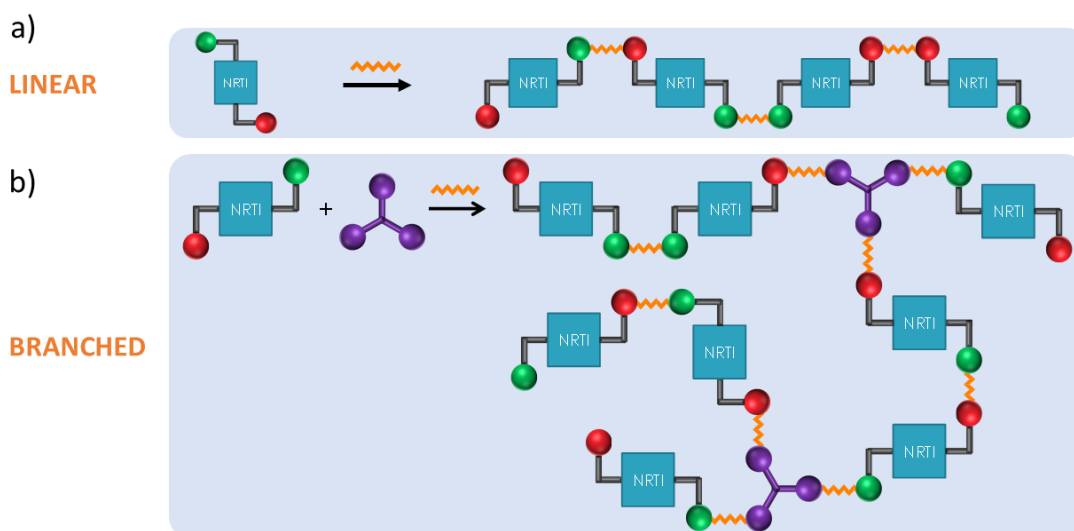
In January 2021 there were two approved long-acting ARV formulations, Ibalizumab, approved by the US food and drug administration (FDA) and Aluviritide approved in China, both INSTIs (Flexner, Owen, Siccardi, & Swindells, 2021). Long-acting intramuscular formulations of both cabotegravir, an INSTI, and rilpivirine, an NNRTI, have since been approved in combination with each other as a dual combination alternative to oral therapy by both the National Institute for Health and Care Excellence (NICE) in the UK and the FDA in the US (Venkatesan, 2022). Subcutaneous administration of implants has also been explored previously for ARV delivery for the INSTI dolutegravir and NRTI tenofovir alafenamide (TAF) (Gunawardana et al., 2022; Kovarova et al., 2018; Su et al., 2020). However, one of the previous TAF long-acting implants have shown significant toxicity in the immediate environment of the implant, drug release profiles must be considered due to their environment, high concentrations in the skin could be more toxic (Su et al., 2020). The other TAF and dolutegravir implant however showed no signs of overt toxicity at the implantation site. A foreign body reaction occurred in response to the TAF implants in mice, with a thin gelatinous capsule surrounding the implant with blood capillaries encircling it (Gunawardana et al., 2022).

1.3 POP long-acting materials assessed in the thesis

The work contained within this thesis, formed part of a larger project, funded by the National Institutes of Health, to develop long-acting formulations of HIV antiretrovirals termed Polymer of prodrug (POP). These POP formulations were designed as fully biodegradable implants, which don't require an implant system. As discussed earlier in the thesis, there is a need for long-acting delivery of ARVs and particularly NRTIs due to their water solubility. Three drugs were being explored for the POP formulations: emtricitabine (FTC), lamivudine (3TC) and tenofovir. Two different types of POP materials were assessed in this thesis, the

first contained the drug FTC and the second contained the drug TAF. Due to their stage in development, the FTC containing materials were explored in more depth, whereas only a preliminary screen was conducted for the TAF POP materials as they were still in the prodrug development phase, the TAF materials are introduced in Chapter 4.

The FTC POP materials assessed were prepared in the Chemistry department at the University of Liverpool by Dr Faye Hern and Dr Anika Shakil. The basis of the FTC work built on previously developed carbamate/carbonate prodrugs of FTC in order to generate linear or branched polymers containing FTC (Hobson et al., 2019; Shakil et al., 2022). The orientation of the FTC in the resulting polymers is statistical, so a mixture of carbamate and carbonate groups may occur in any order along the backbone. At this stage in the development the exact polymer formation and therefore the breakdown products of the polymers created and the implants has not yet been predicted.



c)

Polymer	Monomer A	Monomer B	Monomer C
Linear poly(FTC)	FTC 		
CPI (Linear)	$\text{H}_2\text{N}-\text{CH}_2-\text{CH}_2-\text{CH}_2-\text{CH}_2-\text{CH}_2-\text{CH}_2-\text{NH}_2$		
Branched poly(FTC) 1	FTC 		
Branched poly(FTC) 2	FTC 		

Figure 1.2: POP materials strategy of polymer generation for FTC. On FTC the green end indicates the amine functional group, and the red end indicates the hydroxyl functional group. On the polymers formed from both the linear and branched methods the green end indicates the carbamate group formed and the red end indicates the carbonyl group. a) Demonstrates the Linear method of polymer formation, b) Illustrates the branched method

of polymer formation, and c) Demonstrates the method of formation and the monomers used to create the four polymer implants linear poly(FTC), CPI, and branched poly(FTC) 1 and 2. Figure adapted from a figure made by Dr Faye Hern and Dr Anika Shakil (Shakil et al., 2022).

Linear poly(FTC) and the control polymer implant (CPI) were prepared using the linear method, demonstrated in Figure 1.2 a) and c). The CPI was designed to not breakdown and release any of its formation products. Branched poly(FTC) 1 and branched poly(FTC) 2 were prepared using the branched method, demonstrated in Figure 1.2 b) and c). The repeating monomer units of each of the final polymer implants produced are shown in Figure 1.3 a-d).

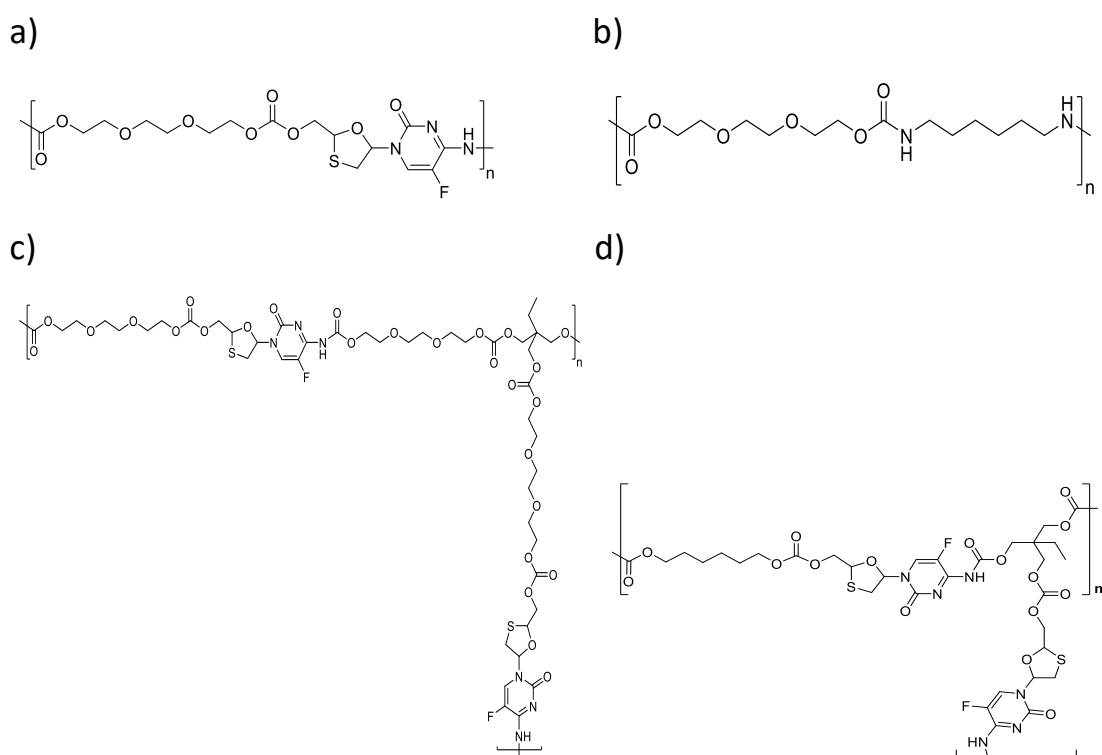


Figure 1.3: Structures of the FTC containing POP polymers in the implants. a) linear poly(FTC) polymer structure. b) CPI polymer structure. c) Branched poly(FTC) 1 polymer structure. d) Branched poly(FTC) 2 polymer structure.

A series of different length polymer chains of the linear poly(FTC) POP material were created to explore the immunomodulatory potential of different length polymer fragments which would theoretically be produced during the degradation of the linear poly(FTC) POP implant *in vivo*. The linker between the poly(FTC) groups in the linear poly(FTC) POP material is tri(ethylene glycol), which is a short chain polyethylene glycol (PEG). Four different materials were created, for ease of interpretation in this thesis, these materials were named linear poly(FTC) Stage 2 (S2), linear poly(FTC) Stage 3 (S3), linear poly(FTC) Stage 4 (S4), and linear

poly(FTC) Stage 5 (S5), with decreasing polymer chain lengths, with linear poly(FTC) S5 being the smallest and linear poly(FTC) S2 being the largest fragment. Figure 1.4 shows the oligomer size exclusion chromatography (oligomer-SEC) chromatograms of the five stages of linear poly(FTC) and the potential fragments that occur in each stage of linear poly(FTC). Linear poly(FTC) S5 is a small molecule model for the smallest fragment that may result from degradation of linear poly(FTC). Single FTC molecules have been removed from these fragments during purification.

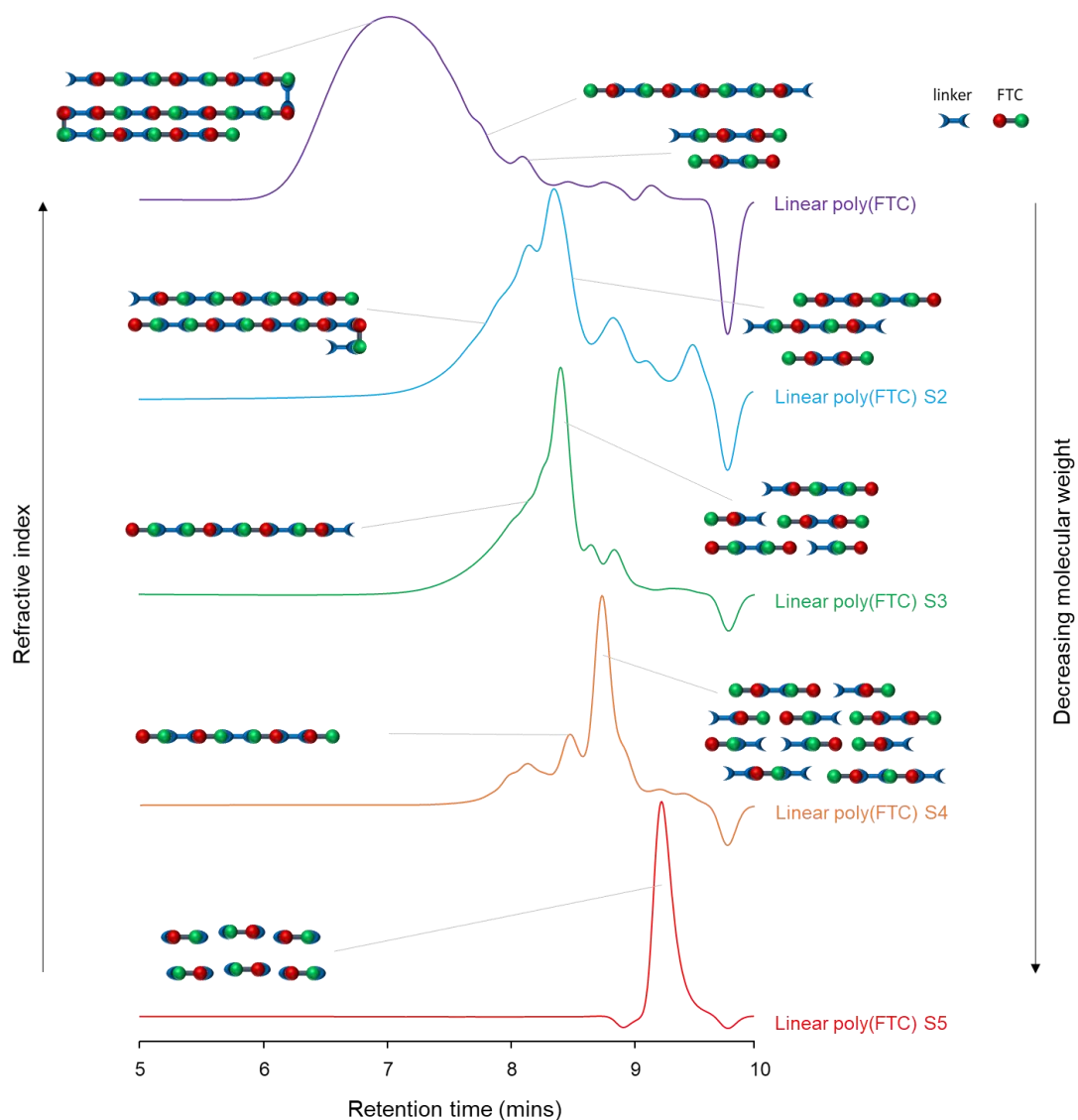


Figure 1.4: Illustrates linear poly(FTC) and the linear poly(FTC) fragments Stages 2-5 and their oligomer-SEC chromatograms. Increased retention time indicates a smaller polymer length. Each major peak is labelled with the potential polymer fragment chains that could be in that material fragment stage. Figure created by Dr Faye Hern.

Linear poly(FTC) and linear poly(FTC) S2-4 have polymeric molecular weight distributions and therefore display multimodal distributions. Linear poly(FTC) S5 is a single molecule, and

therefore possesses a monomodal molecular weight distribution. Dispersity decreases from linear poly(FTC) to linear poly(FTC) S5, as there becomes smaller fragments, and there are fewer possible fragment chains. The number average molecular weight (M_n), weight average molecular weight (M_w) and dispersity (\mathcal{D}) ($\mathcal{D} = \frac{M_w}{M_n}$) for linear poly(FTC) and the four breakdown fragment mimics linear poly(FTC) S2-S5 is shown in Table 1.1.

Table 1.1: M_n , M_w and \mathcal{D} for linear poly(FTC) and the four breakdown fragment mimics linear poly(FTC) S2-S5. Data provided by Dr Faye Hern.

	M_n	M_w	\mathcal{D}
linear poly(FTC)	5880	8530	1.451
linear poly(FTC) S2	3330	3940	1.183
linear poly(FTC) S3	2410	2690	1.116
linear poly(FTC) S4	1840	2000	1.087
linear poly(FTC) S5	447	447	1

1.3 Subcutaneous implant immune cell exposure

Due to the administration route, the exposure of the drug formulation to different subset and profiles of cells, particularly immune cells, varies greatly compared to the oral route, mainly due to the presence of varying immune cell subsets and profiles. The subcutaneous route will also increase exposure of the formulation to these immune cells compared to more traditional routes such as oral or IV delivery, by bypassing metabolism that may occur via these routes. Initially these implants will come into contact with a very different environment and range of immune cells at their administration site in the subcutaneous space. Drugs delivered into subcutaneous tissue will eventually be taken up via the blood capillaries or the lymphatics system and eventually encounter the immune cells in plasma.

1.3.1 Immunology of the epidermis and dermis

The top layer of the skin, the epidermis is composed of dead epidermal cells known as keratinocytes and between these reside Langerhans cells (LCs), a unique antigen presenting cell, and CD8+ resident memory T-cells (Kabashima, Honda, Ginhoux, & Egawa, 2019). These keratinocytes form a part of the innate immune system and have pattern recognition

receptors on their surface and when activated cause the release of cytokines creating local inflammation (Kabashima et al., 2019). Possible immune activation could start from LCs during the insertion, particularly if there is any residue of the formulation on the outside of the needle/implantation device used. In the skin dermis the immune cells that predominate include: Dendritic Cells (DCs), Mast Cells (MCs), macrophages, T-cells, natural killer (NK)-cells and innate lymphoid cells (Kabashima et al., 2019; Nguyen & Soulika, 2019). Activated DCs cells in the skin are known to be able to migrate through the lymphatics in order to present captured antigen to immature T-cells in the lymph node (Russo, Nitschké, & Halin, 2013). The dermis of the skin is highly vascularised with blood vessels and lymphatics and contains a vast vasculature network in order to aid this function (Skobe & Detmar, 2000).

1.3.2 Immunology of the subcutaneous space

The tissue that the subcutaneous implant will reside in will be the adipose tissue located just below the dermis. Adipose tissue is abundant in adipocytes, fibrocytes and immune cells such as T-cells, B-cells and macrophages, following activation they secrete adiponectin, leptin and cytokines such as Interleukin (IL)-1, IL-6 and tumour necrosis factor (TNF)- α (Chung, Nati, Chavakis, & Chatzigeorgiou, 2018; Kabashima et al., 2019; Nguyen & Soulika, 2019). Other immune cells that reside in adipose tissue include eosinophils, neutrophils, DCs, NK-cells and MCs (Chung et al., 2018; Ferrante, 2013). MCs in the skin can produce histamine in response to biomaterial insertion following both subcutaneous and intraperitoneal administration in mice causing the infiltration of other inflammatory cells including phagocytic cells which can adhere to the biomaterial surface (Tang, Jennings, & Eaton, 1998). Therefore, assays used to test these subcutaneously administered implants should reflect the type of cells they are exposed to within the body.

Protein association is particularly important for subcutaneous delivery as the implant breakdown products could encounter many different environments such as the blood, the vasculature, the adipose tissue and the cytosolic fluid in cells. For instance, if in the skin breakdown products of the implant could be seen as safe, but it could be seen as something dangerous to cells in the blood. As the implant degrades over time more of the surface will be exposed altering the protein association and therefore what is seen to the cells surrounding it. If there are many different immune responses to the different fragments seen all over the body this could potentially lead to chronic inflammation. Phagocytosis of these fragments may also lead to redistribution of the fragments.

1.3.2.1 Obesity adipose tissue immunological alterations

The problems with a model is that one size does not always fit all, for example obese individuals have a substantially increased number of macrophages and base level of inflammatory mediators which can sometimes be mistaken for immune activation. Obese individuals have been shown to have pro-inflammatory CD11c+/M1 macrophages dominating expression, compared to lean individuals with anti-inflammatory CD11c-/M2 macrophages making up the majority, maintaining homeostasis (Chung et al., 2018; Ferrante, 2013; Weisberg et al., 2003). Other immune cells such as MCs, neutrophils, B-cells, NK-cells and DCs have also been shown to increase in adipose tissue as a result of obesity and therefore these cells need to be explored and some assays may need to be adapted to demonstrate the different populations (Ferrante, 2013). T-cell increases are also seen in obese individuals, with Th1 CD4+ T-cells predominating compared to Th2 T-cells, with a reduction in Tregs and eosinophils (Ferrante, 2013). Innate lymphoid two cells and NK-cells help to maintain homeostasis in lean individuals, causing maintenance of eosinophil, anti-inflammatory M2 Macrophage and Treg numbers, whereas in obesity innate lymphoid 1 cells cause polarisation to pro-inflammatory M1 macrophages (Chung et al., 2018).

1.3.2.2 HIV infection and adipose tissue alterations

HIV infection can cause alterations to the adipose tissue, HIV-associated adipose redistribution syndrome can occur in some individuals, however this is defined as abnormal accumulation of trunk fat, but can also lead to reduced subcutaneous tissue and affect the health of the individual (Lichtenstein, Balasubramanyam, Sekhar, & Freedland, 2007). The adipose tissue has also been described as a reservoir for HIV (Bourgeois et al., 2019). HIV infection can lead to increased inflammatory mediator release from adipocytes and macrophages within the adipose tissue (Koethe, Hulgán, & Niswender, 2013). Both obesity and HIV infection cause higher CD8+ T-cell levels in adipose tissue, however the reasons for these levels may differ and CD4+ T-cells and macrophage alterations vary (Koethe et al., 2013; Wanjalla, McDonnell, & Koethe, 2018). Some NRTIs, such as stavudine and zidovudine have also been shown to increase macrophage and proinflammatory levels in adipose tissue (Koethe et al., 2013). Patients who are obese and infected with HIV have been shown to have a slower disease progression whilst untreated, but altered CD4+ T-cell recovery counts following treatment (Koethe et al., 2013). These considerations must be taken into account when exploring the immune responses to a subcutaneous implant for the treatment of HIV.

1.3.3 Immunology of vasculature

As the implant degrades the exposure of the breakdown products with change from the skin and will become distributed in the blood via the vasculature. The breakdown products reaching the vasculature could be the drug that is known to be safe for use in humans, but also could be the linker and potentially fragments of the implant. Leukocytes are immune cells in the blood and consist of granulocytes, lymphocytes, monocytes and pre-DCs (Carrick & Begg, 2008). Granulocytes in the blood consist of neutrophils, basophils, and eosinophils. Neutrophils are the first responders to damage in tissues and are recruited via endothelial extravasation following chemotaxis and endothelial cell changes resulting from inflammation signals (Kolaczowska & Kubes, 2013). Basophils make up the smallest population of immune cell type in the blood, they circulate in the blood and function similar to mast cells (Miyake & Karasuyama, 2017). Basophils orchestrate both IgE dependent and independent allergic responses in the blood and can also be recruited to tissues, activation of basophils results in the release of granules including histamine and cytokines such as IL-4 which can activate other immune cells (Miyake & Karasuyama, 2017). Eosinophils play a role in responding to pathogens, their role includes antigen presentation, degranulation in response to pathogens causing the release of chemokines and cytokines, and instruct other immune cells to respond to these pathogens (Ravin & Loy, 2016). Lymphocytes in the blood include: B-cells, T-cells, and NK-cells (LaRosa & Orange, 2008). T-cells are part of the adaptive immune system and lots of sub populations are present in humans, CD8+ and CD4+ T-cells respond to antigens presented on the surface of antigen presenting cells via either MHC class I (CD8+) and II (CD4+) respectively, causing either cytotoxic or effector immune cell responses respectively (LaRosa & Orange, 2008). B-cells play an important role in humoral immunity and the production of antibodies, alongside roles in antigen presentation and complement activation (MacConmara & Lederer, 2005). Monocytes reside in the blood and can differentiate into both macrophages and dendritic cells, they are recruited into tissues as a result of damage or infection (Yona & Jung, 2010). Pre-DCs also reside in the blood and in addition to monocyte-derived dendritic cells (MoDCs), DCs can be differentiated from pre-DCs into plasmacytoid and conventional DCs when migrating into tissues (Sichien, Lambrecht, Guilliams, & Scott, 2017).

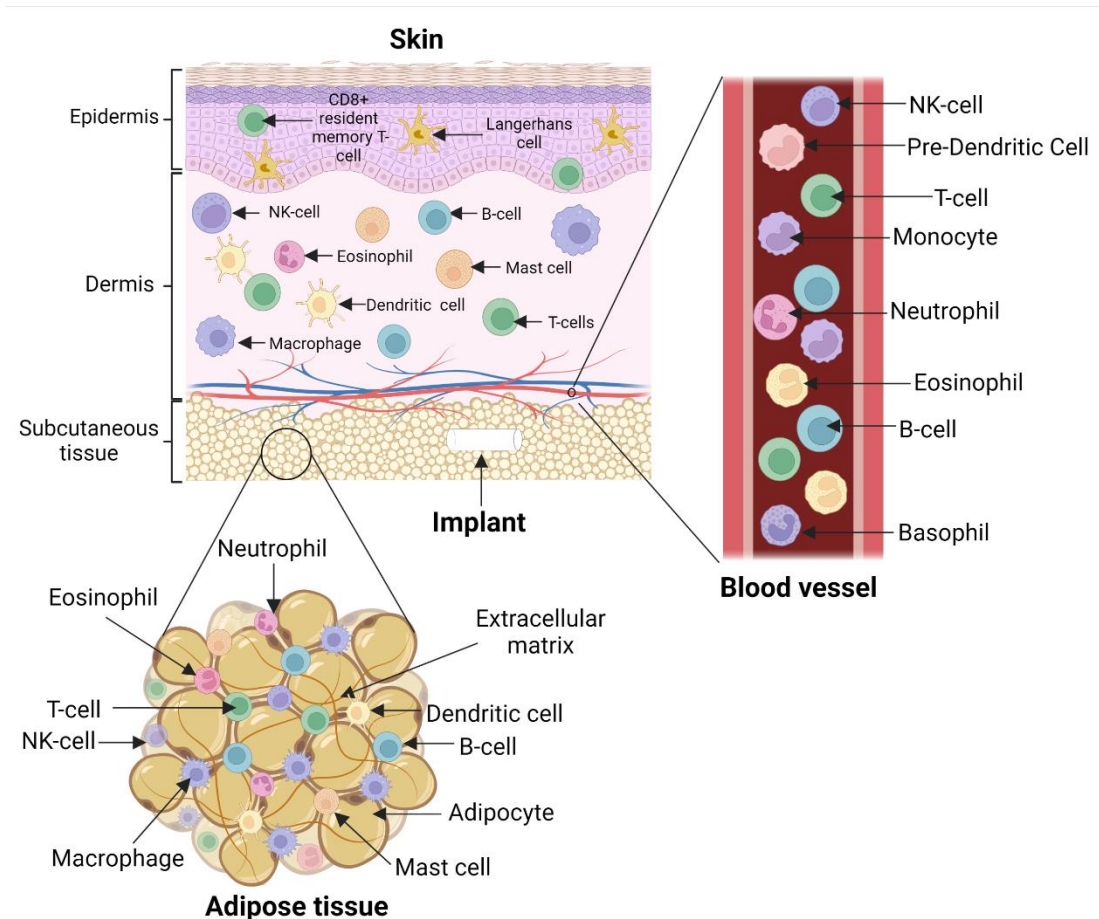


Figure 1.5: Summary of the Immune cells that are hypothetically exposed to the implant and its breakdown products/fragments. Immune cells found in the epidermis include: LCs and CD8+ resident memory T-cells. Immune cells found in the dermis include: B-cells, dendritic cells, eosinophils, macrophages, mast cells, NK-cells and T-cells. Immune cells found in the adipose tissue of healthy individuals between adipocytes in the subcutaneous space include: B-cells, dendritic cells, eosinophils, macrophages, mast cells, NK-cells and T-cells. Immune cells found within blood vessels include: B-cells, basophils, pre-dendritic cells, eosinophils, monocytes, NK-cells and T-cells. Created with BioRender.com

1.3.4 Immune cell responses in wound healing

During the insertion of a subcutaneous implant, the skin is broken, leading to tissue damage, immune activation will start here, although hypodermic needles and implantation devices have been designed to limit the damage to a minimum. Another implication is that as the body's skin is its primary barrier surface from bacteria and other microbes, there is risk of infection or site reaction at the insertion site. Healing of wounds requires coordination of the different cells in the different layers of the skin. There are four key stages to wound healing: homeostasis/coagulation, inflammatory, growth/proliferation and remodelling/re-

epithelialisation (Ellis, Lin, & Tartar, 2018; Nguyen & Soulika, 2019; Rodrigues, Kosaric, Bonham, & Gurtner, 2019; Velnar, Bailey, & Smrkolj, 2009).

A number of immune cells play roles in wound healing, including: Neutrophils, macrophages, DCs, MCs, LCs and T-cells (Nguyen & Soulika, 2019; Rodrigues et al., 2019). Neutrophils are the first responders in the skin to wounds, they respond to Danger Associated molecular patterns (DAMPs), hydrogen peroxide, lipid mediators and chemokines that have been produced by injured cells (Ellis et al., 2018; Rodrigues et al., 2019). Neutrophils carry out three main roles, they secrete proteases and chemoattractants, create neutrophil extracellular traps and carry out phagocytosis of pathogens (Ellis et al., 2018; Nguyen & Soulika, 2019; Rodrigues et al., 2019). Macrophages resident in the skin become activated in wound healing and secrete mediators that recruit monocytes, macrophages and DCs then phagocytose pathogens, and release growth factors promoting angiogenesis or repair (Nguyen & Soulika, 2019; Rodrigues et al., 2019). Pro-inflammatory M1 macrophages carry out these roles and following inflammation the anti-inflammatory M2 macrophages predominate facilitating the growth/proliferation stage (Ellis et al., 2018). Macrophages perform an important role in restoring normal levels of neutrophils and phagocytose them, another route is reverse migration back into the circulation initiating the end of the inflammation stage (Ellis et al., 2018; Nguyen & Soulika, 2019; Rodrigues et al., 2019). Impaired healing leads to chronic wounds and results from prolonged neutrophil infiltration and M1 macrophage levels (Ellis et al., 2018; Rodrigues et al., 2019). The effect of these materials on immune cells involved in wound repair should be considered when assessing subcutaneously administered materials before being used in humans.

1.4 Chronic exposure to long-acting drug formulations

Chronic exposure must be considered for long-acting formulations as they will reside in the body for over 48 hours, longer than most oral or IV administered medicines. Therefore, the adaptive immune response will play a greater role in long-acting responses. On the day of insertion, the contribution of cells in the site surrounding of the formulation can be predicted, however this will change, ultimately resulting in an alteration in how the implant is seen by immune cells. This is due to the cells differentiating and changing their phenotype, as well as new cells entering the site. In particular, T-cells will increase in number following their activation by antigen presenting cells such as macrophages. More specific responses to the materials are made; therefore, longer term continuous preclinical assessment is vital.

1.4.1 Foreign body reactions

These implants reside in the bodies tissues for long periods, which can promote the formation of foreign body granulomas, this usually occurs in response continual pathogen presence or poorly degradable irritating materials, such as splinters (Bouajina et al., 2006; Sanchez, Weston, Yan, Hurt, & Kane, 2011). This has been exhibited in response to nerve neuroprosthetics, cosmetic filler injections, TAF implants, long-acting depots of Paliperidone palmitate and Leuprorelin Acetate (Darville et al., 2016; Gunawardana et al., 2022; Shahrabifarhani, Lerman, Noonan, Kabani, & Woo, 2014; Thway, Strauss, Smith, & Fisher, 2015).

Foreign body reactions start as normal wound healing as discussed in 1.3.4, however the macrophages cannot phagocytose the implant and therefore secrete factors to try to break down the foreign body/implant which causes macrophages to become infiltrated and flatten on the implant surface (Carnicer-Lombarte, Chen, Malliaras, & Barone, 2021). If an implant is degradable this may cause it to become degraded and potentially affect the usefulness of the implant if it is required to release drug for longer periods. Here macrophages also fuse to form polynucleate foreign body giant cells which can phagocytose larger particles (Carnicer-Lombarte et al., 2021; Chandorkar, K, & Basu, 2019). If the macrophages are still unable to degrade the implant, they attract fibroblasts to the surface of the implant causing the formation of fibrinous capsule around the foreign body, alongside the extension of blood vessels to this foreign body (Carnicer-Lombarte et al., 2021; Chandorkar et al., 2019).

Size, stiffness and material surface can affect the extent of foreign body reaction to materials (Chen, Yung, Qian, & Chen, 2018; Thevenot, Hu, & Tang, 2008; Veiseh et al., 2015). It has been suggested that there are a number of ways in which foreign body reactions to implants can be minimised, either by reducing adsorption, by altering the surface of an implant or by co-administration of tissue response modifiers such as dexamethasone to disturb the normal inflammatory process (Carnicer-Lombarte et al., 2021; Chen et al., 2018; Morais, Papadimitrakopoulos, & Burgess, 2010; Ratner, 2002). For an implantable device which is destined to reside in the tissues for a long period co-administration may not be suitable but could be considered for implants for short-term exposure.

1.5 Common acute immunotoxicity assessments for new delivery systems

Nanomaterials have been used as an exemplar novel delivery system, alongside considering the delivery route to base the initial acute immunotoxicity assessments of the POP materials. When assessing the safety of new pre-clinical materials, they must first be pre-screened to ensure they are sterile and not going to cause major reactions in subsequent assays, due to endotoxin or other contamination, which may lead to false-positive interpretations of responses (Marina A. Dobrovolskaia, 2015b; Marina A Dobrovolskaia, Neun, Clogston, Grossman, & McNeil, 2014). Common acute immunotoxicity assessments should next be carried out to determine whether there are any red flags from these complex materials and their fragments. Commonly used acute immunotoxicity assays cover a number of different immunological systems, including, but not limited to: leukocyte proliferation, complement activation and blood cytokine responses (Marina A. Dobrovolskaia, 2015b; Neill J Liptrott, Giardiello, McDonald, Rannard, & Owen, 2017). Where possible within the time frame of this thesis any significant adverse results seen in these assays, are then followed up to determine the pathway and mechanism responsible and determine whether these issues are detrimental for the disease/treatment the materials will be used for.

1.6 Potential innate responses to POP materials

1.6.1 Pattern recognition and the NLRP3 Inflammasome

Pattern recognition receptors (PRR) play a pivotal role in innate immunological responses to Pathogen-Associated Molecular Patterns (PAMPs) and DAMPs (D. Li & Wu, 2021). A cytosolic PRR that responds to PAMPs and DAMPs is, NOD-, LRR- and pyrin domain containing protein 3 (NLRP3), an important component of the NLRP3 inflammasome complex, the inflammasome been previously reviewed extensively (Guo, Callaway, & Ting, 2015; Kelley, Jeltema, Duan, & He, 2019; Zheng, Liwinski, & Elinav, 2020). Inflammasomes are known to be involved in a number of responses to complex medicines, meaning a thorough investigation of their involvement is key (Vandebriel, David, Vermeulen, & Liptrott, 2022). The NLRP3 inflammasome has been shown to require two signals for activation, an initial priming step to activate Nuclear factor kappa-light-chain-enhancer of activated B cells (NF- κ B) signalling, such as LPS interacting with Toll-like receptor (TLR)-4, IL-1 β binding to the IL-1 receptor or TNF binding to the TNF receptor, which causes increased expression of both NLRP3 and pro-IL-1 β (Kelley et al., 2019). When it is produced the NLRP3 protein is ubiquitinated on the LRR domain, deubiquitination is required in order for assembly of the inflammasome, and priming signals also lead to this occurring (Guo et al., 2015; Kelley et al.,

2019). Following priming, the NLRP3 inflammasome complex is activated by one of a number of signals in the cytosol including ionic flux, reactive oxygen species (ROS), mitochondrial dysfunction, and lysosomal damage (Kelley et al., 2019). Assembly of all canonical inflammasomes causes the activation of caspase-1 from its precursor pro-caspase-1 and the conversion of both IL-1 β and IL-18 from their inactive precursors, alongside pyroptosis (Guo et al., 2015).

The POP materials are essentially polymers that are chains of nucleotides joined together by a linker, tri(ethylene glycol), which is a short chain PEG. RNA are single stranded chains of nucleotides, RNA viruses have been previously shown to modulate NLRP3 activity (Choudhury, Ma, Abdullah, & Zheng, 2021; J. Li et al., 2015). The POP materials could potential interact with the NLRP3 inflammasome.

The NLRP3 inflammasome has also been shown to play a role in wound healing and impairment of inflammasome activation in NLRP3 and caspase-1 knockout mice has been shown to reduce immune cell infiltration in wounds(Weinheimer-Haus, Mirza, & Koh, 2015). IL-1 β plays an important role in wound healing, but it is a double edge sword, too much and there are problems with healing of chronic/diabetic wounds and too little and there is impaired healing of the wound (Weinheimer-Haus et al., 2015). Inflammasome components have also been shown to be essential for the formation of the foreign body response to implants, and it's possible that their activation may lead to the initiation of further innate immune responses, such as complement, which may lead to significant injection site reactions (Hervé, Laupèze, Del Giudice, Didierlaurent, & Tavares Da Silva, 2019; Malik et al., 2011; Triantafilou, Hughes, Morgan, & Triantafilou, 2016; van Meer et al., 2016). Incorporation of an NLRP3 inhibitor in the silicone implant coating of an implantable electronic device and has been shown to prevent foreign body reaction from occurring to the implanted device, in contrast to dexamethasone it has been shown to retain the ability to regenerate tissue (Barone et al., 2022)

1.6.2 The Complement system

Complement is an important arm of the innate immune system, which responds to danger signals in the response to pathogens and has previously been well reviewed (Dunkelberger & Song, 2010; Merle, Church, Fremeaux-Bacchi, & Roumenina, 2015; Noris & Remuzzi, 2013). There are three complement pathways that are activated in different ways: classical, lectin and alternative pathways, these pathways all converge into the same pathway by producing C3 convertase (Dunkelberger & Song, 2010; Merle et al., 2015; Noris & Remuzzi, 2013). C3

convertase cleaves C3 into C3a and C3b, C3b forms part of the C5 convertase resulting in the conversion of C5 to C5a and C5b, depending on the pathway of activation C3 and C5 convertase are made of different complement proteins. C3a and C5a are anaphylatoxins and C5b leads to the assembly of the MAC complex (C5b-9) consisting of C5b, C6, C7, C8, and C9, which causes cell lysis.

The classical pathway is activated by antigen binding to IgG or IgM antibodies, C1 has the ability to bind to the antigen bound antibodies resulting in the activation of a portion of C1 which is able to then cleave C2 and C4 into C2a/b and C4a/b which then can form the C3 convertase C4bC2a (Noris & Remuzzi, 2013). The Lectin pathway is activated by mannose-binding lectins (MBLs) and ficolins binding to pathogen surfaces causing the activation of MBL-serine proteases which can then cleave C2 and C4 resulting in the same C3 convertase as the classical pathway (Noris & Remuzzi, 2013). The alternative pathway is activated by spontaneous C3 thioester bond hydrolysis, this creates C3(H₂O) which behaves like C3b, it is able to bind factor B, which following cleavage by factor D is able to create C3(H₂O)Bb which is a C3 convertase (Noris & Remuzzi, 2013). C3b creates an amplification loop which can also activate complement further, C3b can bind to activating surfaces and pathogens, subsequent binding to factor B through Factor D creates C3bBb the C3 convertase (Merle et al., 2015). Factor H and factor I both work to limit complement activation, factor H is an inhibitor of the C3 convertase and factor I degrades C3b and C4b (Dunkelberger & Song, 2010; Merle et al., 2015).

C3a and C5a are both anaphylatoxins, these carry out inflammatory roles by binding to their receptors on immune cells, they can also cause adaptive immune activation (Merle et al., 2015). The MAC complex (C5b-9) is the combination of C5b, C6, C7, C8 and C9 complement proteins, and causes the lysis of cells and calcium flux (Merle et al., 2015) .

Roles of the Complement Cascade in Innate Immunity

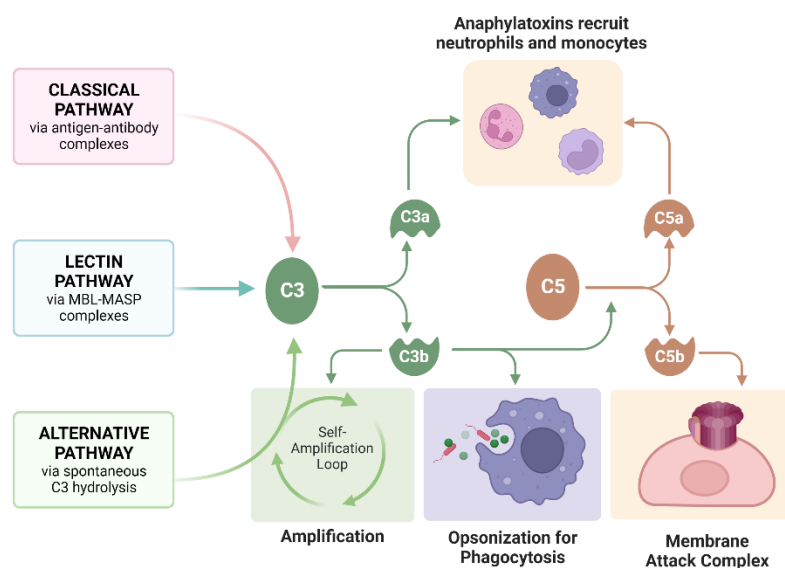


Figure 1.6: Illustrates the common pathway of all three complement pathways. C3 convertase cleaves C3 into C3a and C3b, C3b forms part of the C5 convertase resulting in the conversion of C5 to C5a and C5b. C3a and C5a are anaphylatoxins and C5b leads to the assembly of the membrane attack complex (MAC) complex (C5b-9) consisting of C5b, C6, C7, C8, and C9, which causes cell lysis. Figure taken from BioRender.com (BioRender, 2020b).

Doxil, is the first FDA approved Nanomedicine and is known to cause complement activation-related pseudoallergy (CARPA) syndrome, responses to Doxil are highly variable between patients, with some being able to tolerate it and others having serious anaphylaxis responses (Chanan-Khan et al., 2003). Hydroxyl and amine groups on materials have been shown to induce complement activation and C3b can be spontaneously absorbed to the surface of implanted materials which can lead to C3 convertase activation as discussed above (Arima, Kawagoe, Toda, & Iwata, 2009; Arima, Toda, & Iwata, 2008; Daniël T. Luttkhuizen, 2006). Antibodies bound to implanted materials can also activate complement through the classical pathway, further triggering inflammation during the foreign body reaction to materials (Daniël T. Luttkhuizen, 2006).

1.7 Cell lines used in the thesis

A number of cell lines have been used in the assessment of the POP materials in order to try to create screens of the materials for future assessments. Many cell lines could be used, but

the subsequent cell lines were chosen due to the cell type potential interaction with the implant or its breakdown products and have previously been well defined in the group and literature. These cell lines have been kept undifferentiated to allow for long-term culture and assessment.

1.7.1 CEM cell line

The CEM cell line was isolated from the blood of a child with acute lymphoblastic leukemia, it is a human T lymphoblast cell line (Foley et al., 1965). T-cell responses play an important role in the adaptive arm of the immune system (LaRosa & Orange, 2008).

1.7.2 KU812 cell line

The KU812 cell line was isolated from the blood of a patient with chronic myelogenous leukaemia, it is an immature human basophilic leukocyte cell line (Blom, Huang, Aveskogh, Nilsson, & Hellman, 1992). As discussed above, basophils are a circulating immune cell that play a crucial role in both IgE dependent and independent allergic inflammation (Miyake & Karasuyama, 2017; Plant-Hatelly et al., 2022; Shah, Eisenbarth, Tormey, & Siddon, 2021).

1.7.3 MUTZ-3 cell line

The MUTZ-3 cell line was isolated from the blood of a man with acute myelomonocytic leukaemia, it is an immature human DC cell line (DSMZ). This DC cell line has already been previously demonstrated as a useful model cell line for incorporation into hydrogels for the assessment of subcutaneously administered proteins (Groell, Kalia, Jordan, & Borchard, 2018).

1.7.4 THP-1 cell line

The THP-1 cell line was isolated from the blood of a boy with acute monocytic leukaemia, it is a monocytic cell line (Tsuchiya et al., 1980). Previously the THP-1 cell line has been used to explore monocyte or macrophage responses and inflammasome modulation and is known to produce IL-1 β and increase caspase-1 activation following treatment with known inflammasome inducers (Chanput, Mes, & Wichers, 2014; Guzova et al., 2019; Vandebriel et al., 2022).

1.8 Aims of the thesis

- To screen the POP materials created at both the University of Liverpool and Johns Hopkins University for sterility (Chapter 2).
- To determine whether the POP materials created at University of Liverpool show up any possible red flags in acute immunomodulatory assessments used to assess safety (Chapter 2).
- Explore the role of serum derived exosomes on the modulation of *in vitro* whole blood responses to the POP materials (Chapter 2).
- To determine whether repeat exposure of FTC, 3TC and linear poly(FTC) alter the health and phenotype of cells *in vitro*, using cell lines as a model (Chapter 3).
- To determine whether TAF aryl carbamates that would be used as monomers to enable formulation into a polymer for subcutaneous implant administration are cytotoxic or cause perturbations in cell health (Chapter 4).
- To determine the impact of POP implants on the immunological systems of *in vivo* animal test models (Chapter 5).

Chapter 2

Pre-screen to assess sterility, common Acute Immunotoxicity, and the impact of differential culture on peripheral blood responses to POP materials

2.1 Introduction

Bioburden assessment is standard practice, prior to any immunological assessment; particularly for materials not made to good manufacturing practice (GMP) standards. Following sterility assessment, the materials are evaluated for their cytotoxicity, in order to determine concentrations for consequent assays, and ensure the results in the assays following are not due to cytotoxicity. Common acute immunotoxicity assessments then must be carried out, to ensure that these materials will be safe and rule out any materials which cause red flags in these assays and therefore are predicted to be unsafe in humans. If any significant adverse results are seen in these assays, they are then followed up to determine the pathway and mechanism responsible and determine whether these issues are detrimental for the disease/treatment the materials will be used for. Commonly used acute immunotoxicity assays cover a number of different immunological systems, including, but not limited to: leukocyte proliferation and complement.

Lymphocytes circulate in the blood and provide the body protection from infections. Proliferation of lymphocytes can indicate that there is immune activation as a result of material exposure, and forms part of a material screen for immunological safety of materials.

As discussed in Chapter 1, complement is an important arm of the innate immune system, which responds to danger signals and results in the release of anaphylatoxins and the formation of the MAC. Complement has been shown to be activated in a number of current Nanoformulated drugs, therefore it is key to investigate complement in the pre-clinical assessment of new long-acting delivery systems (La-Beck, Islam, & Markiewski, 2021).

Exploring whole blood responses to new materials can be important in determining their safety if they are expected to enter the blood stream. Previous unpublished work within the group has shown that when A549 cells are grown with basal media supplemented with either fetal bovine serum (FBS) or exosome depleted FBS and treated with TNF- α , IL-8 secretion is significantly higher in the cells which have been cultured in media with serum depleted of exosomes. It has also been demonstrated previously, that exosomes, which are present without disease are involved in downregulating immune processes and termed tolerosomes (Fleshner & Crane, 2017). FBS derived exosomes have been shown to express similar miRNAs to those enriched in human ones, suggesting these exosomes may help to tolerate inflammatory signals to some extent, therefore altering the responses seen *in vivo* with FBS (Fleshner & Crane, 2017). Therefore, the role of exosomes in the serum supplemented in the media used in the dilution of the blood was explored in this chapter.

2.2 Methods

2.2.1 Materials

The POP materials were prepared in the Chemistry department at the University of Liverpool by Dr Faye Hern (Shakil et al., 2022). FTC and 3TC were both purchased from Wischem (Shanghai, China). Phytohaemagglutinin-M (PHA-M) (Sigma Aldrich), Thiazolyl Blue Tetrazolium Bromide (MTT) powder (Sigma Aldrich), Dimethyl sulfoxide (DMSO) (Sigma Aldrich), PyroMAT[®] kit (Millipore), Roswell Park Memorial Institute (RPMI)-1640 (Sigma Aldrich), Phosphate Buffered Solution (PBS) (Sigma Aldrich), Cytotoxicity Detection Kit^{PLUS} (LDH) (Roche) and Cellulose acetate membrane syringe filters (surfactant-free), 28mm, pore size 0.2 μm (Corning) were all purchased from Merck (Darmstadt, Germany). Pyrochrome[®] reagent, control standard endotoxin (CSE), Limulus amoebocyte lysate (LAL) reagent water, K tubes were all purchased from Associates of Cape Cod (Cape Cod, USA). Ficoll-paque was purchased from Fisher Scientific (Loughborough, UK). MicroVue[™] Complement iC3b Enzyme Immunoassay (EIA), Cobra venom factor (CVF) were both purchased from Quidel (California, USA). Doxil (Dox-NP[®]) was purchased from Avanti Polar Lipids (Alabaster, USA). LPS-EK Ultrapure, oligodeoxynucleotide (ODN) 2006, 2'3'- cyclic guanosine monophosphate-adenosine monophosphate (cGAMP), Poly(dG:dC)/LyoVec[™], Herpes Simplex virus (HSV)-60/LyoVec[™] were all purchased from Invivogen (Toulouse, France). 9-plex human Luminex assay (cytokines: Interferon (IFN)- α , IFN- β , IFN- γ , IL-1 β /IL-1F2, IL-6, IL-8/Chemokine (C-X-C motif) ligand (CXCL)-8, IL-10, IL-18/IL-1F4, TNF- α , and IL-1 Receptor Antagonist (RA). Were both purchased from R&D Systems, BioTechne (Minneapolis, USA). Bio-plex 200 system and Sheath fluid were both purchased from Bio-rad (California, USA). The cell lines 5637 (ACC 35) and MUTZ-3 (ACC 295), were purchased from DSMZ (Braunschweig, Germany). Minimum Essential Medium (MEM)- α no phenol red containing ribonucleosides, deoxyribonucleosides and L-glutamine (Gibco), FBS (Gibco) and exosome-depleted FBS (Gibco) were all purchased from ThermoFisher Scientific (Massachusetts, USA). The CEM, KU812 and THP-1 cell lines were all sourced from ATCC (Manassas, Virginia, USA).

2.2.2 POP materials and drug preparation

The POP material linear poly(FTC) was weighed and suspended at 20 mg/mL in DMSO. This was freshly prepared and suspended at the start of each new assay. linear poly(FTC) S5 was weighed and suspended in 1 mL of DMSO until visibly in solution, the final concentration was 9.9 mg/mL. All other materials: linear poly(FTC) S3, linear poly(FTC) S2 and linear poly(FTC)

S4 were too difficult to weigh, and a known weight was suspended into DMSO, 1 mL was added until visibly in solution, final concentrations were 72.76, 76.2 and 22.6 mg/mL respectively. DMSO was chosen, as it is usually one of the vehicles that is used for compounds that are insoluble in water for cellular assays and is usually well tolerated. FTC and 3TC were weighed and suspended at 1 mg/mL in cell culture media. This was freshly prepared and suspended at the start of each new assay.

2.2.3 Pyrogen assessment of the POP materials

2.2.3.1 LAL assessment of POP materials

The chromogenic LAL assay was carried out according to the manufacturer's protocol. The CSE was suspended in the volume stated in the certificate of analysis to obtain a 50 EU/mL stock. A standard curve of the concentrations 5, 0.5, 0.05, 0.005 EU/mL was created in LAL reagent water (endotoxin free) and 1, 0.1, 0.01, 0.001% dilutions of each the POP materials were also made up in LAL reagent water. 200 µL of LAL reagent water served as the blank/negative control, which along with 200 µL of each standard was added to corresponding reaction tubes in duplicate. 200 µL of each of the POP material concentrations to be assayed were added in duplicate to the corresponding reaction tubes. 180 µL of each concentration was added again in duplicate to the corresponding spiked sample reaction tubes, 20 µL of 5 EU/mL CSE was then added to all spiked reaction tubes. Following the set-up of all the reaction tubes, the software was set up on the PKflex. 3.2 mL of endotoxin free water was added to the Pyrochrome® reagent and left to settle at 15-30 °C for ten minutes. When the machine was ready, 50 µL of the lysate was added individually to each reaction tube and the reaction tube immediately placed into the corresponding slot of the reader. The software then created a standard curve for the data and interpreted the sample endotoxin concentrations based on how long it took to reach the end point. The standard curve worked properly, but due to issues with the samples causing interference with the assay example POP materials were taking forward into the MAT assay.

2.2.3.2 Monocyte activation test on POP materials that interfered with the LAL assays

2.2.3.2.1 MAT assay set up with linear poly(FTC) and linear poly(FTC) S3

The PyroMAT® kit was carried out on POP materials linear poly(FTC) and linear poly(FTC) S3 at final concentrations of 10 and 100 µg/mL, following the manufacturer's protocol. An endotoxin standard curve was prepared using LAL reagent water. Seven endotoxin

concentrations (0.0125, 0.025, 0.05, 0.1, 0.2, 0.4, and 0.8 EU/mL) were made to generate the standard curve and are prepared using 1:2 dilutions using the United States Pharmacopeia Reference Standard Endotoxin (RSE) stock solution. To create the first standard (0.8 EU/mL), first 950 μ L of LAL reagent water was added to the 50 μ L aliquot of RSE stock (2,000 EU/mL) and vortexed at max speed. 200 μ L of this RSE dilution was then added to 800 μ L of LAL reagent water in a non-endotoxin absorbing glass tube. To get the first standard 80 μ L of this RSE dilution was then added to 1920 μ L of LAL reagent water. To create the rest of the standard curve, 1:2 dilution (1000 μ L of the previous dilution was added to 1000 μ L of LAL reagent water), between each dilution the tube was vortexed at max speed for 30 seconds. To each of the two dilutions of test POP material concentrations RSE was spiked in at a final concentration of 0.2 EU/mL of endotoxin and these were also assayed in quadruplicate. 50 μ L of the blank, standards and samples were added to the corresponding wells and assayed in quadruplicate.

Two 50 mL endotoxin-free tubes were filled with pre-warmed RPMI-1640 media and two vials of PyroMAT™ cells from cryogenic storage were thawed in a water bath at 37°C. 1 mL of pre-warmed RPMI-1640 media was added to each vial, mixed by pipetting and transferred into respective tubes with pre-warmed media. The tubes were then spun at 210xg-force (g) for five minutes at 15-30 °C, the supernatants discarded and the pellet suspended in the remaining media and the two tubes combined and a small amount of media was used to wash the now empty tube. Warmed RPMI-1640 was then added to a total volume of 20 mL and 200 μ L of cells added to every well on the plate and incubated for 22 hours at 37 °C without Carbon dioxide (CO₂).

2.2.3.2.1 MAT IL-6 Enzyme-linked immunosorbent assay (ELISA) procedure

All components included in the kit were warmed to 15-30 °C and the manufacturer's protocol was followed. 100 μ L of assay diluent was added to all the wells being used on the 96-well plate. 100 μ L of the cell supernatant from the MTT set-up plate was then added to the corresponding wells on the ELISA plate, the plate, was sealed and incubated at 15-30 °C for two hours. Wash buffer was made up by adding 20 mL of 25x wash buffer to 480 mL of purified water. The contents of each well of the plate were then aspirated and the plate was then washed four times by adding 400 μ L of wash buffer each time using the plate washer. Following final aspiration, 200 μ L of IL-6 conjugate was added to each well, the plate was sealed and incubated for two hours at 15-30 °C. Following incubation, the previous wash step was repeated and the substrate solution was prepared by adding the entire contents of the

colour reagent A bottle to the colour reagent B bottle and mixed by inversion. 200 µL of substrate solution was then added to each well immediately after it was made and incubated at 15-30 °C for 20 minutes protected from light. Immediately after incubation 50 µL of stop solution was added to each well and mixed by pipetting up and down. The optical density (OD) at 450 nm and a reference wavelength of 630 nm was immediately read using the CLARIOstar plate reader.

2.2.4 Cytotoxicity assessment of FTC, 3TC and the POP materials using the MTT and Lactate dehydrogenase (LDH) assays

2.2.4.1 Routine culture of cell lines

2.2.4.1.1 Culture of CEM cells

The human peripheral blood acute lymphoblastic leukaemia T lymphoblast cell line, CEM cells were maintained in a routine cell culture medium of RPMI-1640 supplemented with 10% v/v FBS. All cells were incubated at 37°C, with 5% CO₂.

2.2.4.1.2 Culture of KU812 cells

The human peripheral blood myeloblast basophil cell line, KU812 cells were maintained in a routine cell culture medium of RPMI-1640 supplemented with 10% v/v FBS.

2.2.4.1.3 Culture of MUTZ-3 cells

The human urinary bladder carcinoma cell line 5637 cells were maintained in a routine cell culture medium of RPMI-1640 supplemented with 10% v/v FBS. Conditioned 5637 media was collected once cells reached confluence in T175 flasks, centrifuged for five minutes at 860xg and filtered using cellulose acetate membrane syringe filters (surfactant-free), 28mm, pore size 0.2 µm and frozen at -20 °C until used. The human peripheral blood acute myelomonocytic leukaemia cell line MUTZ-3 cells were maintained in a routine cell culture medium of MEM-α no phenol red containing ribonucleosides, deoxyribonucleosides and L-glutamine supplemented with 20% v/v FBS and 20% v/v 5637 conditioned medium.

2.2.4.1.4 Culture of THP-1 cells

The human peripheral blood acute monocytic leukaemia cell line, THP-1 cells were maintained in a routine cell culture medium of RPMI-1640 supplemented with 10% v/v FBS.

2.2.4.2 Cytotoxicity assessment of FTC and 3TC in the cell lines: CEM, KU812, MUTZ-3 and THP-1 assay set up

50 μ L of media was added to all wells of a 96-well plate and 50 μ L of the respective drug was placed in all wells of column 1. A 1:2 dilution was performed across the plate to column 9, to create a final well concentration range from 250 μ g/mL – 0.977 μ g/mL. 50 μ L cells were plated in column one - twelve rows A-C and rows F-H and 50 μ L of media added to column 1-12 rows D and E, to ensure a cell free control is used to ensure there is no material interference. Each plate was set up in duplicate for each drug (half plate equals one experimental replicate with three technical replicates) and two plates used for each drug for each cell line, per time point. The plates were either incubated for 24-hours or 48-hours. Two untreated cell containing column and a media control was also included. Following incubation 5 μ L of Lysis buffer from Cytotoxicity Detection Kit^{PLUS} (LDH) was added to one of the untreated columns and incubated for a further 15 minutes on a plate shaker set to 250 RPM at 37 °C. Plates were subsequently centrifuged at 860xg for five minutes and the supernatants transferred into 96-well flat bottom plates. MTT powder (thiazolyl blue tetrazolium bromide dye; Sigma-Aldrich, USA) was prepared in sterile PBS at 5mg/mL and 50 μ L was added to the cell pellet of each well and incubated for two hours at 37°C, 5% CO₂.

2.2.4.2.1 LDH assay procedure

Cytotoxicity Detection Kit^{PLUS} (LDH) was then carried out using the supernatants. All contents were allowed to warm up to 15-30 °C prior to the assay being carried out. Reaction mixture was prepared by adding 1 mL of sterile water to the lyphosylate in bottle 1, the whole contents were then transferred into bottle two and vortexed. 100 μ L of freshly prepared reaction mixture was added to every well on the plate and incubated for 30 minutes at 15-30 °C in the dark. 50 μ L of bottle four (stop solution) was added to all wells, the plate was shaken for ten seconds and OD measured at absorbance 493 nm and 600 nm using CLARIOstar plate reader. GraphPad Prism software 9.3.1 was used to calculate effective concentration (EC)₂₀ values for drugs showing complete cytotoxicity.

2.2.4.2.2 MTT assay procedure

Following incubation, the MTT plates were subsequently centrifuged at 1935xg for five minutes followed by aspiration. 100 μ L of DMSO (Sigma-Aldrich, USA) was then added, mixed and OD measured at absorbance 570 nm and 620 nm using CLARIOstar plate reader.

GraphPad Prism software 9.3.1 was used to calculate effective concentration (EC)₂₀ values for drugs showing complete cytotoxicity.

2.2.4.4 Cytotoxicity assessment of the POP materials in THP-1 cells using the MTT and LDH assays

The protocol used in 2.2.4.1 was followed with the following exceptions, only a 24-hour time point was used and a tenth concentration for each test compound was included on a second plate. Each POP material was used at the following concentration ranges illustrated in table 2.1. FTC 250 – 0.977 µg/mL and DMSO 2 – 0.004% were also included.

Table 2.1: POP polymer cytotoxicity concentration ranges tested in the MTT and LDH assays.

POP Polymer	Concentration range assessed (mg/mL)
linear poly(FTC)	0.2 – 0.000391
linear poly(FTC) S2	1.52 – 0.00298
linear poly(FTC) S3	1.46 – 0.00284
linear poly(FTC) S4	0.452 – 0.000882
linear poly(FTC) S5	0.198 – 0.000387

2.2.5 Leukocyte proliferation assessment of POP material linear poly(FTC) and FTC

The Leukocyte proliferation assay was performed as described in (Marina A. Dobrovolskaia, 2015a), except buffy coats were used instead of volunteer blood. Buffy coats were obtained from National Health Service (NHS) blood and transport (BT) service. The blood was layered on top of Ficoll-Paque in a 1:2 ratio and then spun at 860xg for 30 minutes without break. The PBMC layer was then removed and washed with PBS and spun at 860xg for five minutes. The pellet was then suspended in 50 mL of Roswell Park Memorial Institute (RPMI) 1640 media supplemented 10% with FBS and placed in a T175 flask overnight. The next morning each test compound was diluted in media to 2x final concentration and 100 µL was dispensed into the respective wells. Final concentrations of the test compounds were linear poly(FTC) 80 µg/mL, linear poly(FTC) 40 µg/mL, FTC 18 µg/mL and FTC 1.8 µg/mL, these were set up in sextuplicate. These conditions spiked with PHA-M at a final concentration 5 µg/mL were also set up in sextuplicate. Controls were also set up to a final concentration of: PHA-M 2.5, 5 and

10 µg/mL and a DMSO control matching the highest linear poly(FTC) concentration, these were set up in duplicate. The cells were then counted and adjusted to a density of at 1×10^6 cells/mL. 100 µL of cells or media was then plated in the respective wells and incubated at 37°C 5% CO₂ for 72 hours. The plates were then centrifuged at 700xg for five minutes and the supernatant aspirated. 50 µL of MTT (5 mg/mL in PBS) and 200 µL of fresh media was added to each well and incubated for four hours in a humidified incubator at 37°C, 5% CO₂. Following incubation, the plates were centrifuged at 1935xg for five minutes and the supernatants aspirated. 200 µL of DMSO was added to all wells, mixed and the OD read at 570 nm and 620 nm. Data displayed as % of untreated control average, untreated average used from each individual plate. Statistical analysis was performed using GraphPad Prism software 9.3.1, using a one-way Analysis of Variance (ANOVA) test. A p value <0.05 was considered statistically significant. Proliferation Inhibition was calculated as follows,

$$\left(\frac{(\text{mean OD positive control} - \text{mean OD positive control and test compound})}{(\text{mean OD positive control} - \text{mean OD untreated cells})} \right) \times 100\%.$$

2.2.6 Assessment of POP material linear poly(FTC) on complement activation

Assay to assess possible complement was adapted from (Neill J. Liptrott, Giardiello, McDonald, Rannard, & Owen, 2018; Neun, Ilinskaya, & Dobrovolskaia, 2018). Blood was collected fresh from health volunteers using the PharmB ethics in hirudin coated collection tubes. Within 30 minutes of being drawn, the blood was centrifuged at 2500xg for ten minutes. Individual Eppendorf's were then set up in duplicate for each donor with 100 µL of PBS, 100 µL of test compound diluted in PBS and 100 µL of fresh plasma. Final concentrations of the test compounds were linear poly(FTC) 80 µg/mL, linear poly(FTC) 40 µg/mL, FTC 18 µg/mL and FTC 1.8 µg/mL. Alongside this Vehicle control (DMSO), Untreated control (PBS alone) and two Positive controls were set up: Doxil at 200/16.42 µg/mL (total lipid content/Doxorubicin content) and Cobra venom factor (CVF) at 1035 units/mL. All the Eppendorf's were then incubated at 37°C for 30 minutes. Following the incubation period, the samples were immediately analysed in duplicate using the MicroVue™ Complement iC3b EIA following the manufacturer's protocol. Samples were diluted either 1:40 or 1:20 in iC3b specimen diluent for the positive controls and all other samples respectively and assayed. Each of the standards and controls were reconstituted with 2 mL of hydrating reagent, left to sit for 15 minutes, and mixed gently. Wash buffer was made up by diluting the wash buffer concentrate with deionised water with a 1:20 dilution. 100 µL of each the blank, standards, controls, or samples was added to the corresponding wells of the 96-well plate in duplicate,

each FTC 1.8 µg/mL and linear poly(FTC) 40 µg/mL were assayed in singlicate due to space constraints on the iC3b ELISA plates. OD was read at 405 nm and data analysed by removing the blank and plotting the Concentration (x-axis) against Absorbance (y-axis) and the test sample concentrations interpolated from the curve created using GraphPad Prism software 9.3.1, table 2.1-2.3 demonstrate the validation of the assay and the concentrations of the standard curve and therefore limits of detection. Statistical analysis was performed using the same GraphPad Prism software 9.3.1. Statistical significance was evaluated using a one-way ANOVA test. A p value <0.05 was considered statistically significant. Percentage increases calculated as follows, $\left(\frac{(\text{Concentration } iC3b \text{ test compound} - \text{Concentration } iC3b \text{ untreated})}{\text{Concentration } iC3b \text{ untreated}}\right) \times 100\%$.

Table 2.2: Demonstrates the Minimum and maximum limits of quantification for iC3b in the assay.

Standard	(µg/mL)
A	0.17
B	0.59
C	1.15

Table 2.3: Demonstrates the expected high and low control values and the observed values seen in this experiment.

	Expected (µg/mL)	Observed (µg/mL) donors 1, 2 and 3	Observed (µg/mL) donors 4 and 5
Low	0.25 to 0.42	0.351	0.386
High	0.57 to 1.18	0.987	1.004

Table 2.4: Demonstrates the expected validation criteria for the assay and the observed values seen in this experiment.

	Expected	Observed donors 1, 2 and 3	Observed donors 4 and 5
Correlation coefficient (r)	> 0.95	0.992	0.9984
Slope (m)	Between 0.72 and 1.30	1.061	1.231

Y-intercept	Between 0.70 and 1.39	0.995	1.223
--------------------	--------------------------	-------	-------

2.2.7 Assessment of POP materials in whole blood using control ligand panel

Whole blood assay was adapted from the PBMC cytokine secretion assays used previously by the group (David et al., 2020; Neill J. Liptrott et al., 2018). Blood was collected fresh in tubes containing the anticoagulant Li-heparin from health volunteers using the PharmB ethics. Within 30 minutes of being drawn, the blood was diluted 1:4 with complete culture media (RPMI supplemented 10% v/v FBS), 800 µL of diluted blood was then seeded into 24-well plates and 200 µL of each diluted test compound added. The following final concentration of the agonist compounds set up in duplicate were: LPS 20 ng/mL, the principal component of gram-negative bacteria, which acts on and activates TLR-4, PHA-M 10 µg/mL, a potent mitogen that crosslinks the human T lymphocyte antigen receptor (Ti), media (Blank), PBS (Negative Control), ODN 2006 19.2/38.5 ng/mL, contains CpG motifs that act on and activate TLR-9, 2'3'- cGAMP 5/10 µg/mL, a STING agonist, Poly(dG:dC)/LyoVec™ 2.5/5 µg/mL, HSV-60/LyoVec™ 2.5/5 µg/mL, both act on Cytosolic DNA sensors (CDS). The samples were incubated for 24 hours at 37°C, 5% CO₂. Samples were then centrifuged at 860xg for five minutes and 100 µL aliquots of the supernatants frozen at -80 °C until analysis.

Supernatants were thawed and cytokine analysis carried out following the Human Magnetic Luminex Assay protocol. The Bio-Plex 200 Luminex system (Bio-Rad Laboratories, Hemel Hempstead, UK) was started and allowed to warm up to working temperature. Samples, standards and all reagents were allowed to equilibrate to 15-30 °C. Each of the four standards provided in the kit were reconstituted with Calibrator Diluent RD6-52 using the volumes specified on the certificate of analysis and allowed to stand for 15 minutes with gentle agitation. 100 µL of each were then combined together with 600 µL Calibrator Diluent RD6-52 to create standard 1. 200 µL of Calibrator Diluent RD6-52 was then pipetted into five tubes and labelled standards 2-6. 100 µL from standard one was then used to perform a 3-fold dilution series. Wash buffer was made by adding 20 mL of wash buffer concentrate to 480 mL of distilled water. Microparticle cocktail, biotin-antibody cocktail, Streptavidin-phycoerythrin (PE) vials were all centrifuged at 1000xg for 30 seconds. Biotin-antibody cocktail was vortexed to suspend the microparticles and 500 µL was added to 5 mL of Diluent RD2-1 to create the Diluted biotin-antibody cocktail. Streptavidin-PE concentrate was

vortexed and 220 μ L added to 5.35 mL of Wash buffer in a polypropylene test tube wrapped with aluminium foil to protect it from light. Samples were centrifuged at 860xg for five minutes and 50 μ L of sample or standards plated in their respective wells, all standards were read in duplicate, and each blood sample was read in singlicate. Human magnetic microparticle cocktail was vortexed and 500 μ L added to 5 mL of Diluent RD2-1 to create the diluted microparticle cocktail. 50 μ L of microparticle cocktail was added to every well on the 96-well plate and incubated at 15-30 $^{\circ}$ C on a plate shaker set at 800 RPM for two hours. The plate was washed three times with addition of 100 μ L of wash buffer. 50 μ L of diluted Biotin antibody cocktail was added to each well and incubated at 15-30 $^{\circ}$ C on a plate shaker set at 800 RPM for one hour. During this incubation the Bio-Plex 200 Luminex was calibrated, and bead regions and standard values entered into the software. The plate wash was repeated and 50 μ L of diluted streptavidin-PE added to each well and incubated at 15-30 $^{\circ}$ C on a plate shaker set at 800 RPM for 30 minutes. The plate wash was repeated and 100 μ L of wash buffer was added to each well and incubated for two minutes on a plate shaker set to 800 RPM. The plate was analysed using the Bio-Plex 200 Luminex setting the sample volume at 50 μ L, bead type as Bio-Plex MagPlex Beads, set double discriminator gates at 8000 and 23000, reporter gain settings set to low RP1 target value for CAL2 setting, 50 counts/region and collect median fluorescence intensity (MFI). The minimum and maximum limits of quantification for these cytokines are displayed in table 2.4. Statistical analysis was performed using GraphPad Prism software 9.3.1. Statistical significance was evaluated using a one-way ANOVA test. A p value <0.05 was considered statistically significant.

Table 2.5: Demonstrates the Minimum and maximum limits of quantification for each panel of analytes for the early development of the whole blood assay assessment.

Analyte	Minimum (μ g/mL)	Maximum (μ g/mL)
IFN- α	10.02	2510
IFN- β	11.445	2800
IFN- γ	49.58	12330
IL-1 β /IL-1F2	19.55	4810
IL-6	5.705	1400
IL-8/CXCL-8	4.275	1050
IL-10	4.805	1190
IL-18/IL-1F4	11.95	3020

TNF- α	9.23	2260
---------------	------	------

The above protocol was then repeated following the same steps as described above but the complete culture media used to dilute the blood was either supplement with FBS or Exosome-depleted FBS with the same conditions repeated for either media with n=2. The minimum and maximum limits of quantification for the cytokines assayed are displayed in table 2.4.

Following analysis of the results, the highest concentration of each agonist was then used following the protocol described above with the two types of FBS for donors 1-3, with the exception that whole blood was obtained from NHS BT service using the anticoagulant sodium citrate and each sample was only set up in singlicate but ran in the Luminex assay in duplicate. The following additional POP materials were also assayed: linear poly(FTC) 80 $\mu\text{g}/\text{mL}$, linear poly(FTC) S2 80 $\mu\text{g}/\text{mL}$, linear poly(FTC) S3 60 $\mu\text{g}/\text{mL}$, linear poly(FTC) S4 80 $\mu\text{g}/\text{mL}$, and linear poly(FTC) S5 80 $\mu\text{g}/\text{mL}$. The minimum and maximum limits of quantification for the cytokines assayed are displayed in table 2.5.

The above protocol for Donors 1-3 was then repeated again for donors 4-6 using blood that was collected fresh from health volunteers using the PharmB ethics and an extra concentration of linear poly(FTC) at 40 $\mu\text{g}/\text{mL}$ was included. The intentions of this experiment were not to compare the blood source and responses, but due to the COVID-19 pandemic blood had to be sourced externally for donors 1-3. The minimum and maximum limits of quantification for the cytokines assayed are displayed in table 2.5. The average concentrations calculated for each cytokine were plotted, values that were above the limit of quantification were plotted at the limit of detection and values below the limit of detection were plotted as 0. Samples that had one replicate within the range were plotted at the value that was in range alone. A dashed line has been used to indicate where these limits of detection are on the graphs that contained samples that were either above or below the limit of detection. The average concentration for the seven donors supplemented with either normal or exosome-depleted serum was averaged and plotted in a heat map with the colour scheme for each cytokine being determined by the highest and lowest concentrations all in pg/mL . Donors that were under the limit of detection were excluded from that cytokine analysis and the average taken from the remaining donors. GraphPad Prism software 9.3.1 was used to display the data.

Table 2.6: Demonstrates the Minimum and maximum limits of quantification for each panel of analytes for Donors 1-6 of in the whole blood assay assessment of the POP materials.

Analyte	Donor 1-3	Donor 1-3	Donor 4-6	Donor 4-6
	Minimum (pg/mL)	Maximum (pg/mL)	Minimum (pg/mL)	Maximum (pg/mL)
IFN- α	10.02	2510	9.63	2340
IFN- β	11.445	2800	16.20	3390
IFN- γ	49.58	12330	48.601	11810
IL-1 β /IL-1F2	19.55	4810	13.951	3990
IL-6	5.705	1400	4.074	990
IL-8/CXCL-8	4.275	1050	3.909	950
IL-10	4.805	1190	-	-
IL-18/IL-1F4	11.95	3020	16.543	4020
TNF- α	9.23	2260	7.325	1780
IL-1 Receptor Antagonist (RA)	-	-	25.844	6280

2.3 Results

2.3.1 Pyrogen assessment of POP materials measured by MAT assay

The MAT assay was used to detect whether the materials tested contained pyrogens. No detectable levels of endotoxin were found in the POP material samples: linear poly(FTC) and linear poly(FTC) S3 analysed using the MAT assay (Figure 2.1). Both concentrations of linear poly(FTC) and linear poly(FTC) S3 spiked samples had between 50 - 200% endotoxin spike recoveries, 50 - 200% is the acceptable range of recovery for the assay. linear poly(FTC) S3 at both concentrations gave consistent recovery levels, 10 $\mu\text{g/mL}$ and 100 $\mu\text{g/mL}$ respectively were 88.8% and 82.8%. Whereas the average % recovery for linear poly(FTC) 10 $\mu\text{g/mL}$ was 105% and 100 $\mu\text{g/mL}$ was 70.67%. This data suggests that the level of pyrogen contamination in the sample is acceptable.

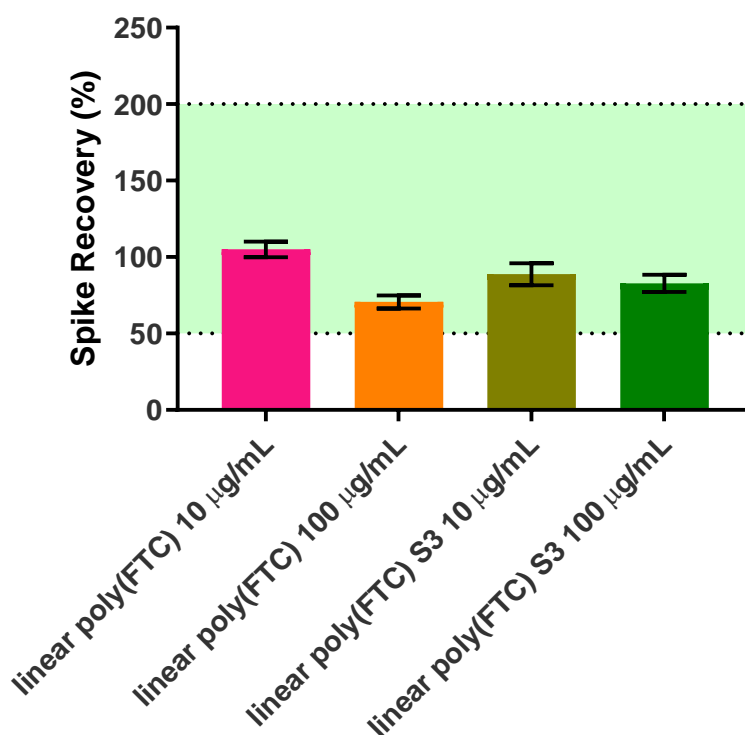


Figure 2.1: MAT recovery of RSE from samples of linear poly(FTC) and linear poly(FTC) S3 10 and 100 $\mu\text{g/mL}$ spiked with RSE at a final concentration of 0.2 EU/mL. All unspiked samples were below the limit of detection of the assay. Data displayed as n=4, mean (\pm standard deviation). Spike recovery, green area indicates 50-200% recovery following LPS spike.

This data suggests that the level of pyrogen contamination in the sample is acceptable.

2.3.2 Cytotoxicity assessment of Antiretrovirals and POP materials

Cytotoxicity assessment was carried out on the antiretrovirals FTC and 3TC, alongside the POP fragments in order to find appropriate concentrations to test in subsequent immunocompatibility assays.

2.3.2.1 FTC and 3TC cytotoxicity assessment in the four cell lines: CEM, KU812, THP-1 and MUTZ-3.

Neither FTC nor 3TC caused overt toxicity in any of the four cell lines over 24 or 48 hours, in either the MTT or LDH assay up to 250 $\mu\text{g}/\text{mL}$ and therefore EC_{20} values for the drugs were not able to be calculated (Figures 2.2 – 2.9). As a result of this data, concentrations up to 250 $\mu\text{g}/\text{mL}$ can be used in subsequent assays in these cell lines.

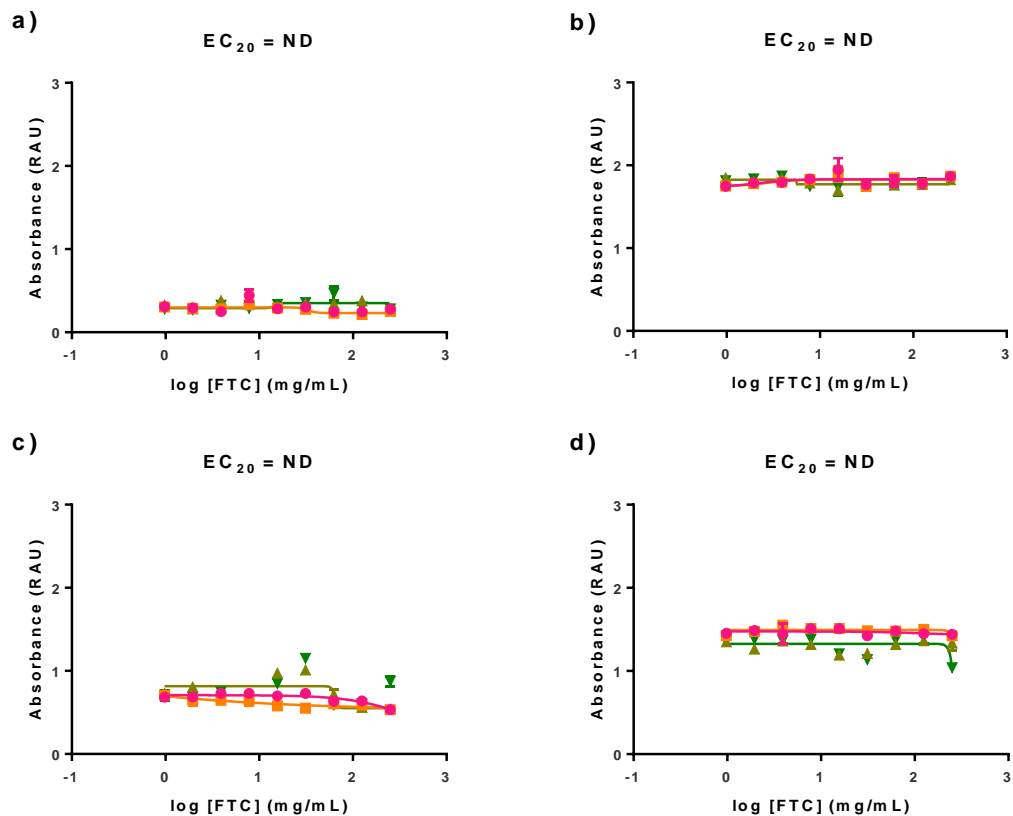


Figure 2.2: Cytotoxicity assessment of FTC in the CEM cell line a) 24 hours MTT, b) 24 hours LDH, c) 48 hours MTT and d) 48 hours LDH. Data displayed as n=3 technical replicates mean (\pm Standard Deviation) and n=4 experimental replicates, each displayed in a different colour. EC_{20} values calculated using EC anything calculator from EC_{50} values and the Hill Slope using GraphPad Prism software 9.3.1, not determined (ND) is used to describe values that were unable to be computed due to incomplete cytotoxicity curves.

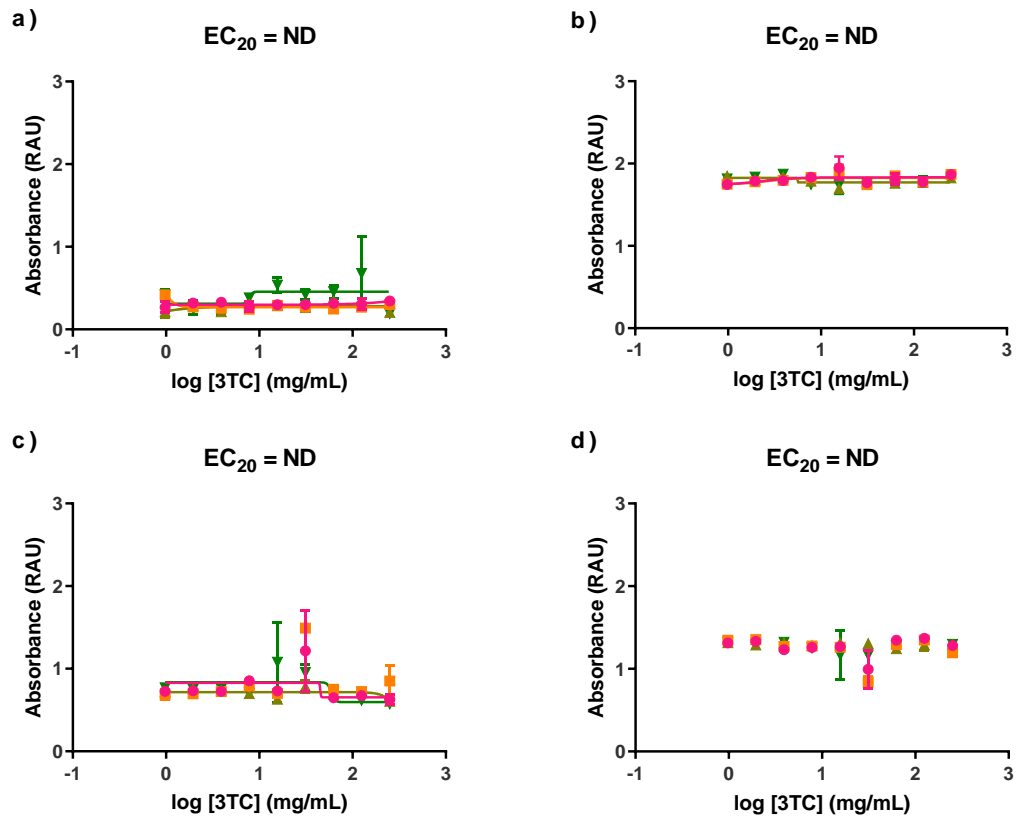


Figure 2.3: Cytotoxicity assessment of 3TC in the CEM cell line a) 24 hours MTT, b) 24 hours LDH, c) 48 hours MTT and d) 48 hours LDH. Data displayed as n=3 technical replicates mean (\pm Standard Deviation) and n=4 experimental replicates, each displayed in a different colour. EC_{20} values calculated using EC anything calculator from EC_{50} values and the Hill Slope using GraphPad Prism software 9.3.1, not determined (ND) is used to describe values that were unable to be computed due to incomplete cytotoxicity curves.

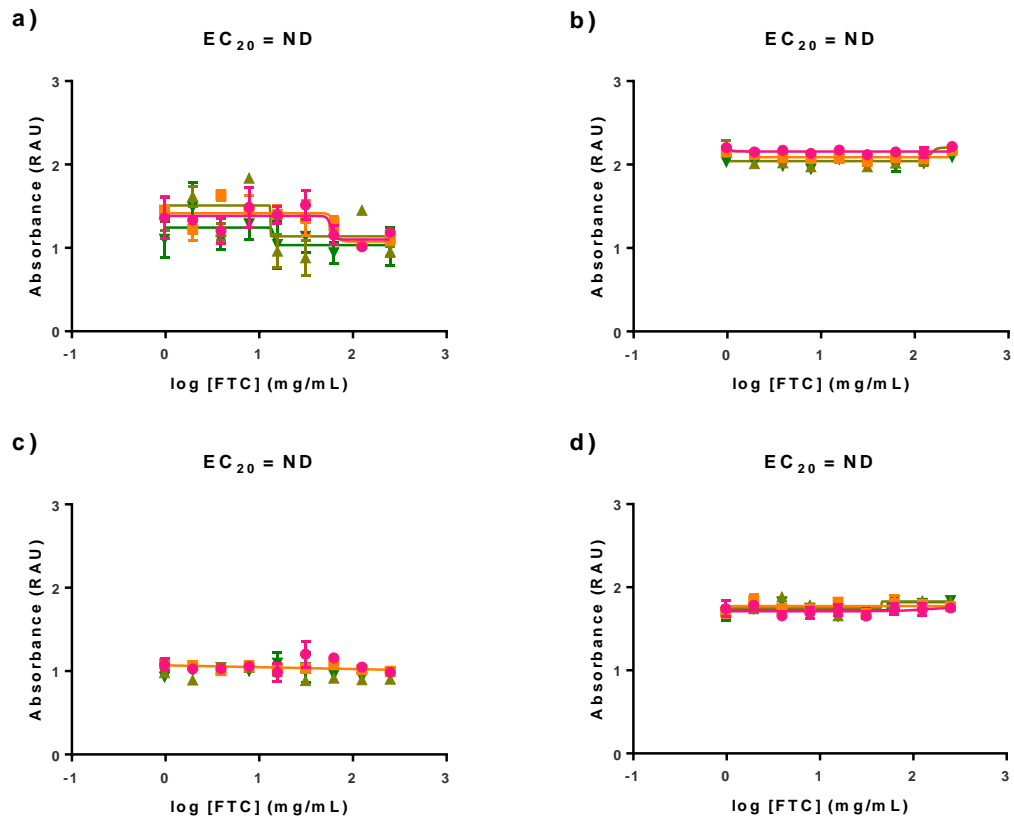


Figure 2.4: Cytotoxicity assessment of FTC in the KU812 cell line a) 24 hours MTT, b) 24 hours LDH, c) 48 hours MTT and d) 48 hours LDH. Data displayed as n=3 technical replicates mean (\pm Standard Deviation) and n=4 experimental replicates, each displayed in a different colour. EC_{20} values calculated using EC anything calculator from EC_{50} values and the Hill Slope using GraphPad Prism software 9.3.1, not determined (ND) is used to describe values that were unable to be computed due to incomplete cytotoxicity curves.

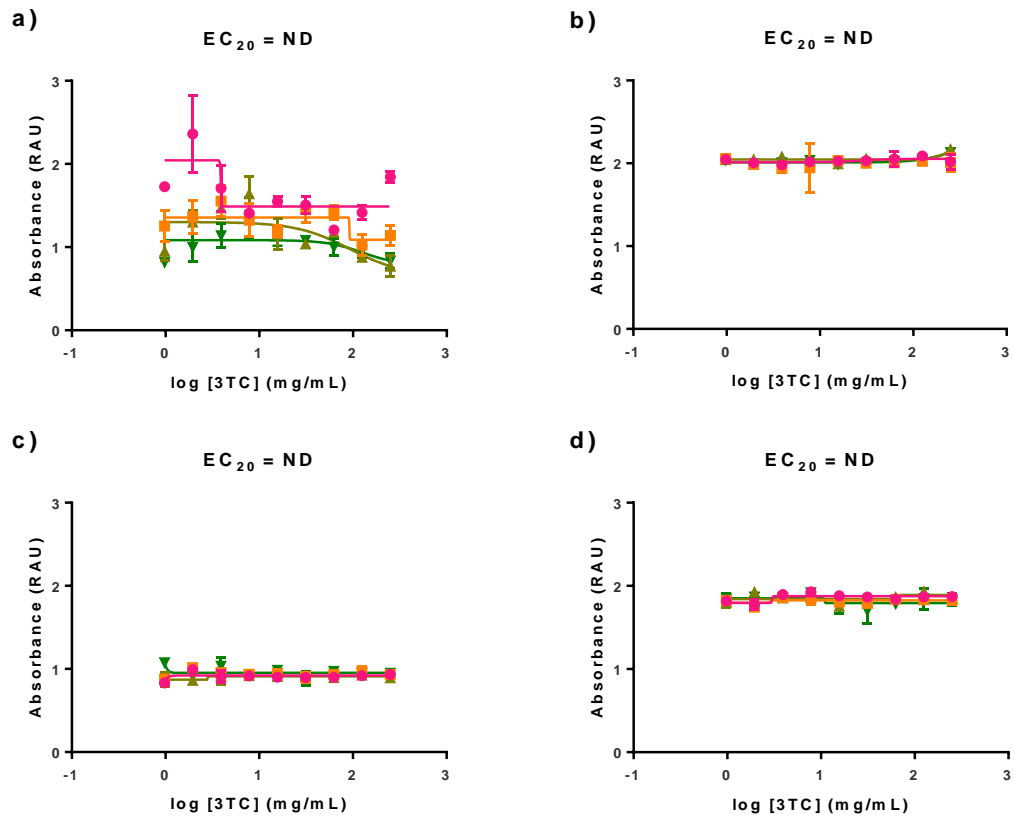


Figure 2.5: Cytotoxicity assessment of 3TC in the KU812 cell line a) 24 hours MTT, b) 24 hours LDH, c) 48 hours MTT and d) 48 hours LDH. Data displayed as n=3 technical replicates mean (\pm Standard Deviation) and n=4 experimental replicates, each displayed in a different colour. EC₂₀ values calculated using EC anything calculator from EC₅₀ values and the Hill Slope using GraphPad Prism software 9.3.1, not determined (ND) is used to describe values that were unable to be computed due to incomplete cytotoxicity curves.

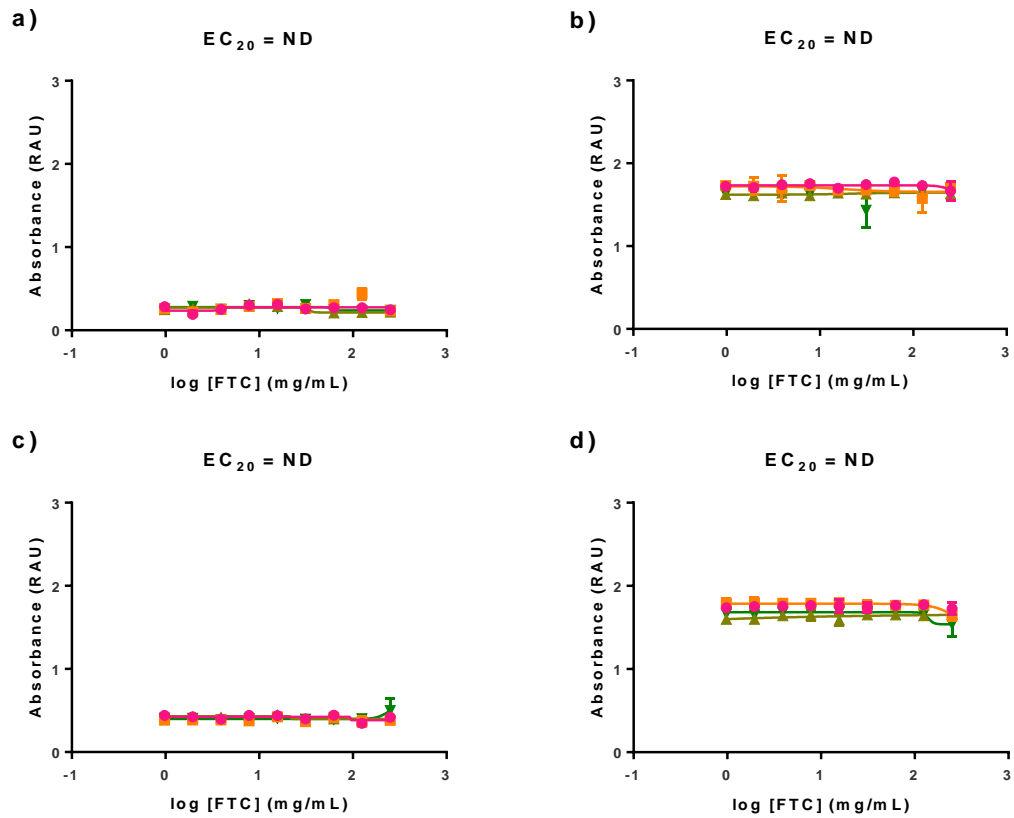


Figure 2.6: Cytotoxicity assessment of FTC in the MUTZ-3 cell line a) 24 hours MTT, b) 24 hours LDH, c) 48 hours MTT and d) 48 hours LDH. Data displayed as n=3 technical replicates mean (\pm Standard Deviation) and n=4 experimental replicates, each displayed in a different colour. EC_{20} values calculated using EC anything calculator from EC_{50} values and the Hill Slope using GraphPad Prism software 9.3.1, not determined (ND) is used to describe values that were unable to be computed due to incomplete cytotoxicity curves.

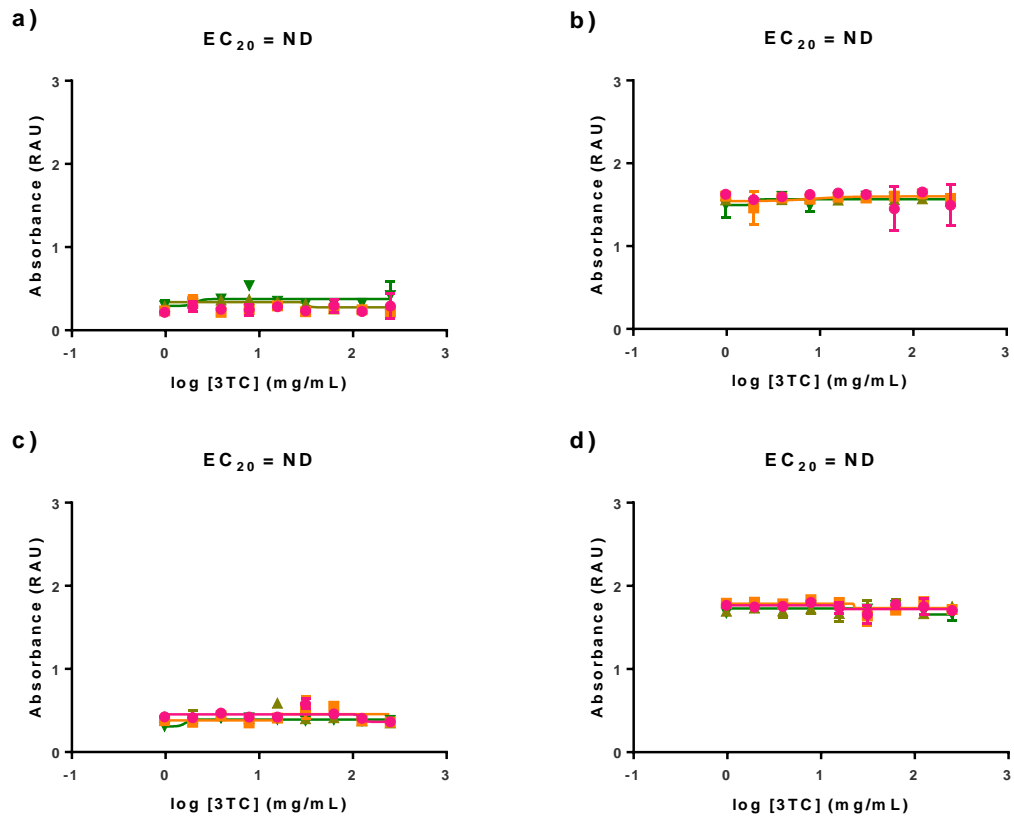


Figure 2.7: Cytotoxicity assessment of 3TC in the MUTZ-3 cell line a) 24 hours MTT, b) 24 hours LDH, c) 48 hours MTT and d) 48 hours LDH. Data displayed as n=3 technical replicates mean (\pm Standard Deviation) and n=4 experimental replicates, each displayed in a different colour. EC₂₀ values calculated using EC anything calculator from EC₅₀ values and the Hill Slope using GraphPad Prism software 9.3.1, not determined (ND) is used to describe values that were unable to be computed due to incomplete cytotoxicity curves.

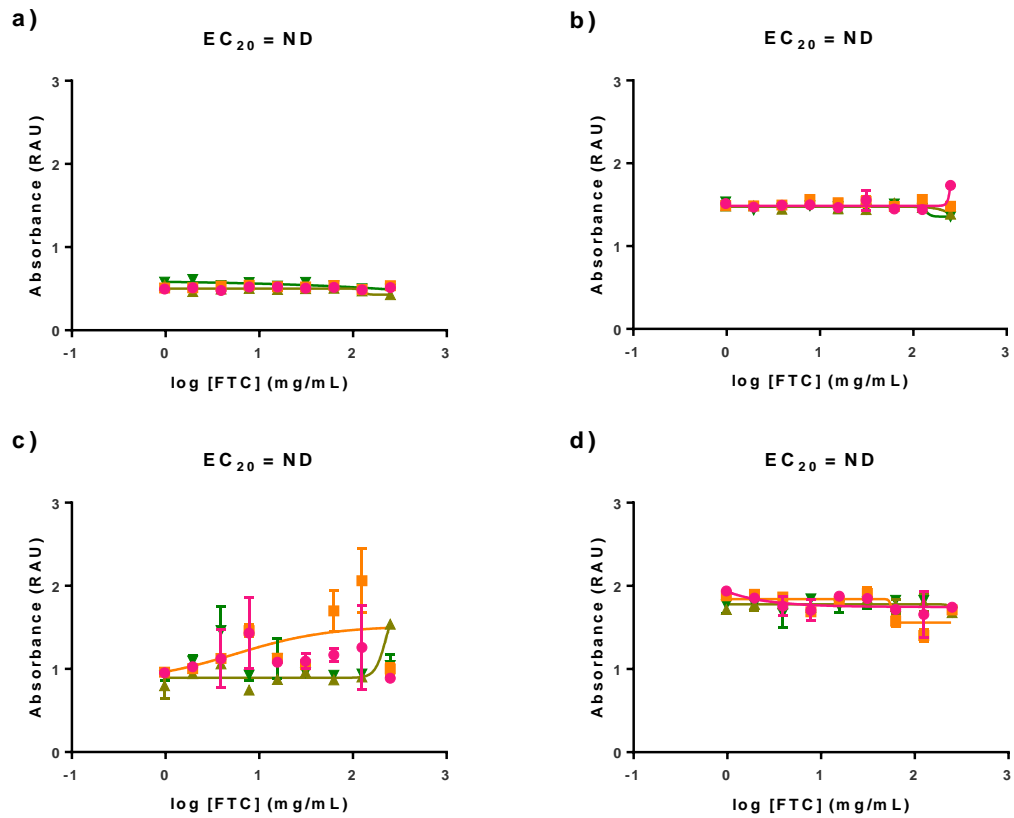


Figure 2.8: Cytotoxicity assessment of FTC in the THP-1 cell line a) 24 hours MTT, b) 24 hours LDH, c) 48 hours MTT and d) 48 hours LDH. Data displayed as n=3 technical replicates mean (\pm Standard Deviation) and n=4 experimental replicates, each displayed in a different colour. EC₂₀ values calculated using EC anything calculator from EC₅₀ values and the Hill Slope using GraphPad Prism software 9.3.1, not determined (ND) is used to describe values that were unable to be computed due to incomplete cytotoxicity curves.

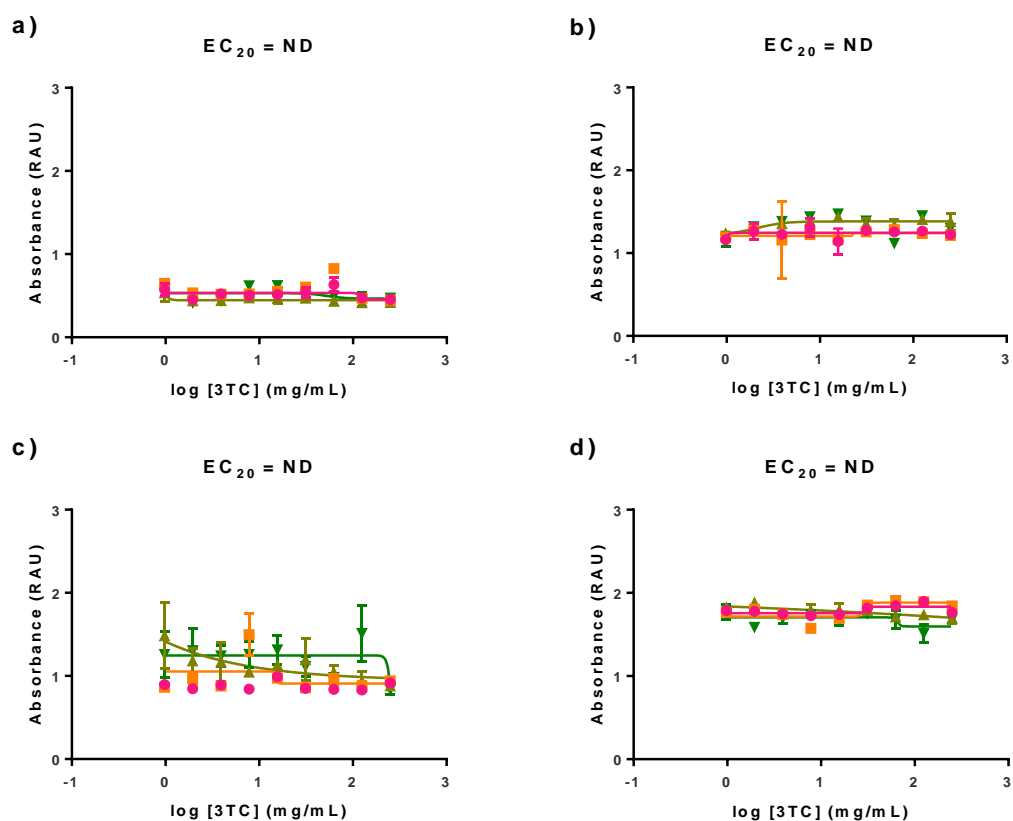


Figure 2.9: Cytotoxicity assessment of 3TC in the THP-1 cell line a) 24 hours exposure MTT, b) 24 hours exposure LDH, c) 48 hours exposure MTT and d) 48 hours exposure LDH. Data displayed as n=3 technical replicates mean (\pm Standard Deviation) and n=4 experimental replicates, each displayed in a different colour. EC_{20} values calculated using EC anything calculator from EC_{50} values and the Hill Slope using GraphPad Prism software 9.3.1, not determined (ND) is used to describe values that were unable to be computed due to incomplete cytotoxicity curves.

As a result of this data, concentrations up to 250 $\mu\text{g}/\text{mL}$ can be used in subsequent assays in these cell lines.

2.3.2.2 POP material cytotoxicity assessment in the monocytic THP-1 cell line

DMSO at the percentages tested did not cause any overt toxicity in either the MTT or LDH assay over 24 hours and therefore EC_{20} values were not able to be calculated (Figure 2.10). FTC caused no overt toxicity at the concentrations tested in either the MTT or LDH assay over 24 hours (Figure 2.11). Linear poly(FTC), S2 and S4 caused no overt toxicity in either of the cytotoxicity assays either (Figures 2.12, 2.13 and 2.15). Linear poly(FTC) S3 however did cause cytotoxicity in both the MTT and the LDH assays following 24 hour exposure, the MTT EC_{20}

values calculated for the four experimental repeats were: 0.133, 0.042, 0.032 and 0.078, with the average EC_{20} being 0.071 mg/mL (Figure 2.14). The LDH EC_{20} values for linear poly(FTC) S3 were: 0.249, 0.749, 0.352 and 0.141, with the average EC_{20} being 0.373 mg/mL (Figure 2.14). Linear poly(FTC) S5 also caused cytotoxicity in both the MTT and LDH assays, the EC_{20} values for the MTT assay were 0.107, 0.101, 0.109, 0.102 and the average EC_{20} was 0.105 mg/mL (Figure 2.16). The EC_{20} values for the LDH assay were: 0.091, 0.104, 0.111 and 0.109, with the average EC_{20} values being 0.104 mg/mL (Figure 2.16). Due to toxicity at the concentrations tested, 80 μ g/mL was taken forward for all the linear poly(FTC) fragments except, linear poly(FTC) S3 in which 60 μ g/mL was used.

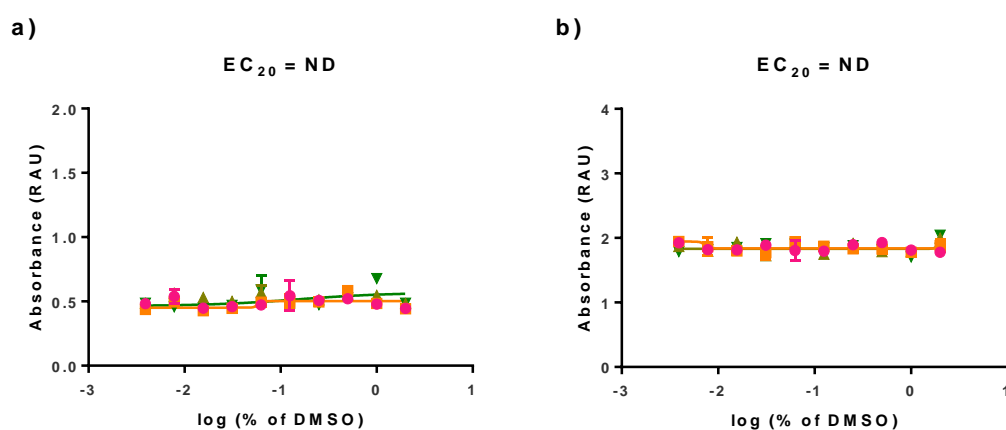


Figure 2.10: Cytotoxicity assessment of DMSO vehicle control in THP-1 cells following 24 hours exposure a) MTT, b) LDH. Data displayed n=3 technical replicates mean (\pm Standard Deviation) and n=4 experimental replicates, each displayed in a different colour. EC_{20} values calculated using EC anything calculator from EC_{50} values and the Hill Slope using GraphPad Prism software 9.3.1, not determined (ND) is used to describe values that were unable to be computed due to incomplete cytotoxicity curves.

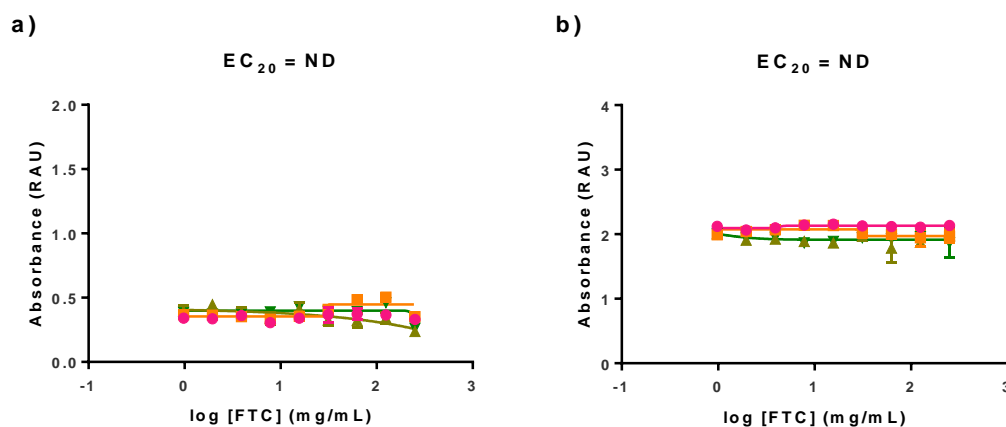


Figure 2.11: Cytotoxicity assessment of FTC in THP-1 cells following 24 hours exposure a) MTT, b) LDH. Data displayed n=3 technical replicates mean (\pm Standard Deviation) and n=4 experimental replicates, each displayed in a different colour. EC_{20} values calculated using EC anything calculator from EC_{50} values and the Hill Slope using GraphPad Prism software 9.3.1, not determined (ND) is used to describe values that were unable to be computed due to incomplete cytotoxicity curves.

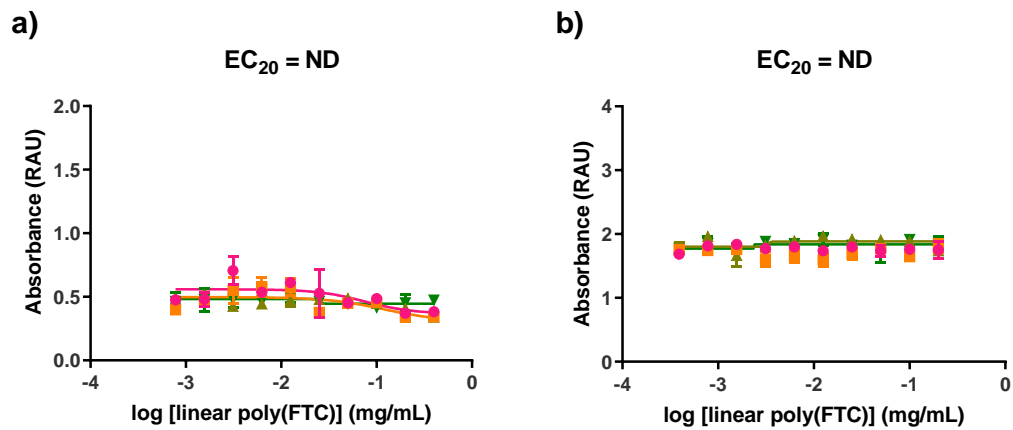


Figure 2.12: Cytotoxicity assessment of linear poly(FTC) in THP-1 cells following 24 hours exposure a) MTT, b) LDH. Data displayed n=3 technical replicates mean (\pm Standard Deviation) and n=4 experimental replicates, each displayed in a different colour. EC_{20} values calculated using EC anything calculator from EC_{50} values and the Hill Slope using GraphPad Prism software 9.3.1, not determined (ND) is used to describe values that were unable to be computed due to incomplete cytotoxicity curves.

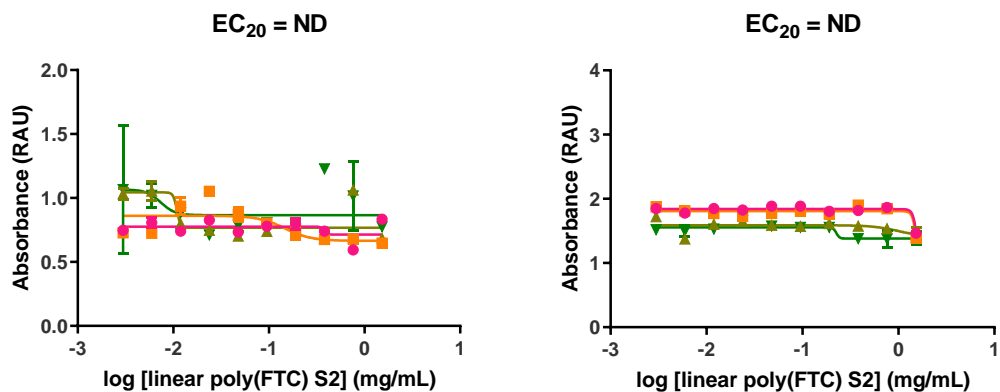


Figure 2.13: Cytotoxicity assessment of linear poly(FTC) S2 in THP-1 cells following 24 hours exposure a) MTT, b) LDH. Data displayed n=3 technical replicates mean (\pm Standard

Deviation) and n=4 experimental replicates, each displayed in a different colour. EC₂₀ values calculated using EC anything calculator from EC₅₀ values and the Hill Slope using GraphPad Prism software 9.3.1, not determined (ND) is used to describe values that were unable to be computed due to incomplete cytotoxicity curves.

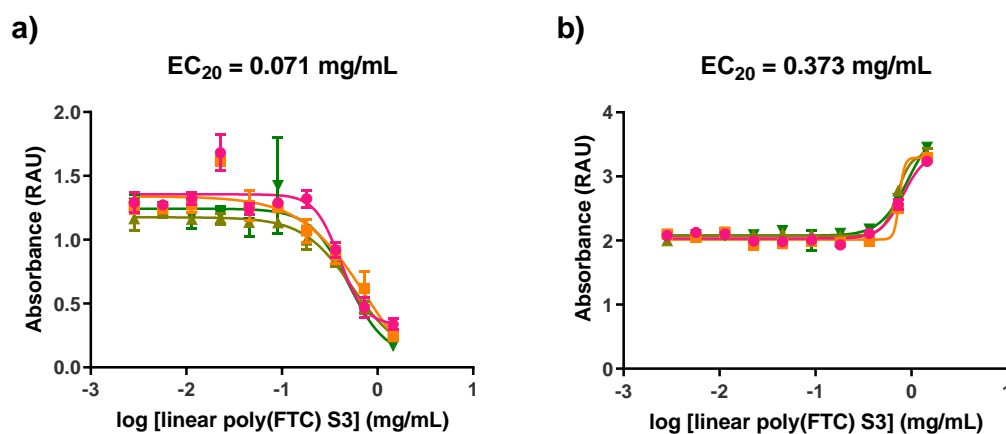


Figure 2.14: Cytotoxicity assessment of linear poly(FTC) S3 in THP-1 cells following 24 hours exposure a) MTT, b) LDH. Data displayed n=3 technical replicates mean (\pm Standard Deviation) and n=4 experimental replicates, each displayed in a different colour. EC₂₀ values calculated using EC anything calculator from EC₅₀ values and the Hill Slope using GraphPad Prism software 9.3.1, not determined (ND) is used to describe values that were unable to be computed due to incomplete cytotoxicity curves.

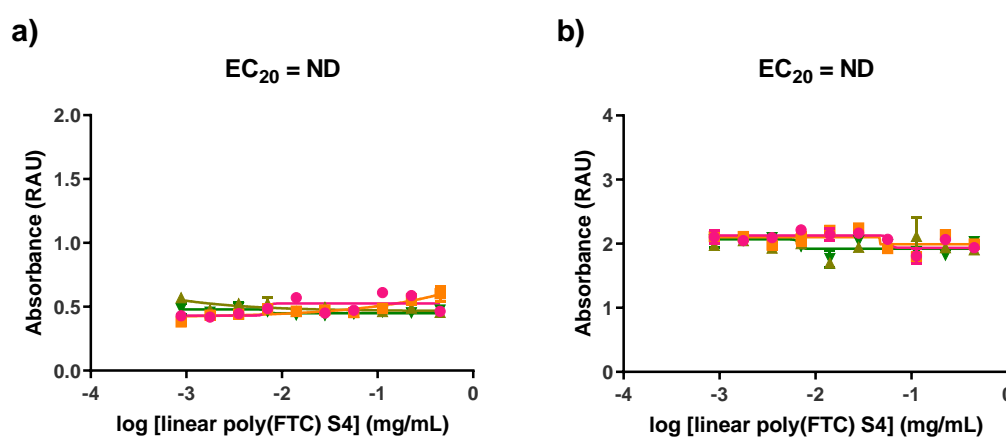


Figure 2.15: Cytotoxicity assessment of linear poly(FTC) S4 in THP-1 cells following 24 hours exposure a) MTT, b) LDH. Data displayed n=3 technical replicates mean (\pm Standard Deviation) and n=4 experimental replicates, each displayed in a different colour. EC₂₀ values

calculated using EC anything calculator from EC₅₀ values and the Hill Slope using GraphPad Prism software 9.3.1, not determined (ND) is used to describe values that were unable to be computed due to incomplete cytotoxicity curves.

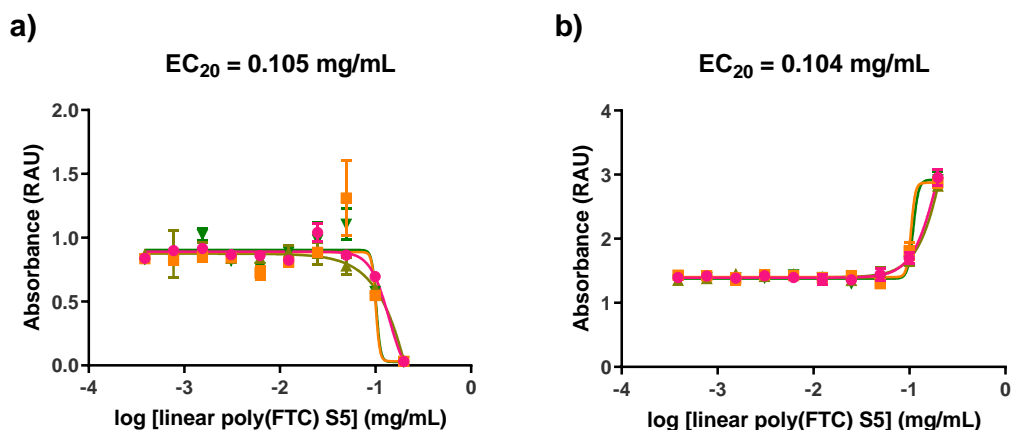


Figure 2.16: Cytotoxicity assessment of linear poly(FTC) S5 in THP-1 cells following 24 hours exposure a) MTT, b) LDH. Data displayed n=3 technical replicates mean (\pm Standard Deviation) and n=4 experimental replicates, each displayed in a different colour. EC₂₀ values calculated using EC anything calculator from EC₅₀ values and the Hill Slope using GraphPad Prism software 9.3.1, not determined (ND) is used to describe values that were unable to be computed due to incomplete cytotoxicity curves.

Due to toxicity with two of the fragments in the concentration range tested, 80 μ g/mL was taken forward for all the linear poly(FTC) fragments except, linear poly(FTC) S3 in which 60 μ g/mL was used.

2.3.3 Leukocyte Proliferation assessment of POP material linear poly(FTC)

Leukocyte proliferation was assessed in order to explore the ability of FTC or linear poly(FTC) to screen for potential immune activation. All three concentrations of PHA-M showed a statistically significant ($p < 0.0001$) higher percentage of the untreated control and therefore proliferation when compared to the untreated cells (Figure 2.17). None of the tested conditions alone (linear poly(FTC), FTC or the vehicle control) caused any significant proliferation (Figure 2.17).

When each sample was spiked with PHA-M at a final concentration of 5 μ g/mL there was no significantly higher proliferation when compared to the PHA-M 5 μ g/mL control alone (Figure 2.18). However, in donor one there was significantly lower % of the untreated control, with

25% proliferation inhibition for linear poly(FTC) 80 $\mu\text{g}/\text{mL}$ ($p < 0.001$), and 15.9% and 18.4% for FTC 1.8 $\mu\text{g}/\text{mL}$ ($p < 0.05$) and FTC 18 $\mu\text{g}/\text{mL}$ ($p < 0.01$) respectively (Figure 2.18).

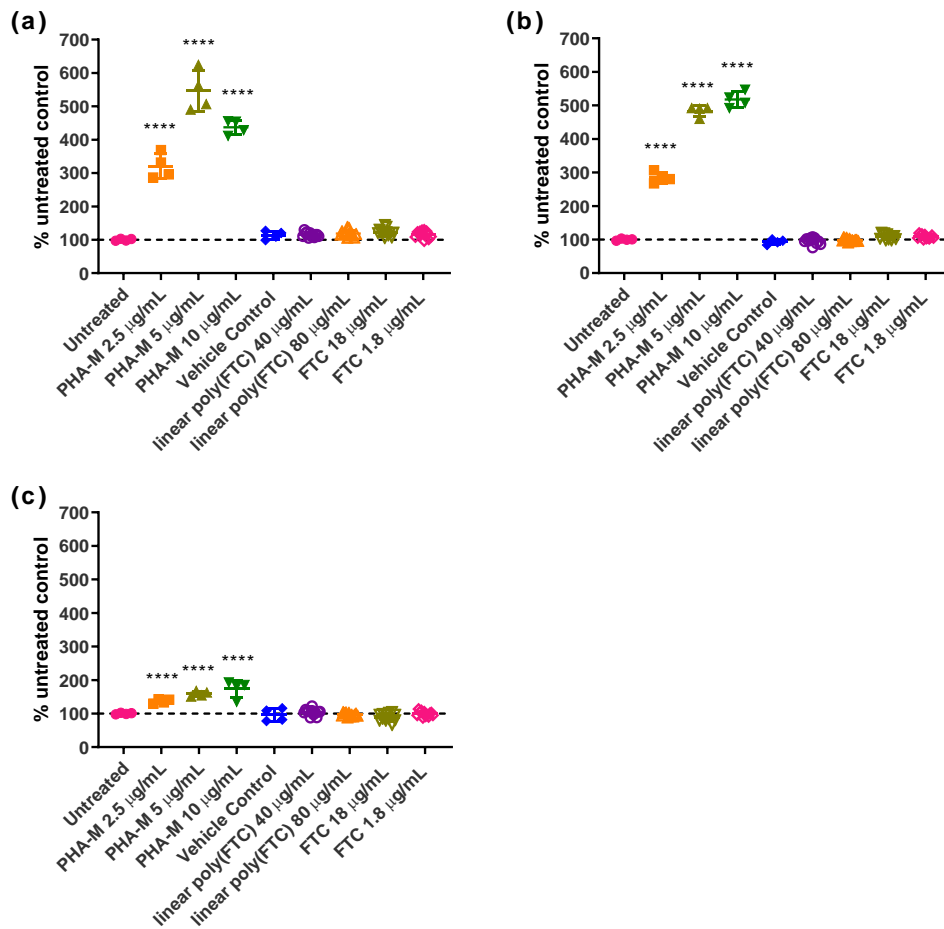


Figure 2.17: Leukocyte proliferation. ANOVA statistical analysis carried out between the untreated and all other conditions, $p < 0.0001 = ****$, $p < 0.001 = ***$, $p < 0.01 = **$ and $p < 0.05 = *$. Data displayed as $n=4$ for Untreated, each PHA-M concentration and vehicle control and $n=12$ for each of the linear poly(FTC)/FTC alone and their spiked samples, mean (\pm standard deviation). Dashed line indicates 100% untreated control.

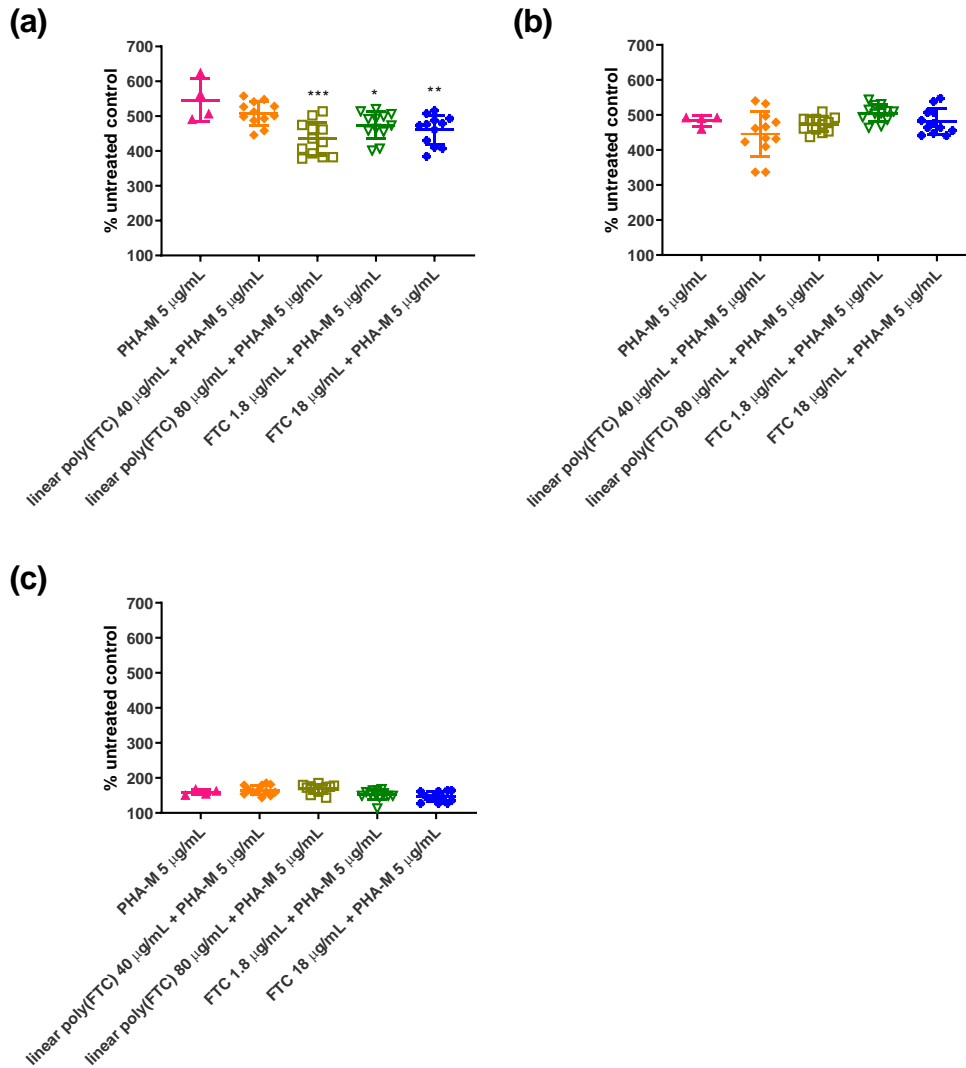


Figure 2.18: Leukocyte proliferation. Each concentration of POP material linear poly(FTC) or FTC was spiked with PHA-M at a final concentration of 5 $\mu\text{g/mL}$. Data displayed as $n=4$ for PHA-M alone and $n=12$ for each of the linear poly(FTC)/FTC spiked samples, mean (\pm standard deviation). ANOVA statistical analysis carried out between PHA-M 5 $\mu\text{g/mL}$ and all the other spiked samples. $p<0.0001 = ****$, $p<0.001 = ***$, $p<0.01 = **$ and $p<0.05 = *$.

Leukocyte proliferation was unaffected by either FTC or linear poly(FTC) at the concentrations tested in donors 2 and 3, however in donor 1 there were some significant alterations in the PHA spiked samples of FTC and linear poly(FTC).

2.3.4 Complement activation induced by POP material linear poly(FTC)

Complement assessment using the surrogate iC3b was used to determine the ability of FTC and linear poly(FTC) to interact with the complement system. Figure 2.19 and 2.20 display the standard curves used to calculate the iC3b concentrations from each sample. When the

average concentration of iC3b for each of the five donors is combined, CVF and Doxil show significantly higher iC3b concentrations ($p < 0.0001$ and $p < 0.001$ respectively) (Figure 2.21). When compared individually CVF caused a significantly higher iC3b concentration in all five donors, with between 649% and 1842% higher iC3b concentrations ($p < 0.0001$) when compared to the untreated (Figure 2.22). Doxil however caused varying responses, with donor one and two having significantly higher iC3b concentration compared to the untreated, 1567% and 1275% respectively ($p < 0.0001$) (Figure 2.22a-b). Whereas donors four and five had a significantly higher iC3b concentration of 281% and 154% respectively ($p < 0.01$) and donor three having insignificant responses, all when compared to the untreated (Figure 2.22c-e). The POP material linear poly(FTC) caused a significantly higher iC3b concentration in donors two, four and five. Donor two showed statically greater significant difference at 80 $\mu\text{g/mL}$ ($p < 0.01$) than at 40 $\mu\text{g/mL}$ ($p < 0.05$) with 274% and 183% higher iC3b concentrations respectively (Figure 2.22b). Donor four showed similar statistical significance for both 40 ($p < 0.05$) and 80 $\mu\text{g/mL}$ ($p < 0.05$) of 213% and 229% greater iC3b (Figure 2.22d). Donor five however showed a concentration dependent significance, 40 $\mu\text{g/mL}$ caused a 127% higher ($p < 0.01$) and 80 $\mu\text{g/mL}$ a 309% higher iC3b concentration ($p < 0.0001$) (Figure 2.22e).

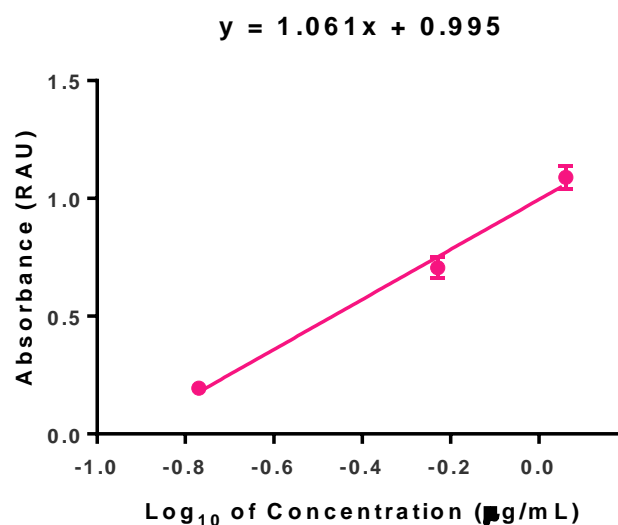


Figure 2.19: Standard curve for donors 1-3, created using the standards provided in the iC3b EIA kit. Data displayed as average of $n=2$, error bars represent mean (\pm standard deviation). Correlation coefficient = 0.992.

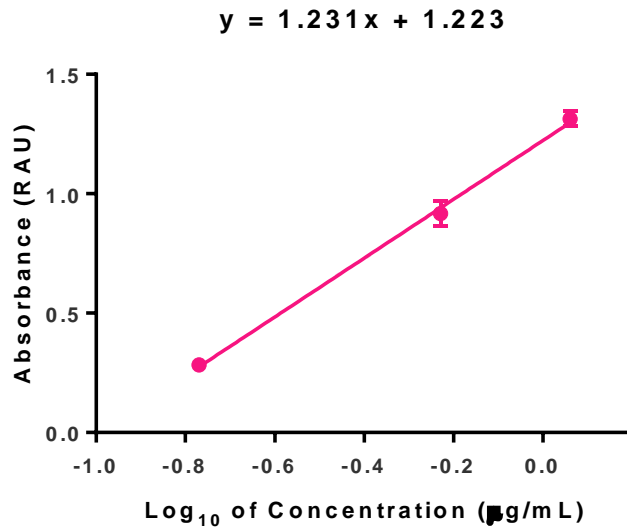


Figure 2.20: Standard curve for donors 4-5, created using the standards provided in the iC3b EIA kit. Data displayed as average of n=2, error bars represent (\pm standard deviation). Correlation coefficient = 0.9984.

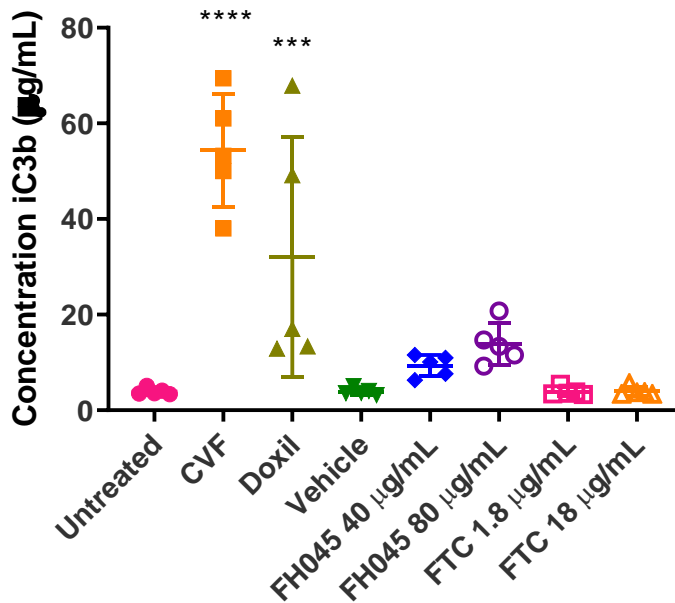


Figure 2.21: Concentration of iC3b determined for the five donors. Data displayed as n=5, mean (\pm standard deviation). ANOVA statistical analysis carried out between the untreated and all other conditions, $p < 0.0001 = ****$, $p < 0.001 = ***$, $p < 0.01 = **$ and $p < 0.05 = *$.

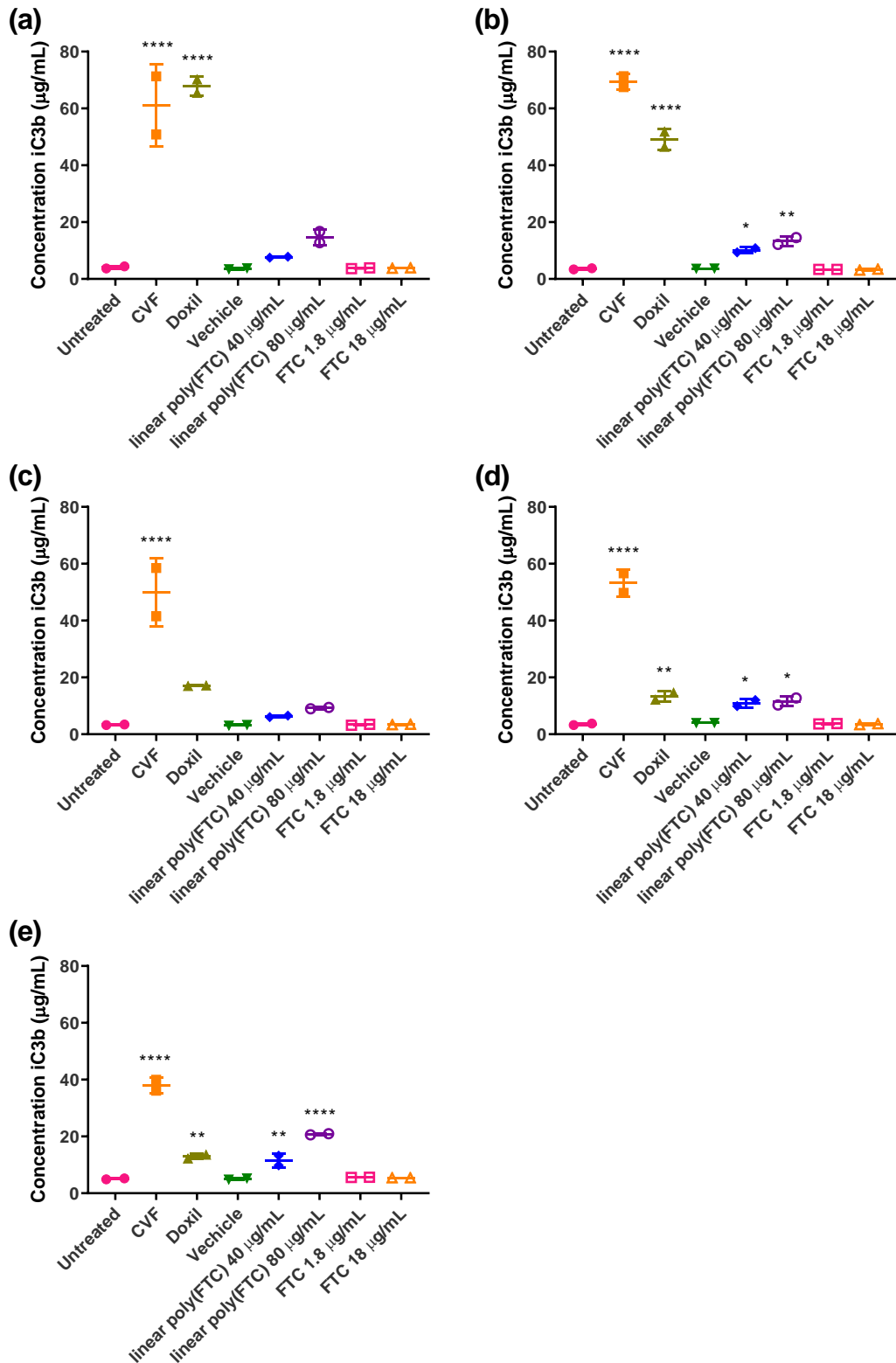


Figure 2.22: Concentration of iC3b determined for (a) Donor 1, (b) Donor 2, (c) Donor 3, (d), Donor 4, (e) Donor 5. Data displayed as n=2 experimental replicates, mean (\pm standard deviation). ANOVA statistical analysis carried out between the untreated and all other conditions, $p < 0.0001 = ****$, $p < 0.001 = ***$, $p < 0.01 = **$ and $p < 0.05 = *$.

Doxil showed interindividual variation in complement activation, linear poly(FTC) caused a concentration dependent increase in complement, as measured by iC3b levels.

2.3.5 Assessment of POP materials in whole blood using control ligand panel, whilst exploring the role of serum exosomes on cellular responses

Known PRR agonists were used to compare against the POP fragments in a whole blood assay, in order to explore whether these fragments interacted with these immune PRR. The different agonists showed responses expected in the initial screen in the whole blood assay (Figure 2.23). LPS caused a significantly higher production of IL-1 β , IL-6, IL-8, IL-10, IL-18, TNF- α ($p < 0.0001$), and IFN γ ($p < 0.01$) (Figure 2.23). PHA-M caused a significantly higher production of IL-6, IL-8, IL-10, IFN- γ ($p < 0.0001$), and TNF- α ($p < 0.05$). ODN 2006 19.2 $\mu\text{g}/\text{mL}$ caused a significantly higher production of IL-6 ($p < 0.0001$) and IFN- α ($p < 0.05$). ODN 2006 38.5 $\mu\text{g}/\text{mL}$ caused a significantly higher production of IL-6, IL-8 ($p < 0.0001$), IL-18 ($p < 0.001$), and IFN- α ($p < 0.05$). 2'3'- cGAMP 10 $\mu\text{g}/\text{mL}$ caused a significantly higher he production of IL-6 ($p < 0.0001$). Poly(dG:dC)/LyoVec™ 2.5 $\mu\text{g}/\text{mL}$ caused a significantly higher production of IL-18 ($p < 0.0001$) and 5 $\mu\text{g}/\text{mL}$ caused significantly higher IL-8 ($p < 0.05$). HSV-60/LyoVec™ 2.5 $\mu\text{g}/\text{mL}$ caused a significantly higher production of IL-18 ($p < 0.01$) and 5 $\mu\text{g}/\text{mL}$ caused significantly higher IFN- α , IFN- β ($p < 0.0001$), and IL-18 ($p < 0.001$).

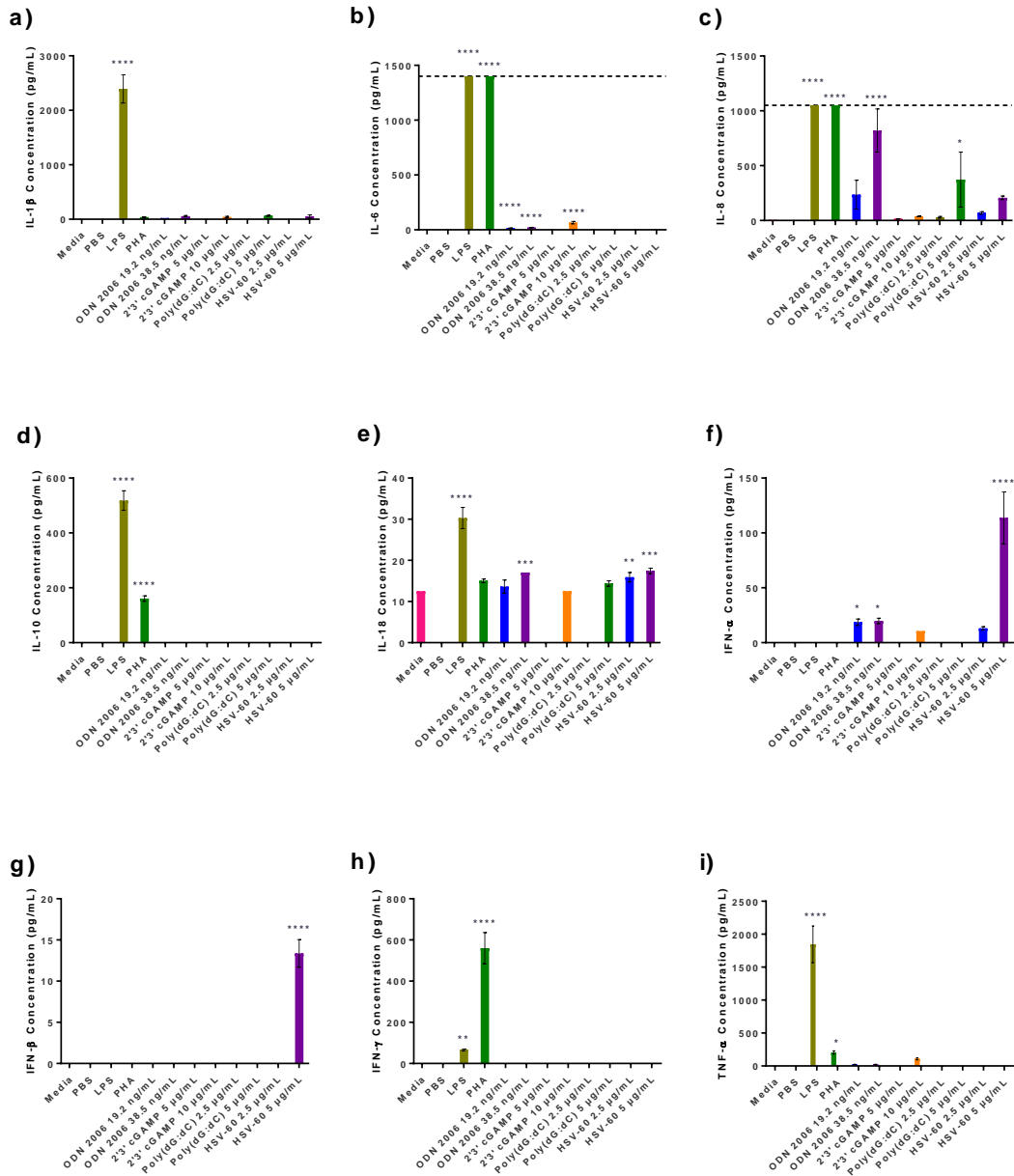


Figure 2.23: Whole blood cytokine concentrations of supernatants treated with control agonists. a) IL-1β, b) IL-6, c) IL-8, d) IL-10, e) IL-18, f) IFN-α, g) IFN-β, h) IFN-γ and i) TNF-α. Data displayed n=3 for all conditions, mean (\pm standard deviation). Dashed lines indicate the top limit of the standard curve. ANOVA statistical analysis carried out between the untreated and all other conditions, $p < 0.0001 = ****$, $p < 0.001 = ***$, $p < 0.01 = **$ and $p < 0.05 = *$.

These known PRR agonists and POP fragments were compared in two types of whole blood, one diluted with media supplemented with normal serum, and one diluted with media supplemented with exosome depleted serum. Figure 2.24 demonstrates the difference in cytokine levels in whole blood from one donor diluted with either media supplemented with

normal serum or media supplemented with exosome-depleted serum, variable responses were seen across the cytokines and agonists with both concentrations.

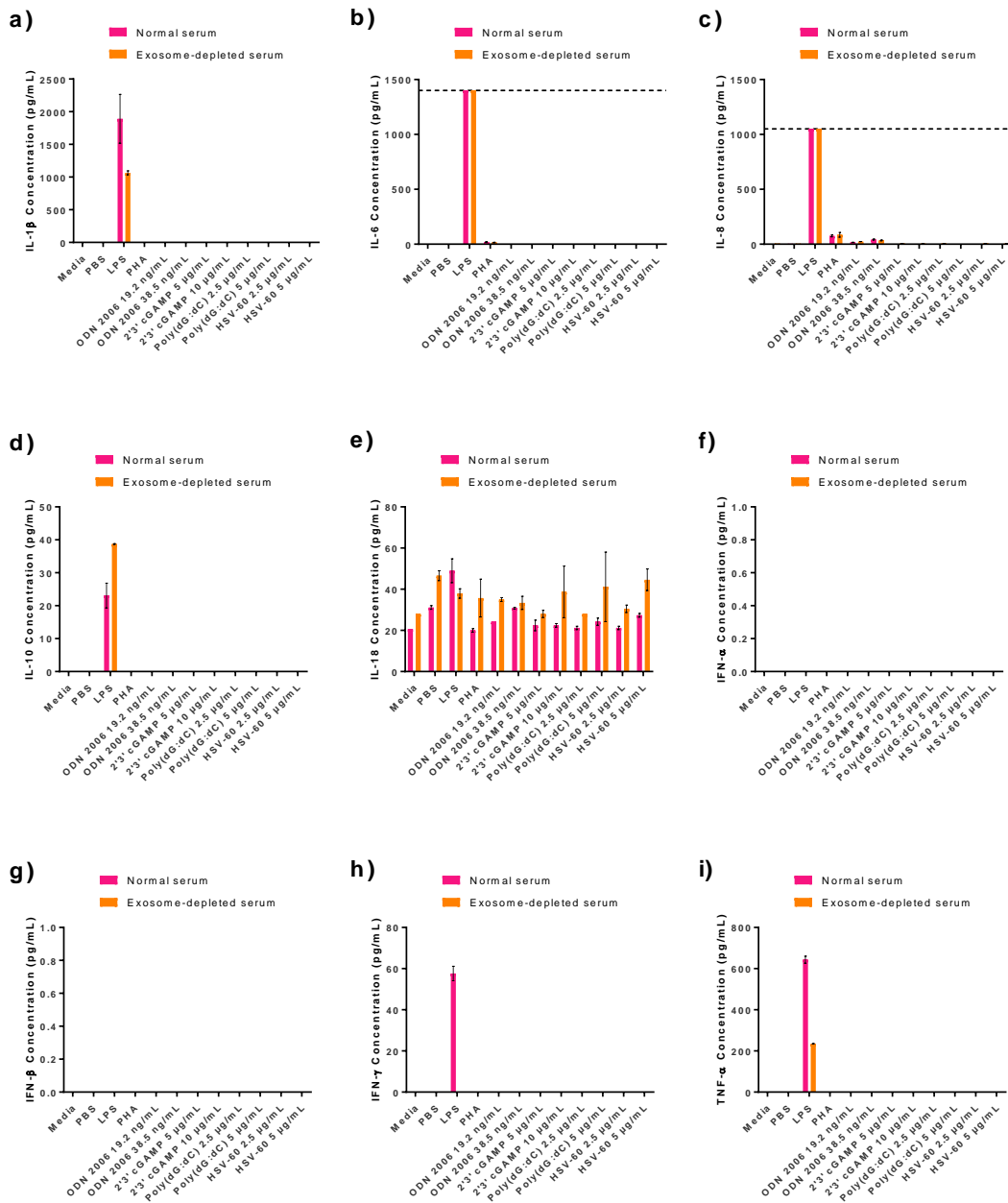


Figure 2.24: Whole blood cytokine concentrations of supernatants treated with control agonists. a) IL-1 β , b) IL-6, c) IL-8, d) IL-10, e) IL-18, f) IFN- α , g) IFN- β , h) IFN- γ and i) TNF- α . Data displayed as n=2, mean (\pm standard deviation). Dashed lines indicate the top of the top limit of the standard curve.

Figures 2.25 – 2.34 shows the secretion of cytokines from donor whole blood from six donors, diluted with either media supplemented with normal serum or media supplemented with exosome-depleted serum. Again, variable responses have been seen across the agonists and

linear poly(FTC) breakdown fragments for each donor and the agonist responses have been summarised in the heatmap Figure 2.35. Cytokine secretion differs between the blood used for donors 1-3 and 4-6. The linear poly(FTC) S3 fragment material gave some elevations in cytokine secretion in the whole blood assay. These differences were typically seen in donors 1-3. Higher secretion of IL-1 β from the linear poly(FTC) S3 treated group was seen when compared to the untreated, which showed undetectable levels (Below the limit of detection, whereas in donor 4-6 IL-1 β levels were undetectable for all the linear poly(FTC) breakdown fragment materials (Figure 2.25). Some elevations were seen in IL-1RA in donors 4-6 following treatment with linear poly(FTC) S3 (Figure 2.26). linear poly(FTC) S3 also caused IL-6 levels above the limit of detection for all donors when the untreated was either below the limit of detection or less than half of the top limit of detection (Figure 2.27). In donors 4-6 however, all the linear poly(FTC) fragment materials were below the limit of detection for IL-6 along with the untreated samples (Figure 2.27). In donors 1-3 the levels of IL-8 were much lower for linear poly(FTC) S5 and Some linear poly(FTC) samples, than all the other linear poly(FTC) breakdown fragment materials and the untreated (Figure 2.28). Whereas in donors 4-6 there were either undetectable or very low levels of IL-8, with some elevations seen with the linear poly(FTC) S3 treated samples (Figure 2.28). linear poly(FTC) S3 donors 1-3 caused a slightly higher IL-10 secretion in some donors, but not all (Figure 2.29). IL-18 in donors 1-3 was very slightly higher compared to the untreated, when treated with linear poly(FTC) S3, but this was not seen in donors 4-6 (Figure 2.29). None of the linear poly(FTC) fragment materials caused any detectable changes in the secretion of IFN- α , IFN- β , and IFN- γ in all 6 donors (Figures 2.30 – 2.32). TNF- α secretion was slightly higher in donors 1-3, with all but the exosome depleted linear poly(FTC) S2 sample being below the limit of detection (Figure 2.33).

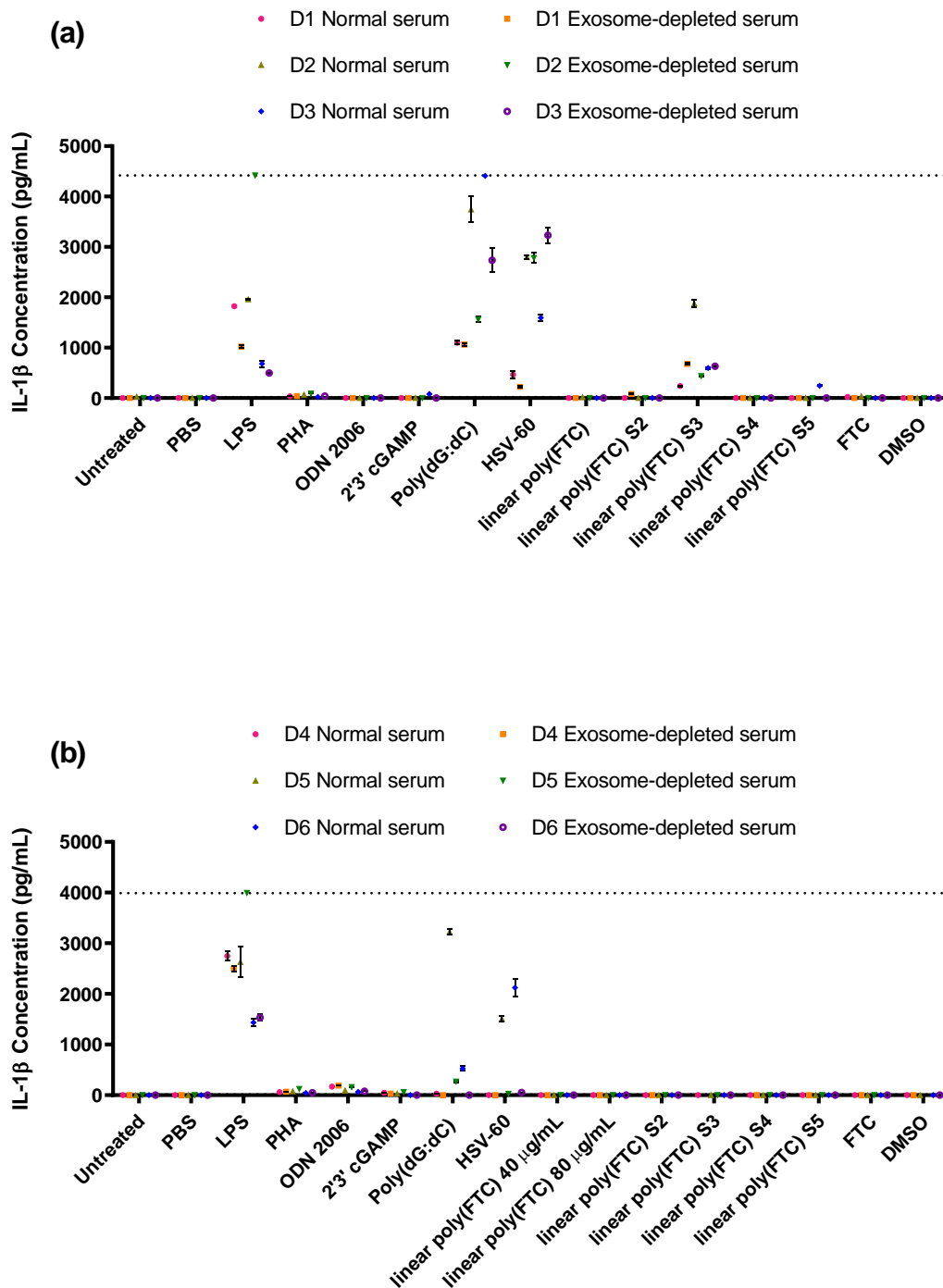


Figure 2.25: IL-1 β . (a) Donor 1-3 and (b) Donor 4-6. Values <OOR and extrapolated from below the standard curve are plotted at 0 and any samples >OOR or extrapolated from above the standard curve are plotted at the highest limit of detection. Data displayed as n=2, mean (\pm standard deviation). Dashed lines indicate the top limit of the standard curve, any points plotted on this line were above the limit of quantification.

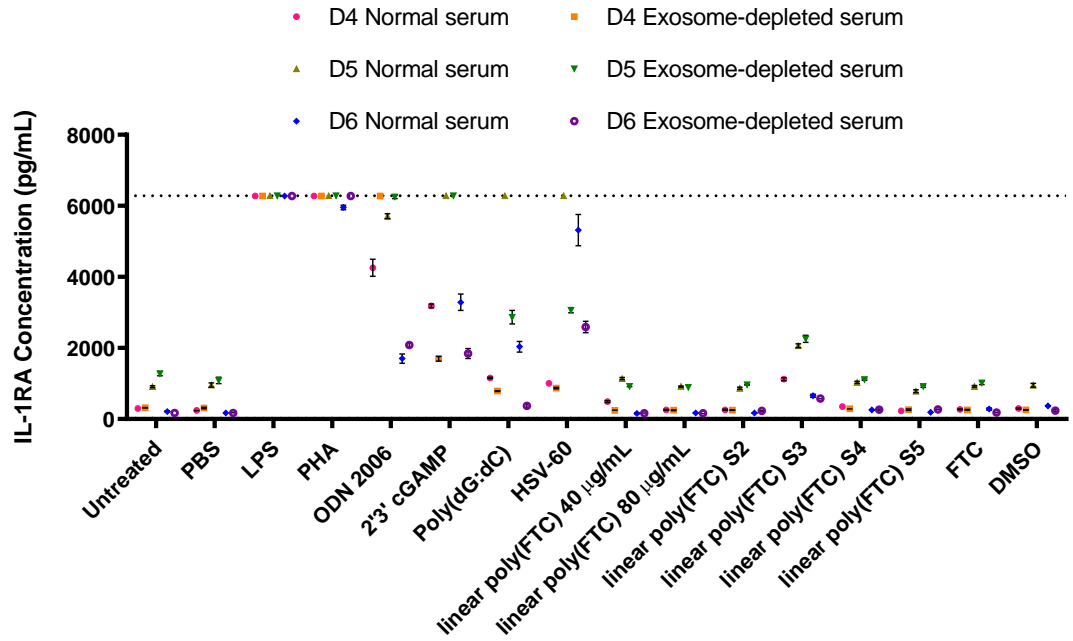


Figure 2.26: IL-1RA. Donor 4-6. Values <OOR and extrapolated from below the standard curve are plotted at 0 and any samples >OOR or extrapolated from above the standard curve are plotted at the highest limit of detection. Data displayed as n=2, mean (\pm standard deviation). Dashed line indicate the top limit of the standard curve, any points plotted on this line were above the limit of quantification.

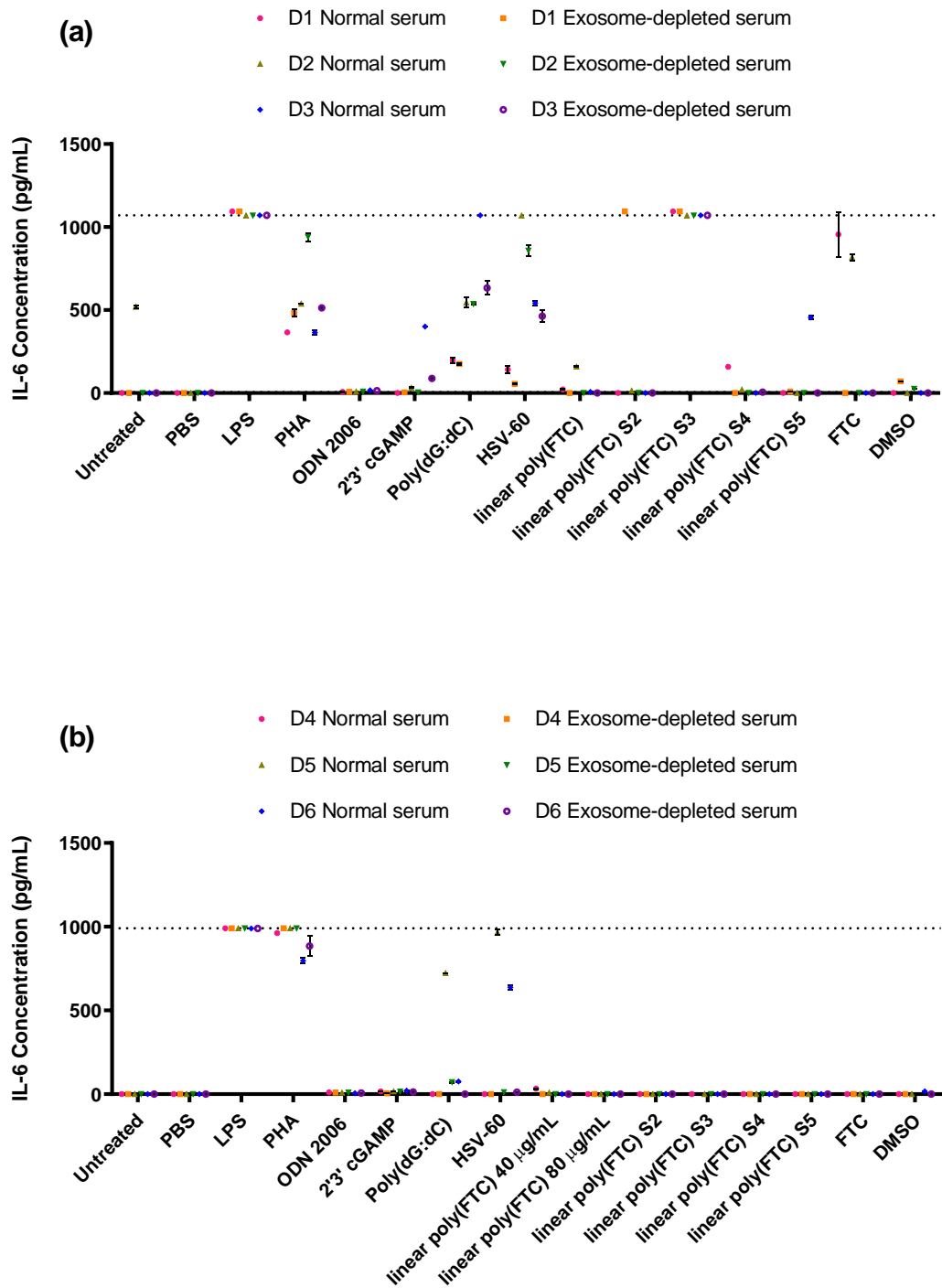


Figure 2.27: IL-6. (a) Donor 1-3 and (b) Donor 4-6. Values <OOR and extrapolated from below the standard curve are plotted at 0 and any samples >OOR or extrapolated from above the standard curve are plotted at the highest limit of detection. Data displayed as n=2, mean (\pm standard deviation). Dashed lines indicate the top limit of the standard curve, any points plotted on this line were above the limit of quantification.

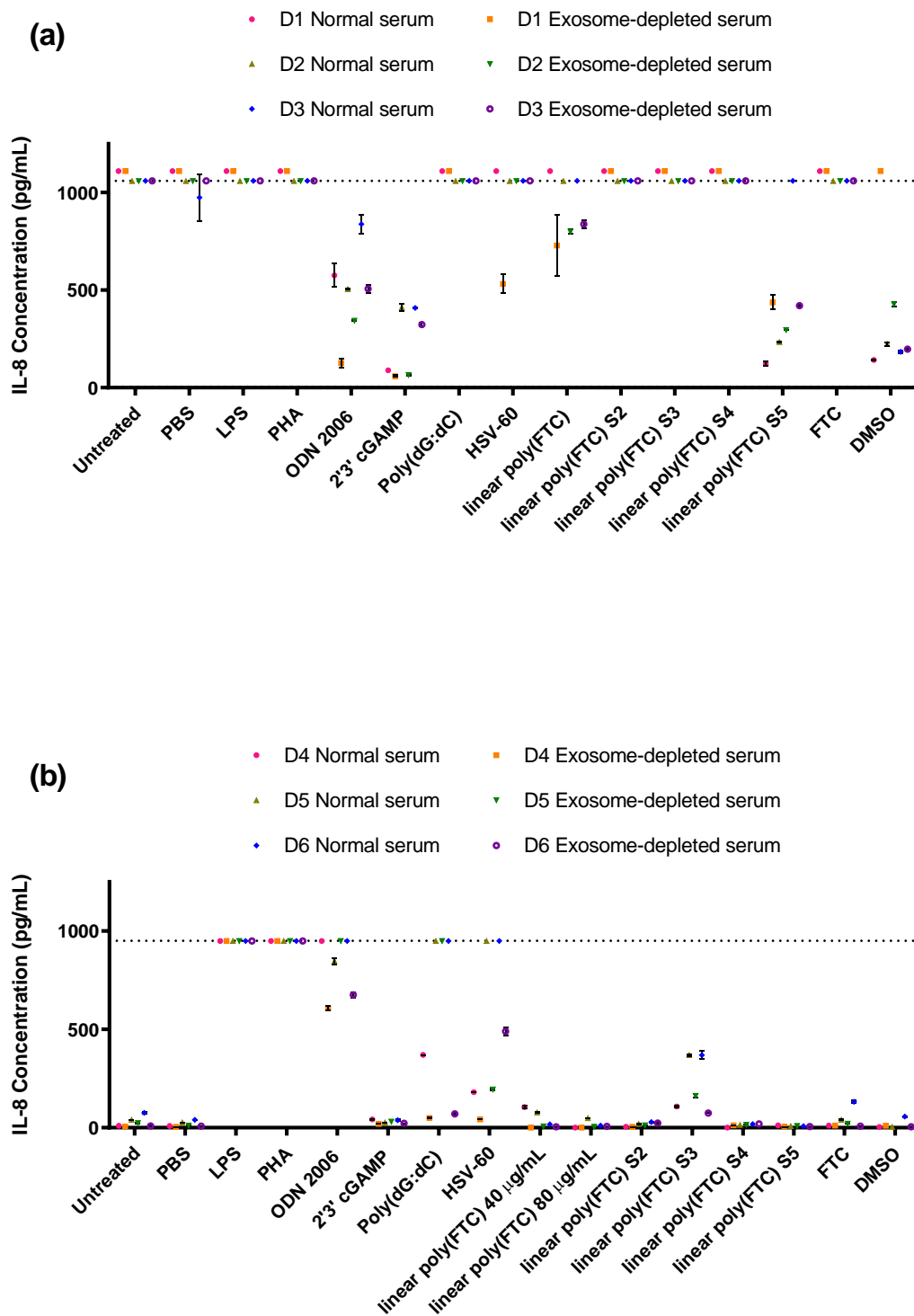


Figure 2.28: IL-8 Concentration. (a) Donor 1-3 and (b) Donor 4-6. Values <ORR and extrapolated from below the standard curve are plotted at 0 and any samples >ORR or extrapolated from above the standard curve are plotted at the highest limit of detection. Data displayed as n=2, mean (\pm standard deviation). Dashed lines indicate the top limit of the standard curve, any points plotted on this line were above the limit of quantification.

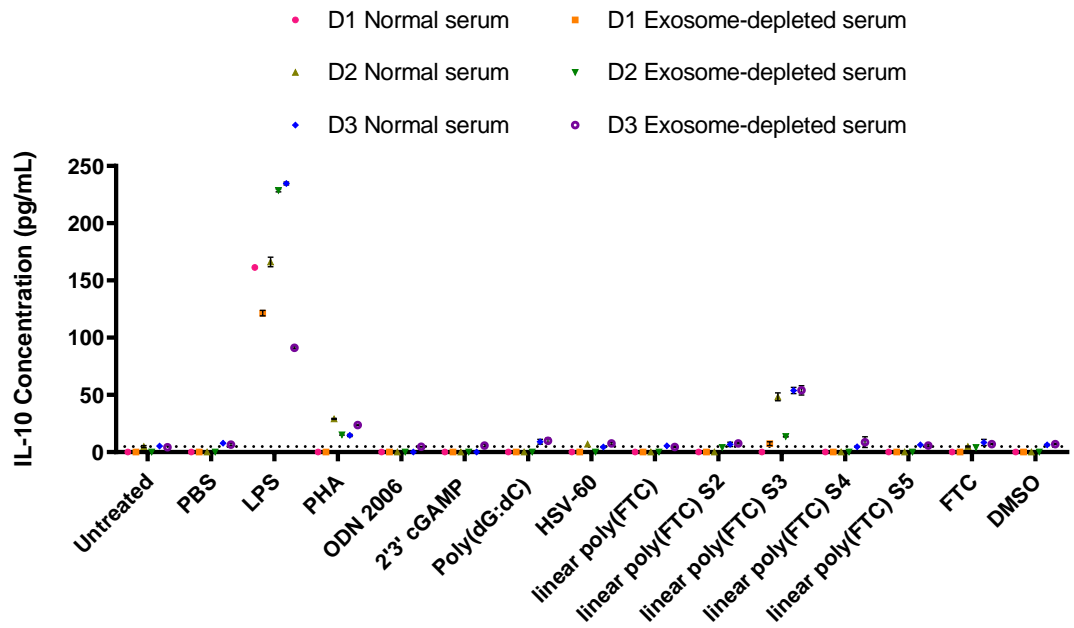


Figure 2.29: IL-10. Donor 1-3. Values <OOR and extrapolated from below the standard curve are plotted at 0 and any samples >OOR or extrapolated from above the standard curve are plotted at the highest limit of detection. Data displayed as n=2, mean (\pm standard deviation). Dashed line indicates the lower limit of the standard curve, all points below the line were below the limit of quantification.

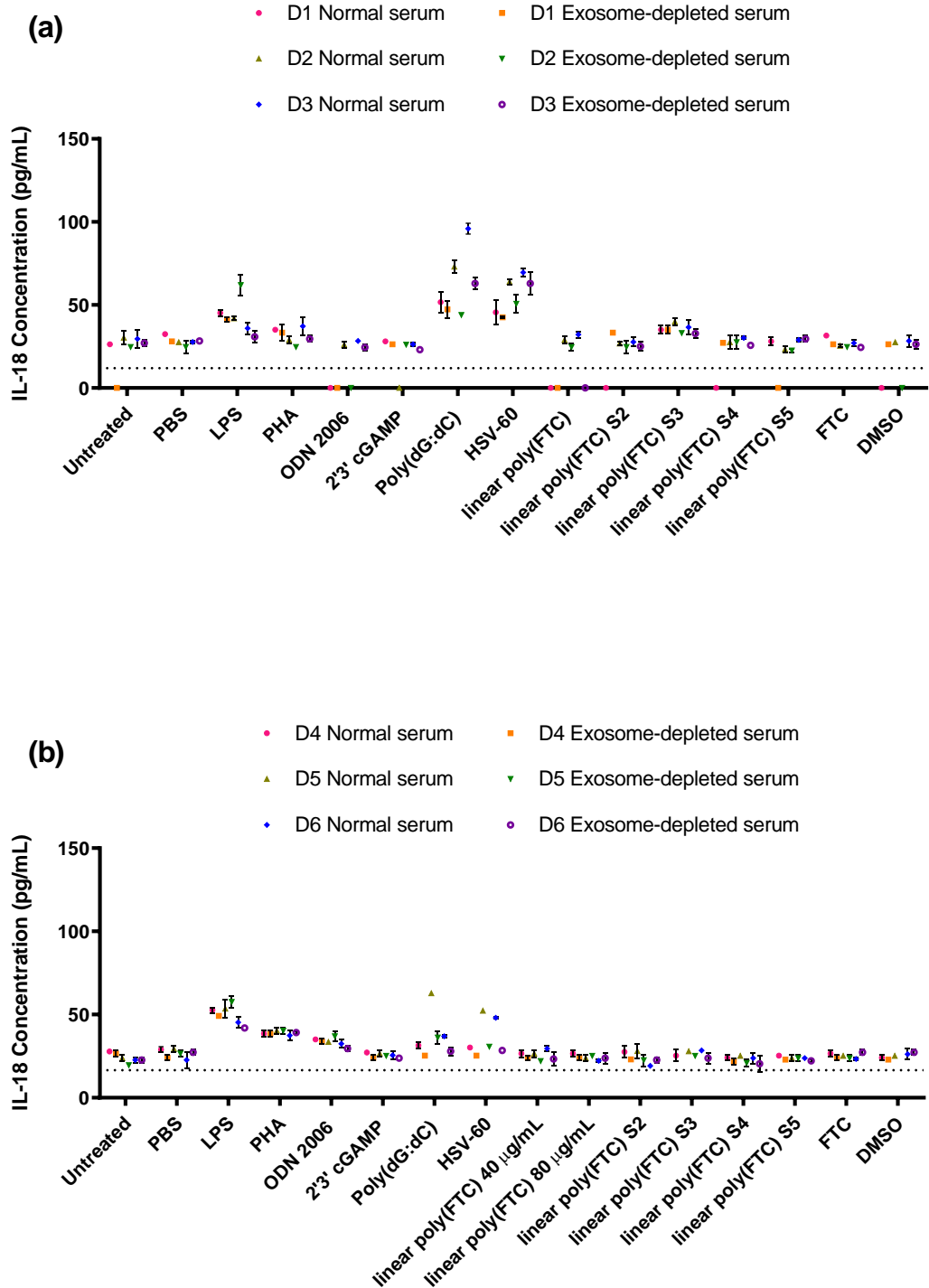


Figure 2.30: IL-18. (a) Donor 1-3 and (b) Donor 4-6. Values <OOR and extrapolated from below the standard curve are plotted at 0 and any samples >OOR or extrapolated from above the standard curve are plotted at the highest limit of detection. Data displayed as n=2, mean (\pm standard deviation). Dashed lines indicates the lower limit of the standard curve, all points below the line were below the limit of quantification.

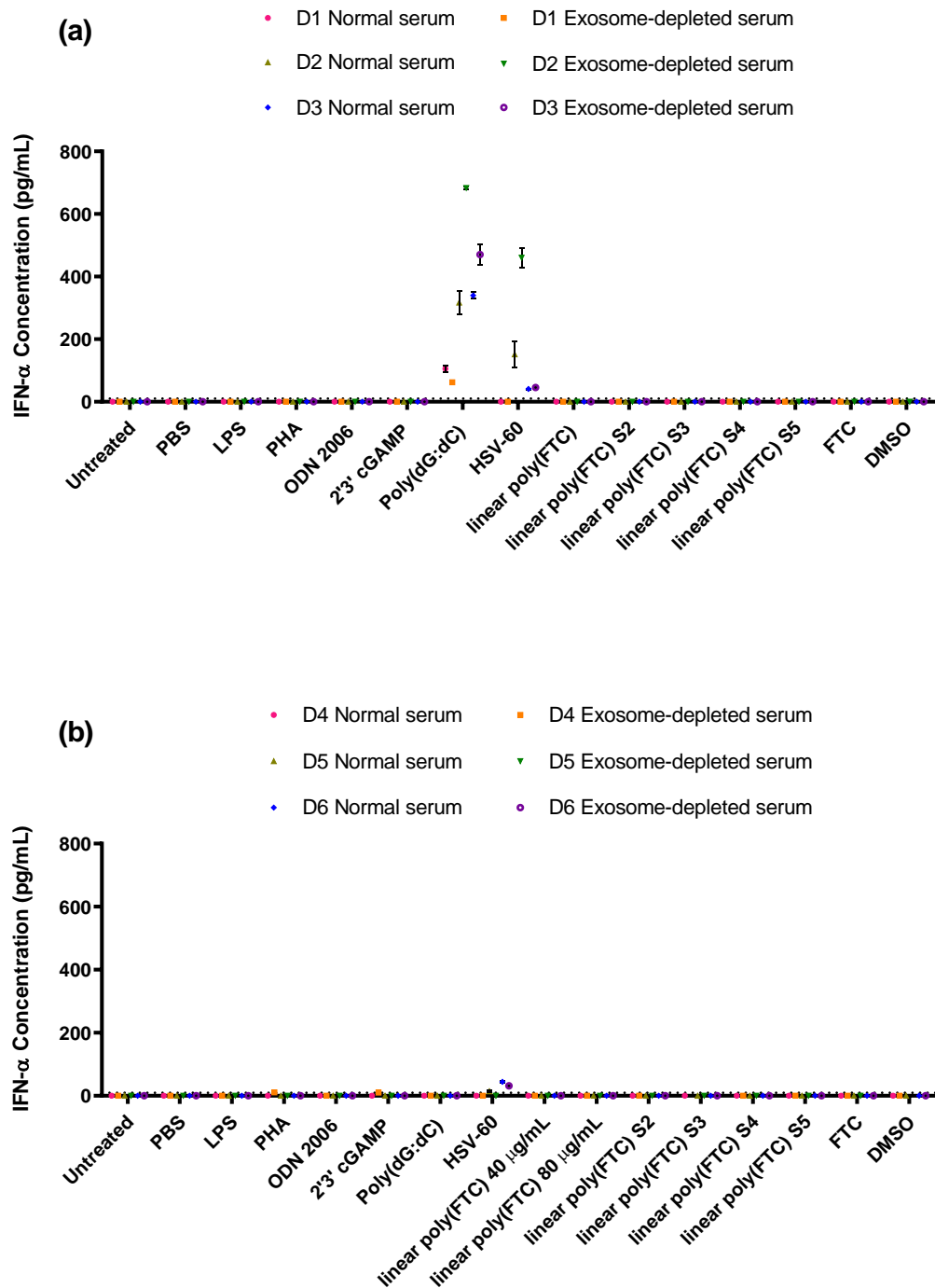


Figure 2.31: IFN- α . (a) Donor 1-3 and (b) Donor 4-6. Values <OOR and extrapolated from below the standard curve are plotted at 0 and any samples >OOR or extrapolated from above the standard curve are plotted at the highest limit of detection. Data displayed as n=2, mean (\pm standard deviation). Dashed lines indicates the lower limit of the standard curve, all points below the line were below the limit of quantification.

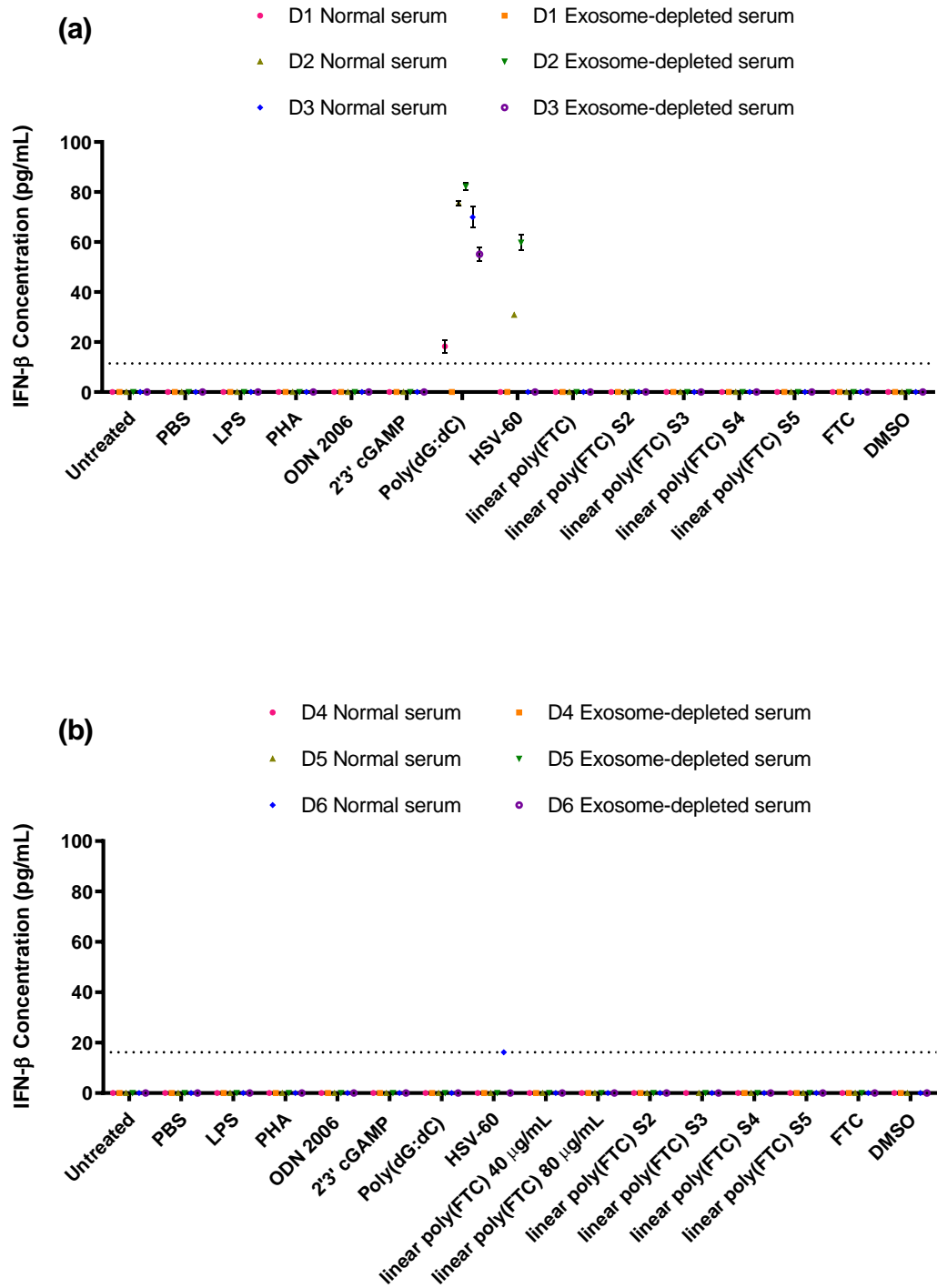


Figure 2.32: IFN- β . (a) Donor 1-3 and (b) Donor 4-6. Values <OOR and extrapolated from below the standard curve are plotted at 0 and any samples >OOR or extrapolated from above the standard curve are plotted at the highest limit of detection. Data displayed as n=2, mean (\pm standard deviation). Dashed lines indicates the lower limit of the standard curve, all points below the line were below the limit of quantification.

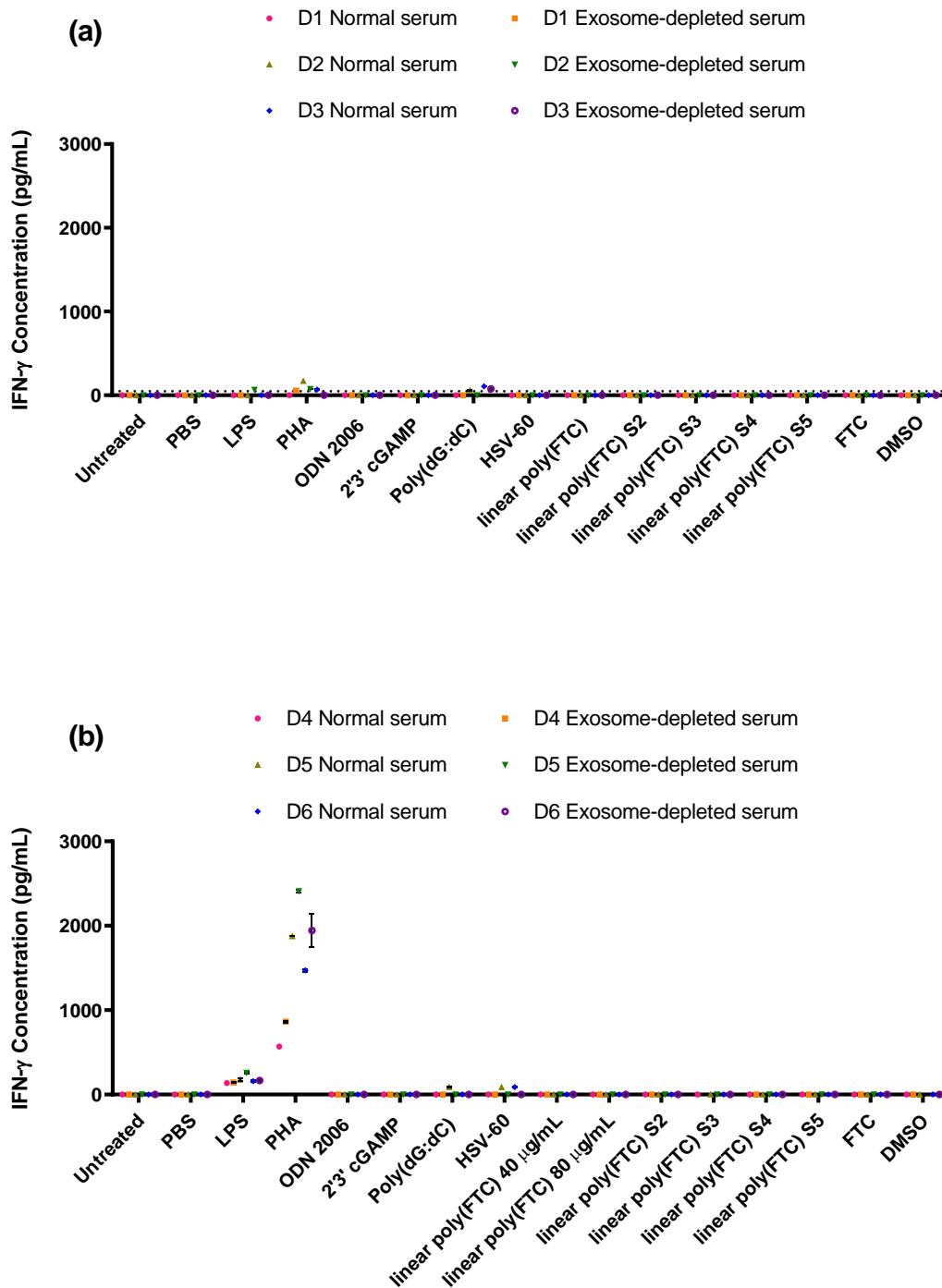


Figure 2.33: IFN- γ . (a) Donor 1-3 and (b) Donor 4-6. Values <OOR and extrapolated from below the standard curve are plotted at 0 and any samples >OOR or extrapolated from above the standard curve are plotted at the highest limit of detection. Data displayed as n=2, mean (\pm standard deviation). Dashed lines indicates the lower limit of the standard curve, all points below the line were below the limit of quantification.

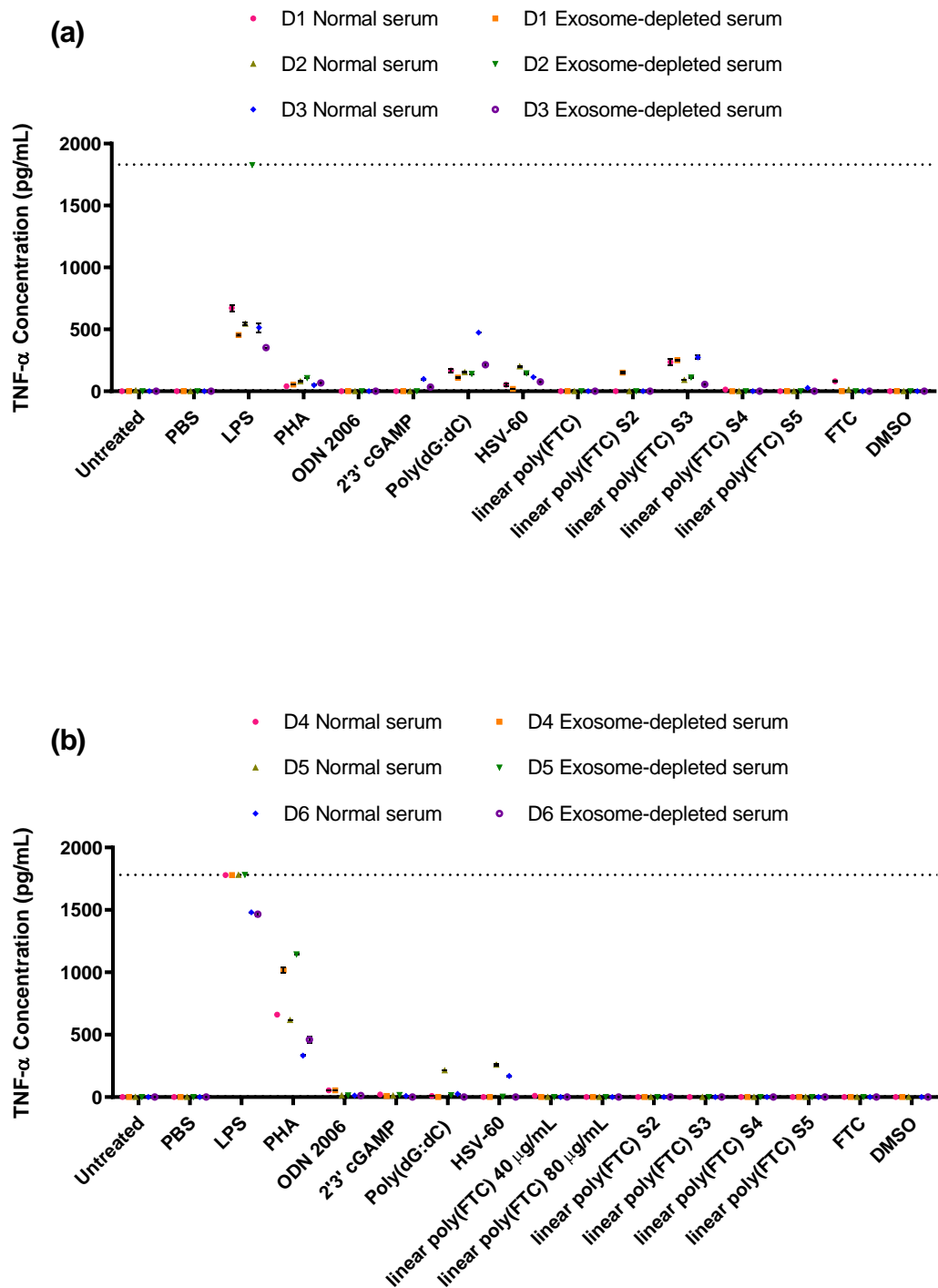


Figure 2.34: TNF- α . (a) Donor 1-3 and (b) Donor 4-6. Values <OOR and extrapolated from below the standard curve are plotted at 0 and any samples >OOR or extrapolated from above the standard curve are plotted at the highest limit of detection. Data displayed as n=2, mean (\pm standard deviation). Dashed lines indicate the top limit of the standard curve, any points plotted on this line were above the limit of quantification.

In donors 1-3 Higher levels were seen for IL-1 β , IL-6, IL-10 and TNF- α , whereas lower levels were seen for IL-8.

PHA-M led to a 32%, 53%, and 59% higher secretion of IL-1 β , INF- γ and TNF- α respectively when serum-derived exosomes are depleted. ODN 2006 led to a 30% and 25% higher secretion of IL-1 β and IL-1RA respectively when serum-derived exosomes are depleted. 2'3'cGAMP caused a 73%, 54%, and 42% lower secretion of IL-6, IL-8, and TNF- α respectively when serum-derived exosomes are depleted. Poly(dGidC)/LyoVec™ causes a 35%, 58%, 32%, and 27% lower secretion of IL-1 β , IL-1RA, IL-6, and TNF- α respectively when serum-derived exosomes are depleted and a 69% higher secretion of IFN- α . HSV-60/LyoVec™ causes a 48%, 57%, and 60% lower secretion of IL-1RA, IL-6, and TNF- α when serum-derived exosomes are depleted and a 63%, 34%, 185%, and 154% higher secretion of IL-8, IFN- α and IFN- β respectively.

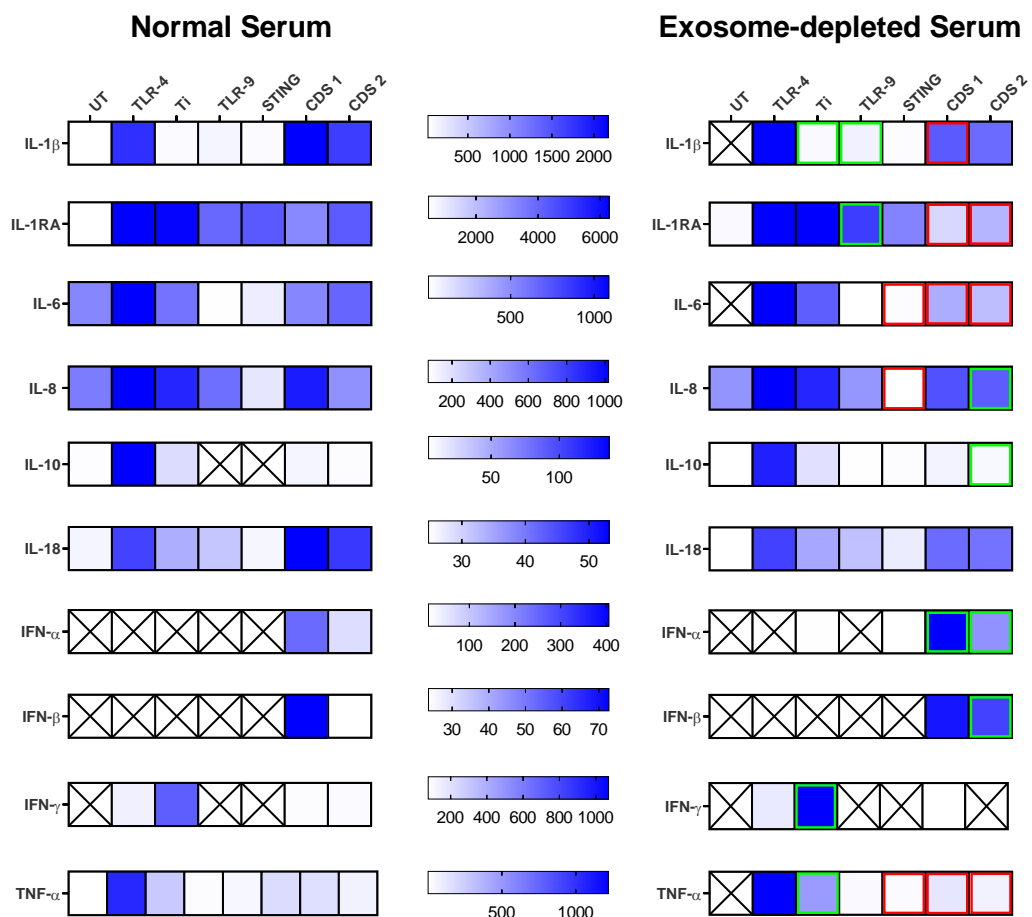


Figure 2.35: Heat map summary of the average concentration of cytokines in the supernatants of whole blood from seven Donors treated with the six agonists: LPS acts on

TLR-4, PHA-M acts on Ti, ODN 2006 acts on TLR-9, 2'3' cGAMP acts on STING, poly(dG:dC)/LyoVec™ acts on CDS, denoted as CDS 1 and HSV-60/LyoVec™ is denoted as CDS 2. All data expressed as an average concentration of the seven donors in pg/mL. Donors that were under the limit of detection were excluded from that cytokine analysis and the average taken from the remaining donors. Each box outlined with red indicates a 25% decrease for the average of each cytokine with the exosome-depleted serum when compared to the same treatment supplemented with normal serum. Each box outlined with green indicates a 25% increase for the average of each cytokine with the exosome-depleted serum when compared to the same treatment supplemented with normal serum. Samples with a cross indicate that none of the donors had detectable cytokines above the lower limit of detection.

Figure 2.36 shows an example cytokine graph (IFN- α) for one agonist, demonstrating the variability seen between donors. Whole blood cytokine secretion varies widely between different donors, IFN- α concentrations on average were higher across all seven donors in response to the CDS Poly(dG:dC) (Figure 2.36), but the variability is very large and the IFN- α concentration was undetectable due to concentrations below the limit of detection in four of the seven donors.

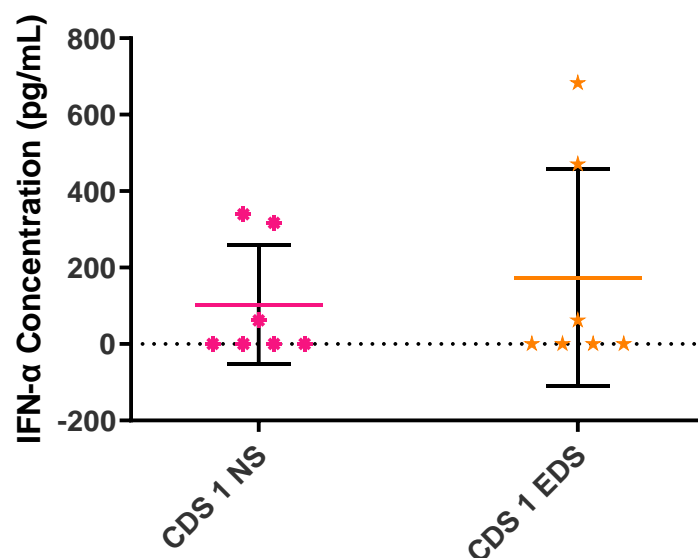


Figure 2.36: IFN- α data used in the heat map for the agonist CDS 1. Data displayed as n=7 donors, mean (\pm standard deviation). Samples plotted at 0 were below the limit of quantification for this assay.

Alterations in cytokine secretion were seen for the PRR agonists tested in whole blood which was either diluted with media that was supplemented with normal FBS or exosome-depleted FBS.

2.4 Discussion

This chapter starts to explore the acute immunotoxicity of the POP polymer linear poly(FTC) and its fragments. It is important to determine this in order to aid the development of these polymers and help improve their translation into the clinic.

Due to the materials interfering with the LAL assay, the MAT assay was used to detect endotoxin contamination. A lack of IL-6 production, in the MAT assay, supports the conclusion that the materials did not contain pyrogen contamination. Endotoxin spiked linear poly(FTC) at the higher concentration (100 $\mu\text{g}/\text{mL}$) showed a greater interference with the assay, due to a reduction in percentage recovery, but the value was still well within the 50-200% recovery limit which is acceptable. This could be due to cell death, although the cytotoxicity assessment suggests that in the other four cell lines tested linear poly(FTC) was not toxic up to 400 $\mu\text{g}/\text{mL}$. Further to these results, significantly higher IL-8 or TNF- α were not seen in the whole blood assay, which would be indicative of endotoxin contamination. Due to the lack of endotoxin contamination the materials were then carried forward into subsequent immunocompatibility assays.

The cells used in the leukocyte proliferation assay include monocytes, and T/B lymphocytes. Therefore, alterations in these cell numbers are important, to understand whether perturbations in immunological homeostasis are being observed. The leukocyte proliferation assay showed no significant proliferation of monocytes or lymphocytes was induced by the POP material linear poly(FTC) and FTC, alone or when spiked with PHA. Although, in donor one there was significantly lower absorbance, indicating a reduction in leukocytes when exposed to linear poly(FTC) 80 $\mu\text{g}/\text{mL}$ and both 1.8 and 18 $\mu\text{g}/\text{mL}$ of FTC in combination with PHA. This could potentially indicate there is a mechanism of inhibition of the monocyte/lymphocyte activation caused by PHA, but this would need to be explored further in more donors to draw any conclusions, as it was only significant in one of the three donors tested. This could potentially be an issue *in vivo*, as the materials may prevent the body responding to subsequent infection exposure appropriately.

Interestingly the results from the iC3b analysis suggest that the POP material linear poly(FTC) at the concentrations tested, weakly activate complement. iC3b is commonly used as a surrogate for complement activation via the classical and Alternative pathway (Cedrone et al., 2017; Neun et al., 2018), iC3b is produced in correlation with the activity of the C3 convertase. Hirudin was used as the anticoagulant for this assay due to previous findings that suggest it allows detection of more sensitive complement responses, due to acting as an

anticoagulant not using ion chelation (Cedrone et al., 2017). iC3b is generated when C3b is cleaved by complement factor I, C3b plays an important role leading to the creation of C5 convertase (Dunkelberger & Song, 2010; Merle et al., 2015). C5b then, along with C6, C7, C8 and C9 combine to form the membrane attack complex (MAC), which results in cell lysis (Bubeck, 2014). Further follow up of these results to determine which pathway in particular is being activated would be needed to draw any further conclusions from this experiment. Of note useful assays are available to determine levels of: soluble C5b-9 (MAC), C4d (Lectin and classical pathway), bb (alternative pathway), factor H (regulates formation of the alternative pathway convertase enzyme).

It is important to recognise that although this POP material causes significant complement activation in three of the five donors tested, the levels of iC3b in four of the five donors were below that of Doxil, a drug which is currently used to treat cancer patients, and known to have clinical adverse reactions. The comparison to Doxil enables a rational determination of the possibility for clinically relevant ADRs. Although treatment for HIV and cancer drugs have very different risk benefit ratios levels, due to the constant demand for new cancer drugs as a result of the severity and consequences of dysregulated tumour growth. Doxil can be well tolerated in most people, if slower infusion rates and premedication of glucocorticoids and antihistamines is carried out (Chanan-Khan et al., 2003). It is also important to point out that these POP materials are designed to be an implant that slowly degrades and releases FTC over time and therefore much larger quantities could potentially be released from the implant, causing a hypothetically greater complement response. This is an important point as previously TAF implants that have been *tested in vivo* have shown the potential to dump a large quantity of TAF at the implant site, which led to high levels of inflammation and necrosis surrounding the implant in both rabbits and rhesus macaques (Su et al., 2020).

CARPA syndrome results from aberrant complement activation, it is a form of non-IgE related hypersensitivity (Janos Szebeni, 2014). An interesting point to make about the results of Doxil, is the variability in responses between donors, Doxil causes CARPA hypersensitivity in certain patients, but is very safe in others. The results seen in this experiments correlates with the variability of complement activation in humans following Doxil administration (Chanan-Khan et al., 2003). As the results are consistent with what is seen *in vivo*, this assay should therefore be a good assessment for predicting whether new materials may cause significant complement activation. Although unlike Doxil, the response to linear poly(FTC) seems to be more consistent across all five donors.

As discussed previously in Chapter 1, the linker between the poly (FTC) groups in the linear poly(FTC) POP material is tri(ethylene glycol), which is a short chain PEG. The linear poly(FTC) polymer is cleaved via esterase activation and will break in a currently unpredictable manner to leave smaller polymer fragment chains, FTC and the linker. Polymer fragments left, will either carry either hydroxyl (FTC or linker end) or an amino end group (FTC end). Hydroxyl groups on materials have been shown to induce complement activation (Arima et al., 2009; Arima et al., 2008). Previously much longer PEG chains in human sera have been shown to increase production of complement activation components, with longer chains causing greater activation (Hamad, Hunter, Szebeni, & Moghimi, 2008). Anti-PEG antibodies have been shown to correlate with complement activation and lead to accelerated clearance of drug formulations (Kozma, Shimizu, Ishida, & Szebeni, 2020). This is an important consideration that should be explored, to further understand the results seen for both Doxil and linear poly(FTC), for example using anti-PEG antibodies ELISAs to determine if they are present in plasma samples from each donor, as this may affect the pharmacokinetics of the implant *in vivo*, as well as the safety. An interesting follow up to these results, would be to explore the four stages of linear poly(FTC) breakdown materials, in order to determine whether the longer or shorter chains cause the same, less or more activation of complement and subsequent higher iC3b or other complement product levels. Better *in vivo* representation of complement activation could also be achieved by exposing the POP fragment pressed rods to the plasma, rather than a solution using DMSO as a vehicle. DMSO may affect the breakdown of the materials and therefore would remove this variable as it wouldn't be used in clinical applications of the material.

Serum such as FBS is commonly used to supplement routine cell culture medium due to its capability to promote growth (Gstraunthaler, 2003). Although FBS can be an unreliable source of nutrients, as it can exhibit batch to batch variation, source and brand variation (Brunner et al., 2010; van der Valk et al., 2010), which therefore can alter cell growth, and consequently lead to variability in assay results. Bovine serum contains many exosomes (Paszkiel et al., 2017), which, like other factors can vary between batches of FBS, although in recent years this variability has been reduced (Eitan, Zhang, Witwer, & Mattson, 2015). Gibco have created an exosome-depleted FBS, which can be used to supplement media, maintain cell culture performance and depletes exosomes more completely than common laboratory protocols (Paszkiel et al., 2017).

Here, in contrast to previous work within the group in cell lines, there is no substantial differences in the results seen from whole blood assays when the blood is supplemented

with culture media containing serum derived exosomes or without. These results are preliminary, as a much larger number of donors would be needed to draw any full conclusions, due to the high variation seen between different donors. Considerably higher or lower results were not seen in any of the cytokines studied, as a result of exposure to the POP linear poly(FTC) stages of breakdown materials. Over the seven donors there are the same trend with the agonists as expected, in both the exosome-depleted and normal serum conditions. The six agonists used as controls in the experiment were used as it was suspected that the POP materials could potentially interact with these receptors or sensors due to their structure, as described in Chapter 1. Due to the complex interactions of all the agonists tested, the large quantity of cytokines measured and the limited number of donors, it is difficult to draw complete conclusions from the work, in terms of the impact of exosomes in serum on the results seen in *in vitro* assays.

Variability in the cytokine secretion responses were seen between donors 1-3 and 4-6, the difference between these blood samples, were the source, the anticoagulant used (donors 1-3 used sodium citrate and donors 4-6 used Lithium heparin), and how long the blood was drawn before being diluted and incubated. In the whole blood assay with freshly drawn blood in house, the blood was diluted within one hour of collection, whereas this couldn't be done with the blood sourced from NHS BT. The results showing higher untreated IL-8 concentrations are in line with previous findings, blood stored at 15-30 °C for 53 hours before being centrifuged leads to higher IL-8 levels in serum and citrate plasma (Kofanova et al., 2018). This is something that needs to be kept consistent for future experiments.

Linear poly(FTC) S3 fragment breakdown material showed particularly different cytokine release profiles in the two sets of donor blood. With donors 1-3 having much higher levels of a number of different cytokines compared to donors 4-6, and higher basal levels of the cytokines in donors 1-3 also led to linear poly(FTC) S3 causing a reduction in certain cytokine levels. In donors 1-3 Higher levels were seen for IL-1 β , IL-6, IL-10 and TNF- α , whereas lower levels were seen for IL-8, the cytokines IL-1 β , IL-6, IL-8 and TNF- α are pro-inflammatory cytokines whereas IL-10 is anti-inflammatory suggesting a complex interaction with cells in the blood. The lower IL-8 levels are also seen from the DMSO vehicle treatment and therefore are probably due to the vehicle and not the fragment itself. However, the other cytokines do not correlate with the DMSO control and look to be caused by the fragment. IL-1 β increases would be indicative of inflammasome activation, which should be followed up. The higher IL-1 β , IL-6, IL-8, IL-10 and TNF- α could be as a result of macrophage activation.

As discussed in Chapter 1, due to the nature of the materials and their early stage of development the exact break-down of the POP materials cannot yet be predicted. As the materials develop there would be the possibility to predict the breakdown of the POP materials, but due to the early stage of development, this is not possible at this moment. Therefore, the best assessment that can be made has been done using the different length chains to predict any red flags using the assays in this chapter. Further testing would be required to distinguish whether the results were due to the fragments in the oligomer-SEC chromatograms or free drug and linker and the degradation of these materials. This is why the focus shifted to using the linear poly(FTC) alone in the screening assays, as this was the most likely material at the time that would be used *in vivo*.

Overall, there were no huge red flags from this biocompatibility screen, although the complement results could impact the safety if the concentrations were much higher at the implant site. Therefore, the POP materials were moved on to determining if there were any other more complex immunological interactions of these materials.

Chapter 3

Assessment of cell health, cell phenotypes and gene expression following continual exposure to FTC, 3TC and linear poly(FTC)

3.1 Introduction

As FTC and 3TC are being developed into POP long-acting delivery systems, the impact of continued exposure to the drugs themselves and the FTC containing linear poly(FTC) POP polymer in a repeated exposure assay was investigated; the reasoning behind this decision is relevant immune cells would be exposed to the drugs, and or the linear poly(FTC) for periods longer than standard drug exposures of 24-48 hours. Previously, studies published have not explored repeat exposure of drugs in cell lines, *in vitro*. A key question in this type of delivery is, with long-acting formulations, does chronic exposure of the drugs to human cells alter their phenotype and therefore do the cells respond differently as a result of this exposure. Assessment of cell phenotype can consider a number of different assessments, including but not limited to assessing: ROS levels, reduced glutathione levels, the mitochondrial membrane potential (MMP) and the activation status of these immune cells by looking at specific marker expression using flow cytometry.

In this chapter, cells were exposed to C_{max} concentrations twice weekly when passaged, to assess potential impact of POP implants to immune cells relevant to the site of administration.

Prior to any assessment in primary cells, immortalised human cells were chosen for the ability for longer term culture. CEM, KU812, MUTZ-3, and THP-1 cell lines were chosen, as models for DCs, T-cells, basophils and monocytes, which will all be immune cells that are potentially exposed to the implant and implant breakdown products. These cell lines were used to determine repeat exposure effects of these drugs or the linear poly(FTC) POP polymer in this chapter.

3.2 Methods

3.2.1 Materials

All the cell lines, FTC, 3TC, DMSO, LPS, PHA, and PBS were all purchased from the companies stated in Chapter 2. The linear poly(FTC) POP material was provided from colleagues at the University of Liverpool as stated in chapter 2. CellROX[®] green reagent (for oxidative stress detection), ThiolTracker[™] Violet dye (Glutathione Detection Reagent) (Invitrogen), JC-1 Dye (MMP Probe) (Invitrogen), DPBS containing Ca²⁺ and Mg²⁺ (Gibco), Nanodrop 1000 Spectrophotometer, and penicillin/streptomycin (Gibco) were all purchased from Thermo Fisher Scientific (Cheshire, UK). MACS Bovine Serum albumin (BSA) stock solution, autoMACS rinsing solution, running buffer, CD14 microbeads and all the REAfinity antibodies and isotype controls used for the CEM (CD25, CD4 and CD69), KU812 (CD63, CD203c and Cd164), MUTZ-3 (CD86, CD80, CD209, CD40, HLA-DR, CD83, CD274 and CD14) and THP-1 (CD64, CD163, CD14) marker expression were all purchased from Milentyi Biotec (Bergisch Gladbach, Germany). Phorbol myristate acetate (PMA) was purchased from Invivogen (Toulouse, France). C5a was purchased from R&D Systems, BioTechne (Minneapolis, USA). RNeasy[®] Mini Kit was purchased from Qiagen (Manchester, UK). Resiquimod (R848) (Sigma) and Calcium Ionophore A23187 (CI) (Sigma) was purchased from Merck (Darmstadt, Germany). nCounter Human Metabolic Pathways panel, and nCounter Master Kit were both purchased from Nanostring (Seattle, USA). Granulocyte-macrophage colony-stimulating factor (GM-CSF) was purchased from PeproTech (London, UK). IL-4 was purchased from Active Bioscience (Hamburg, Germany). Markers used for the MoDC work were: CD274 antibody (eBioscience, Invitrogen) was purchased from Thermo Fisher Scientific, CD209, CD80, CD83, CD14 and CD40 antibodies were all purchased from BD Biosciences (Berkshire, UK), and CD86 and major histocompatibility complex, class II, DR alpha (HLA-DR) antibodies were both purchased from Biolegend (San Diego, USA).

3.2.2 Routine cell culture

CEM, KU812, MUTZ-3 and THP-1 cell lines were all grown using the same method as described in Chapter 2 Section 2.2.4.1. When the cells were growing as expected they were split into three groups: Cells grown untreated, Cells grown in the presence of FTC and Cells grown in the presence of 3TC. (KU812: passage 8, CEM: passage 15, THP-1: passage 11 and MUTZ-3: passage 17 (UT/FTC/3TC/45), passage 15 (UT/DMSO). Cells were cultured in T175 flasks and passaged twice a week and seeded at a suitable density (CEM = 0.2 x10⁶ cells/mL,

THP-1 = 0.4×10^6 cells/mL, KU812 = 0.3×10^6 cells/mL, MUTZ-3 = 0.5×10^6 cells/mL). The drugs were added to the respective flasks directly following passage at a final concentration equivalent to recorded C_{max} values for FTC and 3TC on the HIV drug interactions website (FTC = 1.8 $\mu\text{g/mL}$ and 3TC = 2 $\mu\text{g/mL}$) (HIV Drug Interactions, 2016a, 2016b). Cell health assays were then carried out on the cells following seven weeks of exposure to the drugs (14 passages) and compared to the untreated cells following culture for the same period.

In the MUTZ-3 cell line an exposure to linear poly(FTC) in 100% DMSO to a final concentration of 20 $\mu\text{g/mL}/0.1\%$ DMSO for seven weeks was also carried out and due to the results seen, a DMSO control was also carried out for seven weeks, in order to detect whether changes were due to exposure to the DMSO vehicle. Following experimental culture, aliquots of the repeat exposed cells were frozen in FBS supplemented 10% with DMSO and were stored in liquid nitrogen.

3.2.3 Measurement of Total Reactive Oxygen Species (ROS)

100 μL of cells were seeded at 5×10^5 cells per well in 96-well plate and the final concentration of CellROX[®] green reagent was added at a final concentration of 5 μM , following a prior 1:500 dilution in RPMI supplemented 10% FBS v/v. Each of the conditions for each cell line was carried out in quadruplicate. Cells were incubated for 30 minutes at 37 °C 5% CO_2 , following incubation the cells were centrifuged at 860xg for five minutes and the supernatants removed. Cells were washed three times in PBS, PBS was aspirated, and the cells suspended in 1000 μL MACSQuant running buffer and transferred into a deep well 96-well microplate. Flow cytometric analysis was carried out using the B1 (Fluorescein isothiocyanate (FITC)) channel on the MACSQuant Analyzer 9. The median signal intensity for the corresponding markers for each of the three technical replicates from individual wells were averaged and then the four experimental repeats are displayed as mean (\pm standard deviation) in GraphPad prism 9.3.1.

3.2.4 Measurement of reduced glutathione

100 μL of cells were seeded at 5×10^5 cells per well in 96-well plate and centrifuged at 860xg for five minutes and the supernatant aspirated, the cells were then washed twice with 100 μL Dulbecco's Phosphate Buffered Saline (DPBS) containing Ca^{2+} and Mg^{2+} . During the wash procedure the ThiolTracker™ Violet dye (Glutathione Detection Reagent) was prepared at a final concentration 20 mM in DMSO and further diluted in DPBS containing Ca^{2+} and Mg^{2+} to a final concentration 20 μM and warmed in 37 °C water bath. 100 μL of the dye was added to

each well and incubated for 30 minutes at 37 °C 5% CO₂. Following incubation, the plate was centrifuged at 860xg for five minutes and the supernatants aspirated. The cells were washed in 100 µL DPBS containing Ca²⁺ and Mg²⁺, centrifuged and suspended in 1000 µL MACSQuant running buffer and transferred into a deep well 96-well microplate. Flow cytometric analysis was carried out using the B1 (FITC) channel on the MACSQuant Analyzer 9. The median signal intensity for the corresponding markers for each of the three technical replicates from individual wells were averaged and then the four experimental repeats are displayed as mean (± standard deviation) in GraphPad Prism software 9.3.1.

3.2.5 Measurement of MMP

100 µL of cells were seeded at 5 x 10⁵ cells per well in 96-well plate and centrifuged at 860xg for five minutes and the supernatant aspirated, the cells were then washed twice in PBS. Supernatants were aspirated and JC-1 MMP sensor dye was diluted in RPMI-160 10% v/v FBS at a final concentration of 10 µg/mL added. Dye was incubated at 37 °C 5% CO₂ for ten minutes. Following incubation, the plate was centrifuged at 860xg for five minutes and the supernatants aspirated, cells were washed in PBS and aspirated and suspended in 100 µL MACSQuant running buffer and transferred into a deep well 96-well microplate. Flow cytometric analysis was carried out using the B1 (FITC) and B2 (PE) channels on the MACSQuant Analyzer 9. B2/B1 median fluorescence intensity were averaged and then the four experimental repeats are displayed as mean (± standard deviation) in GraphPad Prism software 9.3.1. B2/B1 median was used to determine MMP, due to the dye accumulating in the mitochondria in a potential dependent manner. When outside the mitochondria the probe is in its monomeric green fluorescence form and inside it forms j-aggregates that have a red fluorescence. A lower B2/B1 median is indicative of membrane depolarisation. Valinomycin 1µM was included as a control for the DMSO control repeat exposure.

3.2.6 Cell line Marker expression assessment

2 mL of cells were seeded at 1 x 10⁶ cells/mL in 12-well plates and the following treatments set up in the different cell lines in triplicate. In the KU812 cells C5a was added to give a final concentration of 50 nM, and together PMA and CI were added to give final concentrations of 80 nM and 2 µM respectively. In the THP-1 cell line the cells were treated with LPS at 1 µg/mL. In the CEM cell line the cells were treated with PHA-M at 10 µg/mL. In the MUTZ-3 cell line marker test the cells were exposed to LPS at 1 µg/mL, for the repeated exposure experiment MUTZ-3 cells the cells were either exposed to R848 at 5 µg/mL or LPS at 1 µg/mL. The cells

were then incubated for 24 hours at 37 °C 5 % CO₂. Each well was then pipetted a few times to mix and then 1 mL from each transferred in respective wells on a 96-well deep well plate. For the MUTZ-3 Cell line 500 µL was transferred to the respective wells as there was two panels of markers to assess. The plates were centrifuged at 860xg for five minutes and the supernatant aspirated. Flow buffer was prepared by diluting MACS BSA stock solution 1:20 with auto MACS rinsing solution. Antibody and isotype control antibody cocktails were created by diluting each antibody 1:50 in flow buffer, as per the manufacturers guidelines. 100 µL of the respective cocktail was then added to each well and incubated at 2-8 °C in the dark for ten minutes. The plate was centrifuged and the supernatant aspirated, each well was then washed twice by adding 1000 µL of flow buffer, centrifuging the plate at 860xg for ten minutes and discarding the supernatant. The final pellet was then suspended in 1000 µL of running buffer. Flow cytometric analysis was carried out using the MACSQuant Analyzer 9, with the following markers, fluorescent dyes and channels illustrated in Table 3.1.

Table 3.1: Displays the cells lines, markers, role of the markers, fluorescent dyes and channels used for the marker analysis of the four cell lines.

Cell line and Panel	Marker	Role of Marker	Fluorescent dye (Excitation (nm), Emission (nm))	MACSQuant Analyzer 9 Channel (Laser (nm), Filter (nm))
KU812	CD63	Activation marker for basophils.	PE-Vio770 (565, 775)	B4 (Blue 488, 750 LP)
	CD203c	Basophil/mast cell activation marker.	PE (565, 578)	B2 (Blue 488, 585/40)
	CD164	Novel basophil activation marker.	Allophycocyanin (APC)-Vio770 (652, 775)	R2 (Red 635, 750 LP)
THP-1	CD64	Key marker of inflammation, Fc receptor that binds IgG antibodies.	PE-Vio770 (565, 775)	B4 (Blue 488, 750 LP)
	CD163	Haemoglobin scavenge receptor, activation marker	PE (565, 578)	B2 (Blue 488, 585/40)

		for monocytes and macrophages.		
	CD14	Activation marker for monocytes and macrophages, binds LPS.	APC-Vio770 (652, 775)	R2 (Red 635, 750 LP)
CEM	CD25	Late activation marker.	PE-Vio770 (565, 775)	B4 (Blue 488, 750 LP)
	CD4	Co-receptor for the T-cell receptor, activated by MHC class II.	PE (565, 578)	B2 (Blue 488, 585/40)
	CD69	T-cell early activation marker.	APC-Vio770 (652, 775)	R2 (Red 635, 750 LP)
MUTZ-3 Panel 1	CD86	Found on APCs, is a co-stimulatory marker for T-cells.	PE-Vio770 (565, 775)	B4 (Blue 488, 750 LP)
	CD80	Found on APCs, is a co-stimulatory marker for T-cells.	PE (565, 578)	B2 (Blue 488, 585/40)
	CD209	Dendritic cell specific PRR, mediates interactions with T-cells.	APC (652, 660)	R1 (Red 635, 655-730)
	CD40	Found on APCs, binds to CD40L on T-cells causing activation.	APC-Vio770 (652, 775)	R2 (Red 635, 750 LP)
MUTZ-3 Panel 2	HLA-DR	MHC class II surface receptor, binds to T-cell receptor.	PE-Vio770 (565, 775)	B4 (Blue 488, 750 LP)
	CD83	APC activation marker.	PE (565, 578)	B2 (Blue 488, 585/40)
	CD274	Chemoattractant for immune cells.	APC (652, 660)	R1 (Red 635, 655-730)
	CD14	Activation marker for monocytes and macrophages, binds LPS.	APC-Vio770 (652, 775)	R2 (Red 635, 750 LP)

The MFI for the corresponding markers for each of the three technical replicates from individual wells were averaged and removed from their corresponding isotype control replicates and then the three experimental repeats are displayed as individual points with mean (\pm standard deviation) in GraphPad Prism software 9.3.1.

3.2.7 Gene expression comparison of the cell lines following repeat exposure

3.2.7.1 RNA isolation

MUTZ-3 Repeat Exposure cells at passage 32 and passage 16 of treatment with either FTC, 3TC or linear poly(FTC) were brought up from cryogenic storage, passaged and split into three flasks for each treatment and grown up until passage 39 and passage 23 of treatment.

The cells were then seeded in singlicate at 2×10^6 cells per well in 2 mL, one well of each condition was treated with R846 at 5 $\mu\text{g}/\text{mL}$ and incubated for 24 hours, the total number of experimental replicates per condition was three. 5 mL was removed from the three corresponding wells and transferred to falcon tubes and spun at 400xg for ten minutes and the supernatants discarded.

RNA isolation was carried out using the RNeasy[®] Mini Kit following the manufacturer's protocol. Each cell pellet was suspended in 350 μL RLT buffer supplemented with 1% β -mercaptoethanol and vortexed. 350 μL of 70% ethanol was added to the lysate and mixed by pipetting. 700 μL of sample was then transferred to a RNeasy Mini spin column in a 2 mL collection tube and centrifuged for 15 seconds at 8000xg and the flow through discarded. 700 μL of Buffer RW1 was added to the spin column and centrifuged for 15 seconds at 8000xg and the flow through discarded. 500 μL of Buffer RPE was added to the spin column and centrifuged for 15 seconds at 8000xg and the flow through discarded. 500 μL of Buffer RPE was added to the spin column and centrifuged for two minutes at 8000xg and the flow through discarded. The spin column was then placed in a new collection tube and 50 μL of RNase-free water was added directly to the spin column membrane and centrifuged at 8000xg to elute the RNA, this was repeated and spun into the same collection tube. RNA was quantified using the Nanodrop 1000 Spectrophotometer. Purity of the samples was analysed in the Centre for Genomics Research at the University of Liverpool using a fragment analyser, due to contamination of two samples with the ladder and low concentrations of RNA, four of the samples were reanalysed using the bioanalyser.

3.2.7.2 Generation of gene expression data using the nCounter system by Nanostring

The Metabolic Pathways code set from Nanostring was ran following manufactures protocols in order to explore gene expression changes in the MUTZ-3 cells following repeat exposure. A thermocycler was pre-heated at 65 °C (lid at 70 °C) and the Reporter CodeSet and Capture ProbeSet thawed at 15-30 °C. Hybridisation master mix was created by adding 70 µL of hybridization buffer to 42 µL of the Reporter CodeSet and then 8 µL of master mix, 5µL of sample at (500 ng/µL) and 2 µL of Capture ProbeSet was added to the corresponding wells of strip tube. The strip tube was then placed in the thermocycler for 20 hours. The strip tubes were then placed in the nCounter prep station and ran at high sensitivity to load the cartridge. The cartridge was then ran on the nCounter analysis system using the reporter library file provided with the kit and the data resolution set to max (550 field of view).

The samples were run on two cartridges on corresponding days, the untreated, untreated treated with R848, FTC cultured, and FTC cultured treated with R848 were analysed on cartridge 1. The 3TC cultured, 3TC cultured treated with R848, linear poly(FTC) cultured and linear poly(FTC) cultured treated with R848 were all ran on cartridge 2.

3.2.7.3 R analysis of nCounter data

R version 4.2.1 was used for all the following data analysis. R analysis was carried out with the help of Francesca Sposito and Dr Christopher David at the University of Liverpool.

The CRAN Package NACHO version 2.0.0 was used to visualise the quality control results of the data collected (Canouil et al., 2019; Mickaël Canouil, and, & Roderick C. Sliker, 2022). Any outlier data files were removed before further analysis. The Bioconductor package NanoStringDiff version 1.26.0 was used to perform normalisation based on the negative, positive and housekeeping factors included in the nCounter metabolic pathways panel of genes, alongside also calculating log₂fold change (log₂FC) and p or q values based on comparisons between the specified groups (Wang et al., 2016). Volcano plots of the group comparisons were created using the Bioconductor package EnhancedVolcano version 1.14.0 from log₂FC and p or q values, with a cut off of 0.05 for the p or q values and 2 or -2 for log₂FC (Blighe K, Rana S, & M, 2022).

The nCounter Human Metabolic Pathways panel splits the genes into five themes, these are: Biosynthesis and Anabolic pathways, cell stress, nutrient capture and catabolic pathways, signalling effecting cellular metabolism, and transcription regulation. Radar plots were

created using these theme classifications to look at how many genes within these themes either had higher or lower expression using the comparisons created in R. The number of genes that had a higher gene expression were classed as a Log2Fold change >2 and genes that had a lower expression were Log2Fold <-2 .

3.3 Results

3.3.1 CEM

ROS, reduced glutathione and MMP were measured following repeat exposure of the CEM cells to FTC and 3TC and compared to untreated cells in order to determine the ability of the treatments to modify cell health. Intracellular ROS levels were significantly higher in the FTC- and 3TC-cultured cells, than the untreated cells ($p < 0.001$ and $p < 0.0001$ respectively), FTC-cultured cells had 12% and 3TC-cultured cells had 14% higher ROS levels (Figure 3.1). No significant differences were seen for the reduced glutathione levels or the MMP for either the FTC- or 3TC-cultured cells.

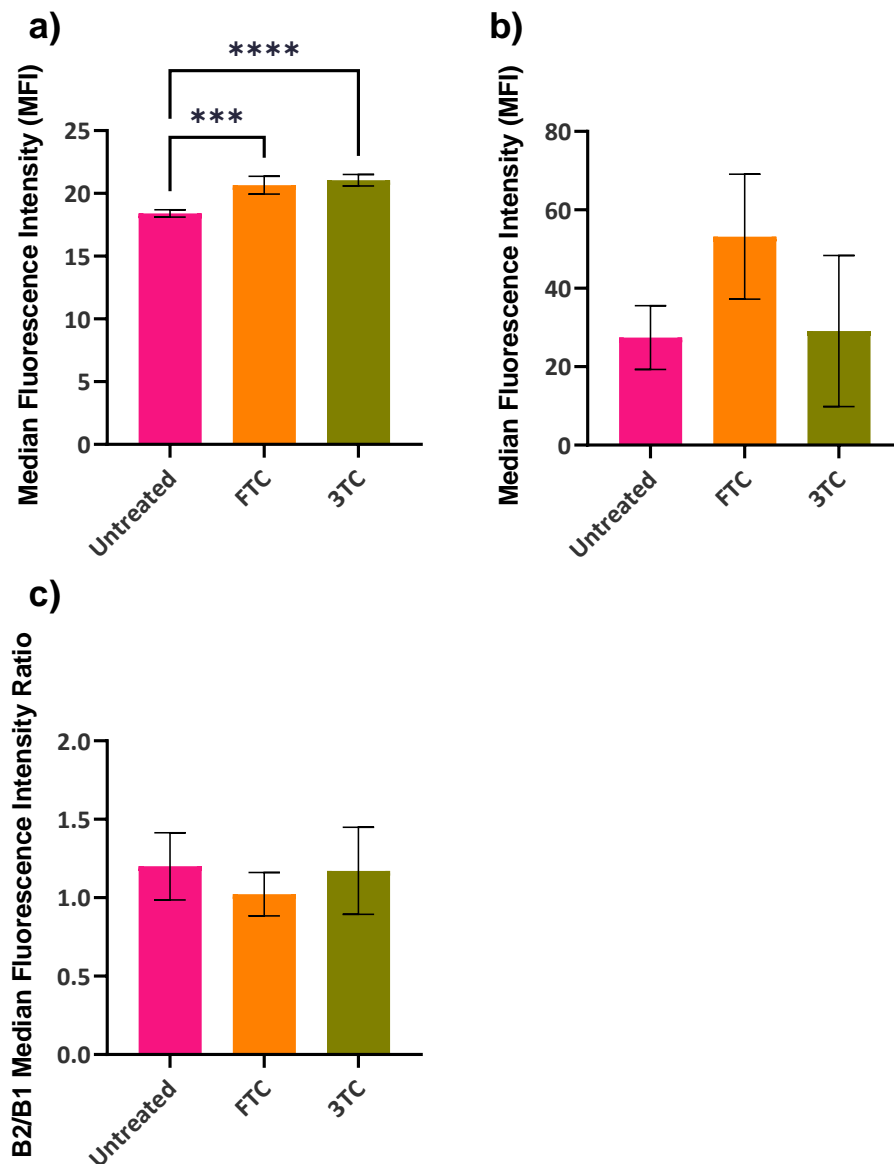


Figure 3.1: CEM cells exposed to FTC, and 3TC, for seven weeks and subsequent phenotypic assessment. a) Intracellular ROS, b) Intracellular reduced glutathione, c) MMP. Data displayed as median fluorescence intensity or B2/B1 median fluorescence intensity of n=4, mean (\pm standard deviation). $p < 0.0001 = ****$, $p < 0.001 = ***$, $p < 0.01 = **$ and $p < 0.05 = *$.

Marker expression of the CEM cells was explored following exposure to FTC and 3TC and compared to the untreated, all cells were compared untreated and treated with a known positive control, for the CEM cell line this was PHA. The markers used were CD4, CD69 and CD25. In both the FTC- and 3TC-cultured cells the treatment of these cells with PHA-M caused a 77% and 42% significantly higher expression of CD69 respectively, this was not significantly higher for the untreated cells ($P < 0.05$ and $p < 0.01$ respectively) (Figure 3.2b). When compared to the Untreated cells, the 3TC-cultured cells showed a significantly higher CD69 expression ($p < 0.05$), with a 47% higher expression (Figure 3.2b). No culture treatments or positive control treatments were significantly different for the markers CD4 and CD25 (Figure 3.2a and c).

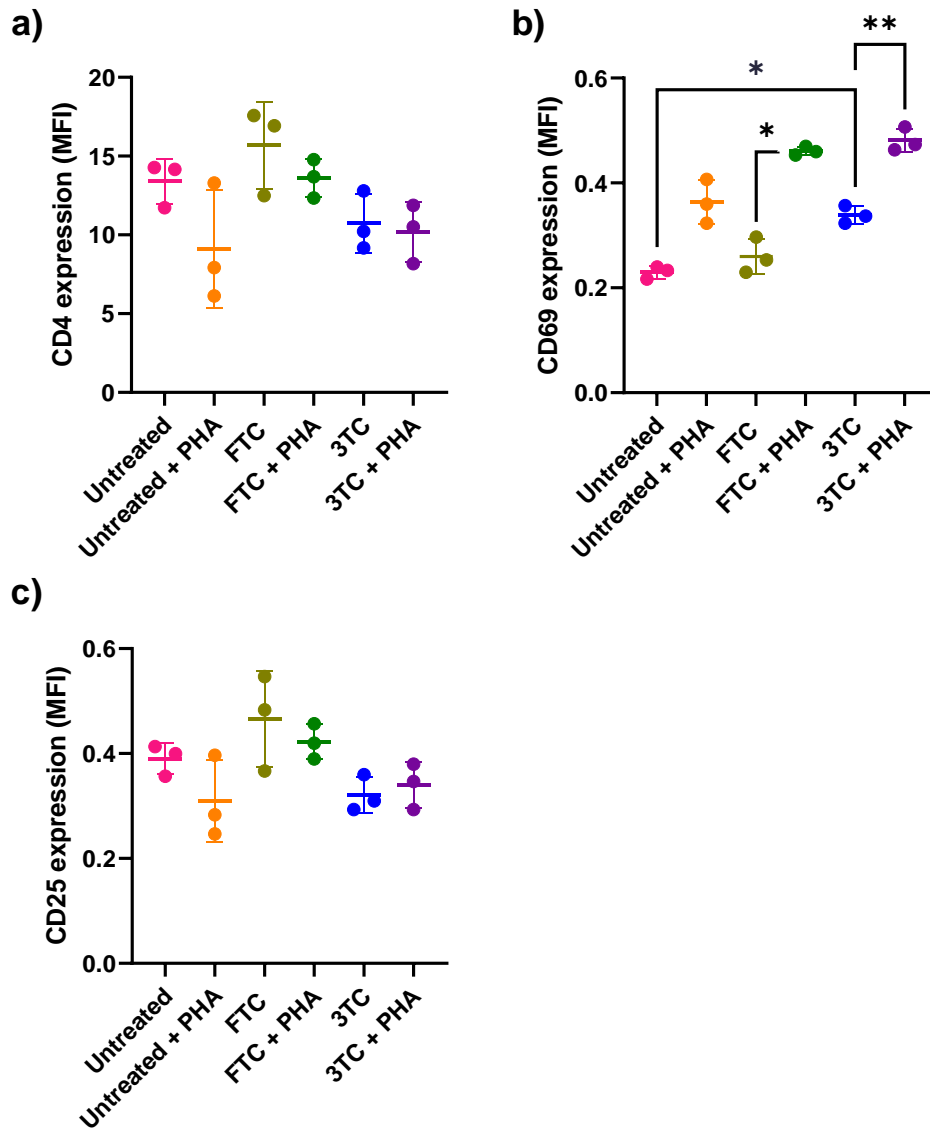


Figure 3.2: CEM cells exposed to FTC, and 3TC, for seven weeks and subsequent marker expression assessment. a) CD4 expression, b) CD69 expression and c) CD25 expression. Data displayed as median fluorescence intensity of $n=3$, mean (\pm standard deviation). $p < 0.0001 = ****$, $p < 0.001 = ***$, $p < 0.01 = **$ and $p < 0.05 = *$.

FTC- and 3TC-cultured cells had significantly higher ROS levels and higher CD69 expression when treated with PHA, 3TC culture alone also caused significantly higher CD69 expression.

3.3.2 KU812

ROS, reduced glutathione and MMP were measured following repeat exposure of the KU812 cells to FTC and 3TC and compared to untreated cells in order to determine the ability of the treatments to modify cell health. Intracellular ROS levels were 55% significantly higher in the

FTC-cultured cells, than the untreated cells ($p < 0.0001$) (Figure 3.3a). FTC- and 3TC-cultured cells displayed a significantly lower B2/B1 fluorescence ratio, by 40% and 33% respectively, indicating a lower MMP ($p < 0.01$) (Figure 3.3c). A lower B2/B1 median is indicative of membrane depolarisation.

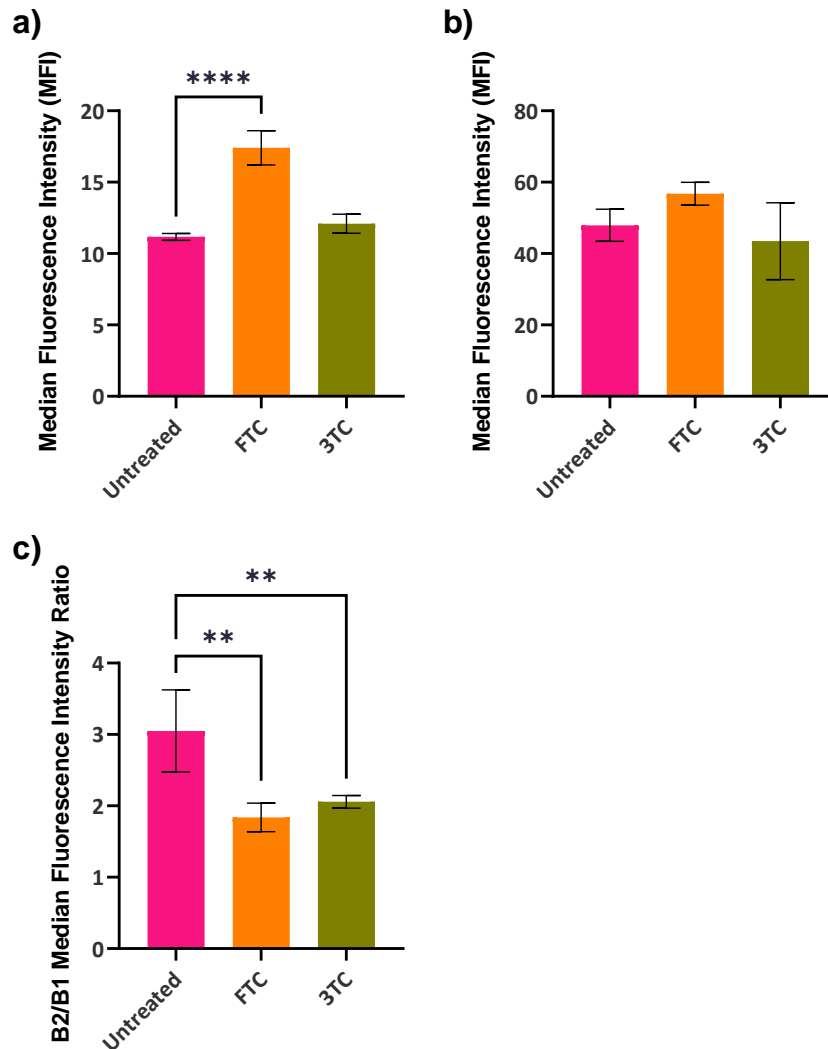


Figure 3.3: KU812 cells exposed to FTC, and 3TC, for seven weeks and subsequent phenotypic assessment. a) Intracellular ROS, b) Intracellular reduced glutathione, c) MMP. Data displayed as median fluorescence intensity or B2/B1 median fluorescence intensity of $n=4$, mean (\pm standard deviation). $p < 0.0001 = ****$, $p < 0.001 = ***$, $p < 0.01 = **$ and $p < 0.05 = *$.

Marker expression of the KU812 cells was explored following exposure to FTC and 3TC and compared to the untreated, all cells were compared untreated and treated with a known positive control, for the KU812 cell line this was C5a or CI and PMA. The markers used were CD63, CD203c and CD164. Both the FTC- and 3TC-cultured cells treated with CI/PMA caused

a 13% and 6% significantly lower expression of CD63, this was not significantly higher for the untreated cells ($p < 0.05$ and $p < 0.01$ respectively) (Figure 3.4a). Also, both the FTC- and 3TC-cultured cells treated CI/PMA caused a 10% and 8% significantly lower expression of CD203c, this was not significantly higher for the untreated cells ($p < 0.05$ and $p < 0.01$ respectively) (Figure 3.4b). The positive controls did not however cause a significantly different expression of CD164 in any of the culture conditions (figure 3.4c). When compared to the untreated cells, both the FTC- and 3TC-cultured cells showed a significantly lower CD63 expression, by 26% or 40% respectively ($p < 0.01$) (Figure 3.4a). FTC- and 3TC-cultured C5a treated cells when compared to the C5a treated cells, showed a 32% and 37% significantly lower CD63 expression respectively ($p < 0.05$ and $p < 0.01$ respectively) (Figure 3.4a). 3TC-cultured cells in comparison with the untreated cells showed significantly 13% higher CD203c expression ($P < 0.01$) (Figure 3.4b). FTC-cultured C5a treated cells when compared to C5a treated cells showed 20% significantly lower CD203c expression ($p < 0.05$) (Figure 3.4b). FTC-cultured C5a treated cells when compared to the C5a treated cells showed a 36% significantly lower CD164 expression ($p < 0.05$) (Figure 3.4c). FTC-exposed CI/PMA treated cells when compared to CI/PMA treated cells had a 30% significantly higher expression of CD164 ($p < 0.01$) (Figure 3.4c).

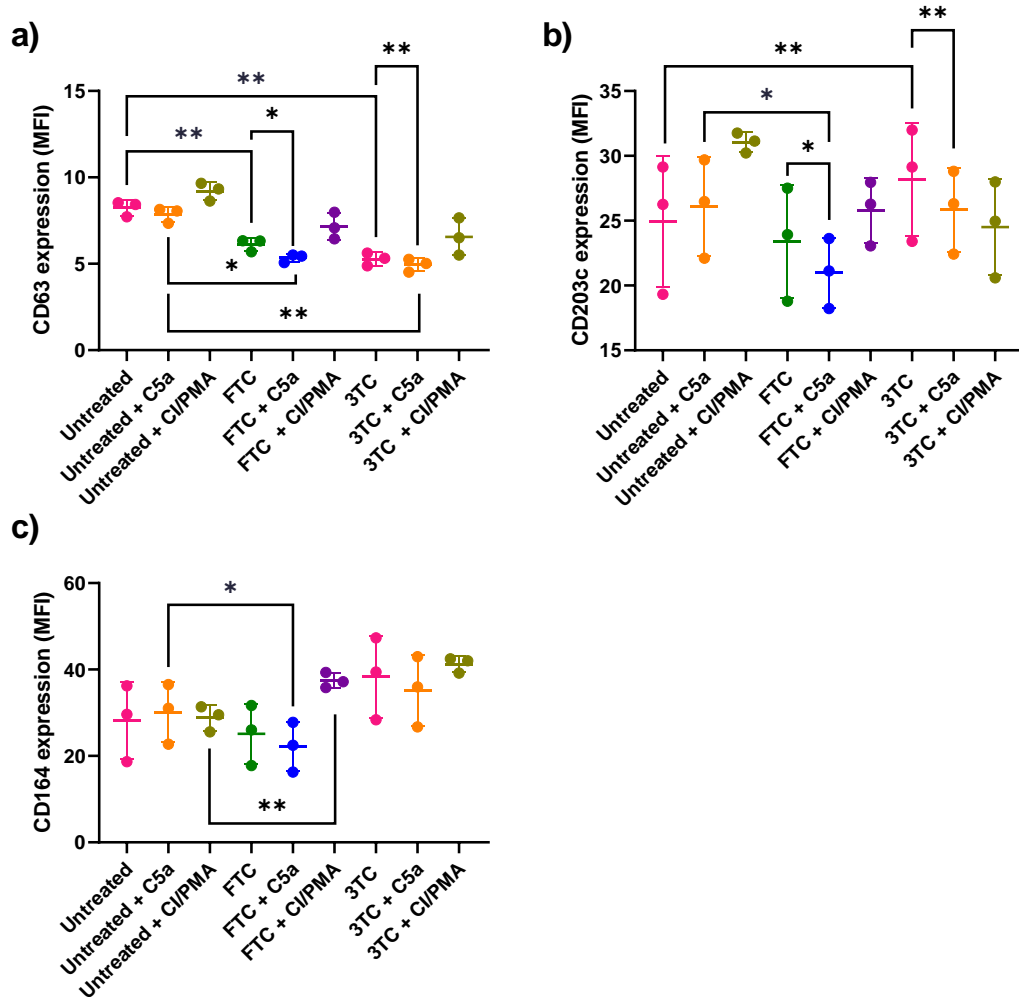


Figure 3.4: KU812 cells exposed to FTC, and 3TC, for seven weeks and subsequent marker expression assessment. a) CD63 expression, b) CD203c expression, c) CD164 expression. Data displayed as median fluorescence intensity of n=3, mean (\pm standard deviation). $p < 0.0001 = ****$, $p < 0.001 = ***$, $p < 0.01 = **$ and $p < 0.05 = *$.

FTC-cultured KU812 cells had significantly higher ROS levels and lower MMP, 3TC-cultured cells also had a lower MMP, indicative of stress. FTC- and 3TC-cultured cells had significantly lower CD63 expression and this was also lower when treated with C5a and compared to the C5a treated cells.

3.3.3 THP-1

ROS, reduced glutathione and MMP were measured following repeat exposure of the THP-1 cells to FTC and 3TC and compared to untreated cells in order to determine the ability of the treatments to modify cell health. Prior to cryogenic storage intracellular reduced glutathione

levels were significantly higher (20% and 54% respectively) in both the FTC- and 3TC-cultured cells compared to those untreated ($p < 0.05$ and $p < 0.0001$ respectively) (Figure 3.5b).

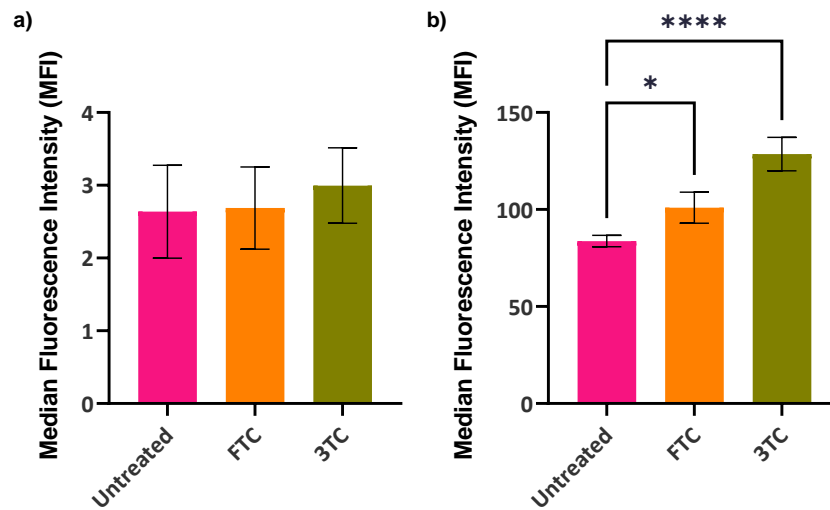


Figure 3.5: THP-1 cells exposed to FTC and 3TC for seven weeks and subsequent phenotypic assessment. a) Intracellular ROS and b) Intracellular reduced glutathione. Data displayed as median fluorescence intensity or B2/B1 median fluorescence intensity of $n=4$, mean (\pm standard deviation). $p < 0.0001 = ****$, $p < 0.001 = ***$, $p < 0.01 = **$ and $p < 0.05 = *$.

However, following cryogenic storage and an extra four passages, no significant differences were seen for either ROS or reduced glutathione levels. MMP was not measured prior to cryogenic storage, following cryogenic storage 3TC-cultured cells demonstrated a 13% significantly lower MMP compared with the untreated cells ($p < 0.01$) (Figure 3.6c). A decrease in the B2/B1 median is indicative of membrane depolarisation.

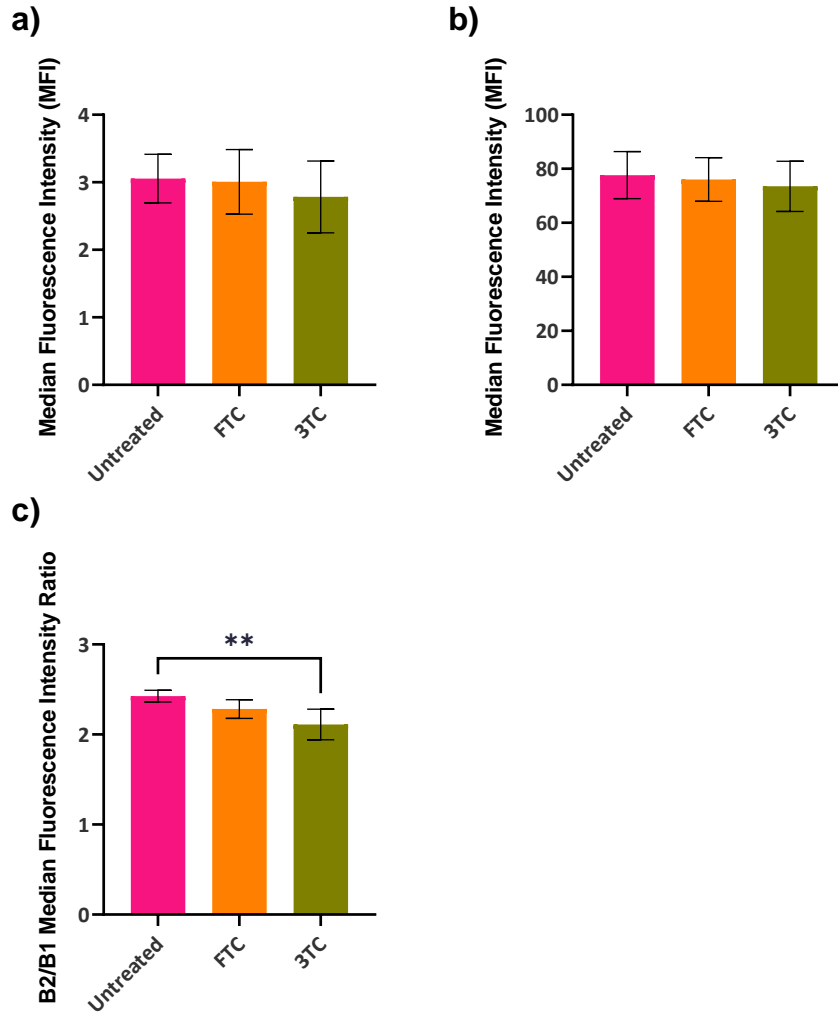


Figure 3.6: THP-1 cells exposed to FTC and 3TC for seven weeks and subsequent phenotypic assessment after frozen for and then passaged four time before analysis. a) Intracellular ROS, b) Intracellular reduced glutathione, c) MMP. Data displayed as median fluorescence intensity or B2/B1 median fluorescence intensity of n=4, mean (\pm standard deviation). $p < 0.0001 = ****$, $p < 0.001 = ***$, $p < 0.01 = **$ and $p < 0.05 = *$.

Marker expression of the THP-1 cells was explored following exposure to FTC and 3TC and compared to the untreated, all cells were compared untreated and treated with a known positive control, for the THP-1 cell line this was LPS. The markers used were CD163, CD64 and CD14. In all of the three culture conditions LPS treatment lead to a 89%, 57%, and 60% significantly higher CD163 expression respectively ($p < 0.0001$, $p < 0.001$, and $p < 0.001$) (Figure 3.7a). The untreated- and FTC-cultured cells when treated LPS caused a 36% and 19% significantly higher expression of CD64 respectively ($p < 0.01$ and $p < 0.05$) (Figure 3.7b). In all of the three culture conditions LPS treatment lead to a 71%, 39%, and 61% significantly higher CD14 expression respectively ($p < 0.0001$, $p < 0.001$, and $p < 0.0001$) (Figure 3.7c). When

compared to the untreated cells, 3TC-cultured cells showed a significantly higher expression of CD14, 22% higher ($p < 0.05$) (Figure 3.7c). When compared to the LPS treated cells, the 3TC-cultured LPS treated cells showed significantly more CD14 expression, 15% higher ($p < 0.05$) (Figure 3.7c).

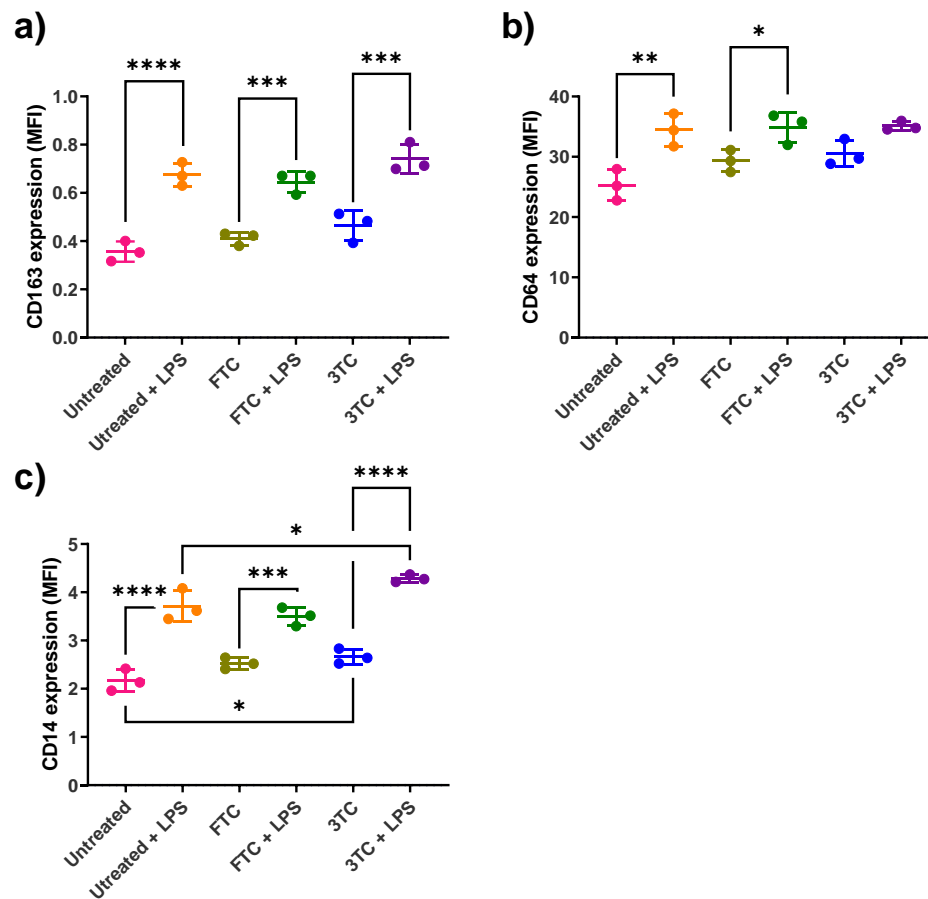


Figure 3.7: THP-1 cells exposed to FTC, and 3TC, for seven weeks and subsequent marker expression assessment after frozen for and then passaged four time before analysis. a) CD163 expression, b) CD64 expression, c) CD14 expression. Data displayed as median fluorescence intensity of $n=3$, mean (\pm standard deviation). $p < 0.0001 = ****$, $p < 0.001 = ***$, $p < 0.01 = **$ and $p < 0.05 = *$.

3TC-cultured cells had significantly lower MMP and higher CD14 expression, which was also higher when treated with LPS and compared to the LPS treated. The CD14 cells treated with LPS also didn't have a significantly higher CD64 expression as seen with the LPS treated cells.

3.3.4 MUTZ-3

3.3.4.1 Cell health and Marker expression

ROS, reduced glutathione and MMP were measured following repeat exposure of the CEM cells to FTC, 3TC and linear poly(FTC) and compared to untreated cells in order to determine the ability of the treatments to modify cell health. Intracellular ROS levels were significantly lower (18% and 21% lower respectively) in the FTC- and 3TC-cultured cells, than the untreated cells ($p < 0.01$) (Figure 3.8a). However, linear poly(FTC)-cultured cells had significantly higher ROS levels, 19% higher than the untreated ($p < 0.01$). FTC- and linear poly(FTC)-cultured THP-1 cells displayed a significantly higher MMP, 29% and 33% higher than the untreated cells ($p < 0.05$) (Figure 3.8c).

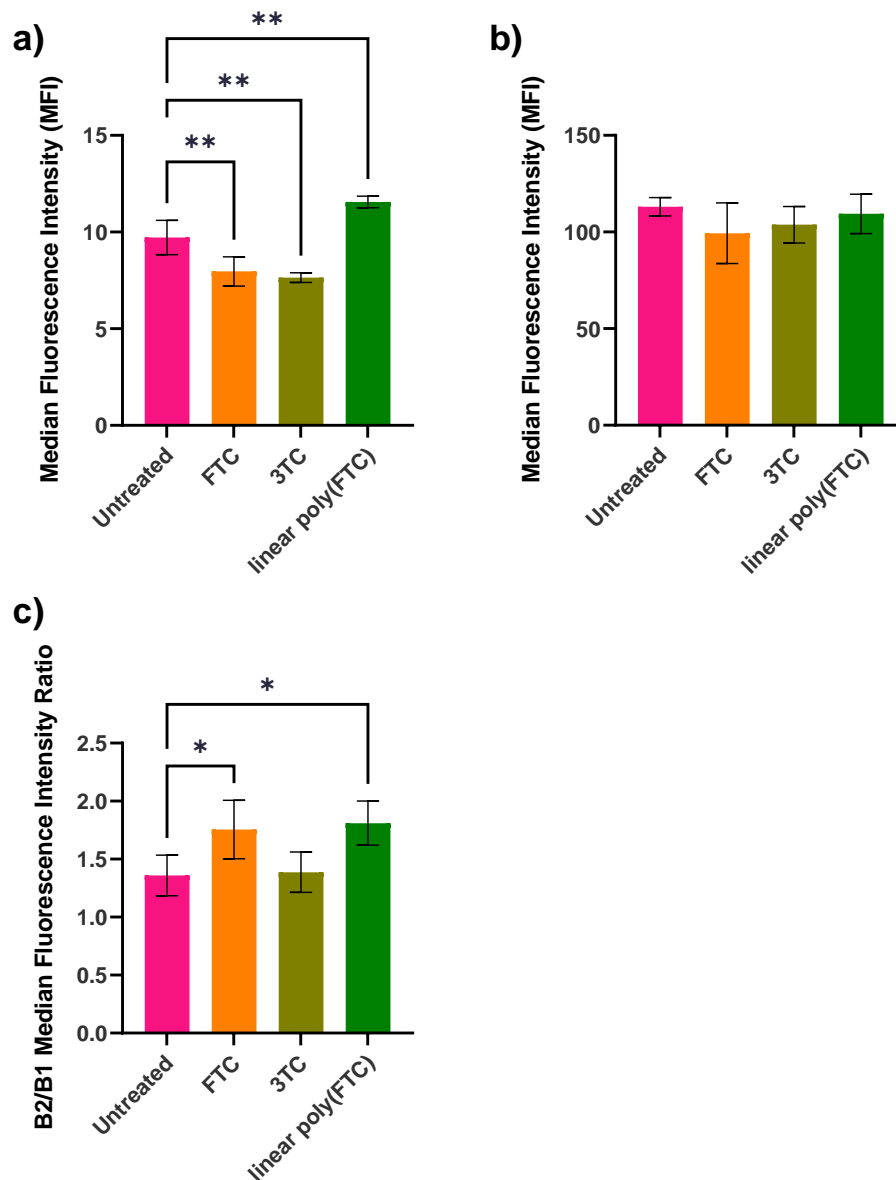


Figure 3.8: MUTZ-3 cells exposed to FTC, 3TC, and linear poly(FTC) for seven weeks and subsequent phenotypic assessment. a) Intracellular ROS, b) Intracellular reduced glutathione, c) MMP. Data displayed as median fluorescence intensity or B2/B1 median fluorescence intensity of n=4, mean (\pm standard deviation). $p < 0.0001 = ****$, $p < 0.001 = ***$, $p < 0.01 = **$ and $p < 0.05 = *$.

Marker expression of the MUTZ-3 cells was explored following exposure to FTC, 3TC and linear poly(FTC) and compared to the untreated, all cells were compared untreated and treated with a known positive control, for the MUTZ-3 cell line this was LPS or R848. The markers used were CD80, CD86, CD209, CD40, CD83, HLA-DR, CD274 and CD14. Linear poly(FTC)-cultured cells had an 89% significantly higher CD80 expression when compared to the untreated cells ($p < 0.05$) (Figure 3.9a). Linear poly(FTC)-cultured R848 treated cells had 172% higher CD86 expression when compared to the R848 cells ($p < 0.05$) (Figure 3.9b). When compared to the untreated cells, the linear poly(FTC)-cultured cells showed a 262% significantly higher CD209 expression ($p < 0.05$), the R848 treated linear poly(FTC)-cultured cells also showed a significantly higher expression of CD209, 56% higher ($p < 0.05$) (Figure 3.9c). LPS treated cells in comparison with the FTC-cultured LPS treated cells showed a 27% significantly lower CD40 expression, ($p < 0.05$) (Figure 3.9d). When compared to the R848 treated cells, the FTC-cultured R848 treated cells showed 25% significantly lower CD40 expression ($p < 0.05$) (Figure 3.9d). Linear poly(FTC)-cultured cells showed a 61% significantly lower expression of HLA-DR, when compared with the untreated cells ($p < 0.05$) (Figure 3.9f). When compared to the R848 treated cells, the linear poly(FTC)-cultured R848 treated cells had a 76% significantly lower expression of HLA-DR ($p < 0.05$) (Figure 3.9f). When compared to the LPS treated cells, the FTC-cultured LPS treated cells showed a 20% significantly lower CD274 expression ($p < 0.05$) (Figure 3.9g). R848 treated cells when compared to the 3TC-cultured, R848 treated cells showed a 13% significantly lower CD274 expression ($p < 0.01$) (Figure 3.9g). Whereas the linear poly(FTC)-cultured R848 treated cells had a 118% significantly higher CD274 expression ($p < 0.01$) (Figure 3.9g).

R848 treatment of the respective cultured cells caused a 768% ($p < 0.01$), 573% ($p < 0.05$) and 273% ($p < 0.01$) higher CD209 expression for the untreated-, FTC- and linear poly(FTC)-cultured cells respectively (Figure 3.9c). R848 treatment of the respective cultured cells also caused a 615% ($p < 0.01$), 489% ($p < 0.01$) and 203% ($p < 0.01$) higher CD40 expression for the untreated-, FTC-, and linear poly(FTC)-cultured cells respectively (Figure 3.9d). LPS treatment of the untreated cells caused a significantly higher expression of CD40, 81% ($p < 0.05$) and CD274, 69% ($p < 0.05$) (Figure 3.9g). In the untreated-, 3TC- and linear poly(FTC)-cultured cells

treated with R848 CD274 expression was also higher than the untreated counterparts, with 310% ($p<0.01$), 196% ($p<0.05$), and 516% ($p<0.01$) higher expression respectively (Figure 3.9g). HLA-DR was not significantly different between any of the cultured cells and those treated with R848, except for the linear poly(FTC)-cultured cells treated with R848, which had a 50 % significantly lower expression of HLA-DR compared to the linear poly(FTC)-cultured cells ($p<0.05$), all other cultured cells treated with R848 had non-significantly higher HLA-DR expression (Figure 3.9f). When the untreated-cultured cells were treated with R848 there was a 59% significantly higher expression of CD83, however none of the other cultured cells showed significant differences ($p<0.05$) (Figure 3.9e). The 3TC-cultured cells showed a 13% significantly higher expression of CD83 when treated with LPS ($p<0.05$) (Figure 3.9e). CD14 expression was significantly higher when the linear poly(FTC)-cultured cells were treated with both LPS and R848, 61% ($p<0.01$) and 237% ($p<0.05$) respectively (Figure 3.9h). CD14 expression was 53% higher when the 3TC-cultured cells were treated with R848 compared to the untreated 3TC-cultured cells ($p<0.05$) (Figure 3.9h).

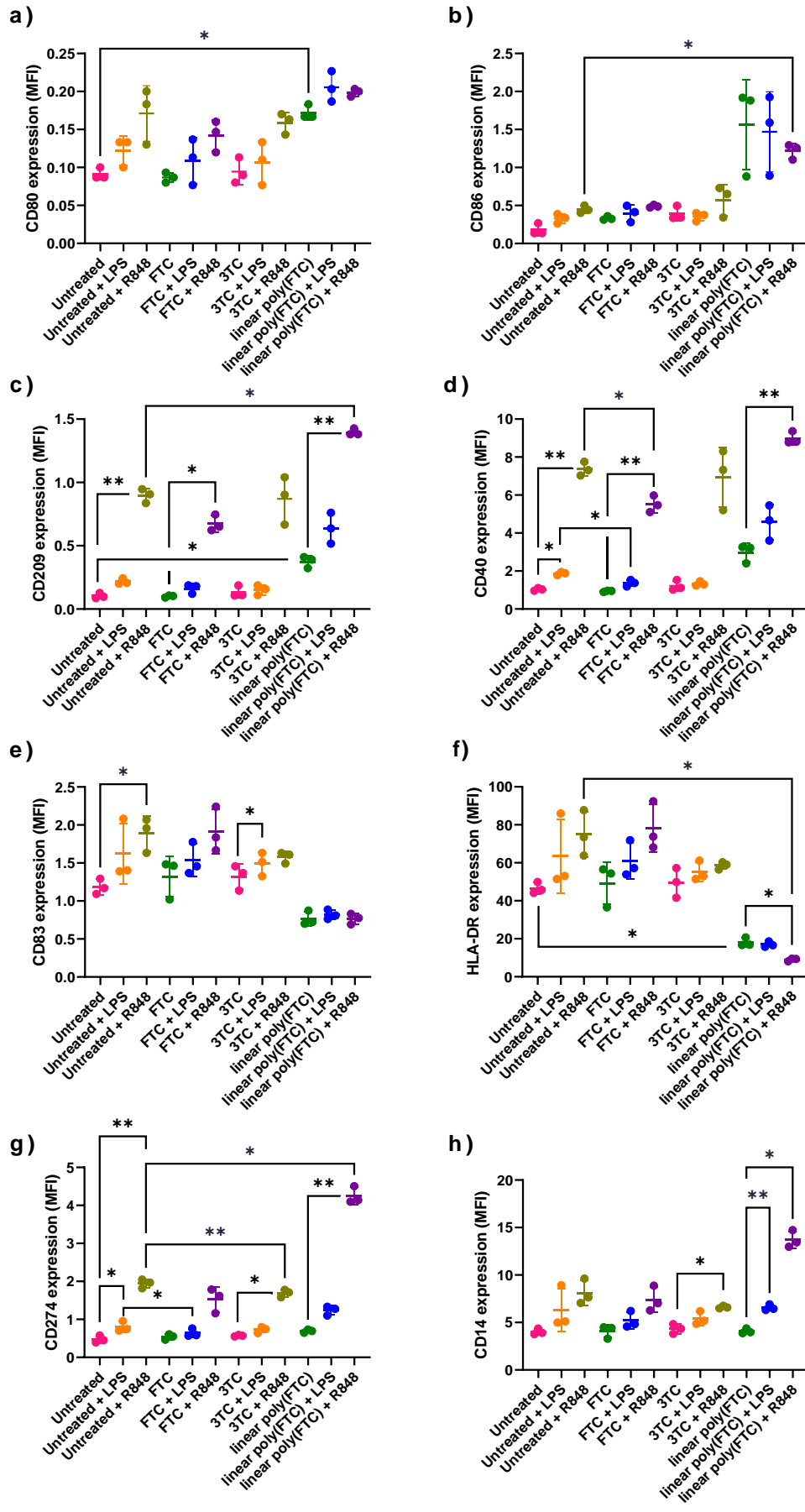


Figure 3.9: MUTZ-3 cells exposed to FTC, 3TC, and linear poly(FTC) for seven weeks and subsequent marker expression assessment. a) CD80 expression, b) CD86 expression, c) CD209 expression, d) CD40 expression, e) CD83 expression, f) HLA-DR expression, g) CD274 expression, and h) CD14 expression. Data displayed as median fluorescence intensity of n=3, mean (\pm standard deviation). $p < 0.0001 = ****$, $p < 0.001 = ***$, $p < 0.01 = **$ and $p < 0.05 = *$.

Linear poly(FTC)-cultured cells had a higher expression of CD80 and CD209 whereas a lower expression of HLA-DR, HLA-DR was further lowered following R848 treatment which differed from the higher expression seen from R848 treatment alone suggesting a reduced ability of the linear poly(FTC)-cultured cells to respond to inflammatory stimuli.

A DMSO cultured cells control was set up in order to explore if the linear poly(FTC) results were influenced by the vehicle DMSO. Cell health assessments were carried out as the same as the linear poly(FTC) cultured cells. DMSO-cultured cells displayed a 25% significantly higher MMP when compared with the untreated cells ($P < 0.001$), whereas the control compound valinomycin showed a 51% significantly lower MMP ($p < 0.0001$) (Figure 3.10c). A decrease in the B2/B1 median is indicative of membrane depolarisation.

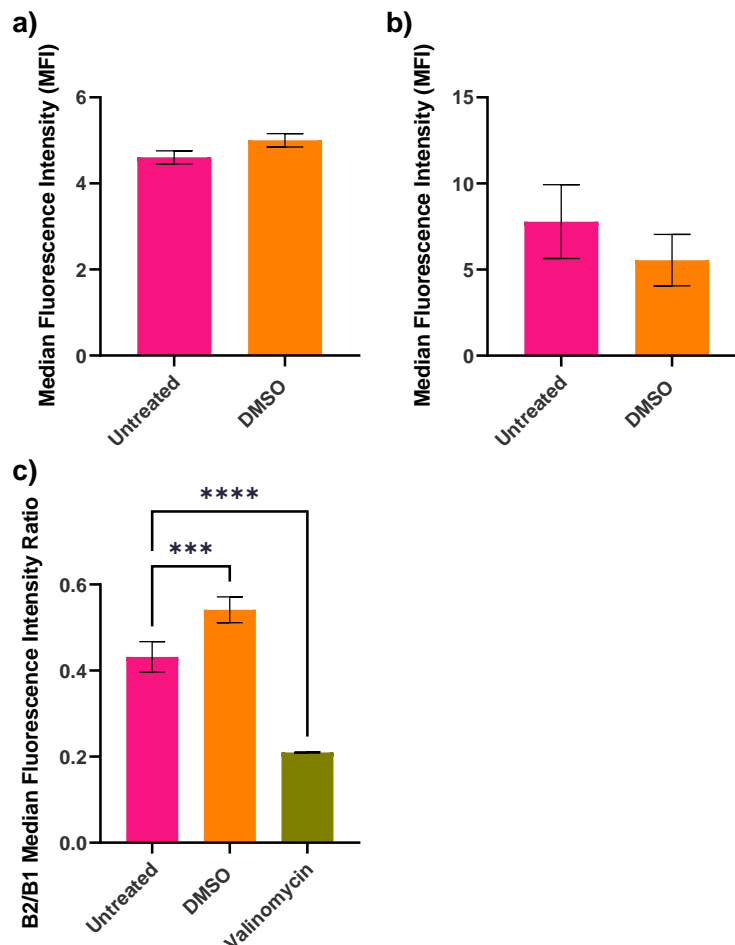
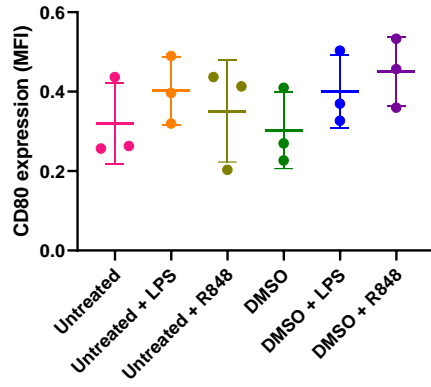


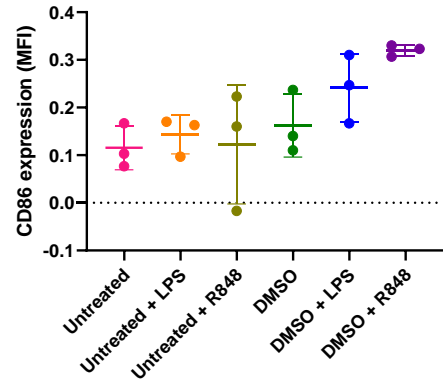
Figure 3.10: MUTZ-3 cells exposed to DMSO for seven weeks and subsequent phenotypic assessment. a) Intracellular ROS, b) Intracellular reduced glutathione, c) MMP. Data displayed as median fluorescence intensity or B2/B1 median fluorescence intensity of n=4, mean (\pm standard deviation). $p < 0.0001 = ****$, $p < 0.001 = ***$, $p < 0.01 = **$ and $p < 0.05 = *$.

The DMSO control cultured cells were also explored in the same marker expression assay that was used for the linear poly(FTC) cultured cells. The DMSO-cultured R848 treated cells had a significantly higher expression of CD209 when compared to the DMSO-cultured cells (percentage unable to be calculated due to the negative value as a result of isotype control correction), however the untreated and untreated R848 treated cells were not significantly different ($p < 0.05$) (Figure 3.11c). Both the untreated- and DMSO-cultured R848 treated cells had higher expression of CD40 when compared their untreated counter parts, with 155% and 188% higher expression respectively ($p < 0.05$) (Figure 3.11d). The DMSO-cultured R848 treated cells had a 64% significantly higher expression of CD274 when compared to the DMSO-cultured cells, however the untreated and untreated R848 treated cells were not significantly different ($p < 0.01$) (Figure 3.11g). No other significant alterations were seen for any of the markers assessed in the MUTZ-3 panel for the DMSO-cultured cells (Figure 3.11).

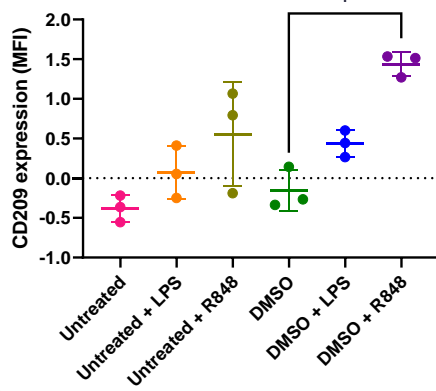
a)



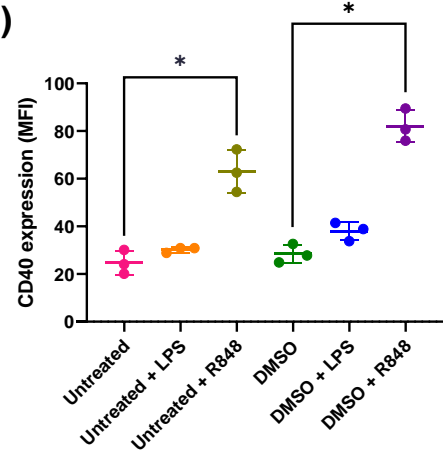
b)



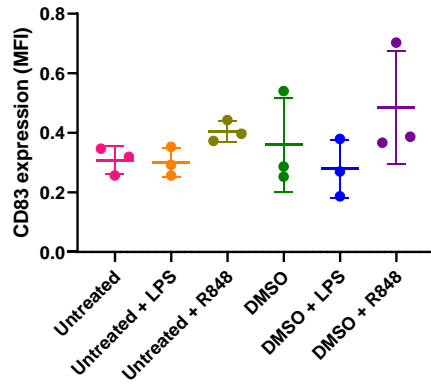
c)



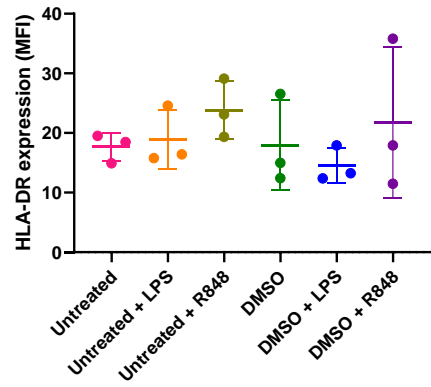
d)



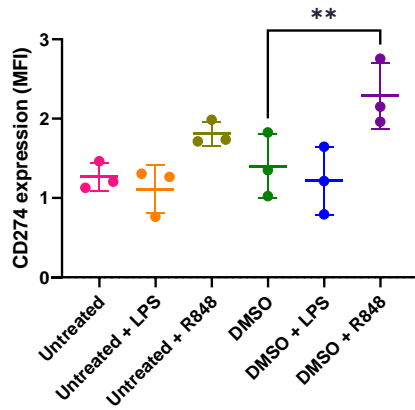
e)



f)



g)



h)

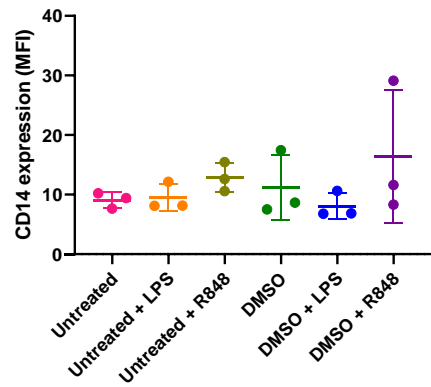


Figure 3.11: MUTZ-3 cells exposed to DMSO, for seven weeks and subsequent marker expression assessment. a) CD80 expression, b) CD86 expression, c) CD209 expression, d) CD40 expression, e) CD83 expression, f) HLA-DR expression, g) CD274 expression, and h) CD14 expression. Data displayed as median fluorescence intensity of n=3, mean (\pm standard deviation). $p < 0.0001 = ****$, $p < 0.001 = ***$, $p < 0.01 = **$ and $p < 0.05 = *$.

DMSO did not appear to cause the changes seen from the linear poly(FTC)-cultured cells.

Table 3.2: Summary of figures 3.1, 3.3, 3.6, 3.9 and 3.11 and the Cell Health changes across the 4 cell lines tested. \uparrow indicates a higher level when compared to the untreated and \downarrow indicates a lower level when compared to the untreated.

Cell line	Culture treatment	ROS levels	Reduced glutathione levels	MMP
CEM	UT	N/A	N/A	N/A
	FTC	\uparrow	-	-
	3TC	\uparrow	-	-
KU812	UT	N/A	N/A	N/A
	FTC	\uparrow	-	\downarrow
	3TC	-	-	\downarrow
THP-1	UT	N/A	N/A	N/A
	FTC	-	-	-
	3TC	-	-	\downarrow
MUTZ-3	UT	N/A	N/A	N/A
	FTC	\downarrow	-	\uparrow
	3TC	\downarrow	-	-
	Linear poly(FTC)	\uparrow	-	\uparrow
	DMSO	-	-	\uparrow

Table 3.3: Summary of figures 3.2, 3.4, 3.7, 3.10 and 3.12 and the marker expression changes across the 4 cell lines. \uparrow indicates a higher expression and \downarrow indicates a lower expression $p < 0.0001 = ****$, $p < 0.001 = ***$, $p < 0.01 = **$ and $p < 0.05 = *$.

Cell Line	Comparison Culture/treatment	Expression change treatment/Culture	Marker expression changes
CEM	UT	PHA	-
		FTC	-
		3TC	CD69 \uparrow *
	UT + PHA	FTC + PHA	-
		3TC + PHA	-
		FTC	CD69 \uparrow *
3TC	3TC + PHA	CD69 \uparrow **	
KU812	UT	C5a	-
		Cl/PMA	-
		FTC	CD63 \downarrow **

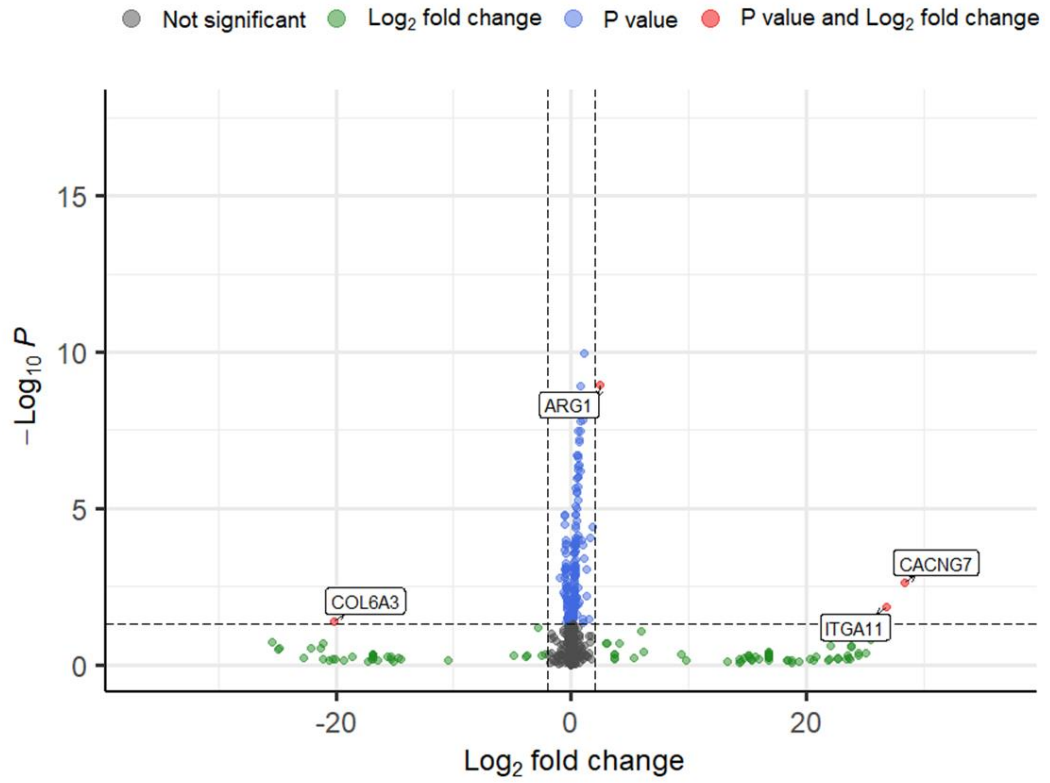
		3TC	CD63 ↓ ** CD203c ↑ **
	UT + C5a	FTC + C5a	CD63 ↓ * CD203c ↓ * CD164 ↓ *
		3TC + C5a	CD63 ↓ **
	UT + CI/PMA	FTC + CI/PMA	CD164 ↑ **
		3TC + CI/PMA	-
	FTC	FTC + C5a	CD63 ↓ * CD203c ↓ *
		FTC + CI/PMA	-
	3TC	3TC + C5a	CD63 ↓ ** CD203c ↓ **
		3TC + CI/PMA	-
	THP-1	UT	LPS
FTC			-
3TC			CD14 ↑ *
UT + LPS		FTC + LPS	-
		3TC + LPS	CD14 ↑ *
FTC		FTC + LPS	CD163 ↑ *** CD64 ↑ * CD14 ↑ ***
3TC		3TC + LPS	CD163 ↑ *** CD14 ↑ ****
MUTZ-3		UT	LPS
	R848		CD209 ↑ ** CD40 ↑ ** CD83 ↑ * CD274 ↑ **
	FTC		
	3TC		
	linear poly(FTC)		CD80 ↑ * CD209 ↑ * HLA-DR ↓ *
	DMSO		
	UT + LPS	FTC + LPS	CD40 ↑ * CD274 ↓ *
		3TC + LPS	
		linear poly(FTC) + LPS	
		DMSO + LPS	
	UT + R848	FTC + R848	CD40 ↑ *
		3TC + R848	CD274 ↓ **
linear poly(FTC) + R848		CD86 ↑ * CD209 ↑ * CD40 ↑ * HLA-DR ↓ * CD274 ↑ *	

		DMSO + R848	
	FTC	FTC + LPS	
		FTC + R848	CD209 ↑ *
	3TC	3TC + LPS	CD83 ↑ *
		3TC + R848	CD274 ↑ * CD14 ↑ *
	linear poly(FTC)	linear poly(FTC) + LPS	CD14 ↑ **
		linear poly(FTC) + R848	CD209 ↑ ** CD40 ↑ ** HLA-DR ↓ * CD274 ↑ ** CD14 ↑ *
	DMSO	DMSO + LPS	
		DMSO + R848	CD209 ↑ * CD40 ↑ * CD274 ↑ **

3.3.4.2 nCounter analysis

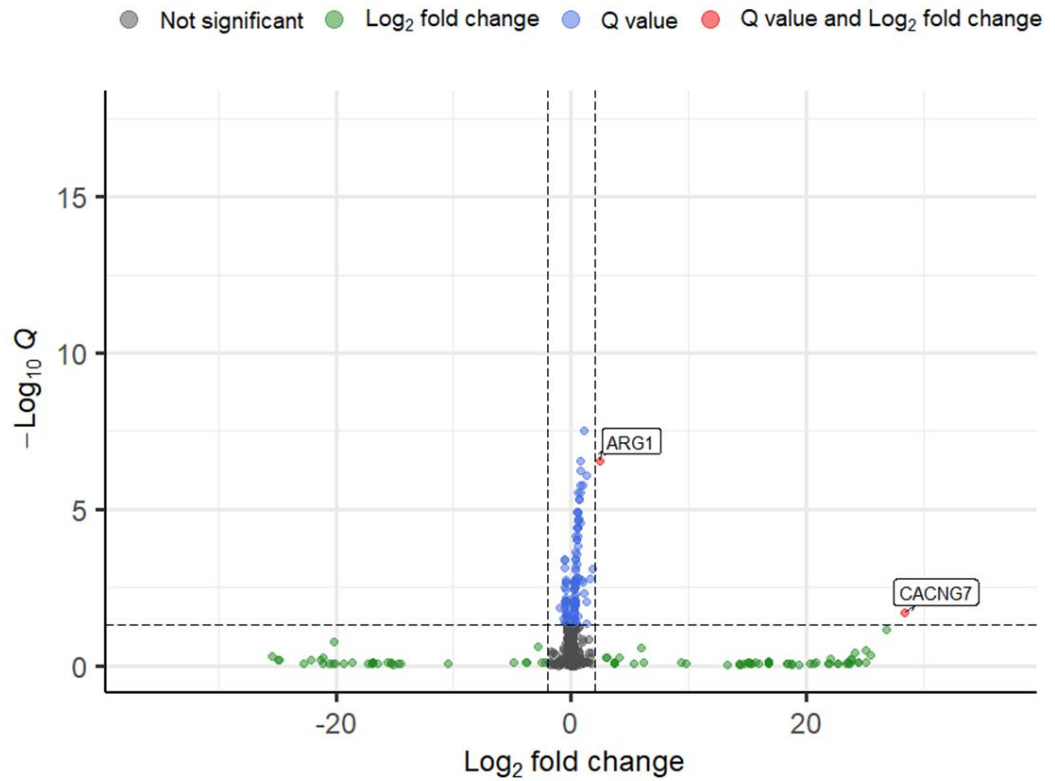
Following the interesting results seen for the marker expression assessment in the MUTZ-3 cell line, they were taken forward into nCounter analysis to explore if any changes are seen in gene expression using the metabolic pathways panel. Volcano plots were created for comparisons between the cultured and treated cells. When the FTC-cultured cells were compared to the untreated cells using a q value cut off of 0.05 the genes which had a $\log_2FC > 2$ and therefore a significantly higher expression are: arginase 1 (ARG1), and calcium voltage-gated channel auxiliary subunit gamma (CACNG) 7 (Figure 3.12b). When using a p < cut off of 0.05 the additional genes which had a $\log_2FC > 2$ and therefore a significantly lower expression are: integrin subunit alpha 11 (ITGA11), whereas collagen type VI alpha 3 chain (COL6A3) has a $\log_2FC < -2$ (Figure 3.12a).

a)



total = 748 variables

b)

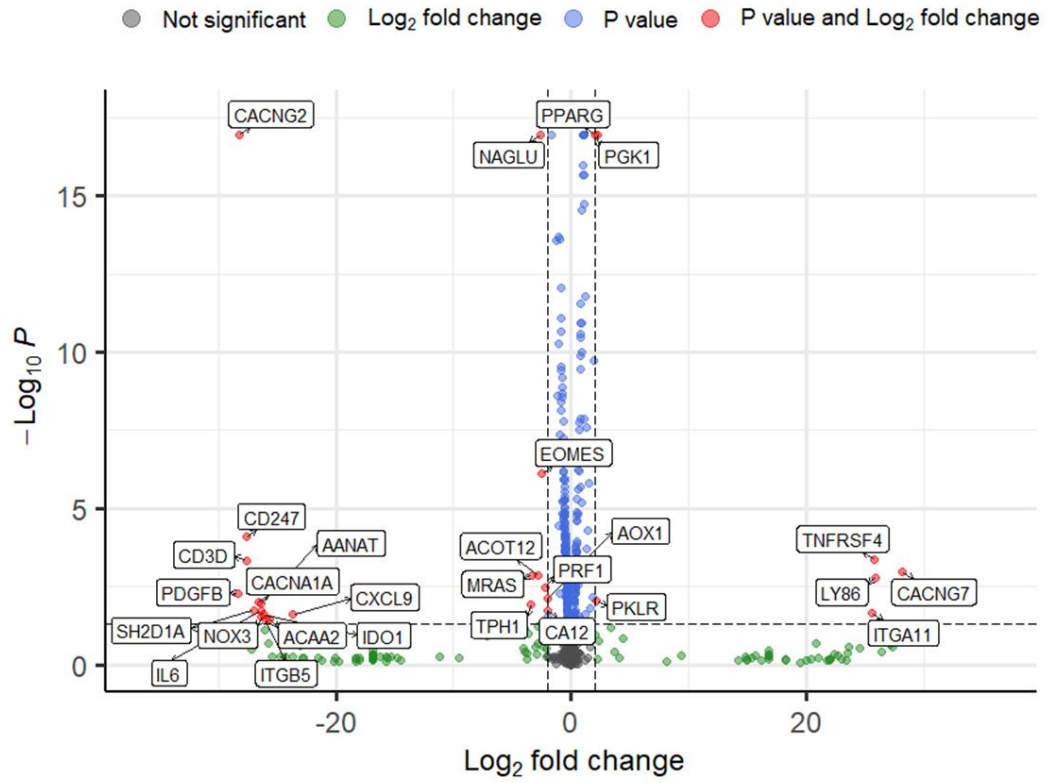


total = 748 variables

Figure 3.12: Untreated vs FTC a) p value 0.05, and b) q value 0.05

When the 3TC-cultured cells were compared to the untreated cells using a q value cut off of 0.05 the genes which had a $\log_2FC > 2$ and therefore a significantly higher expression are: CACNG7, lymphocyte antigen 86 (LY86), platelet derived growth factor subunit B (PDGFB), phosphoglycerate kinase 1 (PGK1), pyruvate kinase L/R (PKLR), peroxisome proliferator activated receptor gamma (PPARG), and TNF receptor superfamily member 4 (TNFRSF4) (Figure 3.13b). Whereas the following genes had an $q \text{ value} < 0.05$ and $\log_2FC < -2$ and therefore a significantly lower expression are: aralkylamine N-acetyltransferase (AANAT), acyl-CoA thioesterase 12 (ACOT12), aldehyde oxidase 1 (AOX1), calcium voltage-gated channel subunit alpha1 A (CACNA1A), CACNG2, CD247, CD3D, eomesodermin (EOMES), muscle RAS oncogene homolog (MRAS), N-acetyl-alpha-glucosaminidase (NAGLU), perforin 1 (PRF1), and tryptophan hydroxylase 1 (TPH1) (Figure 3.13b). When using a p value cut off of 0.05 the only additional gene which had a $\log_2FC > 2$ and therefore a significantly higher expression was ITGA11 (Figure 3.13a). Whereas $p \text{ value} < 0.05$ and $\log_2FC < -2$ additional genes and therefore a significantly lower expression are: acetyl-CoA acyltransferase 2 (ACAA2), carbonic anhydrase 12 (CA12), CXCL9, indoleamine 2,3-dioxygenase 1 (IDO1), IL-6, integrin subunit beta 5 (ITGB5), NADPH oxidase 3 (NOX3), and SH2 domain containing 1A (SH2D1A) (Figure 3.13a).

a)



b)

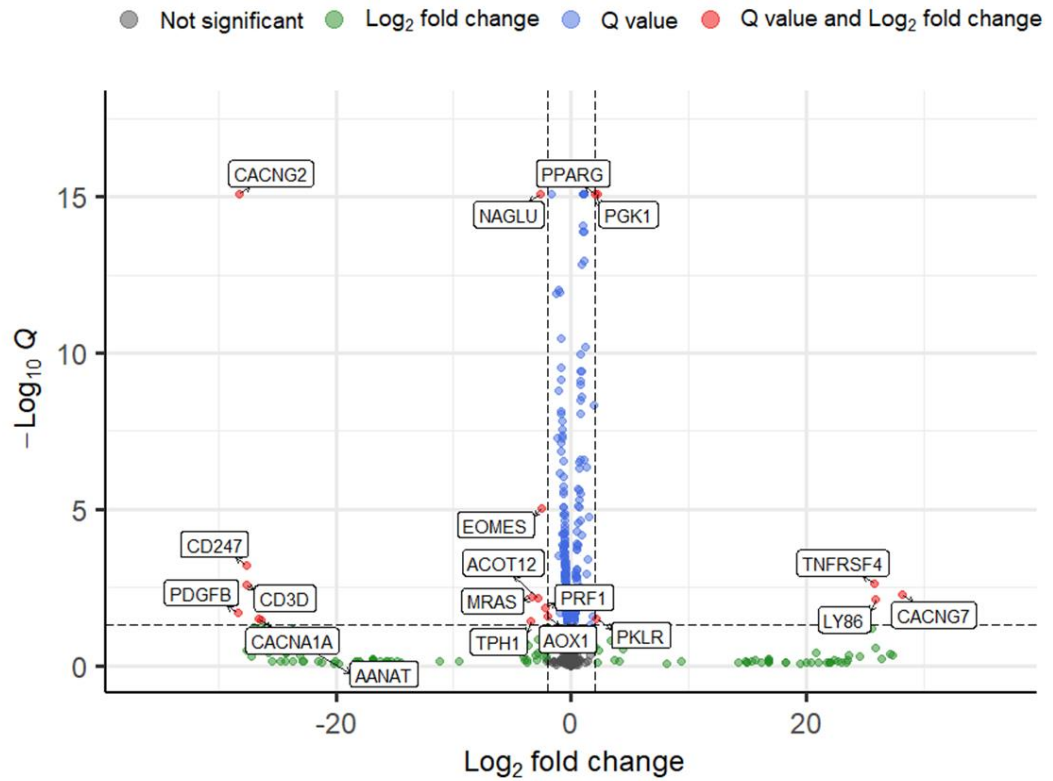
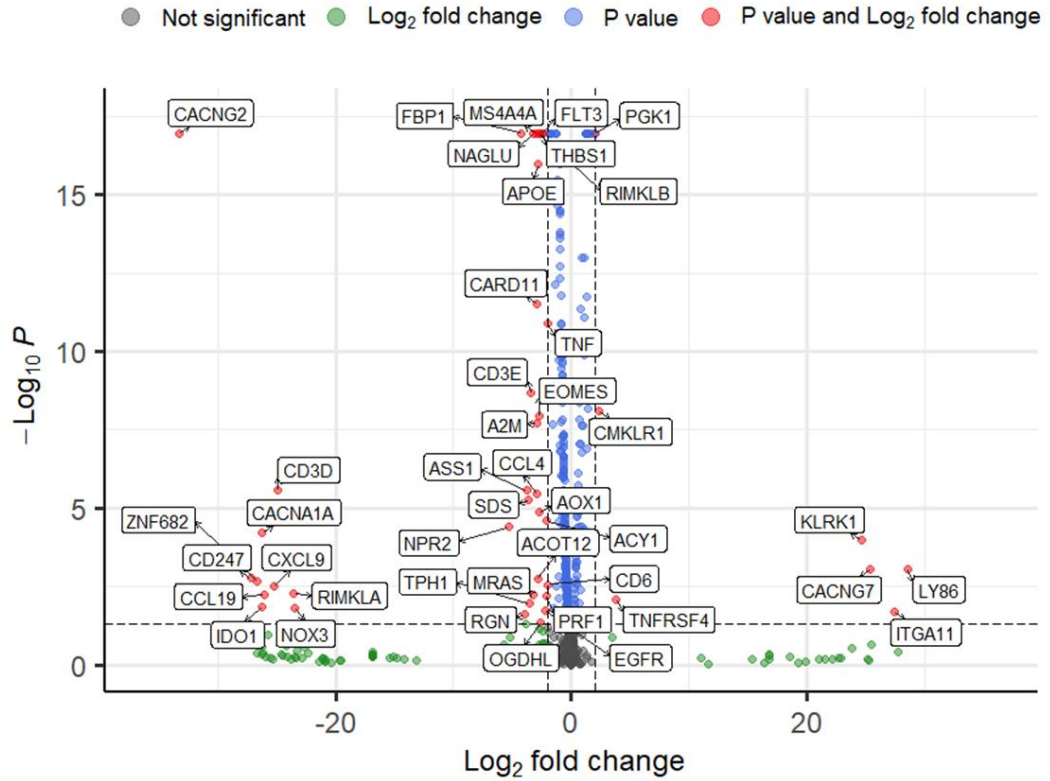


Figure 3.13: Untreated vs 3TC a) p value 0.05, and b) q value 0.05

When the linear poly(FTC)-cultured cells were compared to the untreated cells using a q value cut off of 0.05 the genes which had a $\log_2FC > 2$ and therefore a significantly higher expression are: CACNG7, chemerin chemokine-like receptor 1 (CMKLR1), ITGA11, killer cell lectin like receptor K1 (KLRK1), LY86, PGK1, and TNFRSF4 (Figure 3.14b). However, the following genes had an q value < 0.05 and $\log_2FC < -2$ and therefore a significantly lower expression: alpha-2-macroglobulin (A2M), ACOT12, aminoacylase 1 (ACY1), AOX1, apolipoprotein E (APOE), argininosuccinate synthase 1 (ASS1), CACNA1A, CACNG2, caspase recruitment domain family member 11 (CARD11), CCL19, CCL4, CD247, CD3D, CD3E, CD6, CXCL9, epidermal growth factor receptor (EGFR), EOMES, fructose-bisphosphatase 1 (FBP1), fms related tyrosine kinase 3 (FLT3), IDO1, MRAS, membrane spanning 4-domains A4A (MS4A4A), NAGLU, NOX3, natriuretic peptide receptor 2 (NPR2), PRF1, ribosomal modification protein rimK like family member (RIMKL) A, RIMKLB, serine dehydratase (SDS), thrombospondin 1 (THBS1), TNF, TPH1, and zinc finger protein 682 (ZNF682) (Figure 3.14b). When using a p value cut off of 0.05 the additional genes which had a $\log_2FC < -2$ and therefore a significantly lower expression are: oxoglutarate dehydrogenase like (OGDHL), and regucalcin (RGN) (Figure 3.14a).

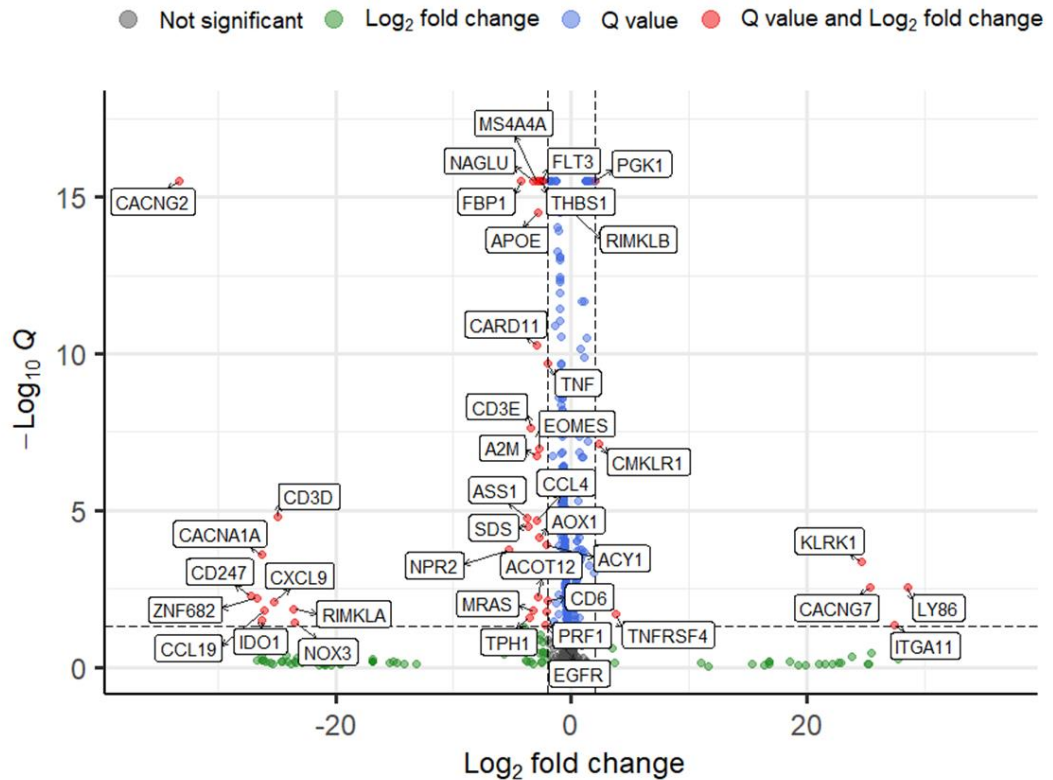
When looking at the gene expression in the Untreated vs any of the three drug-cultured cells both CACNG7 and ITGA11 genes always had a higher expression in the drug-cultured cells ($\log_2FC > 2$, $p > 0.05$) (Figures 3.12-3.14).

a)



total = 748 variables

b)

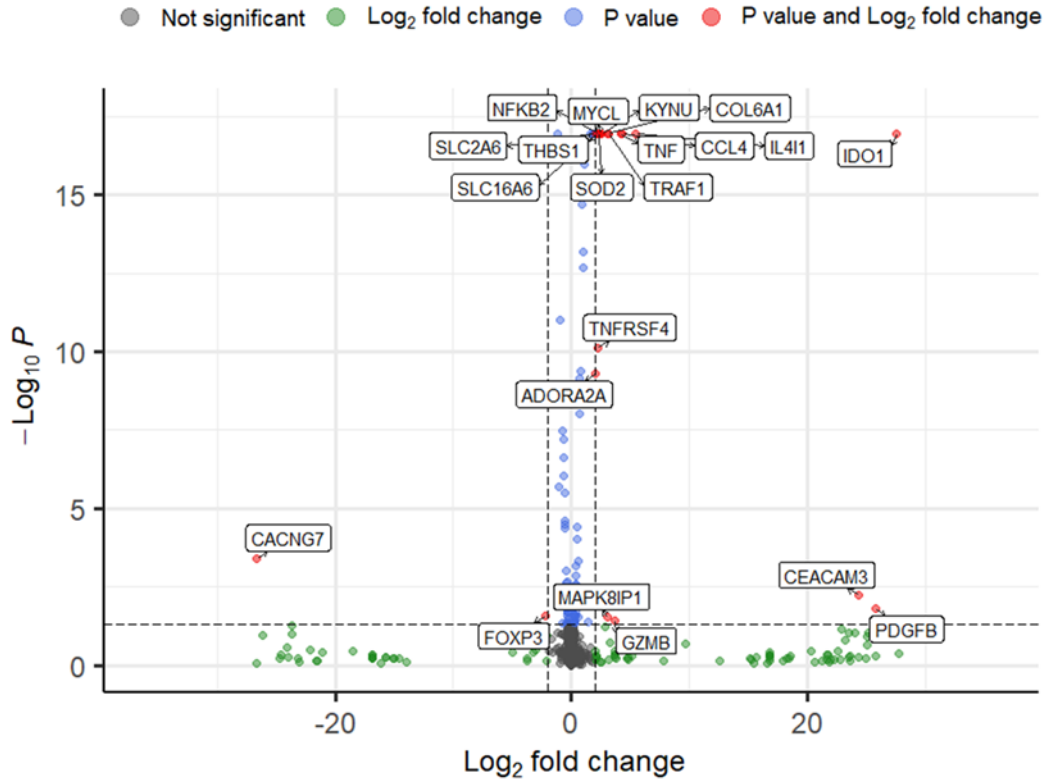


total = 748 variables

Figure 3.14: Untreated vs linear poly(FTC) a) p value 0.05, and b) q value 0.05

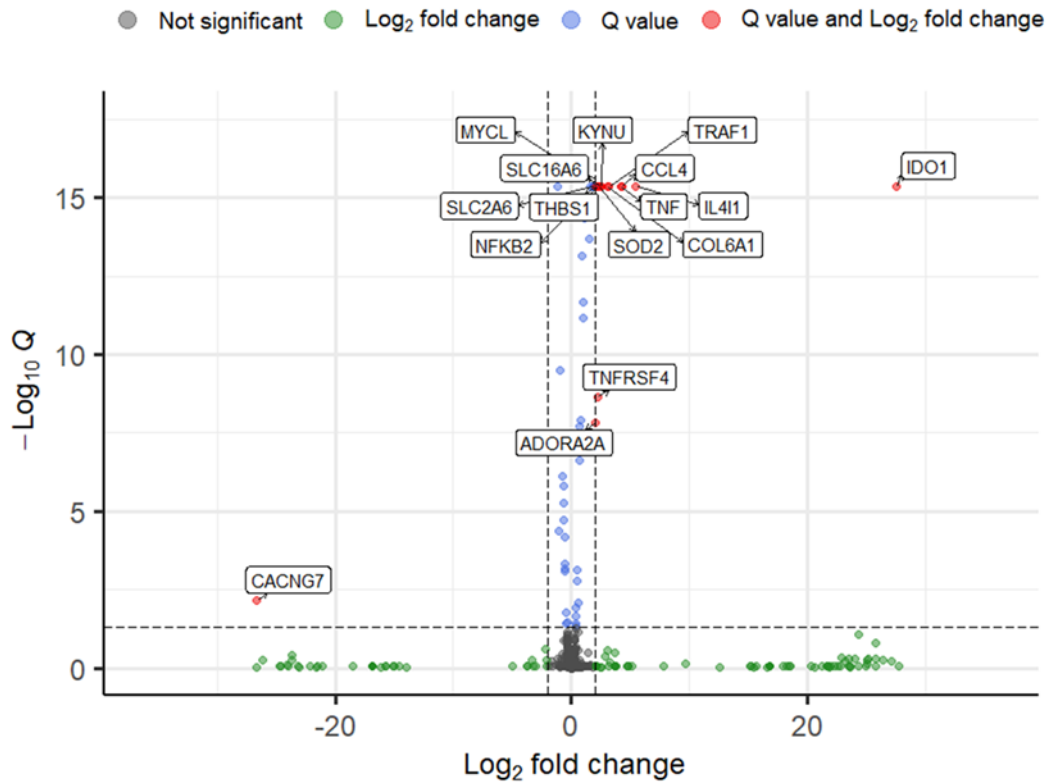
When the R848 treated cells were compared to the untreated cells using a q value cut off of 0.05 the genes which had a $\log_2FC > 2$ and therefore a significantly higher expression are: adenosine A2a receptor (ADORA2A), CCL4, collagen type VI alpha 1 chain (COL6A1), IDO1, IL-4 induced 1 (IL-4I1), kynureninase (KYNU), MYCL proto-oncogene, bHLH transcription factor (MYCL), nuclear factor kappa B subunit 2 (NFKB2), solute carrier family 16 member 6 (SLC16A6), solute carrier family 2 member 6 (SLC2A6), superoxide dismutase 2 (SOD2), THBS1, TNF, TNFRSF4, and TNF receptor associated factor 1 (TRAF1) (Figure 3.15b). The following genes had a q value < 0.05 and $\log_2FC < -2$ and therefore a significantly lower expression of: CACNG7 (Figure 3.15b), and when using $p < 0.05$ forkhead box P3 (FOXP3) is also included (Figure 3.15a). When using a p value cut off of 0.05 the additional genes which had a $\log_2FC > 2$ and therefore a significantly higher expression: carcinoembryonic antigen related cell adhesion molecule 3 (CEACAM3), granzyme B (GZMB), mitogen-activated protein kinase 8 interacting protein 1 (MAPK8IP1), and PDGFB (Figure 3.15a).

a)



total = 748 variables

b)

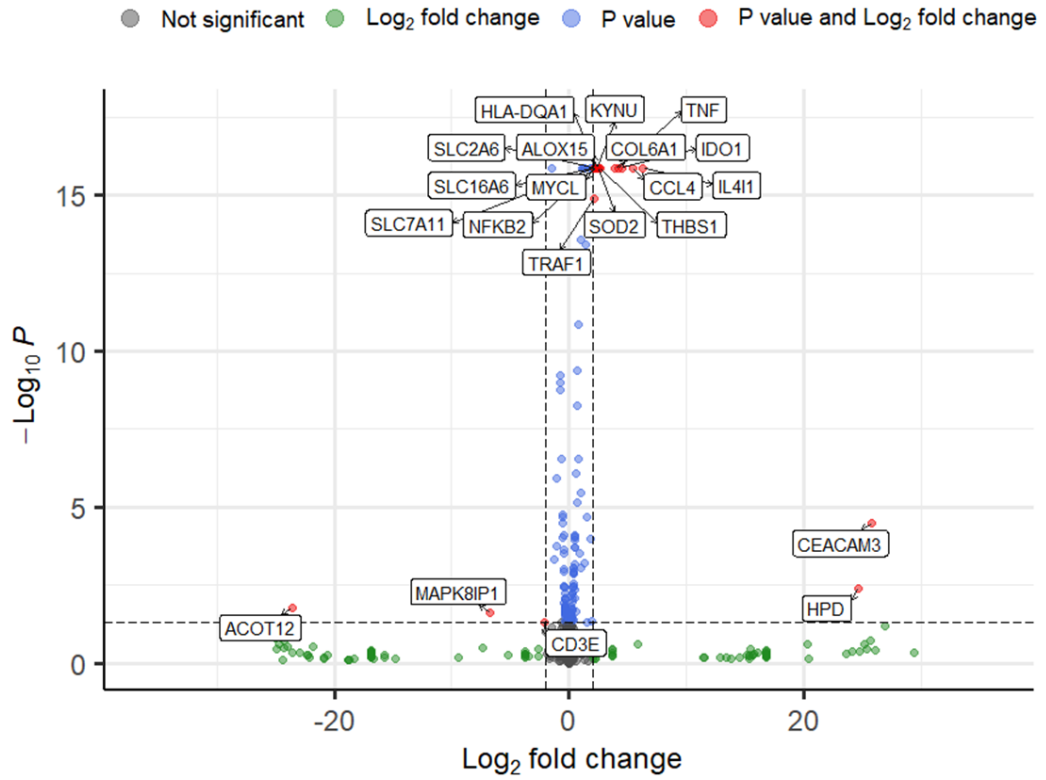


total = 748 variables

Figure 3.15: Untreated vs R848 a) p value 0.05, and b) q value 0.05

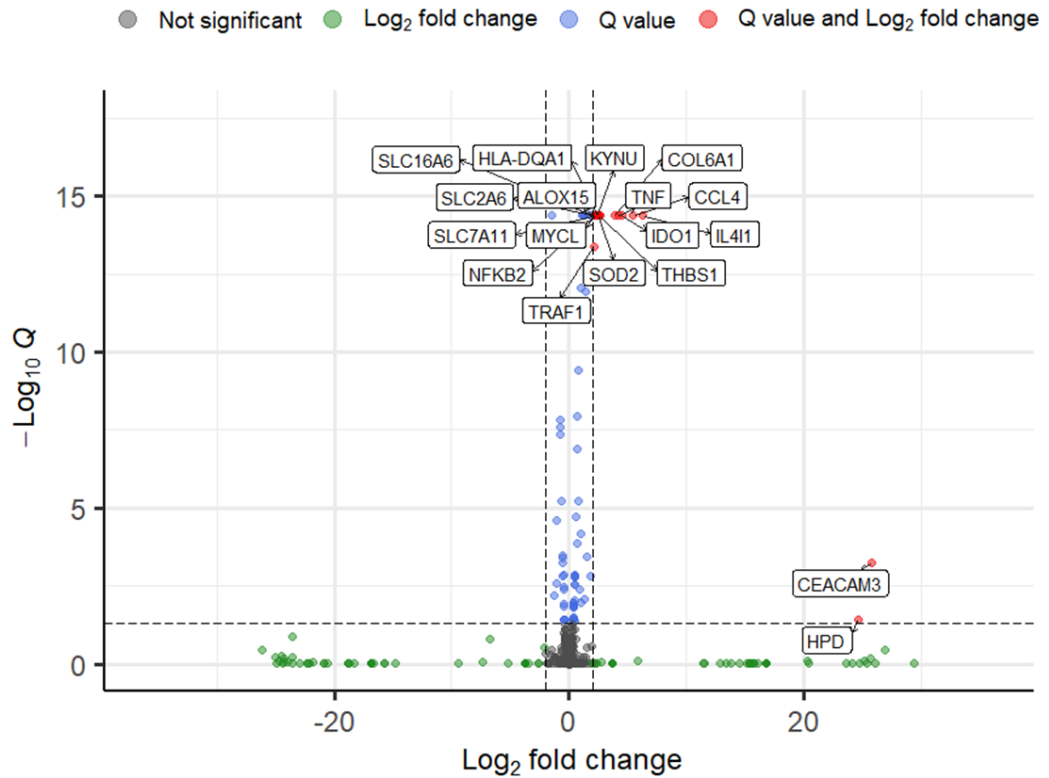
When the FTC-cultured R848 treated cells were compared to the FTC-cultured cells using a q value cut off of 0.05 the genes which had a $\log_2FC > 2$ and therefore a significantly higher expression are: arachidonate 15-lipoxygenase (ALOX15), CCL4, CEACAM3, COL6A1, major histocompatibility complex, class II, DQ alpha 1 (HLA-DQA1), 4-hydroxyphenylpyruvate dioxygenase (HPD), IDO1, IL-4I1, KYNU, MYCL, NFKB2, SLC16A6, SLC2A6, solute carrier family 7 member 11 (SLC7A11), SOD2, THBS1, TNF, and TRAF1 (Figure 3.16b). When using a p value cut off of 0.05 the additional genes which had a $\log_2FC < -2$ and therefore a significantly lower expression are: ACOT12, CD3E, and MAPK8IP1 (Figure 3.16a).

a)



total = 748 variables

b)

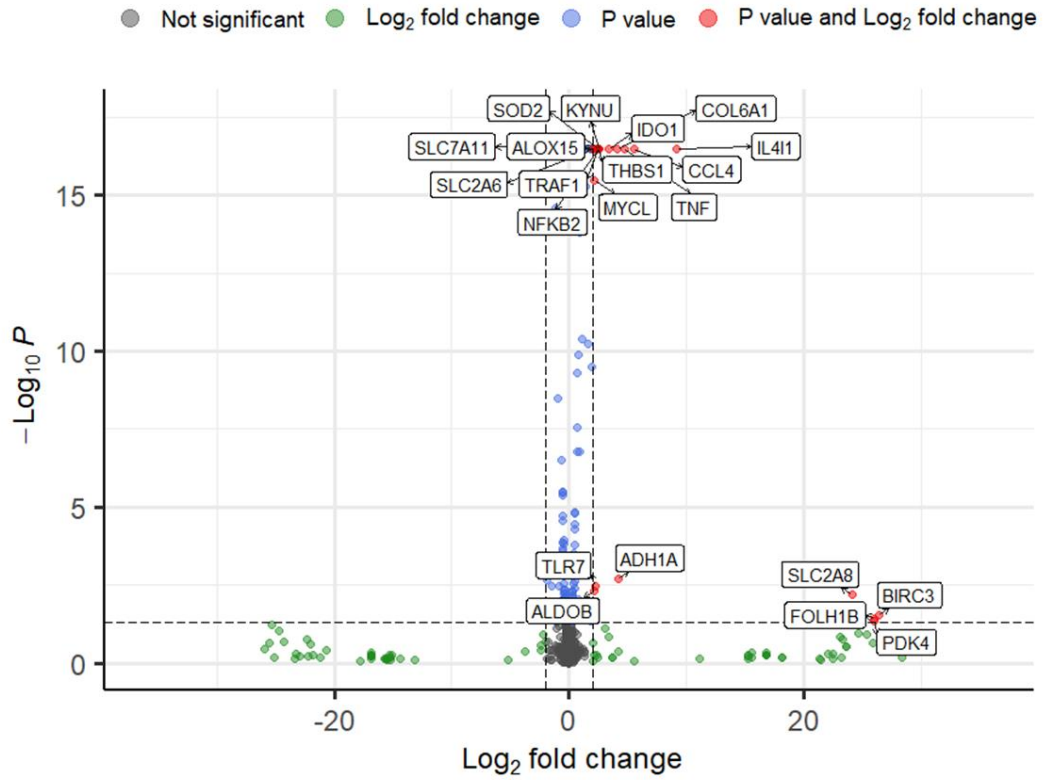


total = 748 variables

Figure 3.16: FTC vs FTC and R848 a) p value 0.05, and b) q value 0.05

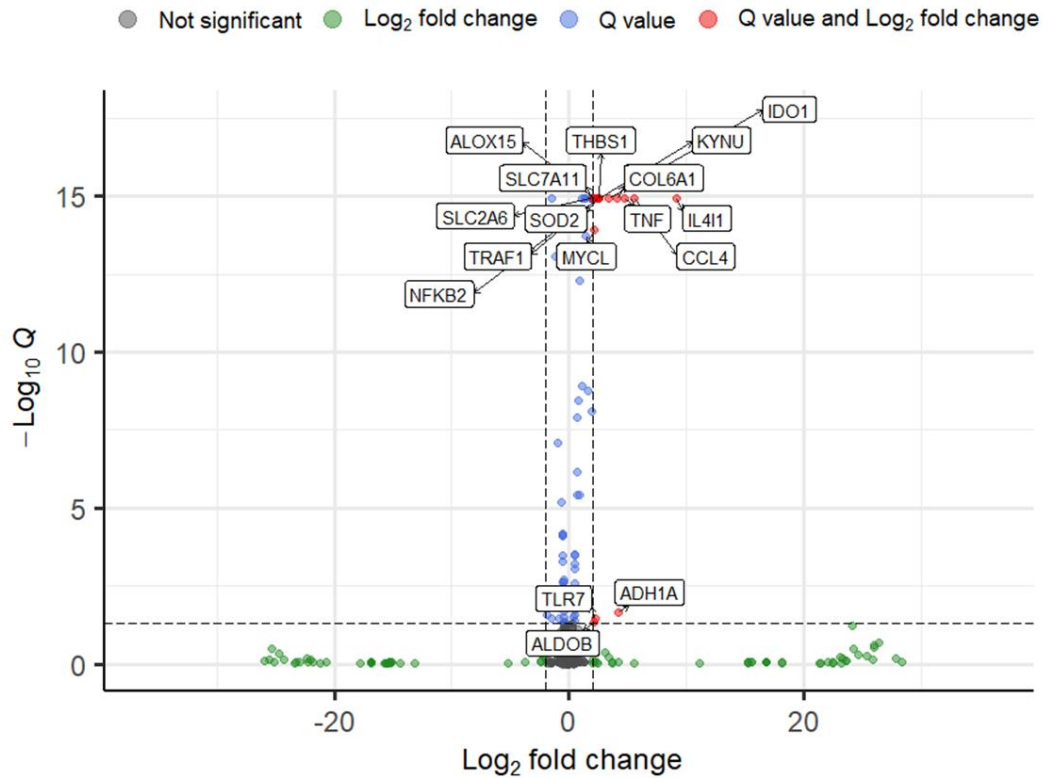
When the 3TC-cultured R848 treated cells were compared to the 3TC-cultured cells using a q value cut off of 0.05 the genes which had a $\log_2FC > 2$ and therefore a significantly higher expression are: alcohol dehydrogenase 1A (class I) alpha polypeptide (ADH1A), aldolase, fructose-bisphosphate B (ALDOB), ALOX15, CCL4, COL6A1, IDO1, IL-4I1, KYNU, MYCL, NFKB2, SLC2A6, SLC7A11, SOD2, THBS1, TLR-7, TNF, and TRAF1 (Figure 3.17b). When using a p value cut off of 0.05 the additional genes which had a $\log_2FC > 2$ and therefore a significantly higher expression are: baculoviral IAP repeat containing 3 (BIRC3), folate hydrolase 1B (FOLH1B), pyruvate dehydrogenase kinase 4 (PDK4), and solute carrier family 2 member 8 (SLC2A8) (Figure 3.17a).

a)



total = 748 variables

b)



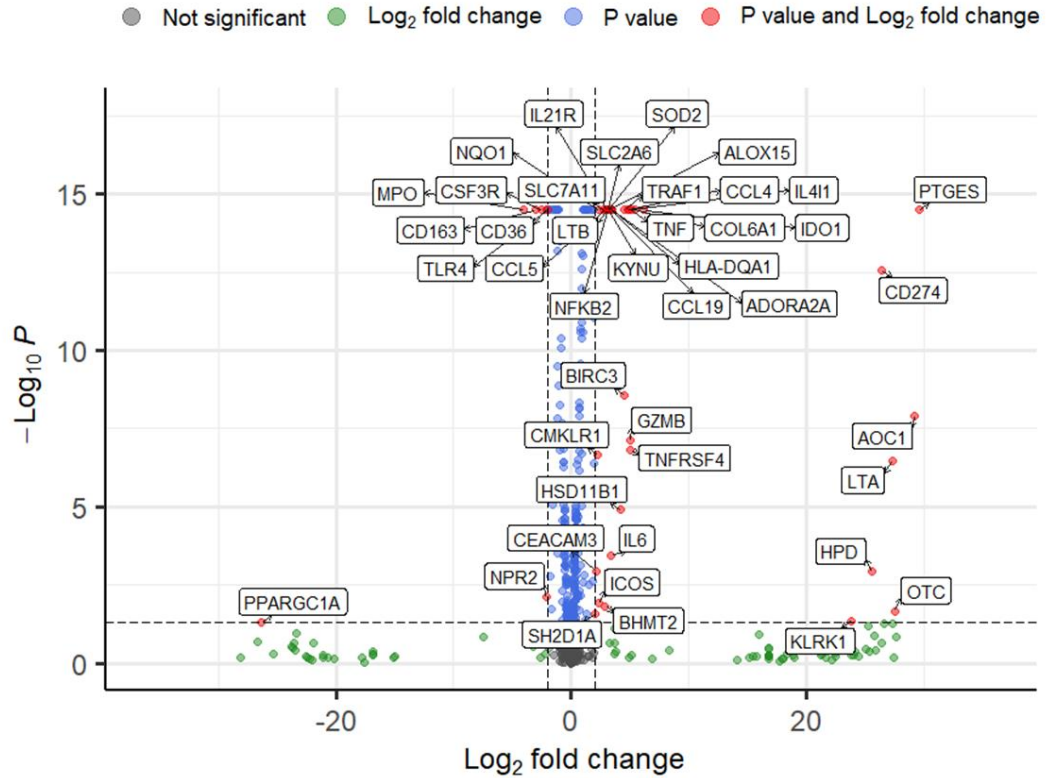
total = 748 variables

Figure 3.17: 3TC vs 3TC and R848 a) p value 0.05, and b) q value 0.05

When the linear poly(FTC)-cultured R848 treated cells were compared to the linear poly(FTC)-cultured cells using a q value cut off of 0.05 the genes which had a $\log_2FC > 2$ and therefore a significantly higher expression are: ADORA2A, ALOX15, amine oxidase copper containing 1 (AOC1), betaine--homocysteine S-methyltransferase 2 (BHMT2), BIRC3, CCL19, CCL4, CCL5, CD274, CEACAM3, CMKLR1, COL6A1, colony stimulating factor 3 receptor (CSF3R), GZMB, HLA-DQA1, HPD, hydroxysteroid 11-beta dehydrogenase 1 (HSD11B1), inducible T-cell costimulator (ICOS), IDO1, IL-21 receptor, IL-4I1, IL-6, KYNU, lymphotoxin alpha (LTA), lymphotoxin beta (LTB), NFKB2, NAD(P)H quinone dehydrogenase 1 (NQO1), prostaglandin E synthase (PTGES), SLC2A6, SLC7A11, SOD2, TNF, TNFRSF4, and TRAF1 (Figure 3.18b). Whereas the following genes which had a q value < 0.05 and $\log_2FC < -2$ and therefore a significantly lower expression are: CD163 CD163, CD36, myeloperoxidase (MPO), NPR2, and TLR-4 (Figure 3.18b). When using a p value cut off of 0.05 the additional genes which had a $\log_2FC > 2$ and therefore a significantly higher expression are: KLRK1, ornithine carbamoyltransferase (OTC), and SH2D1A, and PPARG coactivator 1 alpha (PPARGC1A) is the only genes with $\log_2FC < -2$ (Figure 3.18a).

When looking at the untreated or any of the three drug-cultured cells vs the corresponding R848 treatment you consistently observe higher expression of the genes: CCL4, COL6A1, IDO1, IL-4I1, KYNU, NFKB2, SLC2A6, SOD2, TNF, and TRAF1 in the R848 treated ($\log_2FC > 2$, $p < 0.05$) (Figures 3.16-3.18).

a)



b)

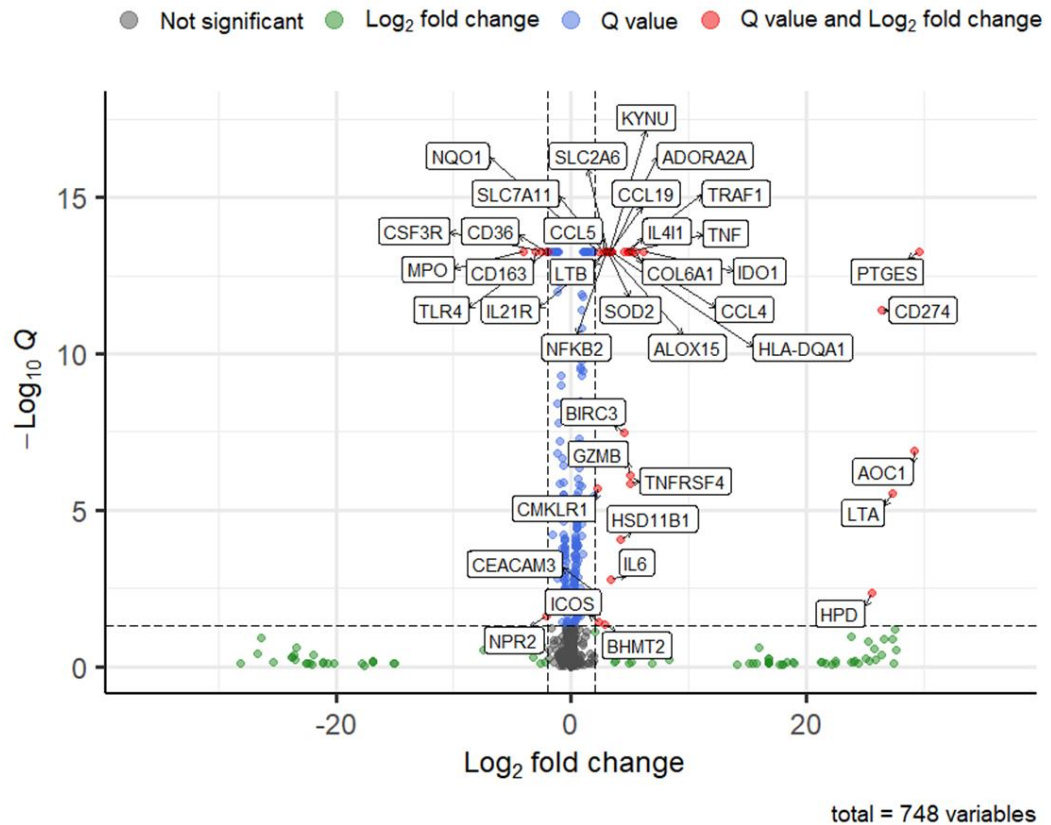
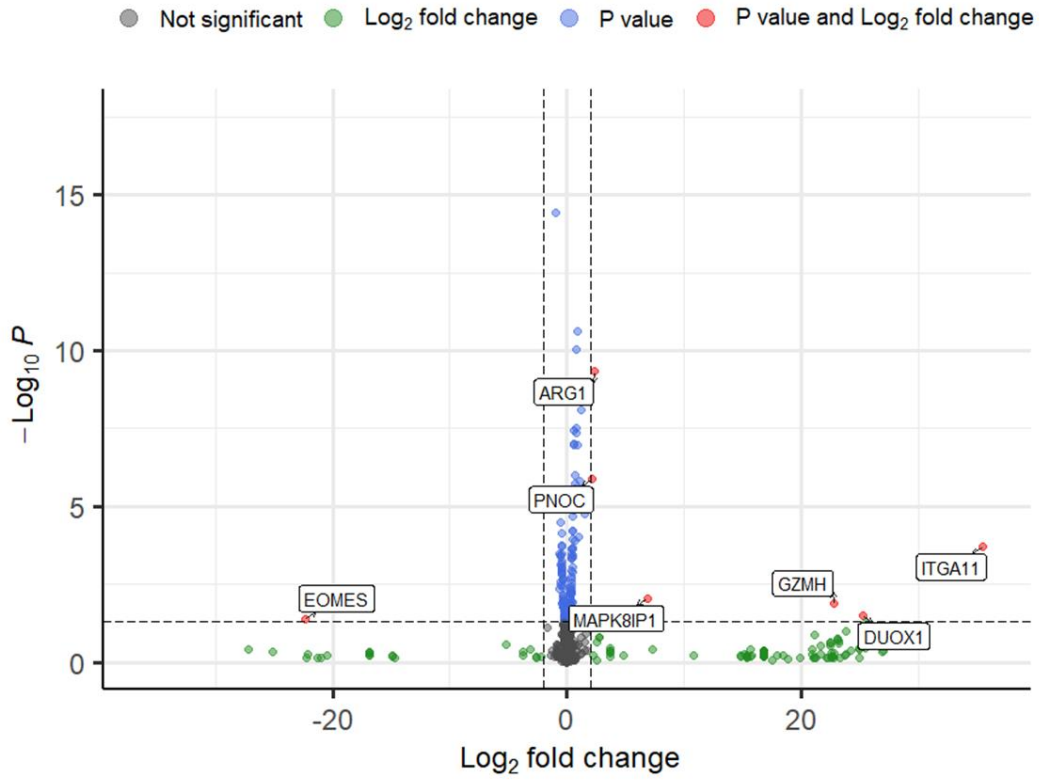


Figure 3.18: linear poly(FTC) vs linear poly(FTC) and R848 a) p value 0.05, and b) q value 0.05

When the FTC-cultured R848 treated cells were compared to the R848 treated cells using a q value cut off of 0.05 the genes which had a $\log_2FC > 2$ and therefore a significantly higher expression are: prepronociceptin (PNOC), ARG1, and ITGA11 (Figure 3.19b). When using a p value cut off of 0.05 the additional genes which had a $\log_2FC > 2$ and therefore a significantly higher expression are: MAPK8IP1, granzyme H (GZMH), and dual oxidase 1 (DUOX1), whereas $\log_2FC < -2$ also highlights that the gene EOMES has a significantly lower expression (Figure 3.19a).

a)



b)

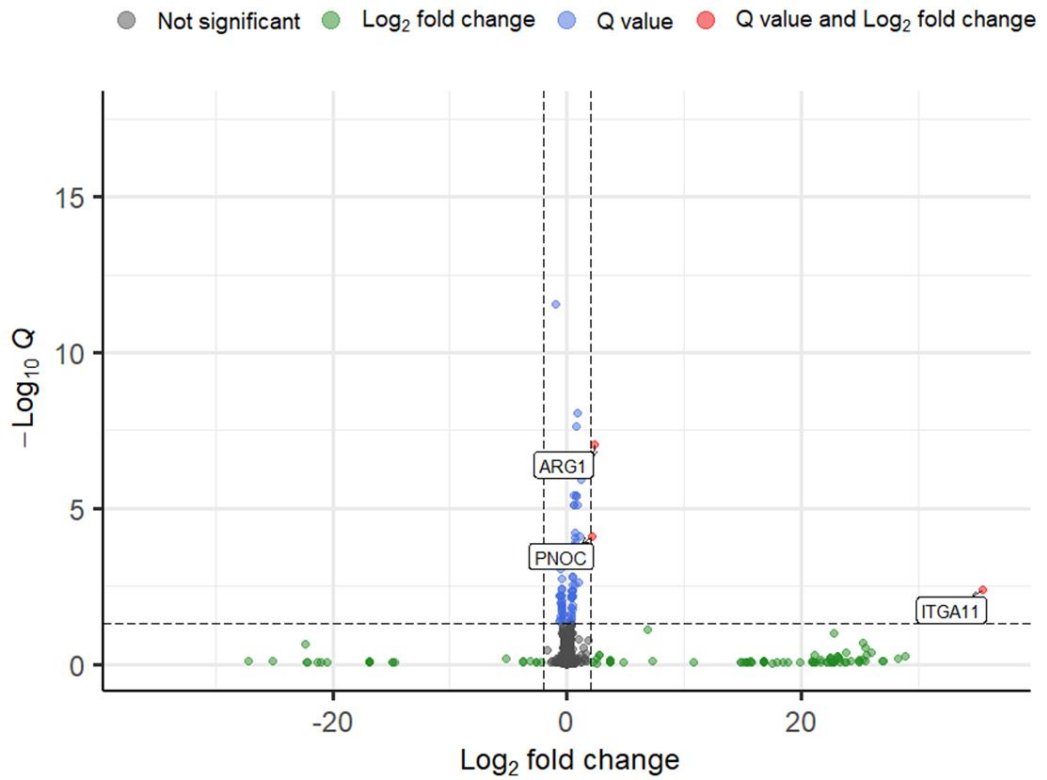
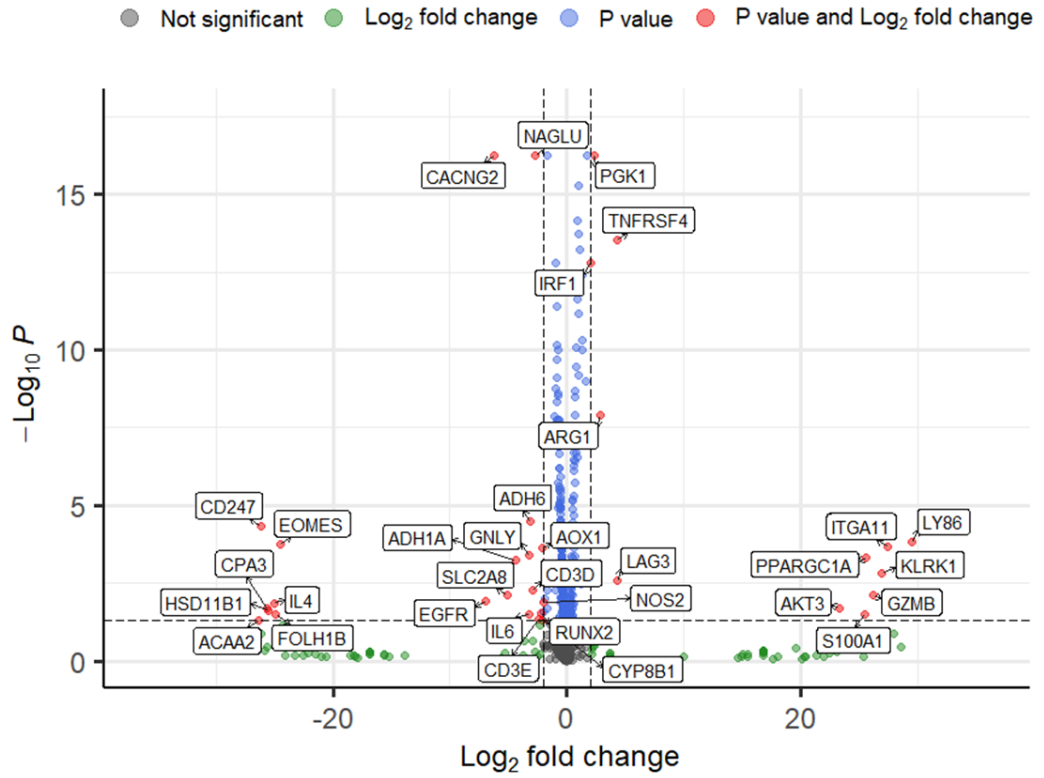


Figure 3.19: R848 vs FTC and R848 a) p value 0.05, and b) q value 0.05

When the 3TC-cultured R848 treated cells were compared to the R848 treated cells using a q value cut off of 0.05 the genes which had a $\log_2FC > 2$ and therefore a significantly higher expression are: ARG1, GZMB, interferon regulatory factor 1 (IRF1), ITGA11, KLRK1, lymphocyte activating 3 (LAG3), LY86, PGK1, PPARGC1A, and TNFRSF4 (Figure 3.20b). Whereas those that had a $\log_2FC < -2$ and therefore a significantly lower expression are: ADH1A, alcohol dehydrogenase 6 (class V) (ADH6), AOX1, CACNG2, CD247, CD3D, EGFR, EOMES, granulysin (GNLY), IL-4, NAGLU, nitric oxide synthase 2 (NOS2), and SLC2A8 (Figure 3.20b). When using a p value cut off of 0.05 the additional genes which had a $\log_2FC > 2$ and therefore a significantly higher expression are: AKT serine/threonine kinase 3 (AKT3), and S100A1 (Figure 3.20a). When using a p value cut off of 0.05 the additional genes which had a $\log_2FC < -2$ and therefore a significantly lower expression are: ACAA2, CD3E, carboxypeptidase A3 (CPA3), cytochrome P450 family 8 subfamily B member 1 (CYP8B1), FOLH1B, HSD11B1, IL-6, and runt related transcription factor 2 (RUNX2) (Figure 3.20a).

a)



b)

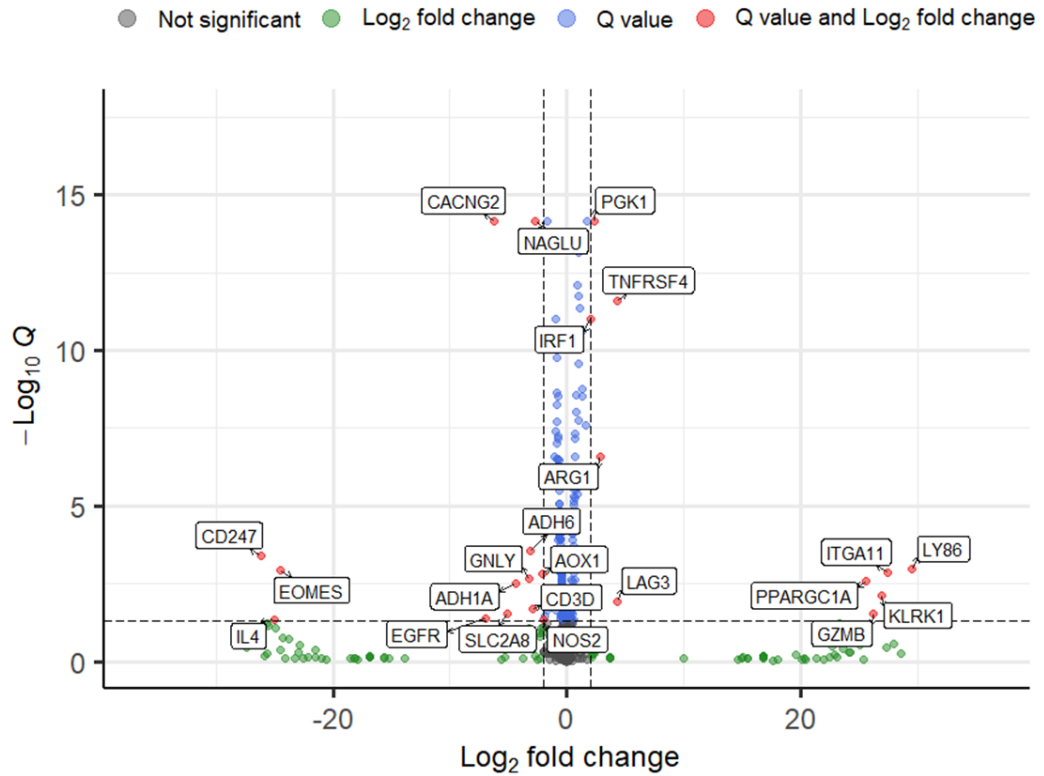
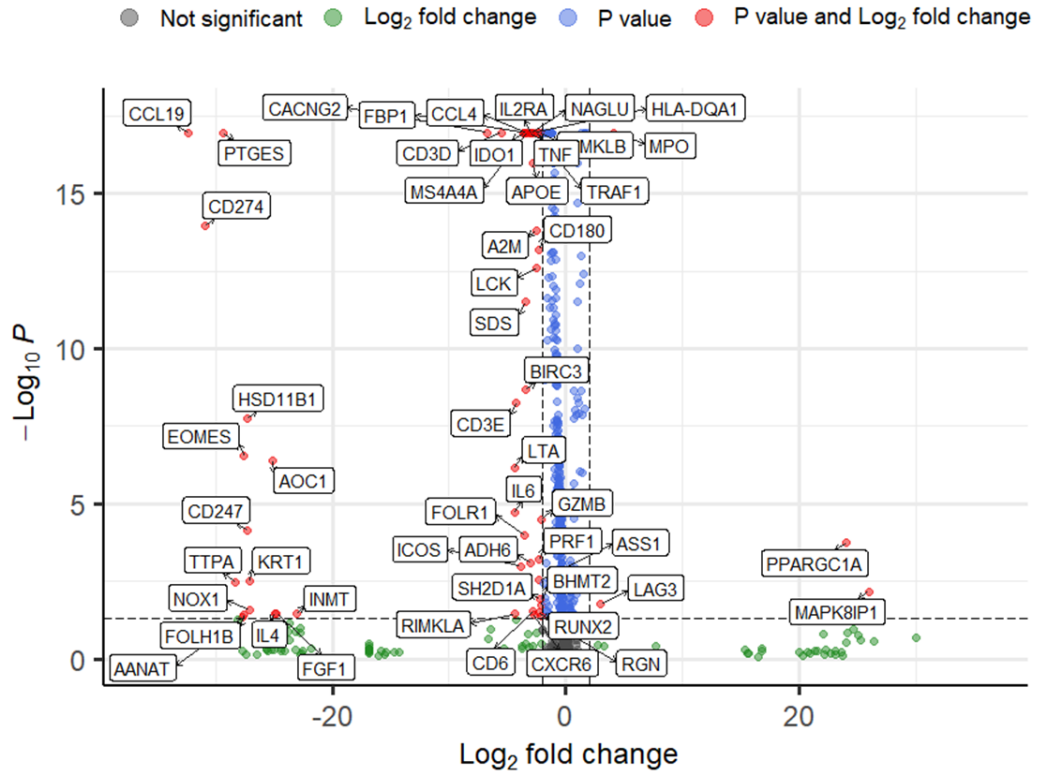


Figure 3.20: R848 vs 3TC and R848 a) p value 0.05, and b) q value 0.05. Data displayed as \log_2FC

When the linear poly(FTC)-cultured R848 treated cells were compared to the R848 treated cells using a q value cut off of 0.05 the genes which had a $\log_2FC > 2$ and therefore a significantly higher expression are: LAG3, MAPK8IP1, MPO, and PPARGC1A (Figure 3.21b). Whereas those with a $q < 0.05$ and $\log_2FC < -2$ and therefore a significantly lower expression are: A2M, ADH6, AOC1, APOE, ASS1, BHMT2, BIRC3, CACNG2, CCL19, CCL4, CD180, CD247, CD274, CD3D, CD3E, EOMES, FBP1, folate receptor 1 (FOLR1), GZMB, HLA-DQA1, HSD11B1, ICOS, IDO1, IL-2 receptor subunit alpha (IL-2RA), IL-6, keratin 1 (KRT1), LCK proto-oncogene, Src family tyrosine kinase (LCK), LTA, MS4A4A, NAGLU, PRF1, PTGES, RIMKLB, SDS, SH2D1A, TNF, TRAF1, and alpha tocopherol transfer protein (TTPA) (Figure 3.21b). However, when using a p value cut off of 0.05 the additional genes which had a $\log_2FC < -2$ and therefore a significantly lower expression are: AANAT, CD6, CXCR6, fibroblast growth factor 1 (FGF1), FOLH1B, IL-4, indolethylamine N-methyltransferase (INMT), NOX1, RGN, RIMKLA, and RUNX2 (Figure 3.21a).

When looking at the R848 treated cells vs the three drug-cultured cells treated with R848 only EOMES always has a significantly lower expression in the cultured R848 treated cells ($\log_2FC < -2$, $p < 0.05$) (Figures 3.19-3.21).

a)



b)

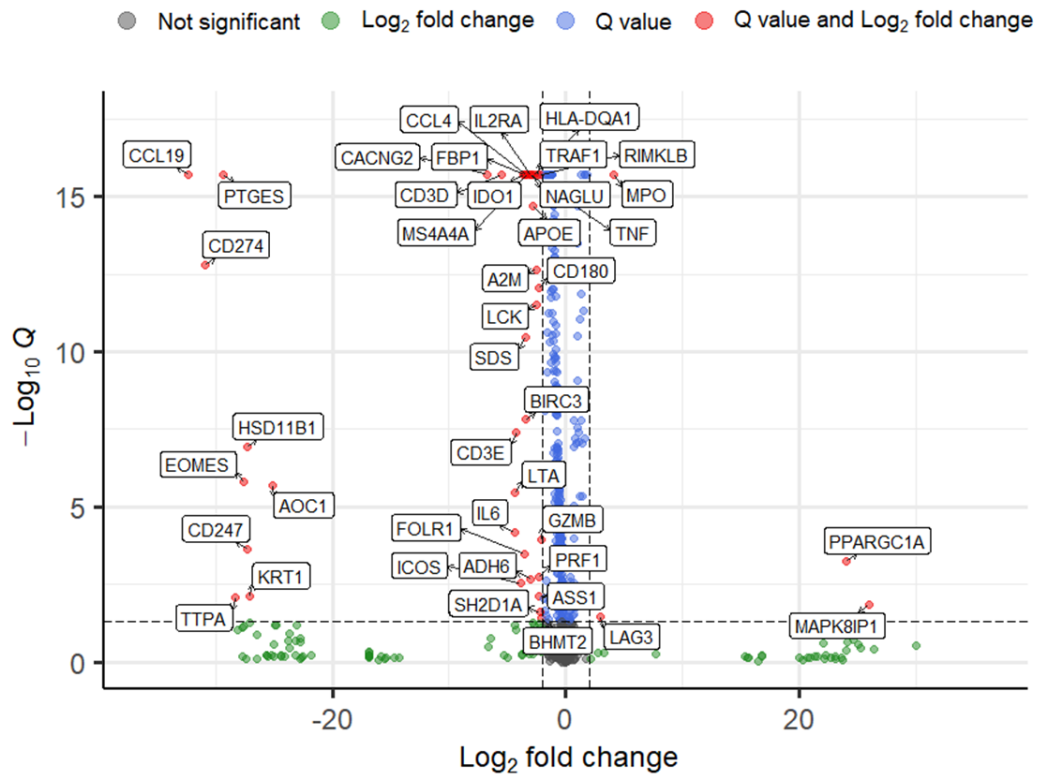


Figure 3.21: R848 vs linear poly(FTC) and R848 a) p value 0.05, and b) q value 0.05

Radar plots were used to explore changes in the 5 pathways that the nCounter panel is separated into. When the FTC-cultured cells were compared to untreated the number of genes that had a higher expression in each theme are: Biosynthesis and Anabolic Pathways 35 genes, Cell Stress five genes, Nutrient Capture and Catabolic Pathways six genes, Signalling Effecting Cellular Metabolism 32 genes, and Transcription Regulation eight genes (Figure 3.22a). When the FTC-cultured cells are compared to the untreated the number of genes that had a lower expression in each theme are: Biosynthesis and Anabolic Pathways 17 genes, Cell Stress one gene, Nutrient Capture and Catabolic Pathways three genes, Signalling Effecting Cellular Metabolism 18 genes, and Transcription Regulation one gene (Figure 3.22b).

When the 3TC-cultured cells were compared to untreated the number of genes that had a higher expression in each theme are: Biosynthesis and Anabolic Pathways 21 genes, Cell Stress two genes, Nutrient Capture and Catabolic Pathways four genes, Signalling Effecting Cellular Metabolism 20 genes, and Transcription Regulation five genes (Figure 3.22a). When the 3TC-cultured cells were compared to the untreated the number of genes that had a lower expression in each theme are: Biosynthesis and Anabolic Pathways 39 genes, Cell Stress four genes, Nutrient Capture and Catabolic Pathways 15 genes, Signalling Effecting Cellular Metabolism 44 genes, and Transcription Regulation six genes.

When the linear poly(FTC)-cultured cells were compared to untreated the number of genes that had a higher expression in each theme are: Biosynthesis and Anabolic Pathways 11 genes, Cell Stress two genes, Nutrient Capture and Catabolic Pathways three genes, Signalling Effecting Cellular Metabolism 20 genes, and Transcription Regulation zero genes (Figure 3.22a). When the linear poly(FTC)-cultured cells were compared to the untreated the number of genes that had a lower expression in each theme are: Biosynthesis and Anabolic Pathways 51 genes, Cell Stress seven genes, Nutrient Capture and Catabolic Pathways 18 genes, Signalling Effecting Cellular Metabolism 52 genes, and Transcription Regulation nine genes (Figure 3.22b).

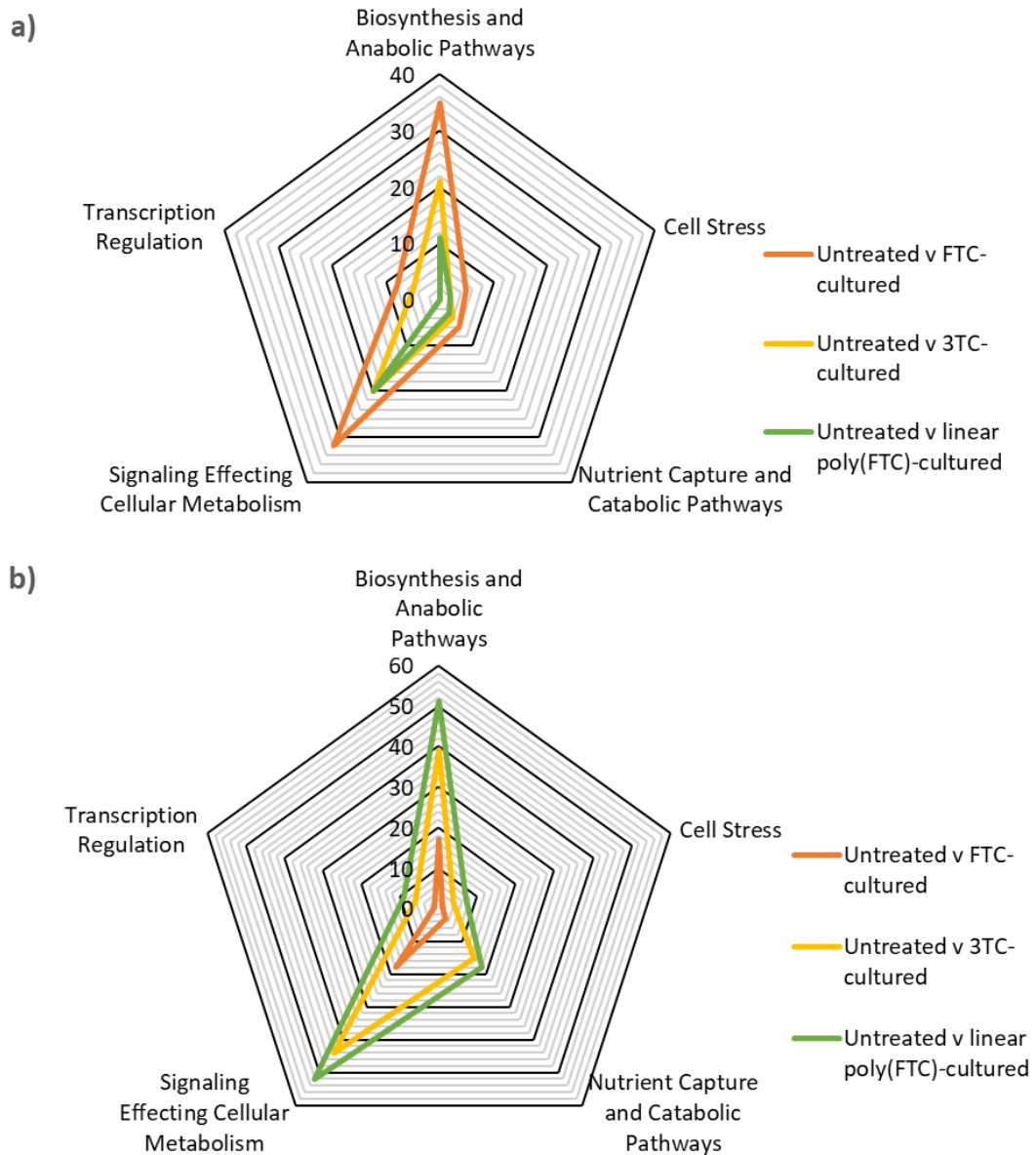


Figure 3.22: Number of genes in each Nanostring metabolic pathways theme that had an a) higher expression, and b) lower expression categorised by a Log2Fold Change either >2 or <-2.

When compared to the untreated the FTC-cultured cells had the highest number of genes with increased expression and within two main themes, Biosynthesis and anabolic pathways and signalling effecting cellular metabolism. The 3TC- and linear poly(FTC)-cultured cells then had a lower number of genes with higher expression, but the majority still fell into the same two themes. This showed the same pattern for genes that had lower expression except it was

the opposite way round and the linear poly(FTC)-, then the 3TC-cultured and then the FTC-cultured cells had a greater number of genes with lower expression.

When the untreated cells were compared to the R848 treated the number of genes that had a higher expression in each theme are: Biosynthesis and Anabolic Pathways 39 genes, Cell Stress 3 genes, Nutrient Capture and Catabolic Pathways 13 genes, Signaling Effecting Cellular Metabolism 47 genes, and Transcription Regulation seven genes (Figure 3.23a). When the untreated cells were compared to the R848 treated the number of genes that had a lower expression in each theme are: Biosynthesis and Anabolic Pathways 15 genes, Cell Stress four genes, Nutrient Capture and Catabolic Pathways five genes, Signaling Effecting Cellular Metabolism 15 genes, and Transcription Regulation five genes (Figure 3.23b).

When the FTC-cultured cells were compared to the FTC-cultured R848 treated the number of genes that had a higher expression in each theme are: Biosynthesis and Anabolic Pathways 36 genes, Cell Stress three genes, Nutrient Capture and Catabolic Pathways nine genes, Signaling Effecting Cellular Metabolism 39 genes, and Transcription Regulation nine genes (Figure 3.23a). When the FTC-cultured cells are compared to the FTC-cultured R848 treated the number of genes that had a lower expression in each theme are: Biosynthesis and Anabolic Pathways 22 genes, Cell Stress seven genes, Nutrient Capture and Catabolic Pathways seven genes, Signaling Effecting Cellular Metabolism 23 genes, and Transcription Regulation four genes (Figure 3.23b).

When the 3TC-cultured cells were compared to the 3TC-cultured R848 treated the number of genes that had a higher expression in each theme are: Biosynthesis and Anabolic Pathways 36 genes, Cell Stress six genes, Nutrient Capture and Catabolic Pathways seven genes, Signaling Effecting Cellular Metabolism 28 genes, and Transcription Regulation ten genes (Figure 3.23a). When the 3TC-cultured cells are compared to the 3TC-cultured R848 treated the number of genes that had a lower expression in each theme are: Biosynthesis and Anabolic Pathways 19 genes, Cell Stress one gene, Nutrient Capture and Catabolic Pathways 11 genes, Signaling Effecting Cellular Metabolism 24 genes, and Transcription Regulation two genes (Figure 3.23b).

When the linear poly(FTC)-cultured cells were compared to the linear poly(FTC)-cultured R848 treated the number of genes that had a higher expression in each theme are: Biosynthesis and Anabolic Pathways 30 genes, Cell Stress five genes, Nutrient Capture and Catabolic Pathways nine genes, Signaling Effecting Cellular Metabolism 46 genes, and Transcription Regulation zero genes (Figure 3.23a). When the linear poly(FTC)-cultured cells

are compared to the linear poly(FTC)-cultured R848 treated the number of genes that had a lower expression in each theme are: Biosynthesis and Anabolic Pathways 23 genes, Cell Stress two genes, Nutrient Capture and Catabolic Pathways seven genes, Signaling Effecting Cellular Metabolism 18 genes, and Transcription Regulation one gene (Figure 3.23b).

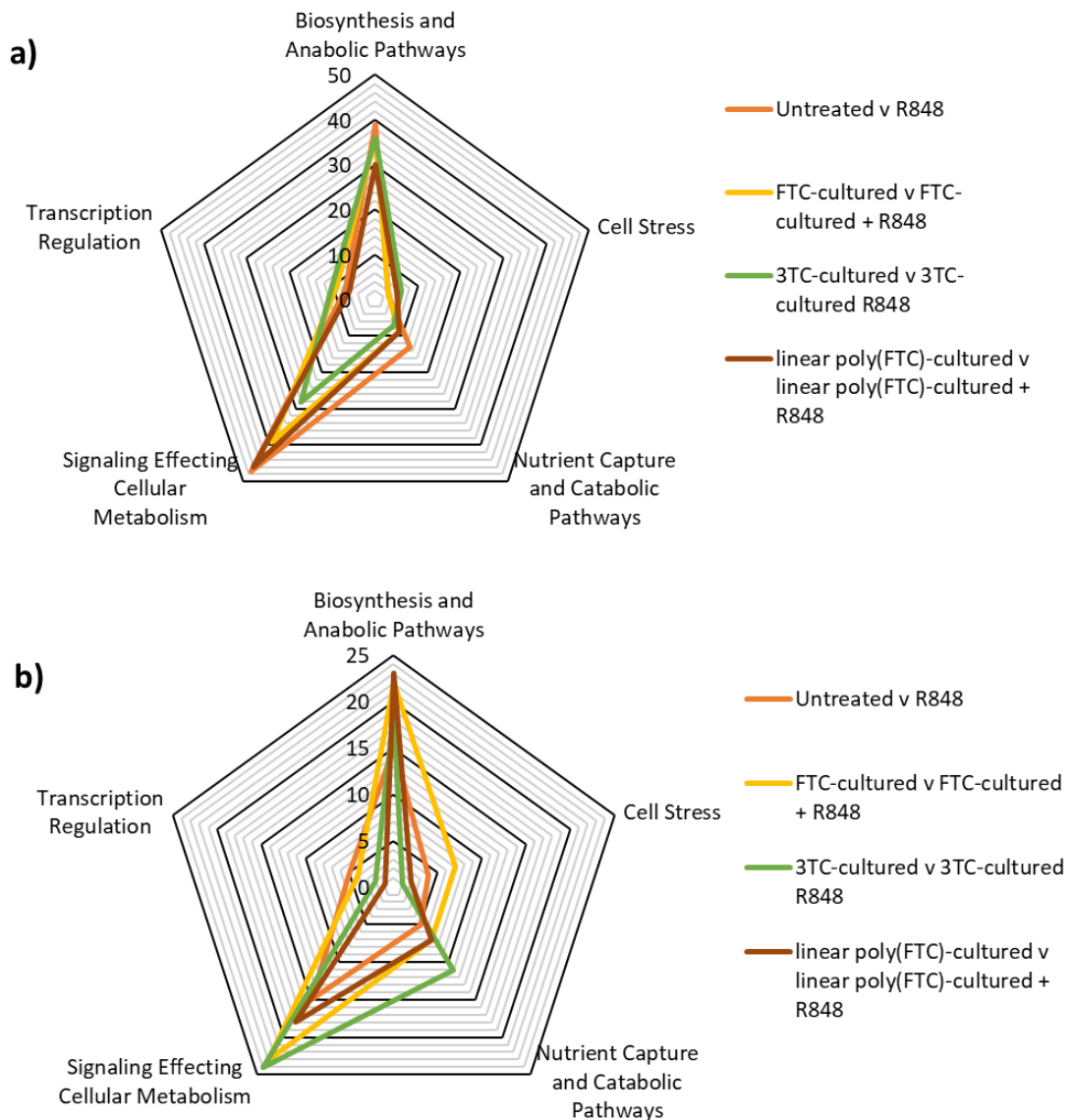


Figure 3.23: Number of genes in each Nanostring theme that had a a) higher expression, and b) lower expression categorised by a Log2Fold Change either >2 or <-2.

When comparing the cultured cells to the cultured cells with R848 treatment the number of genes with higher expression was pretty similar and mostly fell into the Biosynthesis and anabolic pathways and signalling effecting cellular metabolism themes. This was more variable for genes with lower expression, however it followed a similar pattern.

When the FTC-cultured R848 treated cells were compared to the R848 treated the number of genes that had a higher expression in each theme are: Biosynthesis and Anabolic Pathways 39 genes, Cell Stress eight genes, Nutrient Capture and Catabolic Pathways 12 genes, Signaling Effecting Cellular Metabolism 37 genes, and Transcription Regulation eight genes (Figure 3.24a). When the FTC-cultured R848 treated cells are compared to the R848 treated the number of genes that had

a lower expression in each theme are: Biosynthesis and Anabolic Pathways 15 genes, Cell Stress three genes, Nutrient Capture and Catabolic Pathways six genes, Signaling Effecting Cellular Metabolism 13 genes, and Transcription Regulation four genes (Figure 3.24b).

When the 3TC-cultured R848 treated cells were compared to the R848 treated the number of genes that had a higher expression in each theme are: Biosynthesis and Anabolic Pathways 34 genes, Cell Stress six genes, Nutrient Capture and Catabolic Pathways 13 genes, Signaling Effecting Cellular Metabolism 30 genes, and Transcription Regulation seven genes (Figure 3.24a). When the 3TC-cultured R848 treated cells were compared to the R848 treated the number of genes that had a lower expression in each theme are: Biosynthesis and Anabolic Pathways 34 genes, Cell Stress six genes, Nutrient Capture and Catabolic Pathways 13 genes, Signaling Effecting Cellular Metabolism 30 genes, and Transcription Regulation seven genes (Figure 3.24b).

When the linear poly(FTC)-cultured R848 treated cells were compared to the R848 treated the number of genes that had a higher expression in each theme are: Biosynthesis and Anabolic Pathways 17 genes, Cell Stress one gene, Nutrient Capture and Catabolic Pathways five genes, Signaling Effecting Cellular Metabolism 18 genes, and Transcription Regulation three genes (Figure 3.24a). When the linear poly(FTC)-cultured R848 treated cells were compared to the R848 treated the number of genes that had a lower expression in each theme are: Biosynthesis and Anabolic Pathways 45 genes, Cell Stress eight genes, Nutrient Capture and Catabolic Pathways 17 genes, Signaling Effecting Cellular Metabolism 54 genes, and Transcription Regulation ten genes (Figure 3.24b).

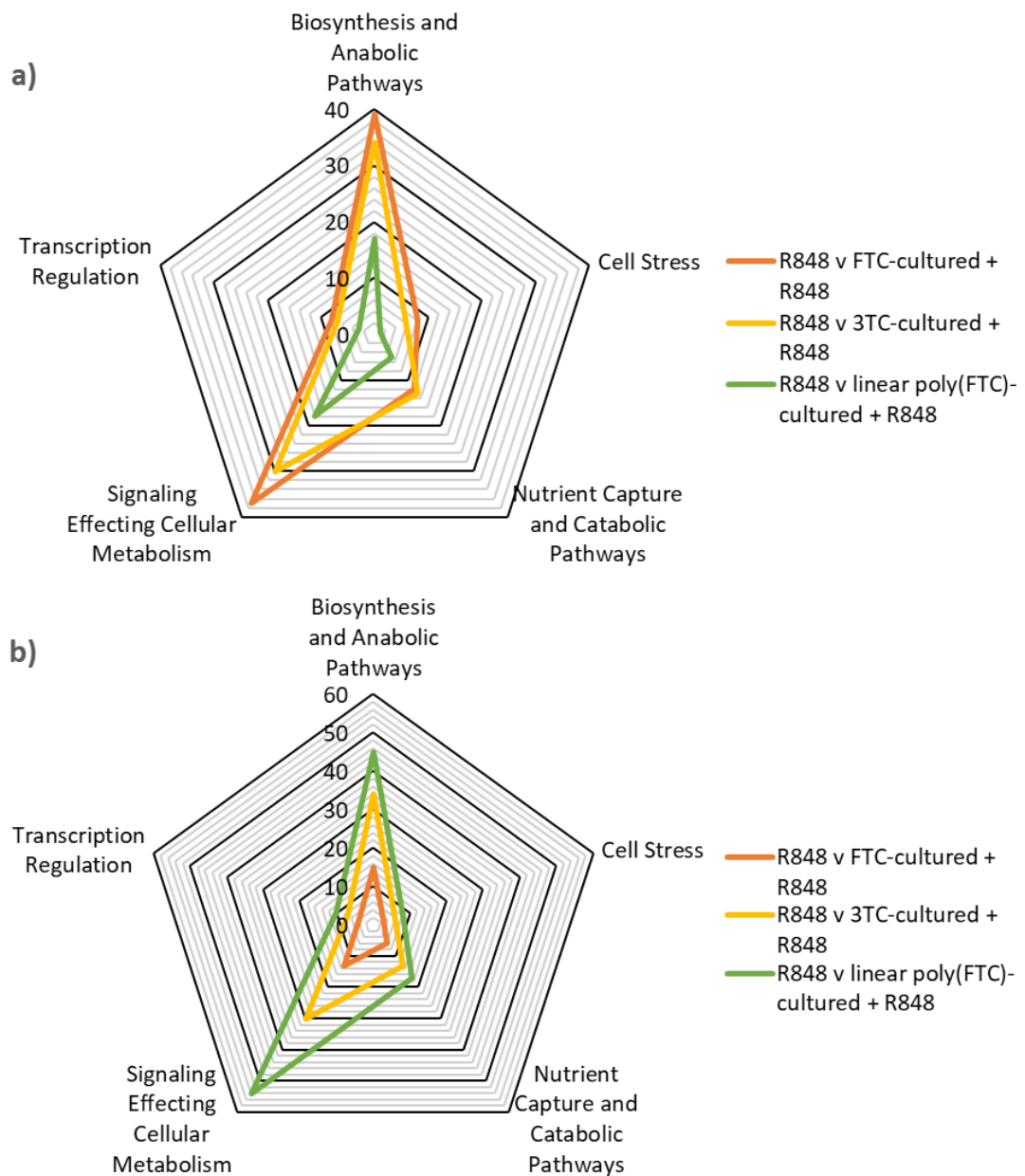


Figure 3.24: Number of genes in each Nanostring theme that had an a) higher expression, and b) lower expression categorised by a Log2Fold Change either >2 or <-2.

When comparing the R848 treated cells to the cultured R848 treated cells the same pattern occurred as with the untreated and cultured cells and these genes also commonly fell into the same 2 themes.

3.4 Discussion

Exploring these materials over long exposure periods is important in order to mimic the exposures that will be seen during the implantation period. This chapter has started to develop an assay that can be used to help assess the potential for inflammatory responses to long-acting drug formulations.

Initially measurement of total ROS, reduced glutathione, and Mitochondrial Membrane Polarisation was carried out to explore the health of the cells following exposure, prior to investigation of activation profiles in response to agonists and drug exposure. The MUTZ-3 cell line was chosen to be taken forward into the Nanostring nCounter experiment, as a paradigm for future assessments, due to the significant changes seen in marker expression following exposure to linear poly(FTC)-cultured cells, as well as significant changes in the FTC- and 3TC-cultured cells.

The significantly higher ROS seen for both the FTC- and 3TC-cultured **CEM** cells, suggests these cells have become stressed, however no significant changes were seen for either reduced glutathione or MMP. The 3TC-cultured cells also showed significantly higher CD69 expression when compared to the untreated cells. CD69 is expressed at the early stages on activated T-cells, it has been shown to peak at 12 hours following stimulation with PMA and starts to reduce by 18 hours (López-Cabrera et al., 1993). No significantly higher expression between the untreated and the PHA-M treated cells following 24 hour exposure, could be due to reduced expression at this time point. The FTC- and 3TC-cultured cells however show a significantly higher CD69 expression following treatment with PHA, which may suggest altered activation profiles following repeat exposure to these drugs. The 3TC-cultured cells have higher basal CD69 expression, suggesting higher basal T-cell activation.

In the **KU812** cell line significantly higher ROS was seen in the FTC-cultured cells compared to the Untreated, MMP was also significantly lower suggesting that there is depolarisation, both these are indicative of cell stress. The 3TC-cultured cells also showed significantly lower MMP, however no significant difference between the ROS or reduced glutathione. C5a is an anaphylatoxin which can bind to its receptor, causing activation of basophils in an IgE independent manner (Shah et al., 2021). CI is used to increase the cells permeability of Ca^{2+} and PMA is a known protein kinase C activator, CI alone and PMA together with another ionophore ionomycin have been shown to lead to higher CD63 and CD203c expression on basophils (Chirumbolo et al., 2008; Ebo et al., 2012). CD164 is a novel basophil activation marker, which has been shown to have higher expression following stimulation with anti-IgE,

its expression profile over time following activation has shown parallels with that of CD203c, its suggested CD63 is a slow responder and CD164 and CD203c are fast responders (Hennersdorf et al., 2005). When compared to the untreated neither of these positive controls caused a significantly higher or lower expression of the three markers assessed, PMA and CI did cause a non-significant higher expression of CD63 in all culture groups when compared with the respective cultured cells. However, both the FTC- and 3TC-cultured alone and treated with C5a caused respectively lower CD63 expression when compared to the untreated or C5a treated cells. The 3TC-cultured cells compared to the untreated had higher expression of CD203c, whereas the FTC-cultured C5a treated cells had lower CD203c. The FTC-cultured and FTC, C5a treated had a lower expression of CD164 when compared to the C5a treated cells. However, the FTC-cultured CI and PMA treated, expressed higher levels of CD164 when compared to the CI/PMA treated cells. CD63, CD203c and CD164 are all markers of basophil activation, the changes in these markers at basal levels and following exposure to known activators may play an important role in allergic responses following repeated exposure. Particularly, the reduced basal level and response to the C5a anaphylatoxin in the drug-cultured cells could potentially mean that these cells may not be able to respond correctly to subsequent allergen exposure.

Due to equipment failure only the ROS and reduced glutathione cell health measurements were able to be carried out after seven weeks of exposure in the **THP-1** cell line, therefore the cells were frozen and passaged a further four times in the presence of the drugs once brought out of liquid nitrogen storage before carrying out the full panel of cell health and marker expression assessments. Prior to storage significantly higher levels of reduced glutathione were seen in the FTC- and 3TC-cultured cells, however following freezing there was no significant difference seen for any of the cultured cells in the reduced glutathione assay and the ROS levels for 3TC showed the opposite trend seen prior to freezing. There was however a significantly lower MMP seen for the 3TC-cultured cells following storage in liquid nitrogen. The 3TC-cultured and 3TC-cultured LPS treated both showed significantly higher CD14 expression when compared to the untreated and the LPS treated respectively. CD14 expression is known to have a higher expression as a result of LPS challenge (Zamani, Zare Shahneh, Aghebati-Maleki, & Baradaran, 2013). Following repeated exposure of the cells to 3TC caused a higher basal CD14 expression, this may potentially impact subsequent exposure of cells to subsequent infection. In any follow up experiments, all cell health and marker expression assays should be carried out prior to any storage due to the changes seen with the THP-1 cells post freezing.

The **MUTZ-3** cell line is a human acute myelomonocytic leukaemia cell line, which expresses the CD34 marker common to hematopoietic progenitor cells, the cell line has the characteristics of a monocytic cell and weakly expresses CD14 (Masterson et al., 2002). and can be differentiated into cells with either display characteristics reflecting immature DC or LCs, which can be activated in mature phenotypes (Masterson et al., 2002). Although there are differences between MoDCs and MUTZ-3 cell expression of DC markers following stimulation with LPS they follow a similar activation pattern, these differences could also be due to concentration and treatment time differences.

Both FTC- and 3TC-cultured MUTZ-3 cells had significantly lower ROS when compared to the untreated. Whereas linear poly(FTC)-cultured cells had significantly higher ROS levels compared to the untreated, this suggests that the linear poly(FTC)-cultured cells were stressed. Both the FTC-cultured and the linear poly(FTC)-cultured cells had significantly higher MMP, this is interesting as it would be expected higher ROS levels correlate with depolarization in the stressed linear poly(FTC)-cultured cells.

Significantly higher expression of CD80 was seen when comparing the linear poly(FTC)-cultured cells to the untreated. CD86 expression was higher when comparing the linear poly(FTC)-cultured R848 treated to the R848 treated MUTZ-3 cells. CD80 and CD86 are both costimulatory molecules found on antigen presenting cells that bind to both CD28 or CD152/CTLA-4 either promoting or inhibiting T-cell activation respectively in combination with MHC/antigen interaction with the T-cell receptor and other costimulatory signals (Sansom, Manzotti, & Zheng, 2003). Higher expression of both these molecules suggest that the cells have become activated in response to repeat exposure to linear poly(FTC). CD209, also known as DC-SIGN has three main functions, it can act as a pattern recognition receptor causing a specific response depending on the pathogen it senses and internalisation of antigens for MHC presentation, bind Intercellular adhesion molecule (ICAM)-2 modulating DC migration into the blood, or ICAM-3 on T-cells modulating DC-T-cell initial interactions (T. B. Geijtenbeek, Dunnen, & Gringhuis, 2009; T. B. H. Geijtenbeek, Krooshoop, et al., 2000; T. B. H. Geijtenbeek, Torensma, et al., 2000). Interestingly CD209 expression was significantly higher in both the linear poly(FTC)-cultured and linear poly(FTC)-cultured R848 treated cells when compared to the untreated or R848 treated cells respectively, suggesting again that linear poly(FTC) is activating the cells in some way. CD40 is upregulated on activated DCs, a lower expression of CD40 in the FTC-cultured LPS and R848 treated cells when compared to their treated comparison, suggests that repeat exposure to FTC may have impacted the MUTZ-3 cells ability to respond to DC-specific positive controls (Ma & Clark, 2009). This could

potentially imply that repeated exposure could cause a reduced ability of the bodies DCs to fight off immunological challenges whilst undergoing repeat treatment with FTC. HLA-DR is an isotype of the MHC class II cell surface receptor, DC cells present peptides to CD4+ T-cells using the MHC class II receptor in order to promote T-cell activation (Choo, 2007). Previously 48 hour treatment with R848 has been shown to upregulate HLA-DR expression in human MoDCs (Alam, Yang, Trivett, Meyer, & Oppenheim, 2018). Linear poly(FTC)-cultured cells alone and treated with R848 both caused a significantly lower expression of HLA-DR when compared to the untreated or R848 treated respectively. When the untreated, FTC-, and 3TC-cultured cells are compared to their LPS and R848 treated equivalents there is a non-significantly higher HLA-DR expression, however when the linear poly(FTC)-cultured cells are treated with either LPS or R848 there is a non-significant or significantly lower HLA-DR expression. A lack of response to known activation agents, suggests there may be some alterations in immune response as a result of linear poly(FTC) treatment. CD274, also known as programmed death ligand 1 (PD-L1), plays a role in controlling T-cell responses via the receptor PD-1 (Hudson, Cross, Jordan-Mahy, & Leyland, 2020). LPS treated FTC-cultured cells caused a significantly lower expression of CD274 when compared to FTC-cultured cells, 3TC-cultured R848 treated also showed a lower expression when compared to the R848 treated cells. However linear poly(FTC)-cultured R848 treated caused a significantly lower expression of CD274 compared to the R848 treated. This again poses the question whether repeated exposure may prevent the immune system from carrying out its normal roles. Non-significantly and significantly higher CD83 expression was seen respectively with LPS and R848 treatment in the untreated, FTC-cultured and 3TC-cultured. The linear poly(FTC)-cultured cells however had a non-significantly lower expression that was consistent for all three conditions. CD83 is known to have higher expression on antigen presenting cells such as DCs upon activation (Z. Li et al., 2019). The lack of change in CD83 expression yet again suggests a lack of ability of the linear poly(FTC)-cultured cells to respond to inflammatory stimuli.

From the follow up experiment exploring the influence of repeat exposure of DMSO on the MUTZ-3 cells, it has been demonstrated that the results seen for linear poly(FTC) exposure do not look to be due to exposure of the DMSO vehicle used, no significant changes were seen in ROS, reduced glutathione or marker expression. However, as little as 0.1% DMSO has previously been shown to affect gene expression, microRNA expression, and the epigenetic landscape (Verheijen et al., 2019). The DMSO-cultured cells did show a significantly higher MMP and this correlated with the change seen for linear poly(FTC). Future analysis of the

DMSO cultured cells using the nCounter could be useful to rule out further the role of DMSO in the responses seen.

When looking at the nCounter results it must be taken into account that this is calculated based on mRNA levels and therefore higher gene expression does not always mean an higher level of protein (Liu, Beyer, & Aebersold, 2016). Further proteomics analysis would be useful in order to determine whether this translates into protein level variations.

Interestingly the R848 treated cells all show a significantly higher expression of CCL4, COL6A1, IDO1, IL-4I1, KYNU, NFKB2, SLC2A6, SOD2, TNF, and TRAF1 when compared to their untreated counterparts. The chemokine CCL4, also known as macrophage inflammatory protein (MIP)-1 β) has previously been shown to have a higher secretion in MoDCs stimulated with R848, and the current work is in agreement with that supporting this approach (Jensen & Gad, 2010). IDO is the enzyme that catalyzes the rate-limiting step in the catabolism of tryptophan via the kyurenine pathway, higher IDO correlates with previously reported higher gene expression in antigen presenting cells treated with R848, however this has been shown not to occur with immature DCs (Giesbrecht et al., 2017). IDO can be induced by a number of cytokines including but not limited to IFN- γ and TNF- α , IDO has a number of immunosuppressive functions and plays a role in restoring homeostasis (Giesbrecht et al., 2017; Mándi & Vécsei, 2012). KYNU is an enzyme which converts 3-hydroxykynurenine to 3-hydroxyanthranilic acid further down in the kyurenine pathway, INF- γ is known to induce expression of KYNU, however IFN- γ has not been significantly higher in any of the gene expression comparisons (Mándi & Vécsei, 2012). R848 is a TLR-7 and -8 agonist, all TLRs cause activation of the transcription factor NK- κ B, therefore this may be why NFKB2 has a higher expression and has previously been shown for 48 hour treatment with R848 in MoDCs. SLC2A6 also known as glucose transporter (GLUT)6 was significantly higher in all culture conditions treated with R848, when compared to their untreated counterparts. GLUT6 has been shown to be regulated by the NF- κ B pathway and inflammatory stimuli have been shown to increase its expression and alter inflammatory responses, likely to meet the bioenergetic demands of the cells, following a switch to glycolysis (Krawczyk et al., 2010; Maedera et al., 2019; Møller, Wang, & Ho, 2022). When treated with LPS, mouse peritoneal macrophages had increased GLUT6 expression, altering the immunometabolism via glycolysis activation (Maedera et al., 2019). The mitochondrial antioxidant enzyme SOD2, was expressed at significantly higher levels in all the R848 treated cells, this correlates with previous reports of R848 causing higher SOD2 protein expression in human monocyte derived macrophages (Rakkola, Matikainen, & Nyman, 2007). The higher gene expression of

TNF in all of the R848 treated MUTZ-3 cells correlates to previously shown higher TNF- α gene expression or cytokine secretion when MoDCs are exposed to R848 for 24 hours (Jensen & Gad, 2010; Lombardi, Van Overtvelt, Horiot, & Moingeon, 2009). IL-4I1 and TRAF1 genes have both been shown to have a significantly higher expression in mouse bone marrow-resident DCs in response to intraperitoneally administered R848 treatment (S. Li, Yao, Li, Schmidt, & Link, 2021). These results suggest that the MUTZ-3 cells are all still able to respond in a similar way to primary DCs in response to R848 treatment to an extent.

Interestingly all but the linear poly(FTC)-cultured R848 treated cells only additionally have a significantly higher expression of THBS1. THBS1 plays an important role in modulating inflammation, it's been proposed THBS1 interaction with CD36 among other roles can activate the NF- κ B pathway causing higher expression of TNF- α , IL-6 and STAT3, that all have pro-inflammatory roles (Lopez-Dee, Pidcock, & Gutierrez, 2011). The lack of significant activation of THBS1 in the linear poly(FTC)-cultured cells suggests there may be a reduced ability of these cells to respond to inflammatory stimuli. It is also interesting to point out that when the R848 treated linear poly(FTC)-cultured cells were compared to the poly(FTC)-cultured cells there was a significant reduction in CD36.

IDO1 gene expression is lower when both the 3TC- and linear poly(FTC)-cultured cells are compared to the untreated cells and when the linear poly(FTC)-cultured R848 treated cells are compared to the R848 treated cells. As discussed above, IDO has a number of immunosuppressive functions, this potentially indicates that the cells cultured in 3TC or linear poly(FTC) have a basal level of activation.

Some other statistical differences of note are discussed below. When both the linear poly(FTC)-cultured cells were compared to the untreated cells and the linear poly(FTC)-cultured R848 treated cells were compared to the R848 treated cells there was a significantly lower expression of CCL4, TNF and CCL19. CCL4/MIP-1 β is induced by proinflammatory stimuli and acts as a chemoattractant for other immune cells, alongside a number of other pro-inflammatory responses through binding to G-protein-coupled chemokine receptors (Maurer & von Stebut, 2004). TNF is a pro-inflammatory cytokine that has many different roles and is essential in response to infection (Bradley, 2008). CCL19 can promote DC migration and maturation following CCR7 expression upregulation, which can subsequently stimulate Th1 T-cell responses and produce other pro-inflammatory cytokines (Marsland et al., 2005). All these points suggest that the linear poly(FTC) cultured cells could have an altered response to R848, suggesting potential alterations to the cells capability to respond

to inflammatory stimuli. CCL19 was however, interestingly significantly higher when the linear poly(FTC)-cultured R848 treated cells were compared to the linear poly(FTC)-cultured cells. Gene expression of CXCL9 is lower in the 3TC- and linear poly(FTC)-cultured cells when compared to the untreated. CXCL9 is a chemokine that is induced by IFN- γ and causes migration, differentiation, and activation of lymphocytes through interactions with the CXCR3 receptor (Tokunaga et al., 2018). Both the 3TC- and linear poly(FTC)-cultured cells had a lower expression of the CXCL9 gene suggesting yet again potential reduced immune responses. When compared to the linear poly(FTC)-cultured cells the linear poly(FTC)-cultured R848 treated cells had a significantly higher gene expression of IL-6. This suggests these cells have the capacity to respond appropriately, as it correlates with previously shown higher IL-6 secretion or gene expression when MoDCs are exposed to R848 for 24 hours (Jensen & Gad, 2010; Lombardi et al., 2009). An interesting point to make is, only the linear poly(FTC)-cultured cells caused a significantly higher IL-6 gene expression, further follow up looking at the IL-6 levels from the cell-culture supernatants would be valuable to explore. The 3TC-cultured cells when compared to the untreated cells had a significantly lower IL-6 gene expression. Also, both the 3TC- and linear poly(FTC)-cultured R848 treated cells when compared to the R848 treated cells had lower IL-6 gene expression. As discussed above, this is a key area where proteomics could help to determine the responses seen to the repeated culture conditions. CARD11 can activate NF- κ B through the phosphorylation of BCL10, the exact mechanisms however are still to be defined (Bertin et al., 2001). Gene expression of CARD11 was interestingly reduced in the linear poly(FTC)-cultured cells when compared to the untreated. IL-4 is used to mature CD14⁺ monocytes into immature dendritic cells, IL-4 has been shown to induce Th2 T-cell responses, which subsequently can support B cells and promote immunoglobulin class switching (Choi & Reiser, 1998). When both the 3TC- and linear poly(FTC)-cultured R848 treated cells are compared to the R848 treated cells they both a significantly lower gene expression of IL-4. As discussed throughout this paragraph a number of the changes in gene expression could alter the immune responses in these cells and proteomics data would be useful to further explore these differences.

Nanostring categorise their nCounter panels into themes, the five themes in the Human Metabolic Pathways panel were: Biosynthesis and Anabolic pathways, cell stress, nutrient capture and catabolic pathways, signalling effecting cellular metabolism, and transcription regulation. Figures 3.21-23 summarise the gross change in genes that have higher or lower expression. It is interesting to point out that in all comparisons that were made, the most changes occur to the signalling affecting cellular metabolism and biosynthesis and anabolic

pathways. Further analysis on the effects of the drugs and the POP materials on metabolic processes in future work would be useful to determine the reason for the gene expression changes in these cells. Previously efavirenz and lopinavir have led to lower glucose uptake and caused bioenergetic modifications to cells, it would be useful to explore the methods used to determine if FTC, 3TC and linear poly(FTC) also alter these profiles (Heaton et al., 2022).

The nCounter metabolic pathways panel included CD274, CD209, CD14, and HLA-DRB1, it did not include CD80, CD86, CD83, and CD40. Gene expression of CD274 is significantly higher in the linear poly(FTC)-cultured cells treated with R848 compared to the linear poly(FTC)-cultured cells, interestingly this is consistent with the marker expression results for the same comparison. The marker expression also showed significant changes in untreated and 3TC-cultured cells treated with R848, these higher percentages were much lower than seen for linear poly(FTC), which may be why significant differences aren't seen in gene expression for these conditions. However, gene expression of CD274 is lower in the linear poly(FTC)-cultured R848 treated cells when compared to the R848 treated cells, this contradicts what was seen in the marker expression experiment. CD40 is not measured, but CD40 ligand is, however no significant gene expression changes in the ligand were seen. HLA-DRB1 did not show any significant changes in gene expression, however HLA-DQA1 did show significant changes in its expression profiles. HLA-DQ is another MHC class II isotype, the gene HLA-DQA1 codes for the α chain, which forms HLA-DQ when in combination with a β chain (Choo, 2007). In both the FTC- and linear poly(FTC)-cultured cells that are treated with R848 there is a significantly higher HLA-DQA1 expression when compared to the untreated cultured corresponding cells. FTC-cultured cells showed a non-significant higher HLA-DR marker expression and opposingly HLA-DR showed a lower expression with the linear poly(FTC)-cultured cells. Interestingly, there is however also a lower expression in the linear poly(FTC)-cultured R848 treated cells when compared to the R848 treated cells, which corresponds with what was seen in the marker expression results.

The results observed in the analysis of the repeat exposures vary between cell line and drug/POP polymer culture treatment. This poses an interesting question as it suggests there are varying immune responses from these drugs or POP polymer. These results have, potential, consequences for long-acting formulations and implants as they show possible effects of repeat exposure to the FTC and 3TC antiretrovirals used in POP the POP materials. The consequences of these observation should now be assessed in human, primary, cells to validate the work seen here, however, due to the impact of blood supplies during the COVID-

19 pandemic, this was not possible during the current timeframe. It is also possible that some of the differential impacts observed between cell types could relate to the intracellular pharmacology of the cells; varying activity of metabolic enzymes such as the cytochrome P450s (CYP; known metabolisers of ARVs) may link to differential effects on the cells in which they accumulate. Additionally, validation of the transcriptomic data, by proteomic and metabolomic analysis is now warranted. Although the impacts on gene expression observed here, do match up with phenotypic differences, a complete understanding of the linked effects on the cellular proteome and metabolome should be considered.

Chapter 4

Cytotoxicity and cell health assessment of

TAF Carbamate Prodrugs

4.1 Introduction

As discussed in Chapter 1, TAF is a prodrug of tenofovir, an NRTI used in the treatment of HIV. TAF is also effective in treating hepatitis B, comorbidity of hepatitis B and HIV infection is common, due to the similar transmission routes. Further modifications have been made to the TAF prodrug, to produce bio-reversible aryl carbamate prodrugs of TAF. These modified TAF aryl carbamates would then be used as monomers to enable formulation into polymers, using similar strategies to the POP process, for subcutaneous implant administration, like the materials seen in Chapter 2. It is hypothesized that TAF aryl carbamates could be tuned to achieve a range of TAF release rates from the polymer and from TAF polymer fragments in circulation.

Safety of select TAF carbamate prodrugs was explored early in the process of development due to potential toxicity issues with carbamates, ethyl carbamate and insecticide carbamates have been shown *in vitro* to cause both cytotoxicity and genotoxicity (Cui, Wang, Qiu, & Wu, 2016; Guanggang et al., 2013; Soloneski, Kujawski, Scuto, & Larramendy, 2015). Safety issues with previous TAF implants *in vivo*, as discussed in Chapters 1 and 2 also contributed to early testing of these compounds, although a more recently developed TAF releasing implant tested *in vivo* in mice has been shown to be much safer (Gunawardana et al., 2022; Su et al., 2020). The timing of these assessments on the TAF carbamate prodrugs and why this was not done with the FTC monomers, was to prevent potential unnecessary work on something that could be toxic when administered *in vivo*.

Like any materials first the cytotoxic potential of these materials was explored, due to the materials compatibility in vehicles such as DMSO, Acetonitrile (ACN) cytotoxicity was explored. Previously up to 2.5% ACN did not significantly alter cell viability in HK-2 cells (Mapa et al., 2020). Cell health measurements were then carried out on non-toxic concentrations to determine whether there were perturbations in the cells health as a result of exposure to these TAF aryl carbamate prodrugs.

4.2 Methods

4.2.1 Materials

The TAF carbamate prodrugs were prepared at Johns Hopkins University School of Medicine by Dr Kartik Temburnikar. ACN was purchased from Fisher scientific (Loughborough, UK. All the reagents used for the MTT, LDH, ROS and reduced glutathione assays are all purchased from the companies stated in the previous chapters (MTT/LDH Chapter 2, ROS/reduced glutathione Chapter 3).

4.2.2 TAF carbamate prodrug solubilisation

TAF or its carbamate prodrugs were suspended into the following compatible vehicle as advised by the colleagues that made them at Johns Hopkins University (Baltimore, USA): TAF water 1 mg/mL; diphenyl TAF water 1 mg/mL; TAF-2,4,6-trimethylphenyl carbamate ACN 1 mg/mL; TAF-2,4-dimethylphenyl carbamate ACN 1 mg/mL TAF-2-*t*-butylphenyl carbamate ACN 1 mg/mL; and 4-methoxyphenyl carbamate ACN (this was made up immediately before adding to the media as it has been found to only be stable in biological matrixes up to 30 minutes) 1 mg/mL. TAF-*n*-butyl carbamate, a control compound that does not rapidly undergo activation to release TAF TAF-*n*O-butyl carbamate was suspended in water 1mg/ml.

4.2.4 Routine cell culture

Routine cell culture of the THP-1 and MUTZ-3 cell lines were carried out as stated in Chapter 2.

4.2.5 Cytotoxicity Assessment of ACN and TAF carbamate prodrugs

4.2.5.1 ACN cytotoxicity assessment

To check the biocompatibility of ACN as a vehicle a MTT and LDH was first carried out on different concentrations of ACN: 2.5 %, 1%, 0.5%, 0.25%, 0.1%, 0.05%, 0.025%, 0.01% and 0.005%. Both the MTT and LDH assays were carried out as described in Chapter 2.

4.2.5.1 TAF carbamate prodrug cytotoxicity assessment

Both the MTT and LDH assays were carried out as described in Chapter 2. C_{max} levels in the literature were used to determine concentrations for the cytotoxicity. One previous study

reported mean C_{max} values in the literature for TAF in uninfected patients with severe renal impairment was 364 ng/mL or normal renal function 199 ng/mL (Custodio et al., 2016). Another report states a mean of 230.1 ng/mL fasted, HIV infected and fed mean 207.2 ng/mL (Gilead, Sampson, & Younis, 2015). Due to the previous issues with TAF implants and potential burst release of TAF, much higher concentrations than the C_{max} were chosen for testing. The final concentrations assessed for all the TAF carbamate prodrugs were 4000, 2000, 1000, 500, 250, 125, 62.5 and 31.25 ng/mL.

4.2.6 THP-1/MUTZ-3 ROS and reduced glutathione measurement

100 μ L of THP-1/MUTZ-3 cells were seeded at 5×10^5 cells per well in 96-well plate. Each of the TAF carbamate prodrugs was assayed in triplicate at concentrations of 4000, 230 and 31 ng/mL in THP-1 cells and 4000 and 230 ng/mL in MUTZ-3 cells. A positive control treatment with menadione at 100 μ M was also included in triplicate and the plates incubated for 24 hours. Following treatment, the cells were washed and split into two separate plates for subsequent ROS and reduced glutathione analysis. Both the ROS and reduced glutathione analysis were carried out as described in Chapter 3.

4.3 Results

The TAF phenyl carbamates have low stability, by design, in order to release TAF in the body at a pH7.4. TAF is released from TAF-4-methoxyphenyl carbamate the fastest and slowest from TAF-2-*t*-butyphenyl carbamate, as illustrated by the half-lives in Figure 4.1. TAF is not released from TAF-*n*-butyl carbamate, as it a control compound that is not an aryl carbamate.

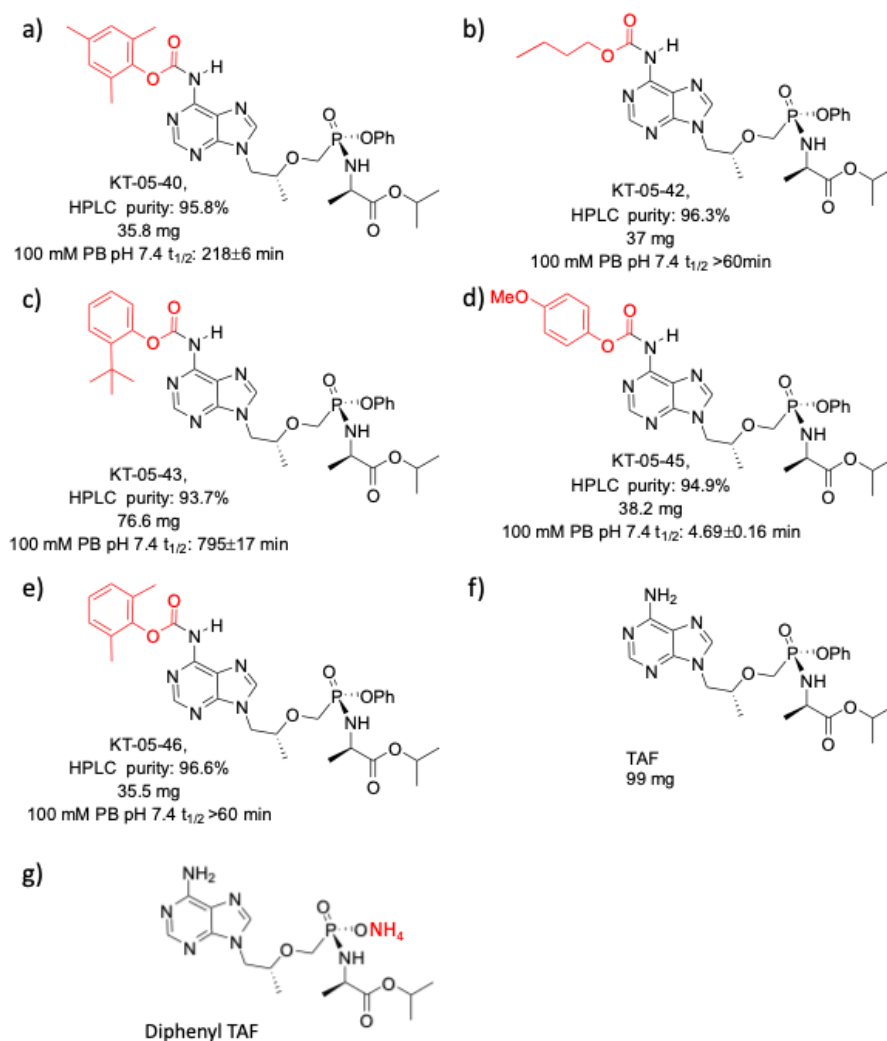


Figure 4.1: Structures of all the TAF carbamate Prodrugs, indicating the stability and purity of the compounds. a) TAF-2,4,6-trimethylphenyl carbamate, b) TAF-*n*-butyl carbamate, c) TAF-2-*t*-butyphenyl carbamate, d) 4-Methoxyphenyl carbamate, e) TAF-2,4-dimethylphenyl carbamate, f) TAF, and g) diphenyl TAF. The materials made at Johns Hopkins University include the HPLC purity and the stability of the compounds. Figure created by Dr Kartik Temburnikar.

4.3.1 ACN cytotoxicity assessment

Due to solubility issues ACN cytotoxicity was explored as a possible vehicle for the TAF carbamate Prodrugs. Figure 4.2 indicates no overt toxicity is caused as a result of ACN exposure between 2.5% and 0.01% ACN.

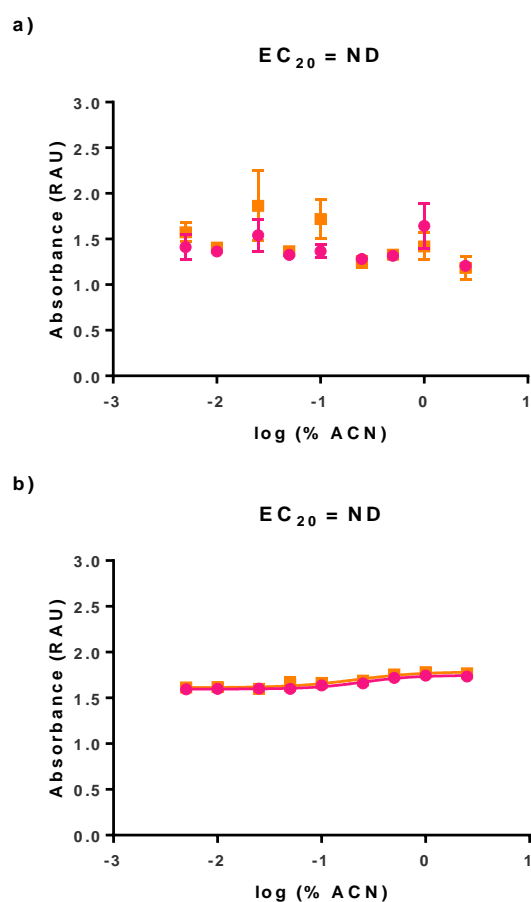


Figure 4.2: Cytotoxicity assessment of % of ACN diluted in media (from in THP-1 cells following 24 hours exposure a) MTT, b) LDH. Data displayed as n=4 technical replicates mean (\pm Standard Deviation) and n=2 experimental replicates, each displayed in a different colour. EC₂₀ values calculated using EC anything calculator from EC₅₀ values and the Hill Slope using GraphPad Prism software 9.3.1, not determined (ND) is used to describe values that were unable to be computed due to incomplete cytotoxicity curves.

Due to the lack of toxicity for ACN, it was carried forward as a vehicle in the subsequent assays.

4.3.2 TAF Carbamate prodrug cytotoxicity assessment

Cytotoxicity assessment was carried out on the TAF carbamate prodrugs in order to find appropriate concentrations to test in subsequent cell health assays. Figures 4.3 – 4.9 show there was no overt toxicity caused by TAF or the TAF carbamate prodrugs up to the concentration of 4000 ng/mL tested.

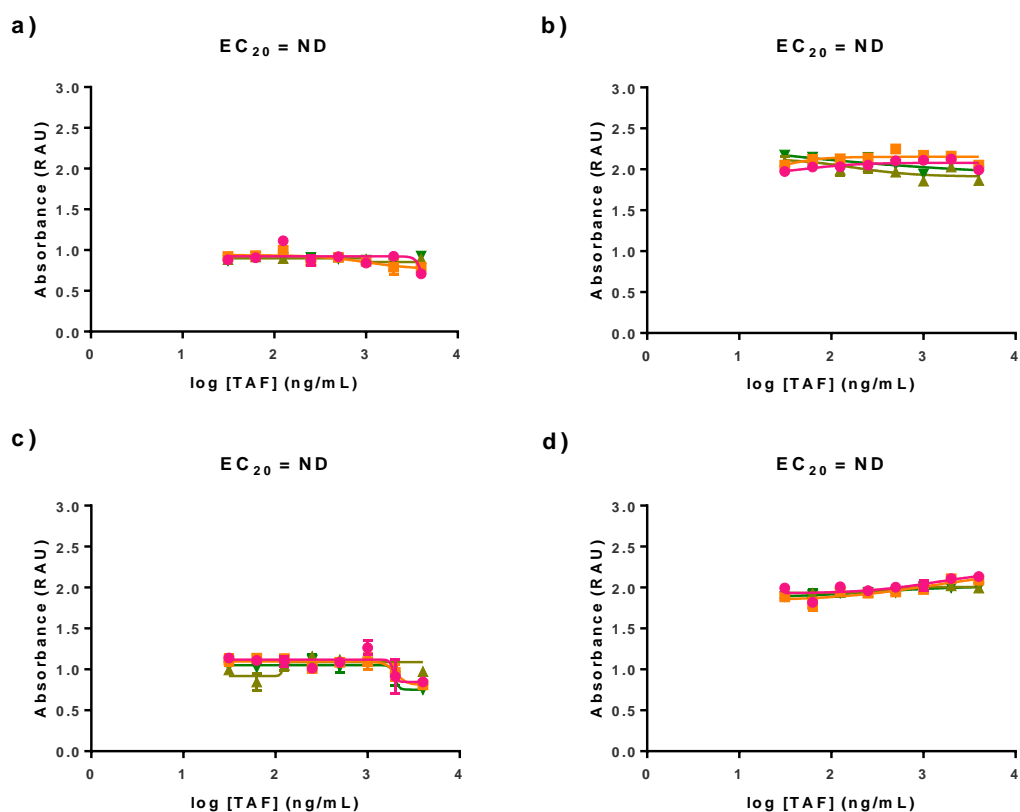


Figure 4.3: Cytotoxicity assessment of TAF in THP-1 cells following 24 hours exposure a) MTT, b) LDH and 48 hours exposure c) MTT, d) LDH. Data displayed as n=3 technical replicates mean (\pm Standard Deviation) and n=4 experimental replicates, each displayed in a different colour. EC_{20} values calculated using EC anything calculator from EC_{50} values and the Hill Slope using GraphPad Prism software 9.3.1, not determined (ND) is used to describe values that were unable to be computed due to incomplete cytotoxicity curves.

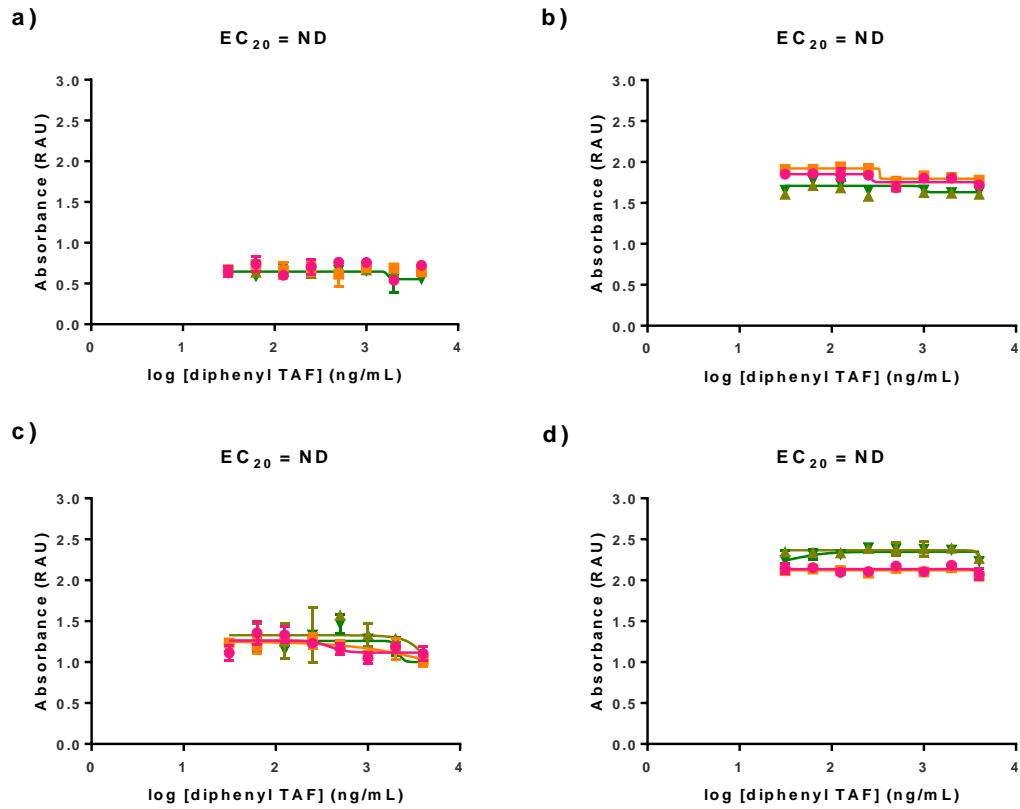


Figure 4.4: Cytotoxicity assessment of diphenyl TAF in THP-1 cells following 24 hours exposure a) MTT, b) LDH and 48 hours exposure c) MTT, d) LDH. Data displayed as n=3 technical replicates mean (\pm Standard Deviation) and n=4 experimental replicates, each displayed in a different colour. EC_{20} values calculated using EC anything calculator from EC_{50} values and the Hill Slope using GraphPad Prism software 9.3.1, not determined (ND) is used to describe values that were unable to be computed due to incomplete cytotoxicity curves.

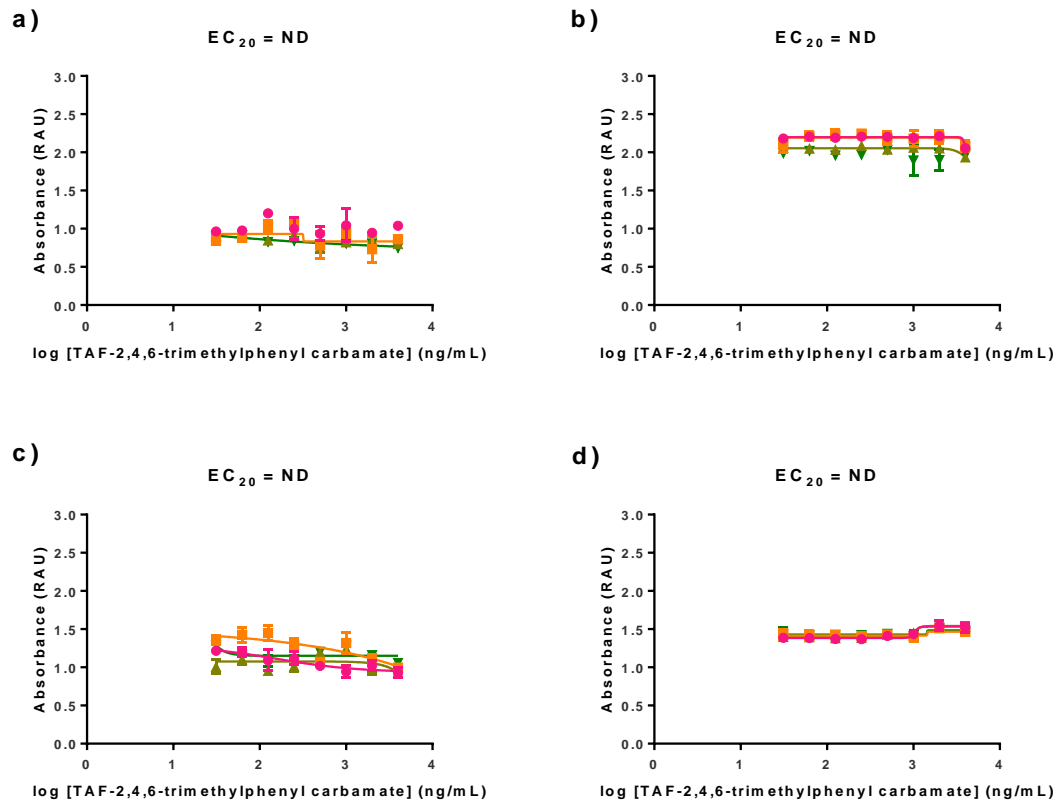


Figure 4.5: Cytotoxicity assessment of TAF-2,4,5-trimethylphenyl carbamate in THP-1 cells following 24 hours exposure a) MTT, b) LDH and 48 hours exposure c) MTT, d) LDH. Data displayed as n=3 technical replicates mean (\pm Standard Deviation) and n=4 experimental replicates, each displayed in a different colour. EC₂₀ values calculated using EC anything calculator from EC₅₀ values and the Hill Slope using GraphPad Prism software 9.3.1, not determined (ND) is used to describe values that were unable to be computed due to incomplete cytotoxicity curves.

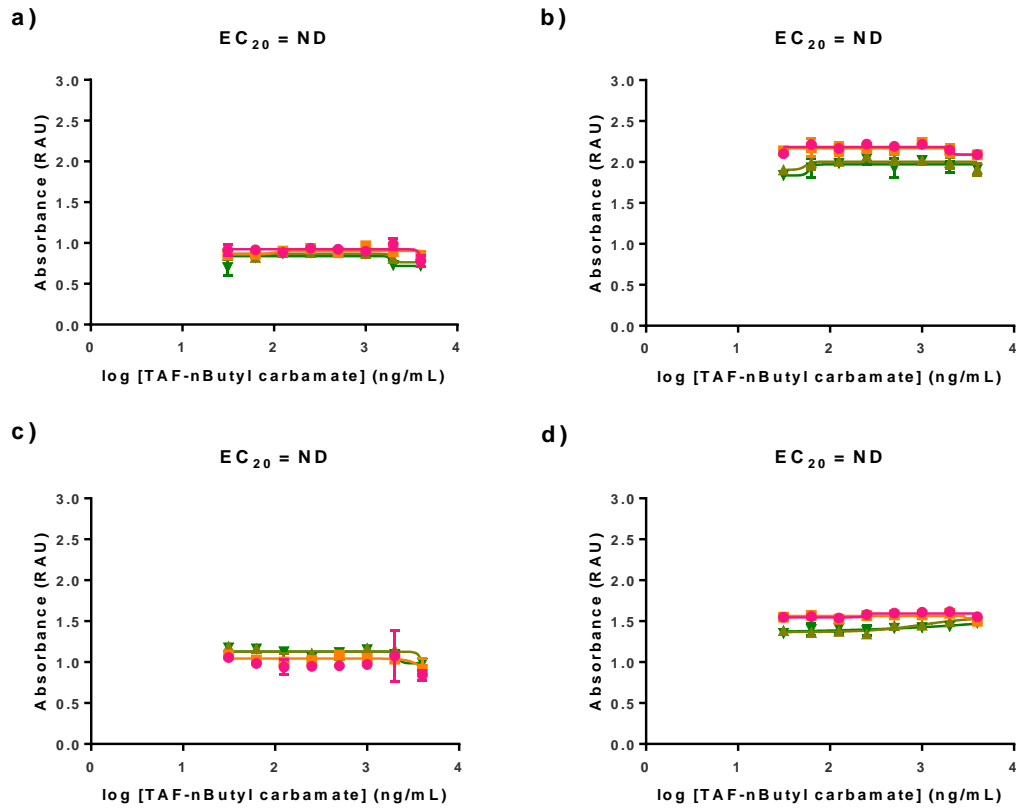


Figure 4.6: Cytotoxicity assessment of TAF-*n*-butyl carbamate in THP-1 cells following 24 hours exposure a) MTT, b) LDH and 48 hours exposure c) MTT, d) LDH. Data displayed as n=3 technical replicates mean (\pm Standard Deviation) and n=4 experimental replicates, each displayed in a different colour. EC₂₀ values calculated using EC anything calculator from EC₅₀ values and the Hill Slope using GraphPad Prism software 9.3.1, not determined (ND) is used to describe values that were unable to be computed due to incomplete cytotoxicity curves.

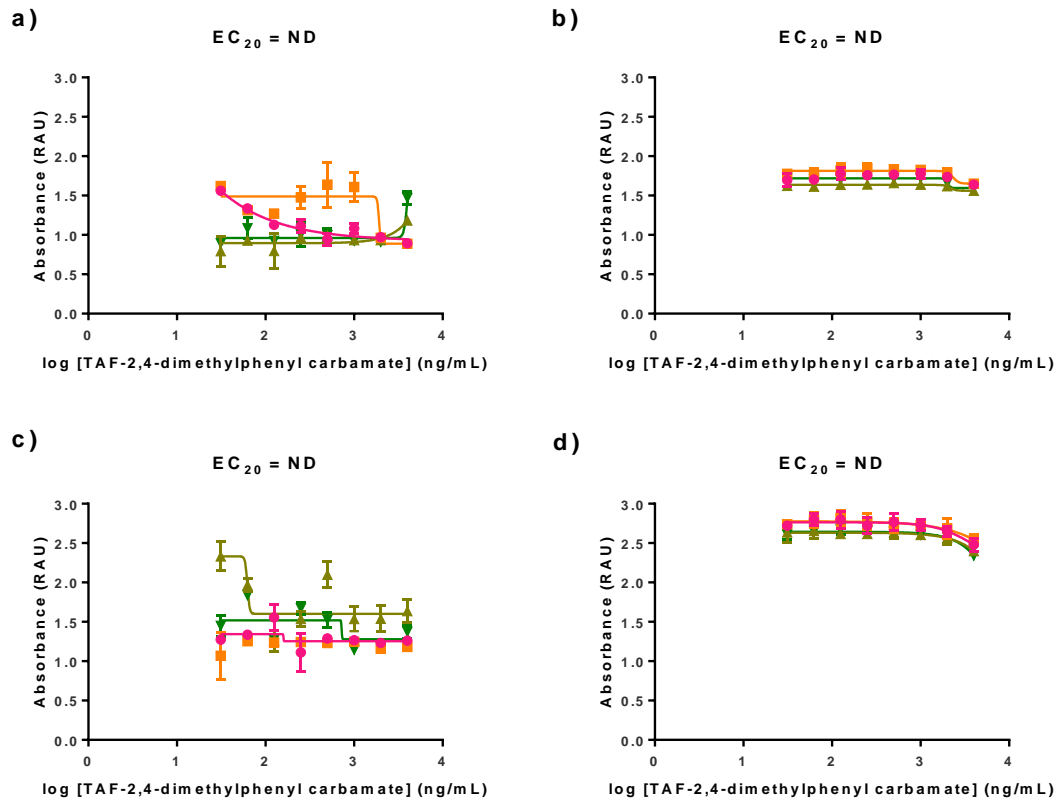


Figure 4.7: Cytotoxicity assessment of TAF-2,4-dimethylphenyl carbamate in THP-1 cells following 24 hours exposure a) MTT, b) LDH and 48 hours exposure c) MTT, d) LDH. Data displayed as n=3 technical replicates mean (\pm Standard Deviation) and n=4 experimental replicates, each displayed in a different colour. EC_{20} values calculated using EC anything calculator from EC_{50} values and the Hill Slope using GraphPad Prism software 9.3.1, not determined (ND) is used to describe values that were unable to be computed due to incomplete cytotoxicity curves.

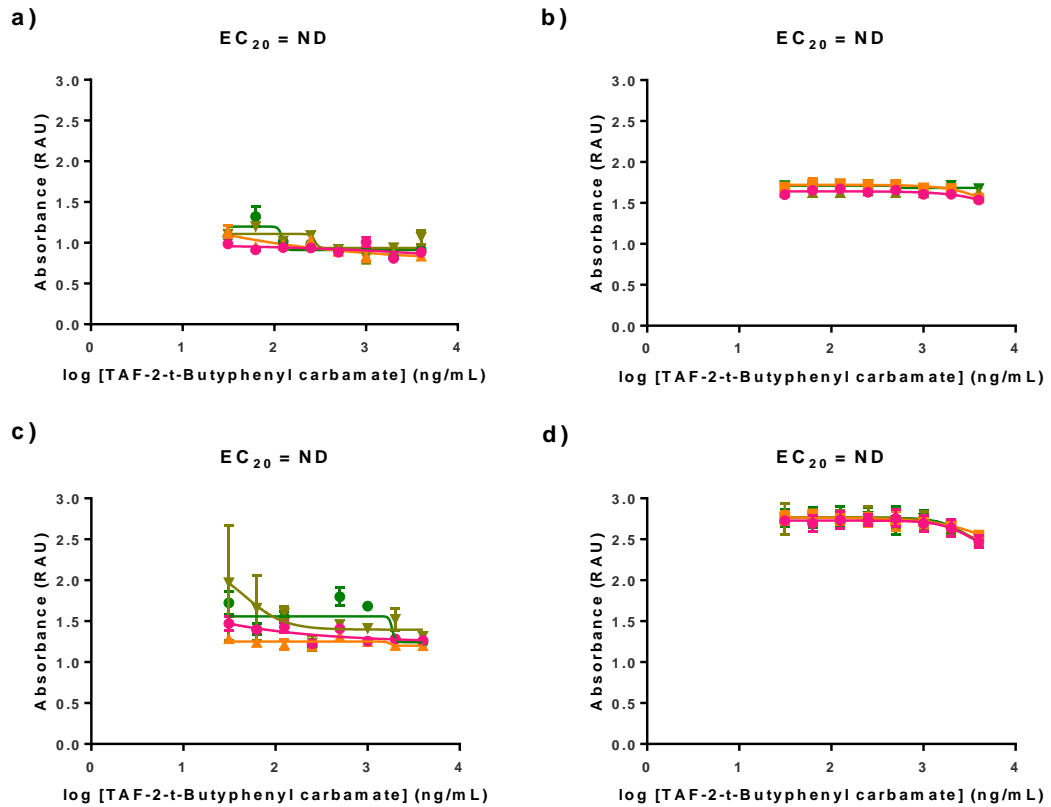


Figure 4.8: Cytotoxicity assessment of TAF-2-*t*-butylphenyl carbamate in THP-1 cells following 24 hours exposure a) MTT, b) LDH and 48 hours exposure c) MTT, d) LDH. Data displayed as n=3 technical replicates mean (\pm Standard Deviation) and n=4 experimental replicates, each displayed in a different colour. EC₂₀ values calculated using EC anything calculator from EC₅₀ values and the Hill Slope using GraphPad Prism software 9.3.1, not determined (ND) is used to describe values that were unable to be computed due to incomplete cytotoxicity curves.

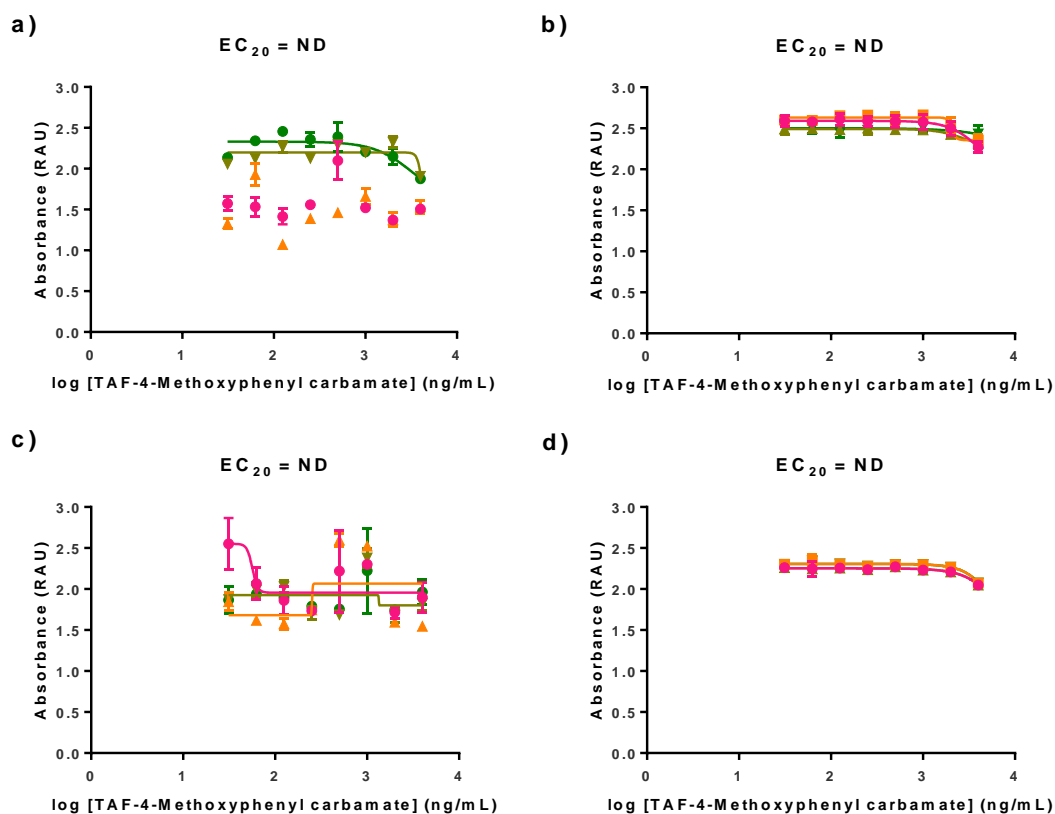


Figure 4.9: Cytotoxicity assessment of TAF-4-methoxyphenyl carbamate in THP-1 cells following 24 hours exposure a) MTT, b) LDH and 48 hours exposure c) MTT, d) LDH. Data displayed as n=3 technical replicates mean (\pm Standard Deviation) and n=4 experimental replicates, each displayed in a different colour. EC₂₀ values calculated using EC anything calculator from EC₅₀ values and the Hill Slope using GraphPad Prism software 9.3.1, not determined (ND) is used to describe values that were unable to be computed due to incomplete cytotoxicity curves.

Due to the lack of toxicity from the TAF carbamate prodrugs, the highest concentration tested was used (4000 ng/mL) in subsequent assays.

4.3.3 TAF carbamate prodrug cell health assessment

ROS and reduced glutathione were measured following 24 hour exposure to the TAF carbamate prodrugs in the THP-1 and MUTZ-3 in order to determine the ability of the treatments to modify cell health.

4.3.3.1 TAF carbamate prodrug cell health assessment in THP-1 Cells

Menadione treated cells had a significantly higher production of intracellular ROS, an average of 1443% compared to the untreated ($p < 0.0001$) (Figure 4.10) and a non-significant lower level of reduced glutathione in THP-1 cells, an average of 24% compared to the untreated (Figure 4.11).

The ACN control showed a significantly higher intracellular ROS, 206% when compared with the untreated ($p < 0.001$) and significantly higher reduced glutathione when compared to the untreated ($p < 0.001$) (Figures 4.10-11). Intracellular ROS was also significantly higher in the cells treated with 230 ng/mL of 4-methoxyphenylcarbamate (205.8%, $p < 0.001$), whereas 4000 ng/mL caused a significantly higher production of reduced glutathione when compared with the untreated (197%, $p < 0.05$) (Figures 4.9 and 10). TAF-2,4-dimethylphenyl carbamate at 230 ng/mL also caused significantly higher levels of reduced glutathione when compared to the untreated (204.1%, $p < 0.01$) (Figure 4.10).

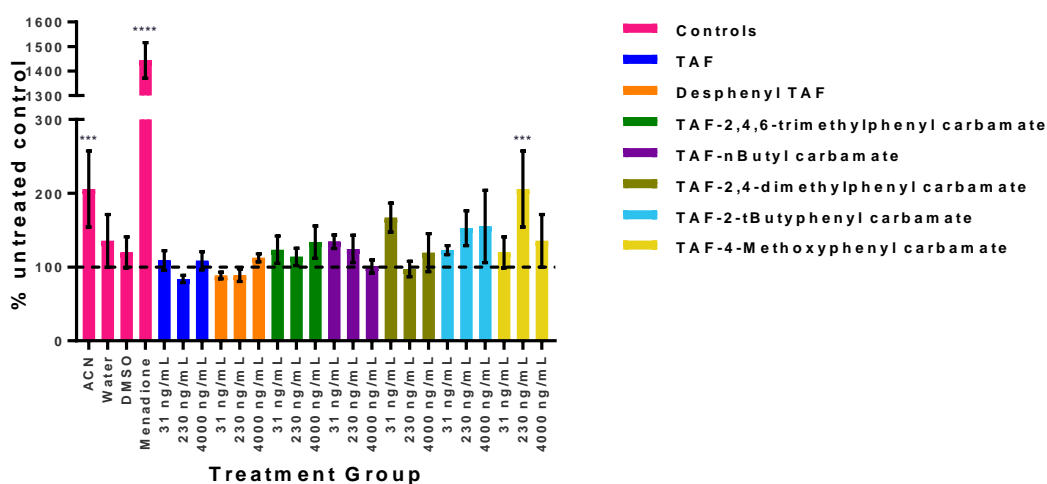


Figure 4.10: THP-1 intracellular ROS levels following 24 hrs exposure to the TAF carbamate prodrugs or controls, as measured using CellROX green reagent and Flow cytometry. Data displayed as median fluorescence intensity % of untreated control of $n=3$ ($n=2$ technical replicates), mean (\pm standard deviation). ANOVA statistical analysis carried out between the untreated (100%) and all other conditions, $p < 0.0001 = ****$, $p < 0.001 = ***$, $p < 0.01 = **$ and $p < 0.05 = *$.

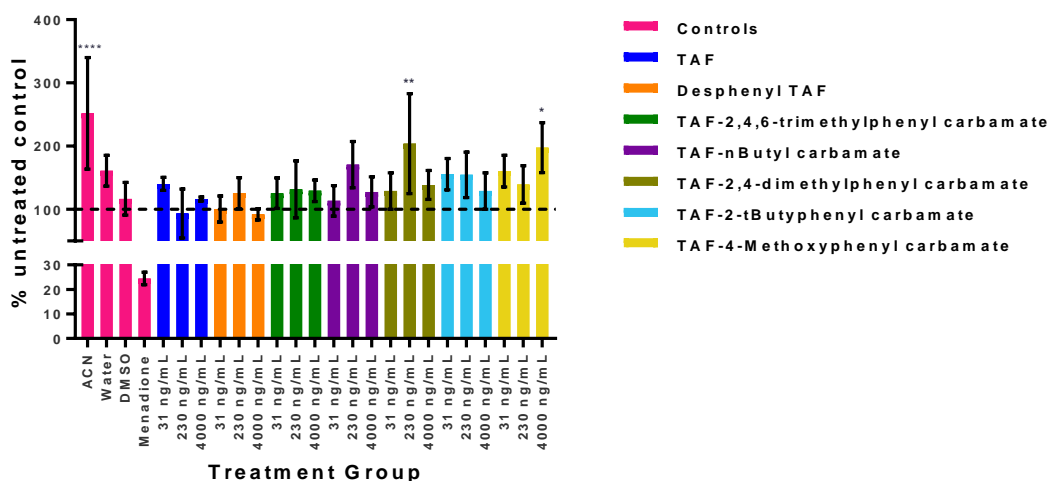


Figure 4.11: THP-1 intracellular reduced glutathione levels following 24 hrs exposure to the TAF carbamate prodrugs or controls, as measured using ThiolTracker violet reagent and Flow cytometry. Data displayed as median fluorescence intensity % of untreated control of n=3 (n=2 technical replicates), mean (\pm standard deviation). ANOVA statistical analysis carried out between the untreated (100%) and all other conditions, $p < 0.0001 = ****$, $p < 0.001 = ***$, $p < 0.01 = **$ and $p < 0.05 = *$.

In the THP-1 cell line significant alterations in ROS and reduced glutathione did not occur at concentration dependent levels from any of the TAF carbamate prodrugs and those that did cause significant alterations were nowhere near that of the control menadione.

4.3.3.2 TAF carbamate prodrug cell health assessment in MUTZ-3 Cells

Menadione treated cells has a significantly higher production of intracellular ROS (average 1131% compared to the untreated) (Figure 4.12) ($p < 0.0001$) and a significantly lower production of reduced glutathione in MUTZ-3 cells, an average of 17% compared to the untreated (Figure 4.13) ($p < 0.0001$). No significant perturbations were seen in the MUTZ-3 cells treated with any of the TAF monomers and the untreated (Figure 4.12 and 13).

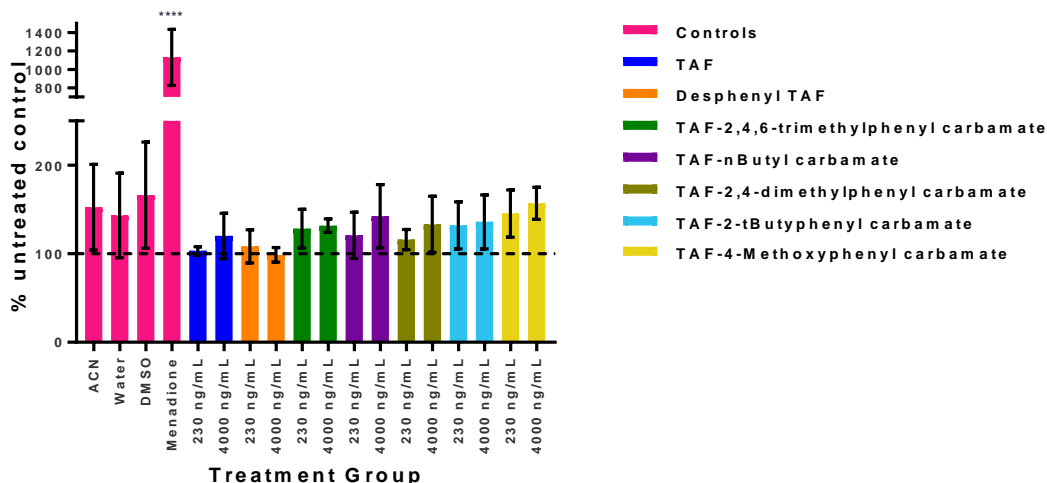


Figure 4.12: MUTZ-3 intracellular ROS levels following 24 hrs exposure to the TAF carbamate prodrugs or controls, as measured using CellROX green reagent and Flow cytometry. Data displayed as median fluorescence intensity % of untreated control of n=3 (n=2 technical replicates), mean (\pm standard deviation). ANOVA statistical analysis carried out between the untreated (100%) and all other conditions, $p < 0.0001 = ****$, $p < 0.001 = ***$, $p < 0.01 = **$ and $p < 0.05 = *$.

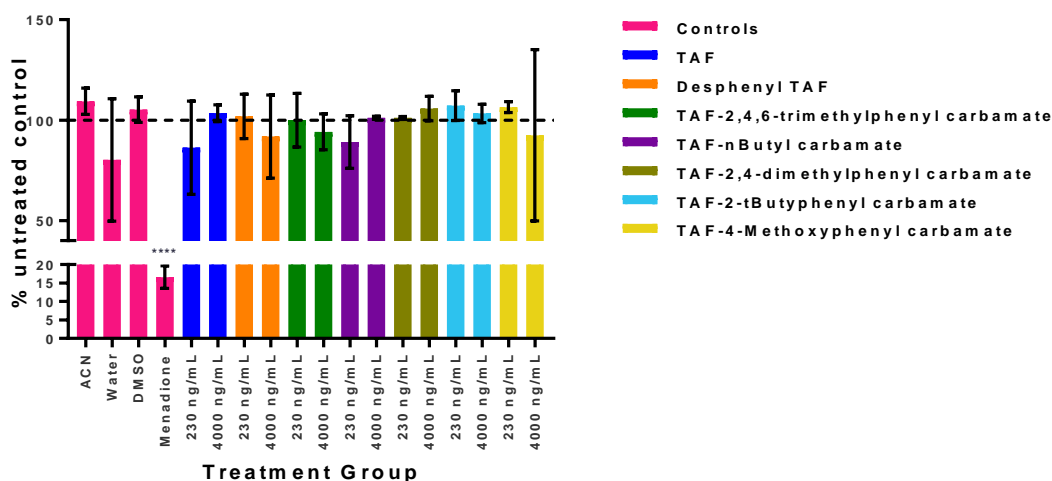


Figure 4.13: MUTZ-3 intracellular reduced glutathione levels following 24 hrs exposure to the TAF carbamate prodrugs or controls, as measured using ThiolTracker violet reagent and Flow cytometry. Data displayed as median fluorescence intensity % of untreated control of n=3 (n=2 technical replicates), mean (\pm standard deviation). ANOVA statistical analysis carried out between the untreated (100%) and all other conditions, $p < 0.0001 = ****$, $p < 0.001 = ***$, $p < 0.01 = **$ and $p < 0.05 = *$.

In the MUTZ-3 cell line significant alterations in ROS and reduced glutathione did not occur from any of the TAF carbamate prodrugs.

4.4 Discussion

TAF is another NRTI drug that is being incorporated into long-acting POP polymers, at the early stage in their development these were explored for their ability to modulate cellular health over short term exposures.

Due to the lack of overt toxicity seen from ACN between 2.5-0.01%, the TAF carbamate prodrugs were all taken forward with a top concentration of 4000 ng/mL at 0.4% ACN. No overt toxicity was seen for any of the TAF carbamate prodrugs tested and therefore the highest concentration of 4000 ng/mL was taken forward into the cell health assessment assays, with two lower concentrations, to explore any possibility of concentration dependent responses. Some variability is seen in the MTT assessment, variability is common with the MTT assay and as the LDH assay showed consistency and no overt toxicity, so therefore the assay was not repeated.

The positive control menadione showed that both intracellular ROS and reduced glutathione can be significantly altered in both the THP-1 and MUTZ-3 cell line following 24-hour exposure, as reported previously in the literature for other cell lines (Kim, Shin, Sohn, & Lee, 2014). A few significant perturbations were seen with intracellular ROS or reduced glutathione, when the cells treated with the TAF carbamate prodrugs were compared to the untreated cells. Although these significant perturbations were only seen in the THP-1 cells and were nowhere near the level of change seen with the positive control menadione.

0.4% ACN treated cells had significantly higher ROS and reduced glutathione, the higher reduced glutathione level is not indicative of ROS stress, due to reduced glutathione usually being depleted as a result of higher ROS production. These results were not replicated in the highest concentrations of test compounds which also contained 0.4 % ACN. The perturbations seen for the reduced glutathione levels in the THP-1 cells was not indicative of stress and does not follow the same direction of menadione, a known inducer of ROS (Kim et al., 2014). The higher perturbations in ROS are not as high as the menadione positive control and are not reflected in the reduced glutathione of the respective conditions for any of the significantly higher ROS results. These results show promise for these TAF carbamate prodrug scaffolds to be potentially successful for formulation into polymers that can be made into implantable rods like the FTC polymers used in the previous chapter. Although further, more detailed analysis, as done for the FTC polymers in Chapters 2, 6 and 7, would be required when or if they reach this stage of development. A repeat of the experiment could be carried out to explore further the potential for dump release of TAF, as previous (Su et al., 2020) TAF

implants toxicity may have been caused via a burst release, therefore exploring the effects of even higher TAF concentrations could potentially be useful. Exposing the cells for longer may also help us to explore this further, as the implant will be left in for longer periods. As previously assessed for FTC and 3TC in Chapter 3, it may be interesting to explore the drug TAF in the same way, in order to distinguish whether this may allude to the problems seen previously with TAF implants.

As mentioned in the introduction, cytotoxicity and genotoxicity has previously been seen with carbamate insecticides and therefore exploring both the cytotoxicity and health before further development of the POP polymers from TAF was important earlier on in the development process (Guanggang et al., 2013; Soloneski et al., 2015). It is also interesting to point out that, these compounds have varying stability as a result of hydrolysis, however the results for toxicity and cell health assessment at the concentrations treated did not significantly differ. When the TAF aryl carbamates undergo hydrolysis to release TAF they produce phenols, some of which are known to be toxic, it is noteworthy that these haven't caused toxicity in these assays. The lack of toxicity is likely either due to the low concentrations released, or failure for the compounds to undergo hydrolysis under the experimental conditions used, this would need to be explored further once concentrations to be used in humans are known.

Cell lines are not ideal for looking at responses, due to the fact they are all derived from a single set of cells and do not represent the inter individual variability seen *in vivo*. Due to the developmental stage of these materials, only a quick pre-screen of the materials was performed, it was determined that no significant perturbations in cytotoxicity or cell health occurs at the concentrations tested and therefore the materials should be developed further and tested as per the other FTC POP materials when they are at the same stage of their development. Genotoxic effects should be explored further into the development once a better understanding of exposure and release is determined.

Chapter 5

Assessment of, potential, *in vivo* adverse reactions to POP implants; links to pharmacokinetic parameters

5.1 Introduction

In vivo pharmacological assessment of a number of initial POP implants was carried out in order to explore the release of FTC, and subsequent pharmacokinetics, in addition to determination of ideal formulations, depending on their chemistry. The model chosen to determine the *in vivo* release of the implants was Wistar rats. *In vitro* candidate screening was carried out first, as part of the larger project, to screen for implants with favourable FTC release profiles. From the *in vivo* exposures, blood samples were taken, from the final cardiac bleed of the rats, for pharmacokinetic determination and preliminary immunological assessment of the animals.

As previously illustrated in chapter 1, the chain composition of the polymer POP materials used to create the implants assessed in this chapter are not uniform and the orientation of the repeat units and the order of these orientations in the polymer chains cannot as yet be predicted. There will therefore be variability in the release of FTC between the different types of implants, which may impact the results seen for the immunological assessment of each group of rats. *In vivo* immunological assessment was important early in the development process due to the previously discussed issues seen *in vivo* with a TAF eluting implant (Su et al., 2020). Implantable biodegradable drug eluting devices are quite new and therefore a decision was to conduct the broadest assessment of soluble immunological responses that was technically, and logistically, practical.

A broad panel of, rat, cytokines were measured, alongside measurement of alanine aminotransferase (ALT) and C-reactive protein (CRP). CRP was measured as it is commonly used to test for inflammation in humans, it produced by the liver hepatocytes and becomes elevated with a number of conditions, such as coronary artery disease (Mortensen, 2001). Increased ALT can indicate liver injury and can help to determine whether the POP implants have the ability to cause liver toxicity alongside the measurement of pro-inflammatory cytokines.

Species differences between humans and rats, including variances in circulating leukocytes and antibody production, and the low number of animals per treatment group suggest this chapter must be taken as a screen which requires other *in vitro/ex vivo* analysis including that carried out in this thesis (Haley, 2003).

5.2 Methods

5.2.1 Materials

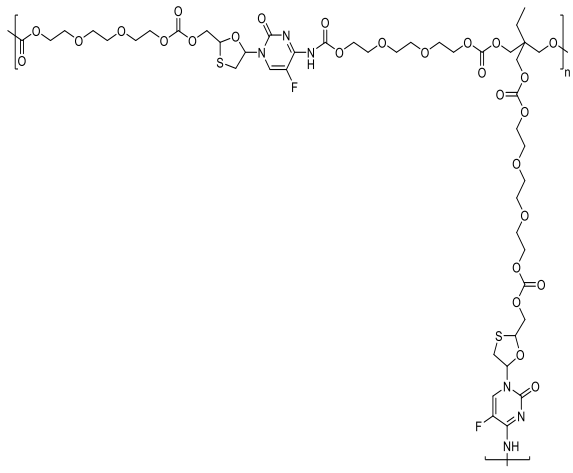
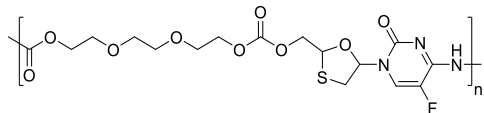
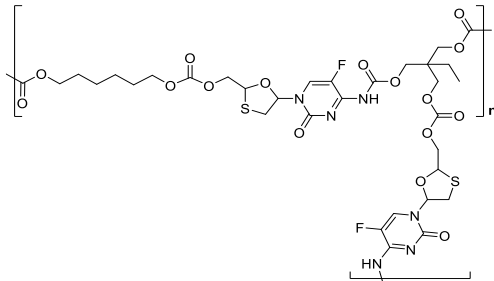
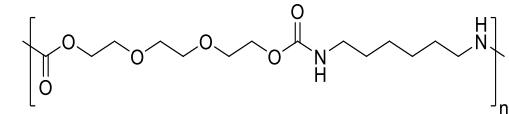
FTC, 3TC and were all purchased as described in the previous chapters. The POP implants were prepared from POP materials by Dr Faye Hern and Dr Anika Shakil from the Chemistry department at the University of Liverpool. Rat Magnetic Luminex, 17-plex (cytokines: CXCL2/growth-regulated oncogene (GRO)- β /MIP-2/ Cytokine-Induced Neutrophil Chemoattractant (CINC)-3, CXCL3/GRO- γ /CINC-2/Dendritic cell inflammatory protein-1 (DCIP-1), GM-CSF, ICAM-1/CD54, IFN- γ , IL-1 α /IL-1F1, IL-1 β /IL-1F2, IL-2, IL-4, IL-6, IL-10, IL-13, IL-18/IL-1F4, L-Selectin/CD62L, Tissue inhibitors of metalloproteinases (TIMP)-1, TNF- α and Vascular endothelial growth factor (VEGF) (R&D systems), CRP ELISA (R&D systems) and DuoSet[®] Ancillary reagent Kit two (R&D systems) were all purchased from Bio-technie (Minneapolis, USA). The Rat ALT SimpleStep ELISA[®] kit was purchased from Abcam (Cambridge, UK).

5.2.2 Exposure of Wistar rats to POP implants

This experimental animal work was planned and carried out by Dr Megan Neary, Dr Jo Sharp and Dr Helen Box at the University of Liverpool. The animal experiment was carried out in two parts. The first involved 4, male, Wistar rats weighing between 326-375g receiving a subcutaneous injection of FTC at 100 mg/kg using water as the vehicle (0.2 mL) within the scapular region and four receiving an IV injection of FTC at 10 mg/kg using water as the vehicle (0.2 mL) via the tail vein. Tail vein bleeds were taken at 24- and 48-hours, for pharmacokinetic assessment. At 72-hours the rats were anaesthetised under 3% isoflurane and cardiac puncture completed using a heparinised syringe. Following cardiac puncture, a lethal injection of pentobarbitone was administered directly into the heart and cessation of breathing was used to confirm death. The second part involved four groups of four male Wistar rats weighing between 300-350g, receiving a subcutaneous administration of four different POP implants for 91 days. Implant diameter was 2 mm and the length 15 mm. The first three groups received different POP implants containing FTC and the final group received a single CPI containing no FTC, Table 6.2.1 details the implants used. To administer the implants the rats were anaesthetised under 3% isoflurane and an incision approximately 5mm in length was made in the subcutaneous layer in the scapular region before a disposable 10mm/8mm implant syringe with a 12-gauge Lauer lock implant needle attached was used to administer the implants on either side of the scapular region. Tail vein bleeds were taken at 1-hour, 2-hours, 4-hours and 1, 2, 3, 4, 7, 10, 14, 21, 28, 35, 42, 49, 56, 63, 70, 77, and 84

days post implantation. On day 91 the rats were anaesthetised under 3% isoflurane and cardiac puncture completed using a heparinised syringe. Following cardiac puncture, a lethal injection of pentobarbitone was administered directly into the heart and cessation of breathing was used to confirm death.

Table 5.1: Summary of the implants used in the animal experiment.

Rat #	Implant Contents	Structure
1-4	Branched poly(FTC) 1 melt prep polymer implant (0.075 mg/day total)	
5-8	Linear poly(FTC) melt prep polymer implant (0.9 mg/day total)	
9-12	Branched poly(FTC) 2 melt prep polymer implant (2.25 mg/day total)	
13-16	CPI, no FTC	

The cardiac bleed from each rat was placed in a heparinised Eppendorf and spun at 860xg for five minutes and the plasma supernatant removed, 75 μ L aliquots were frozen at -80°C until analysis.

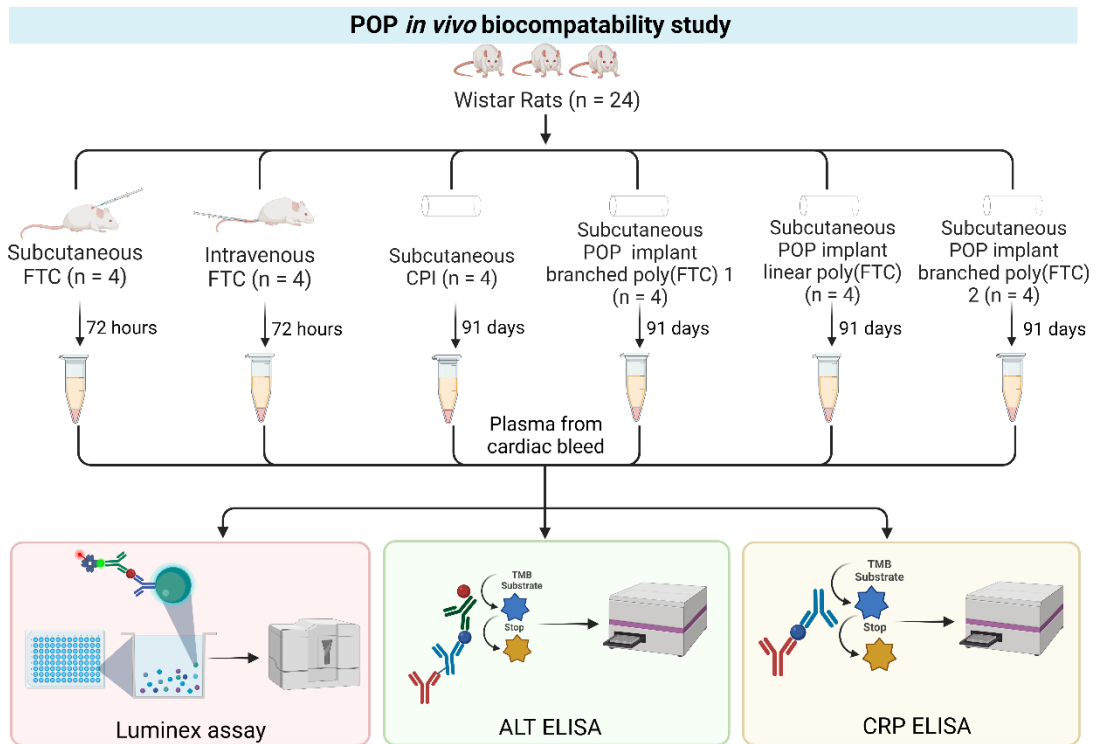


Figure 5.1: POP implant *in vivo* study design for the immune biocompatibility assessment. Created with BioRender.com.

5.2.3 Multiplex measurement of cytokines and chemokines, in rat plasma samples, following exposure to test materials.

Supernatants were thawed and cytokine analysis carried out following the Rat Magnetic Luminex Assay protocol. The Bio-Plex 200 Luminex system was started and allowed to warm up to working temperature. Samples, standards and all reagents were allowed to equilibrate to 15-30 °C. The standard provided in the kit was reconstituted with Calibrator Diluent RD6-52 using the volume specified on the certificate of analysis, in this case 0.8 mL and allowed to stand for 15 minutes with gentle agitation and formed standard 1. 100 µL from standard 1 was then used to perform a 3-fold dilution series using Calibrator Diluent RD6-52 to create the rest of the 6 standards. Wash buffer was made by diluting wash buffer concentrate 1:20 in distilled water. Microparticle cocktail, biotin-antibody cocktail, Streptavidin-PE vials were all centrifuged at 1000xg for 30 seconds. The biotin-antibody cocktail was vortexed to suspend the microparticles and 500 µL was added to 5 mL of Diluent RD2-1 to create the Diluted biotin-antibody cocktail. The streptavidin-PE concentrate was vortexed and 220 µL added to 5.35 mL of Wash buffer in a polypropylene test tube wrapped with aluminium foil to protect it from light. All rat plasma samples were centrifuged at 860xg for five minutes and

diluted 1:2 using calibrator diluent RD6-52. 50 µL of sample or standards plated in their respective wells, all standards were read in duplicate. The rat magnetic microparticle cocktail was vortexed and 500 µL added to 5 mL of Diluent RD2-1 to create the diluted microparticle cocktail. 50 µL of microparticle cocktail was added to every well on the 96-well plate and incubated at 15-30 °C on a plate shaker set at 800 RPM for two hours. The plate was then washed three times with addition of 100 µL of wash buffer using the Bio-Plex Pro™ II plate washer. 50 µL of diluted biotin antibody cocktail was added to each well and incubated at 15-30 °C on a plate shaker set at 800 RPM for one hour. During this incubation the Bio-Plex 200 Luminex was calibrated, and the machine set up with the bead regions and standard concentrations. The plate wash was repeated and 50 µL of diluted streptavidin-PE added to each well and incubated at 15-30 °C on a plate shaker set at 800 RPM for 30 minutes. The plate wash was repeated and 100 µL of wash buffer was added to each well and incubated for two minutes on a plate shaker set to 800 RPM. The plate was then analysed using the Bio-Plex 200 Luminex, setting the sample volume at 50 µL, bead type as Bio-Plex MagPlex Beads, setting double discriminator gates at 8000 and 23000, reporter gain settings set to low RP1 target value for CAL2 setting, 50 counts per region and collect medium fluorescence intensity. The average concentrations calculated for each cytokine were plotted, values that were above the limit of quantification were plotted at the limit of detection and values below the limit of detection were plotted as 0. Samples that had one replicate within the range were plotted at the value that was in range alone. A dashed line has been used to indicate where these limits of detection are on the graphs that contained samples that were either above or below the limit of detection. GraphPad Prism software 9.3.1 was used to display the data.

Table 5.2: Lower and upper limits of quantification for the Rat Magnetic Luminex Assay.

Analyte	Minimum (pg/mL)	Maximum (pg/mL)
CXCL2/GRO-β/MIP-2/CINC-3	30.86	7500
CXCL3/GRO-γ/CINC-2/DCIP-1	27.82	6760
GM-CSF	45.23	10990
ICAM-1/CD54	40.37	9810
IFN-γ	598.97	145550
IL-1 α/IL-1F1	76.87	18680
IL-1β/IL-1F2	15.47	3760
IL-2	27.28	6630

IL-4	14.32	3480
IL-6	198.97	48350
IL-10	24.32	5910
IL-13	6.09	1480
IL-18/IL-1F4	15.76	3830
L-Selectin/CD62L	96.13	23360
TIMP-1	26.91	6540
TNF-α	242.14	58840
VEGF	62.76	15250

The previous experiment was repeated using neat samples from a second plasma aliquot due to the quantity of analytes that were below the limit of detection in a number of samples.

5.2.4 ALT ELISA

Rat plasma aliquots were thawed and the rat ALT SimpleStep ELISA® kit was carried out following the manufacturer's protocol, all reagents and materials were brought to 15-30 °C before starting. Sample diluent NS and enhancer were prepared by diluting cell extraction enhancer with sample diluent NS at a ratio of 1:50. Wash buffer PT was prepared by diluting wash buffer concentrate with deionized water at a ratio of 1:10. The antibody cocktail was made by diluting the capture and detector antibodies with antibody diluent 4BR at a ratio of 1:1:8. The standard curve was made by reconstituting the ALT standard with 500 μ L of sample diluent NS and enhancer, which was mixed gently at 15-30 °C for ten minutes to create a 8,000 ng/mL stock, the standard curve from 1,000-15.6 ng/mL was made by first creating a 1:8 dilution and then six subsequent 1:2 dilutions, all using sample diluent NS and enhancer.

The kit suggested that the typical sample dynamic range for rat plasma, EDTA was 0.125-2%. First a dilution of 1:50 (Rats 1-24, n=2) and 1:100 (Rats 1-16, n=2) was used for all samples, with each sample assayed in duplicate. Then a dilution of 1:500 (Rats 1-24, n=2) and 1:750 (Rats 1-16, n=2) was tried using a second kit due to potential issues with the first plates standards and the very high

OD readings from the first plate.

50 μ L of all standards or diluted samples was added to each well in duplicate, with the sample diluent NS and enhancer being in assayed in duplicate as the blank control. 50 μ L was then also added to all wells, the plate sealed and incubated for one hour at 15-30 °C on a plate

shaker set at 400 RPM. Following incubation, each well was washed using the Bio-Plex Pro™ II plate washer, the wells were aspirated and then 350 µL of wash buffer PT was used to wash all wells three times. After the last wash, the plate was inverted and blotted against clean paper towels to remove any leftover wash buffer. 100 µL of TMB development solution was then added to all wells, the plate sealed with a foil cover, kept in the dark and incubated for ten minutes at 15-30 °C on a plate shaker set at 400 RPM. 100 µL of stop solution was then added to all wells and the plate shook on a plate shaker for one minute followed by immediate reading of OD using the CLARIOstar plate reader at an OD of 450 nm. The average OD for the blank was taken from all other sample values and a standard curve was created in GraphPad Prism software 9.3.1 using a 4-parameter logistic curve-fit, this was used to interpret the values for each sample from the standard curve. GraphPad Prism software 9.3.1 was also used to display the data from the 1:500 dilution shown, as the same samples were also above the limit of detection with the 1:750 dilution also above the limit for all samples and not all samples were analysed at this higher dilution.

5.2.5 CRP ELISA

Supernatants were thawed and cytokine analysis carried out following the CRP ELISA protocol.

CRP ELISA was carried out following the manufacture instructions in both the Rat CRP kit and the DuoSet® Ancillary reagent Kit 2. The Capture antibody was diluted to 4 µg/mL in PBS without protein (ELISA Plate-Coating Buffer) and 100 µL added to each well of a 96-well plate, sealed and incubated overnight at 15-30 °C. The wells were then aspirated and washed three times with 400 µL of wash buffer. The plate was then blocked by adding 300 µL of reagent diluent and incubated at 15-30 °C for one hour and the wash step repeated. A standard curve was generated using a 2-fold dilution series from 10,00-156 pg/mL in reagent diluent.

The kit suggested to start reagent diluent optimisation for plasma samples using 10-50% with animal serum. Seven of the samples had a much larger volume and were used for a test dilution run, all dilutions were made in reagent diluent included in the kit. The first dilution used was 1:2 for samples from animals 2, 4, 6, 8, 9, 10 and 14, a 1:10 dilution was also used for samples. These samples were incredibly darker in colour than the standard curve and the OD much larger than the standard curve samples.

100 µL of each standard or sample was added to the respective well of the 96-well plate, covered, incubated at 15-30 °C for two hours and then the wash step repeated. Detection

antibody was diluted in reagent diluent to 500 ng/mL and 100 µL was then added to each well, covered, incubated at 15-30 °C for two hours and then the wash step repeated. Streptavidin-HRP was diluted 200-fold in reagent diluent and 100 µL added to each well, covered, incubated at 15-30 °C away from direct light for 20 minutes and then the wash step was repeated. Substrate solution was made by mixing colour reagent A (H₂O₂) and colour reagent B (Tetramethylbenzidine) in a 1:1 ratio, then 100 µL added to each well and incubated for 20 minutes at 15-30 °C and avoiding direct light. 100 µL of stop solution was then added to each well and the OD determined using the CLARIOstar at a wavelength of 450 nm and 540 nm. Each well was then corrected by removing the OD at 540 nm from that at 450 nm. The average OD for the blank was taken from all other sample values and a standard curve was created in GraphPad Prism software 9.3.1 using a 4-parameter logistic curve-fit. GraphPad Prism software 9.3.1 was also used to display the data from the 1:500 dilution shown as the 1:5000 also above the limit for all samples and not all samples were analysed at this higher dilution.

For the second attempt, a 1:100 dilution (Rats 1-24, n=2) and a 1:200 dilution (Rats 1-16, n=2). These samples were still also incredibly darker in colour than the standard curve and the OD much higher than the standard curve samples. For the third run, a 1:500 dilution (Rats 1-24, n=2) and a 1:5000 dilution (Rats 1-16, n=2). These samples were closer to the standard curve samples, but still darker in colour than the standard curve and the OD much higher than the standard curve samples.

5.2.6 Histology assessment of biopsies taken from the implantation site

A single biopsy section was taken from one of the implantation sites per rat from the subcutaneous layer containing the implants in the scapular region of the treated rats was taken, stored in formalin and sent off for haematoxylin & eosin stain and Masson trichrome staining. The stained sections are then severity scored and they provide a written comment for each sample as well. This histology work was carried out at the Leahurst University of Liverpool Campus by colleagues Dr Lorenzo Ressel and Emanuele Ricci.

5.3 Results

5.3.1 Multiplex measurement of cytokines and chemokines, in rat plasma samples, following exposure to test materials.

Multiplex analysis of cytokines and chemokines in the plasma from the cardiac bleed of the animals was carried out to explore the immunocompatibility of these materials in vivo. In the diluted samples the analytes IL-1 α , IL-2, IL-4, IL-6, IL-10, IL-13, CXCL-2, GM-CSF, IFN- γ , TNF- α and VEGF were all below the limit of detection in all samples analysed. Although in the diluted samples only L-selectin was above the limit of detection for all samples, with ICAM-1 being above the limit in all but one sample. One of each the rats implanted with either linear poly(FTC) or branched poly(FTC) 1 implants had higher levels of IL-1 β and the linear poly(FTC) animal also had higher IL-18 levels. One of the rats receiving the CPI also showed higher IL-18 levels. Rat 24, that was only included in the short IV study had higher levels of IL-1 β , IL-18, CXCL3, and TIMP-1.

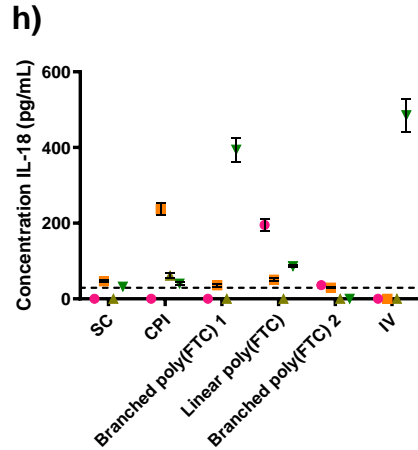
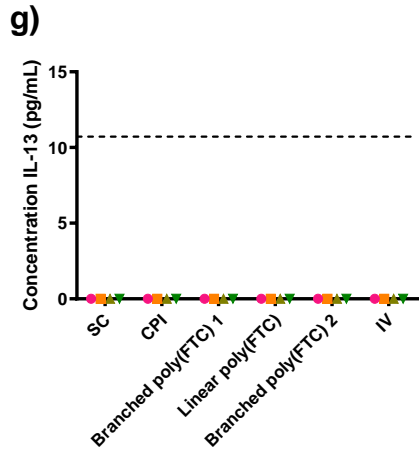
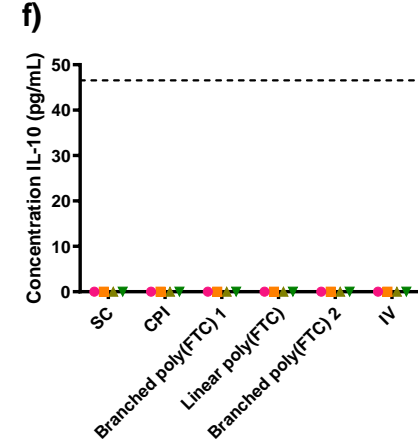
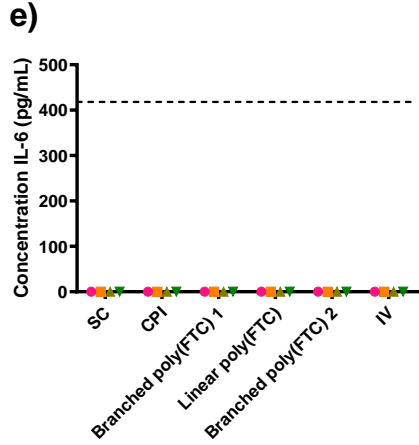
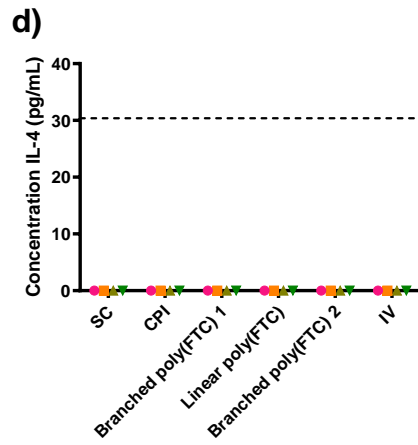
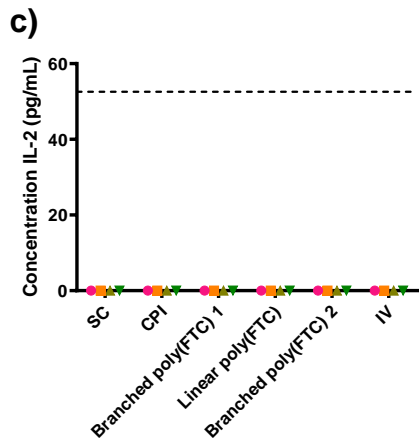
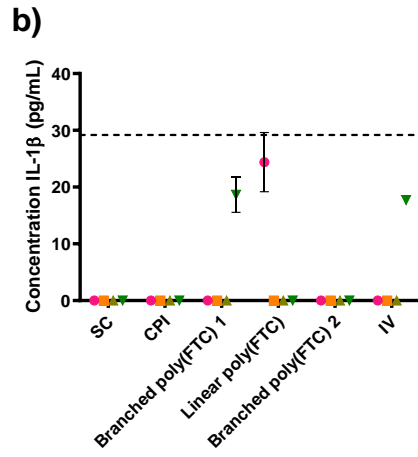
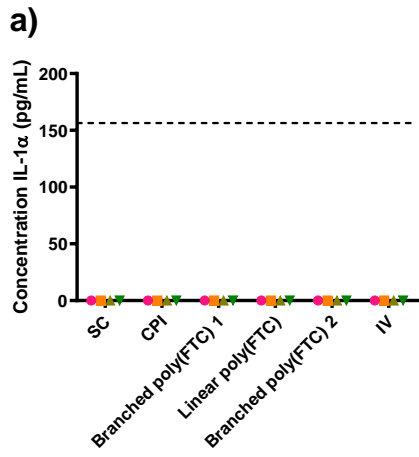


Figure 5.2: Concentrations of IL cytokines measured in rat blood following 91 days of exposure to the POP implants, as measured by Rat Luminex Assay on the Bio-Plex 200 Luminex system. a) IL-1 α , b) IL-1 β , c) IL-2, d) IL-4, e) IL-6, f) IL-10, g) IL-13 and h) IL-18. Data adjusted following 1:2 dilution. Data displayed as n=3, mean (\pm standard deviation). Dashed lines indicate the top limit of the standard curve, # indicates values above the limit of detection. No statistical tests have been carried out due to the variability between rats.

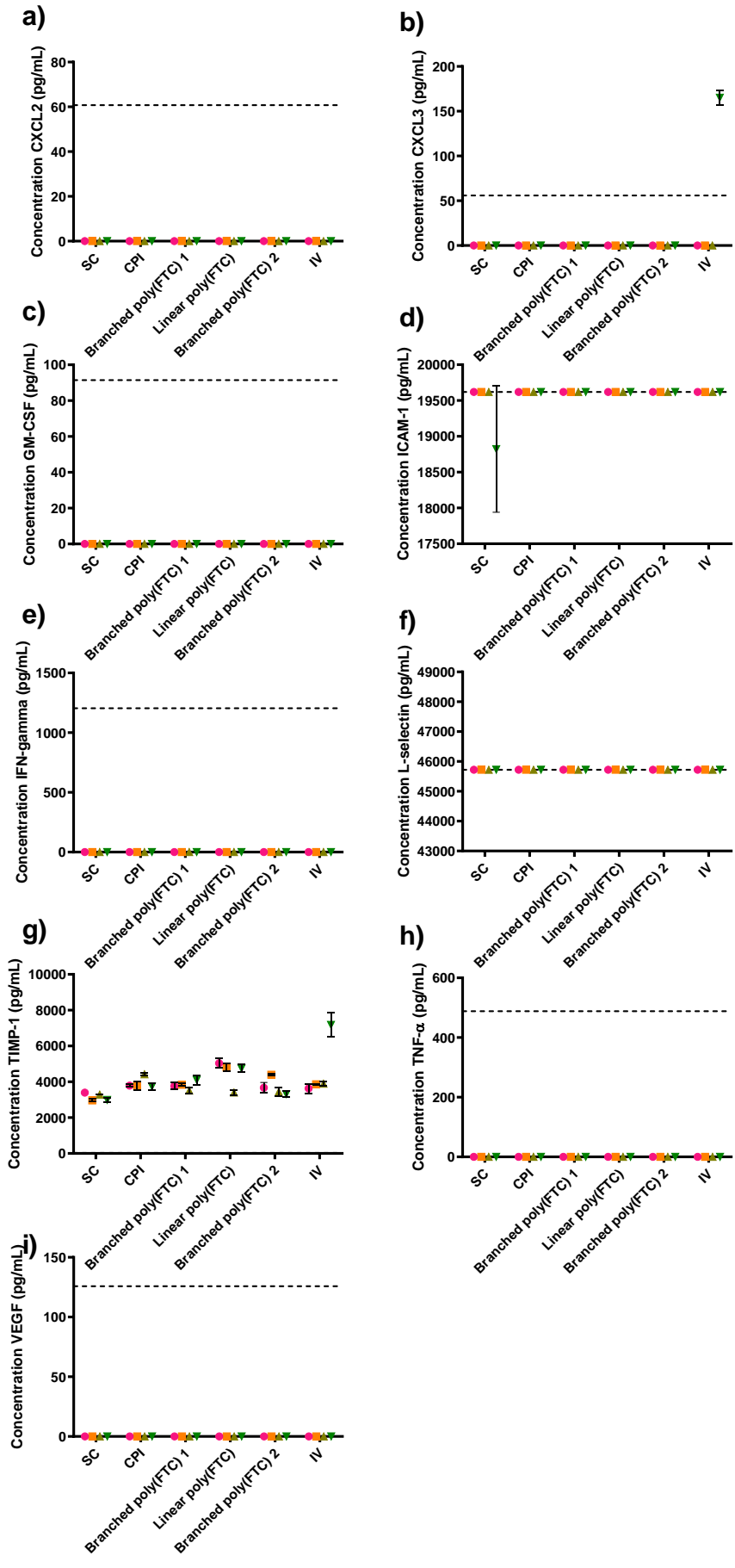


Figure 5.3: Concentrations of cytokines measured in rat blood following 91 days of exposure to the POP implants, as measured by Rat Luminex Assay on the Bio-Plex 200 Luminex system. a) CXCL2, b) CXCL3, c) GM-CSF, d) ICAM-1, e) IFN- γ , f) L-selectin, g) TIMP-1, h) TNF- α and i) VEGF. Data adjusted following 1:2 dilution. Data displayed as n=3, mean (\pm standard deviation). Dashed lines indicate the top limit of the standard curve, # indicates values above the limit of detection. No statistical tests have been carried out due to the variability between rats.

When the samples were run through neat only the analytes IL-1 α , IL-2, IL-4, IL-6, CXCL-2, GM-CSF and TNF- α were all below the limit of detection in all samples analysed. Whereas in the undiluted samples both L-selectin and ICAM-1 were above the limit of detection for all samples. Two of the rats implanted with linear poly(FTC) and one with the branched poly(FTC) 1 implant had higher levels of IL-1 β and one of each the linear poly(FTC) and branched poly(FTC) 1 animals also had higher IL-18 levels. One of the rats receiving the CPI also showed higher IL-18 levels. Rat 24, that was only included in the short IV study had higher levels of IL-18, and CXCL3.

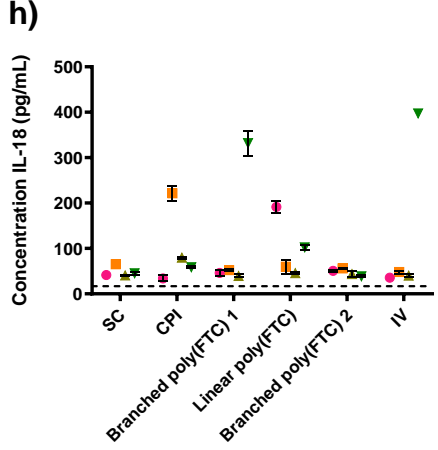
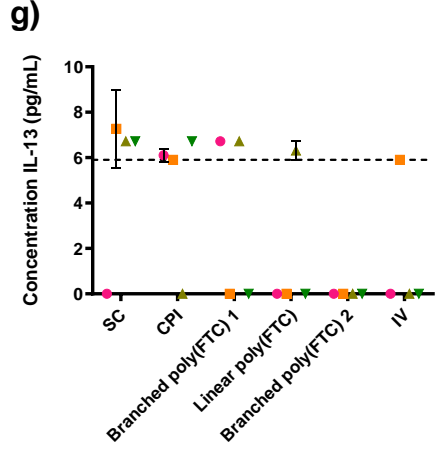
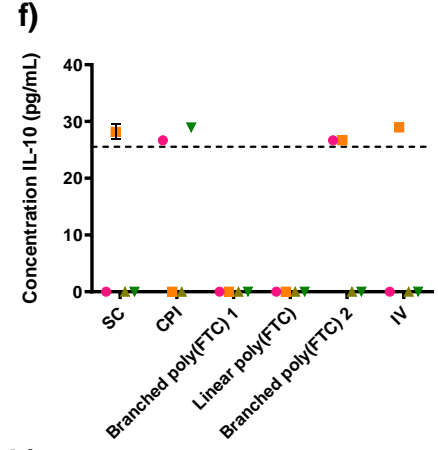
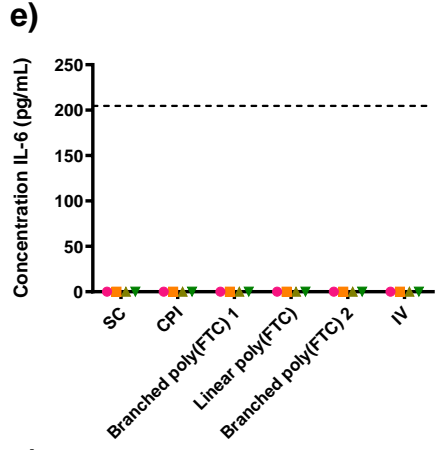
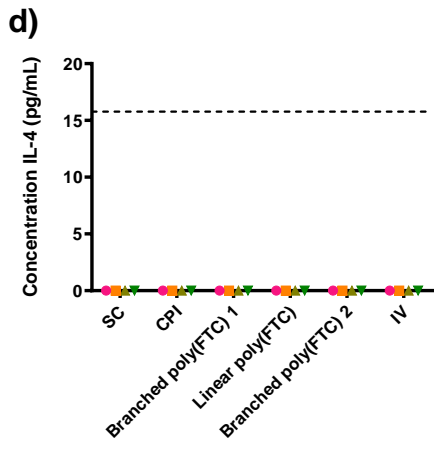
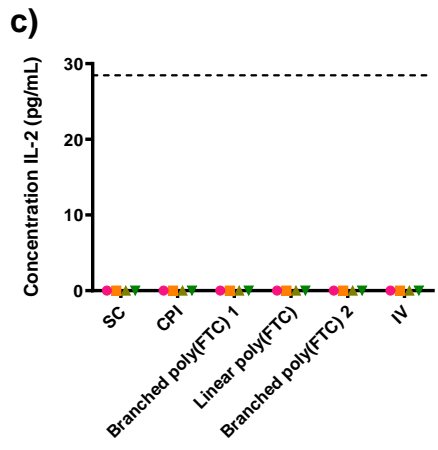
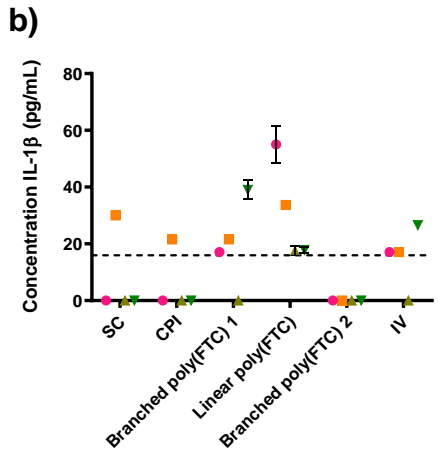
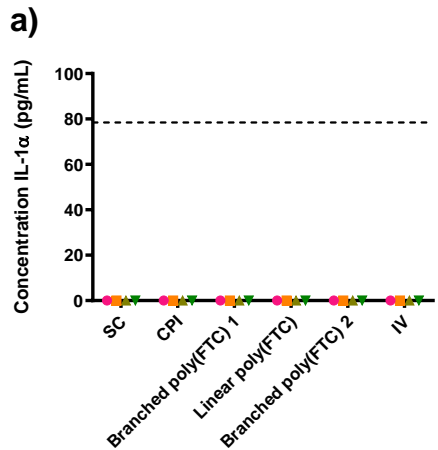


Figure 5.4: Concentrations of IL cytokines measured in rat blood following 91 days of exposure to the POP implants, as measured by Rat Luminex Assay on the Bio-Plex 200 Luminex system. a) IL-1 α , b) IL-1 β , c) IL-2, d) IL-4, e) IL-6, f) IL-10, g) IL-13 and h) IL-18. Data displayed as n=3, mean (\pm standard deviation). Dashed lines indicate the top limit of the standard curve, # indicates values above the limit of detection. No statistical tests have been carried out due to the variability between rats.

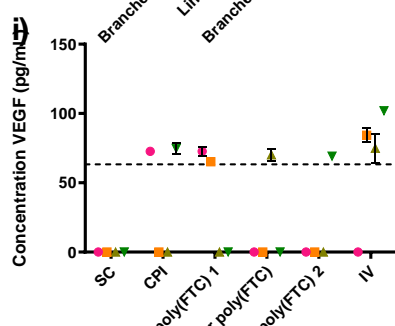
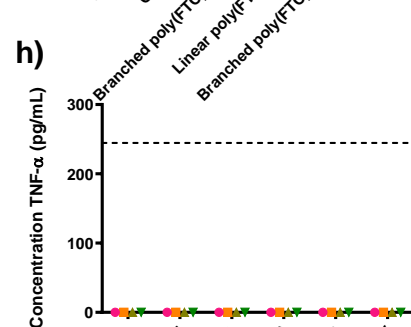
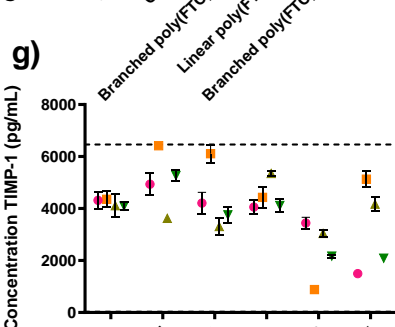
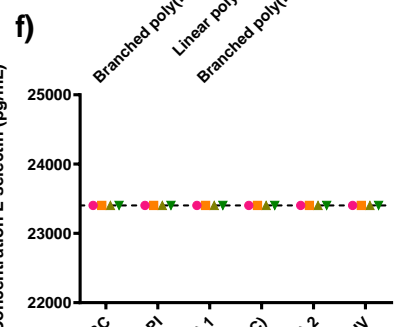
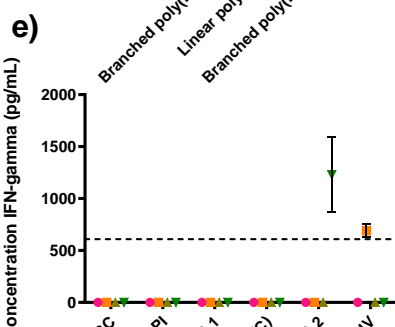
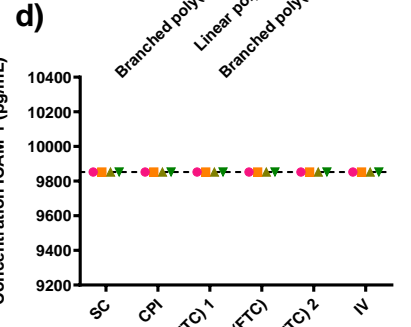
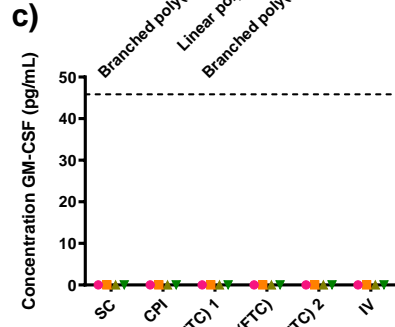
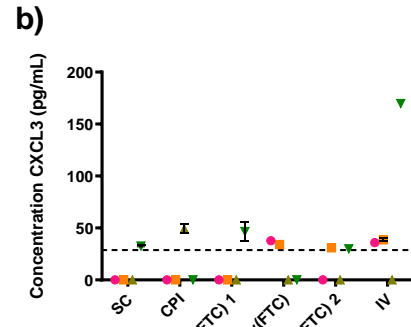
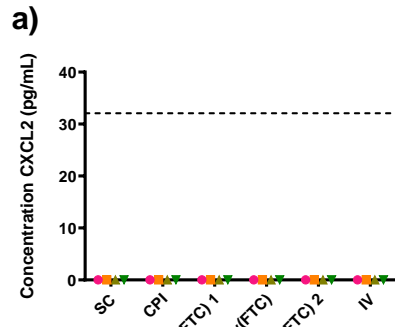


Figure 5.5: Concentrations of cytokines measured in rat blood following 91 days of exposure to the POP implants, as measured by Rat Luminex Assay on the Bio-Plex 200 Luminex system a) CXCL2, b) CXCL3, c) GM-CSF, d) ICAM-1, e) IFN- γ , f) L-selectin, g) TIMP-1, h) TNF- α and i) VEGF. Data displayed as n=3, mean (\pm standard deviation). Dashed lines indicate the top limit of the standard curve, # indicates values above the limit of detection. No statistical tests have been carried out due to the variability between rats.

The levels of FTC in the cardiac bleed and total release across the study were measured by Megan Neary and were explored to see if they correlated with any of the cytokines or chemokines measured. Branched poly(FTC) 2 had the highest total release of FTC over the course of the 91-day study, with an average of 19998.24 ng/mL although also has the highest standard deviation of 6006.86 ng/mL. linear poly(FTC) and branched poly(FTC) 1 had similar release over the course of the study with averages of 5626.80 and 6580.70 ng/mL, with standard deviations of 506.80 and 598.19 ng/mL respectively. However, branched poly(FTC) 2 had the lowest cardiac bleed concentration of 21.06 ng/mL, with a standard deviation of 3.73 ng/mL. Branched poly(FTC) 1 had the highest concentration of FTC in the cardiac bleed, despite having the lowest total release of FTC, with an average of 39.57 ng/mL, although the highest standard deviation for cardiac bleed concentrations of 11.14 ng/mL. linear poly(FTC) had an average cardiac bleed FTC concentration of 27.67 ng/mL and a standard deviation of 5.73 ng/mL.

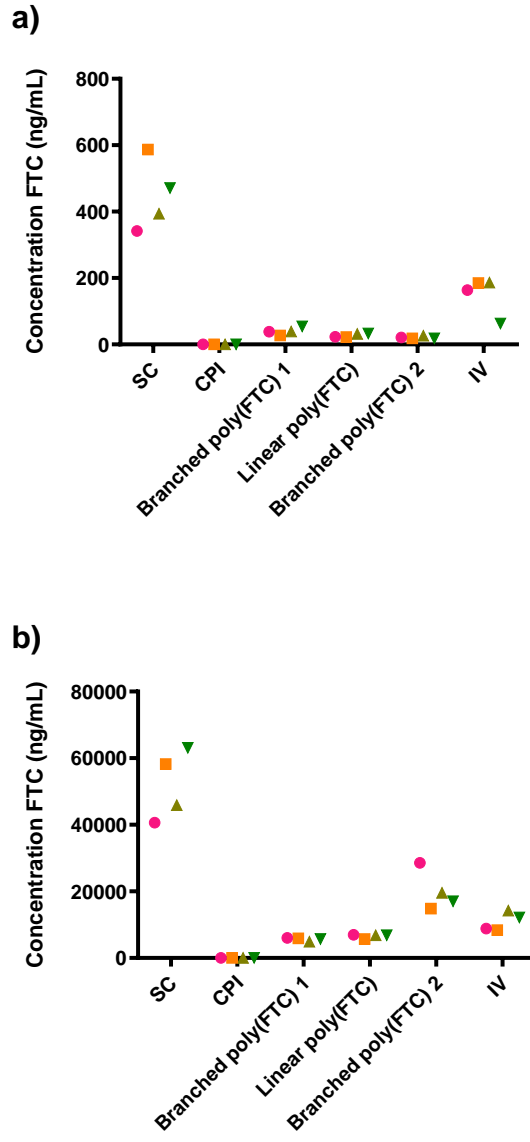


Figure 5.6: a) Concentration of FTC present in the cardiac bleed and b) Total concentration of FTC released over the 91-day study. Data displayed as n=1, mean.

5.3.2 ALT ELISA

ALT was also measured in the plasma from the cardiac bleed to determine whether the implants have the ability to cause liver toxicity. One rat from CPI, branched poly(FTC) 1 and the IV group each had ALT levels above the limit of detection for the assay used following a 1 in 500 dilution. The CPI, branched poly(FTC) 1, linear poly(FTC) and branched poly(FTC) 2 across the board seem to trend towards having higher ALT concentrations compared to the subcutaneous and IV groups, except the above limit IV rat.

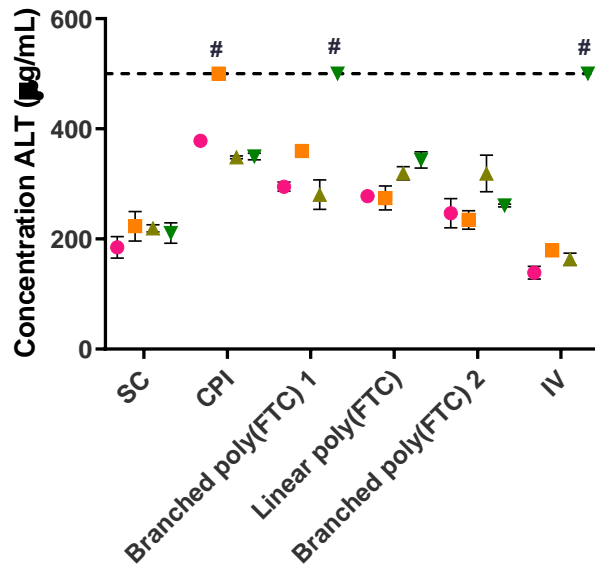


Figure 5.7: ALT concentrations determined by ELISA, using a 1:500 dilution. SC = subcutaneous, CPI = control polymer implant. Data displayed as n=2, mean (\pm standard deviation). Dashed lines indicate the top limit of the standard curve, # indicates values above the limit of detection. No statistical tests have been carried out due to the variability between rats.

5.3.3 CRP ELISA

CRP was also attempted to be measured in the plasma from the cardiac bleed to determine whether the implants have the ability to cause inflammation, as it's a general marker for inflammation. All samples from the rats were outside the limit of quantification for the CRP assay up to a 1:5000 dilution. The results from the 1:500 dilution of all samples was extrapolated from the standard curve to produce concentrations. No differences were seen between the different treatment groups.

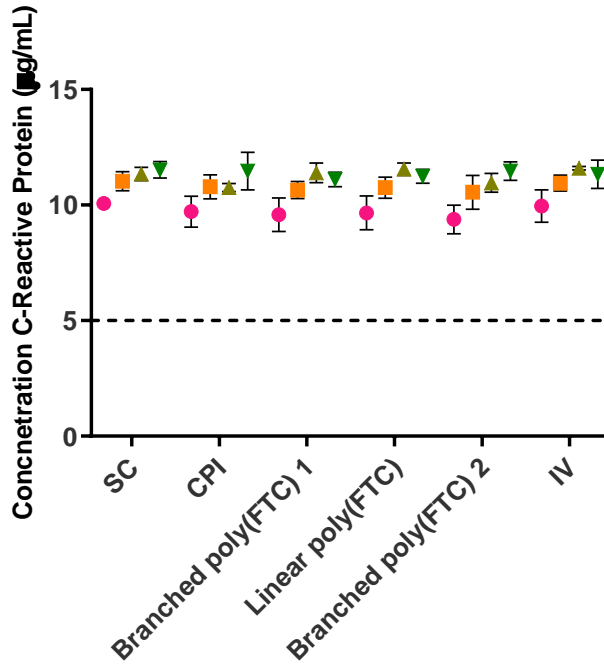


Figure 5.8: CRP concentrations determined by ELISA, 1:500 dilution. SC = subcutaneous, CPI = control polymer implant. Data displayed as n=2, mean (\pm standard deviation). Dashed lines indicate the top limit of the standard curve, all values above the limit of detection. No statistical tests have been carried out due to the variability between rats.

5.3.4 Histology assessment of the implantation site

Histology assessment which included haematoxylin & eosin stain and Masson trichrome staining was used to explore whether the implants caused toxicity at the implantation site. The histology change and severity are displayed in Table 5.3, alongside the cytokines which were altered.

Table 5.3: Summary of histology results carried out by colleges at the University of Liverpool, summary of cytokine levels found in the cardiac bleed of each animal, concentration of FTC detected in the cardiac bleed and Total concentration of FTC released from the implant during the course of the experiment. The cytokines levels using the dilution with the most samples in range for that cytokine are compared using fold change and cytokines with a fold change either <0.5 or >1.5 when compared against the average of any in range values for the CPI are denoted as either being higher or lower respectively.

Study group	Rat number	POP Implant	Change	Severity	Lowered secreted analytes	Higher secreted analytes	Cardiac bleed FTC concentration ng/mL (Average for implant type)	Total concentration of FTC released from implant ng/mL (Average for implant type)
1	1	Branched poly(FTC) 1	focal minor area of fibrosis in the dermis	+/-	IL-18		38.13 (39.57)	6002.87 (5626.8)
	2	Branched poly(FTC) 1	multifocal occasional folliculitis	+	IL-18		27.16 (39.57)	5904.67 (5626.8)
	3	Branched poly(FTC) 1	none		IL-18		38.72 (39.57)	4888.69 (5626.8)
	4	Branched poly(FTC) 1	Cyst/pseudocysts formation containing eosinophilic material under fascia			IL-1 β , IL-18	54.25 (39.57)	5710.96 (5626.8)

2	5	linear poly(FTC)	none			IL-1 β , IL-18	22.84 (27.67)	6954.14 (6580.7)
	6	linear poly(FTC)	none				22.63 (27.67)	5687.02 (6580.7)
	7	linear poly(FTC)	none		IL-18		31.91 (27.67)	6844.52 (6580.7)
	8	linear poly(FTC)	none				33.31 (27.67)	6837.13 (6580.7)
3	9	branched poly(FTC) 2	none				20.88 (21.06)	28534.08 (19998.24)
	10	branched poly(FTC) 2	Mild fibrosis/neovascularisation within connective tissue close to muscle/fascia	+			18.56 (21.06)	14843.38 (19998.24)
	11	branched poly(FTC) 2	very minor inflammation in muscle	+/-	IL-18		26.38 (21.06)	19552.45 (19998.24)

	12	branched poly(FTC) 2	none		IL-18, TMIP-1		18.40 (21.06)	17063.06 (19998.24)
4	13	CPI	none					
	14	CPI	none					
	15	CPI	none					
	16	CPI	none					

Significant alterations in cytokines, chemokines, histology or ALT were seen across the board for the treatment groups, this would suggest that the implants were somewhat tolerated by the animals. Some alterations in IL-1 β and IL-18 did occur in individual animals.

5.4 Discussion

In vivo analysis of three POP implants was carried out in order to explore the pharmacokinetics of FTC release from these implants. Samples were also obtained from the cardiac bleed of these animals following 91 days implantation in order to explore the immunocompatibility.

A number of analytes included in the multiplex panel were below the limit of detection for the assay, even when samples were analysed without dilution. Two analytes were above the limit of detection when using the 1:2 dilution. The quantities of ICAM-1, L-selectin, IL-1 α , IL-2, IL-4, IL-6, CXCL2, GM-CSF, and TNF- α were not able to be quantified using the multiplex luminex panel due to the standard ranges for those analytes in the panel. Of the analytes it was possible to, accurately, quantify there were no substantial differences seen across the board for any of the implants. Due to some variability in the cytokines IL-1 β and IL-18 with some of the POP implants, it would be important to determine the inflammasomes potential role in responding to these FTC containing implants. IL-1 β also showed an increase in the whole blood *in vitro* assay. Follow up of the POP materials used in the implants in systems the immunocompatibility group at the University of Liverpool have developed, to explore inflammasome activation would be useful.

From exploring the data summarised in Table 5.2, neither the concentrations of FTC present in the cardiac bleed, the accumulative release of FTC over the course of the study or the histology results appear to correspond with the cytokine levels detected in the cardiac bleed of the individual animals. Branched poly(FTC) 2 had the highest cumulative release of FTC over the course of the study and linear poly(FTC) had the highest in the cardiac bleed, however the cytokine and histology results didn't seem to reflect this or the individual concentrations in each rat.

As presented in chapter 2, *in vitro* assessment of linear poly(FTC) treated human plasma led to significant alterations in iC3b concentrations when compared to untreated plasma in individual donors. The analyte analysis carried out in this chapter has not been tailored to look for complement activation and therefore it is difficult to draw any conclusions on complement activation *in vivo* for linear poly(FTC) or the other two POP implants branched poly(FTC) 1 and branched poly(FTC) 2. Substantial differences were not seen across the board from all implants in each group in the pro-inflammatory cytokines IL-1 α , IL-1 β , IL-6, IL-8, and TNF- α , which can be suggestive of complement activation in humans, along with a number of other inflammatory responses (Markiewski & Lambris, 2007) .

As discussed in chapter 2, CARPA is a non-IgE related hypersensitivity and can be triggered by Doxil in certain patients, Doxil is administered IV and CARPA reactions are overcome by premedication of immunosuppressive drugs and slower infusion rates (Janos Szebeni, 2014; Janos Szebeni, Simberg, González-Fernández, Barenholz, & Dobrovolskaia, 2018). The pig has been widely used as a model to study CARPA, a result of infusion reactions to novel therapeutic delivery systems such as liposomes (Dézsi et al., 2022; János Szebeni et al., 2007). Comparison of the porcine model with Wistar rats indicated that rats were two to three orders less sensitive to CARPA from liposomal formulations (Dézsi et al., 2014). Interestingly however pigs all respond to Doxil in a similar higher rate manner (János Szebeni et al., 2007). Previously described in the literature and explored using Doxil as a control in chapter 2 of this thesis, Doxil responses in humans vary significantly and causes significant hypersensitivity reactions in a low percentage of patients. Despite this, it has been suggested that the porcine model is still a useful model to screen for potentially dangerous hypersensitivity reactions in humans (J. Szebeni & Bawa, 2020).

It is important to point out however that the route of administration for Doxil and the porcine model use IV administration. The porcine CARPA test model has more recently been used to explore the rare hypersensitivity reactions to the intramuscularly administered COVID-19 mRNA vaccines that contain lipid nanoparticles, but its human relevance to this route and other routes of administration is unknown and would need to be studied further to draw any conclusions on its ability to predict CARPA via other administration routes (Dézsi et al., 2022). Local complement activation has been hypothesised to play a role in the body's natural reaction to damage in the tissue at the site of injection (Dézsi et al., 2022). Local complement activation could also occur during implantation of the POP implants, potentially causing accumulation of complement proteins at the implant site, supplementing the need to further investigate complement responses to the POP implants. As discussed in previous literature, it is important to refine and develop the models to test for CARPA and allow for complement assessment in novel delivery systems like the POP materials tested in this thesis (Janos Szebeni et al., 2018).

In the future it would be important to isolate plasma from the animals for complement analysis as well as the analytes that were successfully detected in this experiment in any further *in vivo* PK analyses. Further analysis of complement activation *in vitro* as previously discussed in chapter 2 and *in vivo* would need to be carried out in order to help determine whether complement plays a role in the immunological response to the POP implants *in vivo* in humans.

Interestingly the samples which had ALT levels above the limit of detection in the assay had corresponding high levels of IL-18. Across the board higher levels are seen for all the rats which had an implant inserted, except for one rat that received IV FTC. No other cytokines correlated with these much higher ALT levels in three of the rats.

Absorbance values within the standard curve for the CRP ELISA range were not obtained, even with using a 1:5000 dilution, therefore a repeat with further dilutions was not carried out, as large differences were not seen in the other analytes measured using the Luminex panel or the CRP ELISA. The dilution used was much greater than the suggested dilution in the kit (1:2 to 1:10) and therefore had a very large quantity of CRP in all the test samples or there was some interference of the samples with this assay.

The results seen in this chapter suggest a safer profile for the POP implants, unlike the TAF non-biodegradable implants however, further experimental work utilising implants incorporating TAF would be required to be sure, and to define if the incompatibility of the TAF implants was drug or device dependant (Su et al., 2020). However, at this stage in development how the POP implants are broken down in a biological context and the exact fragments of the polymer that will be exposed is unable to be predicted.

No severe results were seen from the pathology assessments, and no analytes were seen to correlate with the pathology results seen, suggesting that these implants were tolerated well in the rats. Overall, no consistent, alarming differences were seen across the board for any of the POP implants tested, however, to draw better conclusions on the tolerability of the POP implants, further experiments would be required with a greater n number and at least one other species. This is particularly important to rule out false negative results and rare population responses that may not have been seen in this experiment.

Chapter 6

General Discussion

The development of advanced therapeutics, and complex medicines, requires evaluation of possible impacts on immune responses as part of the regulatory process. Additionally, inflammation has been identified as a key parameter in nearly all adverse outcome pathways (AOP) (Villeneuve et al., 2018). However, little is known on how to consider longer exposure for long-acting therapeutics, with respect to immunocompatibility, particularly for novel therapeutics such as the POP implants investigated as part of the current study. This thesis starts to address the gap in the assessment of the immunocompatibility of long-acting subcutaneously administered novel therapeutic delivery formulations. In this thesis existing, as well as new, methods were applied to assess responses related to the safety of the POP complex pre-clinical formulations.

Once a lack of bioburden, pyrogenicity, and cytotoxicity of the POP materials was established, more involved assessments of their immunocompatibility were carried out. EC₂₀ values calculated from the cytotoxicity curves where relevant and were used to determine concentrations for further testing in whole blood, complement and leukocyte proliferation assessment. In three of five donors complement activation, as determined by significantly higher iC3b levels was seen for both concentrations of linear poly(FTC) tested, non-significantly higher levels were however seen for the other two donors. Interestingly the Nanomedicine Doxil which has known inter individual variation in compatibility responses in humans had much greater levels of variation in responses between donors compared to a low level higher iC3b for linear poly(FTC) (Chanan-Khan et al., 2003). It is possible that this interindividual variability in response to Doxil could be related to the presence/absence of anti-PEG antibodies as this has been implicated previously in pseudoallergic responses to PEG containing materials (Kozma et al., 2020). Although complement activation was observed with POP materials, it did not reach clinically relevant levels as observed for Doxil, and there was no marked interindividual variability in response to these materials, further illustrating the requirement for more comprehensive evaluation of the volunteer samples used in studies such as these for variability in homeostatic and acute-phase responses. Proteomic, and metabolomic, profiling of volunteer samples may reveal temporal variation in such responses, and the entire discipline of chrono-immunology is dedicated to the impact of diurnal patterns on immune cell responses. Although blood samples were collected from volunteers at the same time of day, it is so far unclear how far such assessments should be incorporated into immunocompatibility assessments. Further follow up looking at other complement markers and determining the pathway of activation is needed in order to better understand the responses seen and this is currently being explored in another project

following the interesting data seen in this thesis. Whole blood analysis of the fragments was also carried out to screen potential responses if the POP materials reach the blood, with reference to a number of innate immune system component positive controls, overall no substantial results were seen across the POP fragments or Previously exosomes termed tolerosomes have been revealed to participate in down regulating immune processes (Fleshner & Crane, 2017). This thesis also explored whether exosomes present in FBS could alter these whole blood responses to the POP fragments, varied responses were seen across the controls and cytokines and further repeats of this work using the agonist panel with more donors is required in order to draw conclusions from this work due to high interindividual variation, it would also be useful to use a more refined panel and look at carrying out ELISA analysis with specific analytes with either above or below limit of detection in the multiplex panel, to see if quantifiable responses can be detected.

This thesis also demonstrates the beginning of the development of a chronic exposure cell line assay to determine long-term effects of the drugs used in these complex long-acting formulations and the formulations themselves. This assay found there to be alterations from both repeat exposure to FTC and 3TC which varied between the four cell lines exploited. In the MUTZ-3 cell line, exposure to linear poly(FTC) was also included and caused significant alterations in both marker expression and cell health, this was followed up by looking at metabolic pathways using the nCounter assay to explore gene expression and also showed some interesting differences for all three treatments, that should be explored further with assessment of bioenergetic responses, metabolic proteomic profiling and exploration of epigenetic changes of the cells. Shorter exposure times in primary immune cell cultures could also be useful in order to look at interindividual responses seen in humans.

Due to the stage in which the TAF POP formulations were in their development only prodrugs were available, therefore only a quick pre-screen of these materials was carried out due to their carbamate pro drug structure and previously reported carbamate toxicity (Cui et al., 2016; Guanggang et al., 2013; Soloneski et al., 2015). These materials did not show alterations at the concentrations tested and were moved forward in development, by the partner at Johns Hopkins University. Further analysis consisting of repeat exposure and inflammasome modulation should be carried out further in the development process.

Three FTC containing POP implants were explored in Wistar rats to determine their pharmacokinetics, samples were obtained and subjected to analyte analysis to determine if there were any safety concerns alongside histology assessment. No consistent alterations

were seen across any of the four animals in each group suggestive of a safer profile than the previously tested TAF drug eluting implant (Su et al., 2020). However as discussed in chapter 5, complement responses were not measured and wistar rats are much less sensitive at picking up potential CARPA responses in humans, therefore future experiments should explore complement proteins in plasma and the use of a more sensitive model for exploring CARPA, such as the pig. Further follow-up on the ability of these materials to modulate inflammasome activity would also be useful.

No significant results were seen in the assays used in this thesis that would prevent the development of these implants. However, the occurrence of false negatives must be considered and further repeats of some of this work should be carried out to ensure that no significant immunocompatibility issues have been missed. This is particularly important for the work done using donor human or animal samples, as it could be something that occurs only in a small population of people or animals.

Regulatory bodies provide criteria on the safety assessment of novel implantable devices, however as these are usually novel formulations, the assessment is ever evolving. This thesis has developed current assessments for immunocompatibility of drug formulations focusing on the delivery of the subcutaneously delivered POP formulations. Development of 3D models would be a useful tool to supplement this assessment and work has been started to develop this, but has not been included in this thesis due to the preliminary nature of the development. Building on previous immunocompetent 3D subcutaneous models and *ex vivo* systems used to assess the orientations of immune cells to exposure of the implants would be useful as this thesis only currently looks at 2D exposure systems. 3D assays should try to mimic the environment including the vasculature and lymphatics as closely as possible. It has been suggested that *ex vivo* human tissue is clearly the most relevant model for dermal drug delivery (Flaten et al., 2015). *Ex vivo* full thickness human skin models could also be used to assess the impact of subcutaneous long-acting formulations, which have been shown to be immunologically competent and therefore can be used as a model for immunological interaction, but due to this they are limited for use in long-term exposure assessment (Jardet et al., 2018). Future work should also look at responses to the implant itself rather than just the polymer formulation in these assessments, for example whole blood or macrophage exposure to the implant and measurements for adsorption onto the materials or macrophage marker and secretion analysis would be useful to explore the potential of foreign body responses to the POP implants. It would also be useful to expose the implant to different biological matrices, such as interstitial fluid and lymph, and explore the adsorption of

proteins to the implant surface, which are known to influence “immune visibility”. Taken together, a putative immunocompatibility assessment of the POP materials is presented and shows key points to consider when examining long-acting formulations.

References

- Alam, M. M., Yang, D., Trivett, A., Meyer, T. J., & Oppenheim, J. J. (2018). HMG1 and R848 Synergistically Activate Dendritic Cells Using Multiple Signaling Pathways. *Frontiers in Immunology*, 9. doi:10.3389/fimmu.2018.02982
- Allers, K., Hütter, G., Hofmann, J., Loddenkemper, C., Rieger, K., Thiel, E., & Schneider, T. (2011). Evidence for the cure of HIV infection by CCR5 Δ 32/ Δ 32 stem cell transplantation. *Blood*, 117(10), 2791-2799. doi:<https://doi.org/10.1182/blood-2010-09-309591>
- Arima, Y., Kawagoe, M., Toda, M., & Iwata, H. (2009). Complement Activation by Polymers Carrying Hydroxyl Groups. *ACS Applied Materials & Interfaces*, 1(10), 2400-2407. doi:10.1021/am9005463
- Arima, Y., Toda, M., & Iwata, H. (2008). Complement activation on surfaces modified with ethylene glycol units. *Biomaterials*, 29(5), 551-560. doi:10.1016/j.biomaterials.2007.10.015
- Barone, D. G., Carnicer-Lombarte, A., Tourlomousis, P., Hamilton, R. S., Prater, M., Rutz, A. L., . . . Bryant, C. E. (2022). Prevention of the foreign body response to implantable medical devices by inflammasome inhibition. *Proceedings of the National Academy of Sciences*, 119(12), e2115857119. doi:10.1073/pnas.2115857119
- Bertin, J., Wang, L., Guo, Y., Jacobson, M. D., Poyet, J.-L., Srinivasula, S. M., . . . Alnemri, E. S. (2001). CARD11 and CARD14 Are Novel Caspase Recruitment Domain (CARD)/Membrane-associated Guanylate Kinase (MAGUK) Family Members that Interact with BCL10 and Activate NF- κ B *. *Journal of Biological Chemistry*, 276(15), 11877-11882. doi:10.1074/jbc.M010512200
- BioRender. (2020a). HIV Sites for Therapeutic Intervention. In.
- BioRender. (2020b). Roles of the Complement Cascade in Innate Immunity. In.
- Blighe K, Rana S, & M, L. (2022). EnhancedVolcano: Publication-ready volcano plots with enhanced colouring and labeling., *R package version 1.14.0*. Retrieved from <https://github.com/kevinblighe/EnhancedVolcano>

Blom, T., Huang, R., Aveskogh, M., Nilsson, K., & Hellman, L. (1992). Phenotypic characterization of KU812, a cell line identified as an immature human basophilic leukocyte. *Eur J Immunol*, 22(8), 2025-2032. doi:10.1002/eji.1830220811

Bouajina, E., Harzallah, L., Ghannouchi, M., Hamdi, I., Rammeh, N., Ben Hamida, R., & Kraiem, C. (2006). Foreign body granuloma due to unsuspected wooden splinter. *Joint Bone Spine*, 73(3), 329-331. doi:10.1016/j.jbspin.2005.04.009

Bourgeois, C., Gorwood, J., Barrail-Tran, A., Lagathu, C., Capeau, J., Desjardins, D., . . . Lambotte, O. (2019). Specific Biological Features of Adipose Tissue, and Their Impact on HIV Persistence. *Frontiers in Microbiology*, 10. doi:10.3389/fmicb.2019.02837

Bradley, J. (2008). TNF-mediated inflammatory disease. *The Journal of Pathology*, 214(2), 149-160. doi:<https://doi.org/10.1002/path.2287>

Brown, T. R. (2015). I am the Berlin patient: a personal reflection. *AIDS Res Hum Retroviruses*, 31(1), 2-3. doi:10.1089/aid.2014.0224

Brunner, D., Frank, J., Appl, H., Schöffl, H., Pfaller, W., & Gstraunthaler, G. (2010). Serum-free cell culture: the serum-free media interactive online database. *Altex*, 27(1), 53-62. doi:10.14573/altex.2010.1.53

Bubeck, D. (2014). The making of a macromolecular machine: assembly of the membrane attack complex. *Biochemistry*, 53(12), 1908-1915. doi:10.1021/bi500157z

Canouil, M., Bouland, G. A., Bonnefond, A., Froguel, P., 't Hart, L. M., & Slieker, R. C. (2019). NACHO: an R package for quality control of NanoString nCounter data. *Bioinformatics*, 36(3), 970-971. doi:10.1093/bioinformatics/btz647

Carnicer-Lombarte, A., Chen, S.-T., Malliaras, G. G., & Barone, D. G. (2021). Foreign Body Reaction to Implanted Biomaterials and Its Impact in Nerve Neuroprosthetics. *Frontiers in Bioengineering and Biotechnology*, 9. doi:10.3389/fbioe.2021.622524

Carrick, J. B., & Begg, A. P. (2008). Peripheral Blood Leukocytes. *Veterinary Clinics of North America: Equine Practice*, 24(2), 239-259. doi:<https://doi.org/10.1016/j.cveq.2008.05.003>

Cedrone, E., Neun, B. W., Rodriguez, J., Vermilya, A., Clogston, J. D., McNeil, S. E., . . . Dobrovolskaia, M. A. (2017). Anticoagulants Influence the Performance of In Vitro Assays

Intended for Characterization of Nanotechnology-Based Formulations. *Molecules*, 23(1). doi:10.3390/molecules23010012

Chanan-Khan, A., Szebeni, J., Savay, S., Liebes, L., Rafique, N. M., Alving, C. R., & Muggia, F. M. (2003). Complement activation following first exposure to pegylated liposomal doxorubicin (Doxil®): possible role in hypersensitivity reactions. *Annals of Oncology*, 14(9), 1430-1437. doi:<https://doi.org/10.1093/annonc/mdg374>

Chandiwana, N. C., Serenata, C. M., Owen, A., Rannard, S., Pérez Casas, C., Scott, C., . . . Flexner, C. (2021). Impact of long-acting therapies on the global HIV epidemic. *AIDS*, 35(Supplement 2), S137-S143. doi:10.1097/qad.0000000000003102

Chandorkar, Y., K, R., & Basu, B. (2019). The Foreign Body Response Demystified. *ACS Biomaterials Science & Engineering*, 5(1), 19-44. doi:10.1021/acsbmaterials.8b00252

Chanput, W., Mes, J. J., & Wichers, H. J. (2014). THP-1 cell line: An in vitro cell model for immune modulation approach. *International Immunopharmacology*, 23(1), 37-45. doi:<https://doi.org/10.1016/j.intimp.2014.08.002>

Chen, W., Yung, B. C., Qian, Z., & Chen, X. (2018). Improving long-term subcutaneous drug delivery by regulating material-bioenvironment interaction. *Advanced Drug Delivery Reviews*, 127, 20-34. doi:<https://doi.org/10.1016/j.addr.2018.01.016>

Chirumbolo, S., Vella, A., Ortolani, R., De Gironcoli, M., Solero, P., Tridente, G., & Bellavite, P. (2008). Differential response of human basophil activation markers: a multi-parameter flow cytometry approach. *Clinical and Molecular Allergy*, 6(1), 12. doi:10.1186/1476-7961-6-12

Choi, P., & Reiser, H. (1998). IL-4: role in disease and regulation of production. *Clin Exp Immunol*, 113(3), 317-319. doi:10.1046/j.1365-2249.1998.00690.x

Choo, S. Y. (2007). The HLA system: genetics, immunology, clinical testing, and clinical implications. *Yonsei Med J*, 48(1), 11-23. doi:10.3349/ymj.2007.48.1.11

Choudhury, S. M., Ma, X., Abdullah, S. W., & Zheng, H. (2021). Activation and Inhibition of the NLRP3 Inflammasome by RNA Viruses. *J Inflamm Res*, 14, 1145-1163. doi:10.2147/jir.S295706

Chue, P., Eerdeken, M., Augustyns, I., Lachaux, B., Molčan, P., Eriksson, L., . . . David, A. S. (2005). Comparative efficacy and safety of long-acting risperidone and risperidone oral tablets. *European Neuropsychopharmacology*, *15*(1), 111-117.

doi:<https://doi.org/10.1016/j.euroneuro.2004.07.003>

Chung, K.-J., Nati, M., Chavakis, T., & Chatzigeorgiou, A. (2018). Innate immune cells in the adipose tissue. *Reviews in Endocrine and Metabolic Disorders*, *19*(4), 283-292.

doi:10.1007/s11154-018-9451-6

Croxatto, H. B., Urbancsek, J., Massai, R., Coelingh Bennink, H., & van Beek, A. (1999). A multicentre efficacy and safety study of the single contraceptive implant Implanon. Implanon Study Group. *Hum Reprod*, *14*(4), 976-981. doi:10.1093/humrep/14.4.976

Cui, X., Wang, J., Qiu, N., & Wu, Y. (2016). In vitro toxicological evaluation of ethyl carbamate in human HepG2 cells. *Toxicol Res (Camb)*, *5*(2), 697-702.

doi:10.1039/c5tx00453e

Custodio, J. M., Fordyce, M., Garner, W., Vimal, M., Ling, K. H., Kearney, B. P., & Ramanathan, S. (2016). Pharmacokinetics and Safety of Tenofovir Alafenamide in HIV-Uninfected Subjects with Severe Renal Impairment. *Antimicrob Agents Chemother*, *60*(9), 5135-5140. doi:10.1128/aac.00005-16

Daniël T. Luttikhuisen, M. C. H., and Marja J.A. Van Luyn. (2006). Cellular and Molecular Dynamics in the Foreign Body Reaction. *Tissue Engineering*, *12*(7), 1955-1970.

doi:10.1089/ten.2006.12.1955

Darville, N., van Heerden, M., Mariën, D., De Meulder, M., Rossenu, S., Vermeulen, A., . . . Van den Mooter, G. (2016). The effect of macrophage and angiogenesis inhibition on the drug release and absorption from an intramuscular sustained-release paliperidone palmitate suspension. *J Control Release*, *230*, 95-108. doi:10.1016/j.jconrel.2016.03.041

David, C. A. W., Barrow, M., Murray, P., Rosseinsky, M. J., Owen, A., & Liptrott, N. J. (2020). In Vitro Determination of the Immunogenic Impact of Nanomaterials on Primary Peripheral Blood Mononuclear Cells. *International journal of molecular sciences*, *21*(16), 5610.

doi:10.3390/ijms21165610

de Béthune, M.-P. (2010). Non-nucleoside reverse transcriptase inhibitors (NNRTIs), their discovery, development, and use in the treatment of HIV-1 infection: A review of the last 20

years (1989–2009). *Antiviral Research*, 85(1), 75-90.

doi:<https://doi.org/10.1016/j.antiviral.2009.09.008>

Dézi, L., Fülöp, T., Mészáros, T., Szénási, G., Urbanics, R., Vázsonyi, C., . . . Szebeni, J. (2014). Features of complement activation-related pseudoallergy to liposomes with different surface charge and PEGylation: Comparison of the porcine and rat responses. *Journal of Controlled Release*, 195, 2-10. doi:<https://doi.org/10.1016/j.jconrel.2014.08.009>

Dézi, L., Mészáros, T., Kozma, G., H-Velkei, M., Oláh, C. Z., Szabó, M., . . . Szebeni, J. (2022). A naturally hypersensitive porcine model may help understand the mechanism of COVID-19 mRNA vaccine-induced rare (pseudo) allergic reactions: complement activation as a possible contributing factor. *GeroScience*, 44(2), 597-618. doi:10.1007/s11357-021-00495-y

Dobrovolskaia, M. A. (2015a). *NCL Method ITA-6 - Leukocyte Proliferation Assay*. Nanotechnology Characterization Laboratory, Frederick National Laboratory for Cancer Research, Leidos Biomedical Research, Inc., Frederick, MD 21702 USA.

Dobrovolskaia, M. A. (2015b). Pre-clinical immunotoxicity studies of nanotechnology-formulated drugs: Challenges, considerations and strategy. *Journal of Controlled Release*, 220, 571-583. doi:<https://doi.org/10.1016/j.jconrel.2015.08.056>

Dobrovolskaia, M. A., Neun, B. W., Clogston, J. D., Grossman, J. H., & McNeil, S. E. (2014). Choice of method for endotoxin detection depends on nanoformulation. *Nanomedicine*, 9(12), 1847-1856. doi:10.2217/nnm.13.157

Dolgin, E. (2014). Long-acting HIV drugs advanced to overcome adherence challenge. *Nature Medicine*, 20(4), 323-324. doi:10.1038/nm0414-323

DSMZ. MUTZ-3 ACC 295.

Dunkelberger, J. R., & Song, W.-C. (2010). Complement and its role in innate and adaptive immune responses. *Cell Research*, 20(1), 34-50. doi:10.1038/cr.2009.139

Ebo, D. G., Bridts, C. H., Mertens, C. H., Hagendorens, M. M., Stevens, W. J., & De Clerck, L. S. (2012). Analyzing histamine release by flow cytometry (HistaFlow): A novel instrument to study the degranulation patterns of basophils. *Journal of Immunological Methods*, 375(1), 30-38. doi:<https://doi.org/10.1016/j.jim.2011.09.003>

- Eitan, E., Zhang, S., Witwer, K. W., & Mattson, M. P. (2015). Extracellular vesicle-depleted fetal bovine and human sera have reduced capacity to support cell growth. *Journal of extracellular vesicles*, 4, 26373-26373. doi:10.3402/jev.v4.26373
- Ellis, S., Lin, E. J., & Tartar, D. (2018). Immunology of Wound Healing. *Current Dermatology Reports*, 7(4), 350-358. doi:10.1007/s13671-018-0234-9
- Ferrante, A. W., Jr. (2013). The immune cells in adipose tissue. *Diabetes Obes Metab*, 15 Suppl 3(0 3), 34-38. doi:10.1111/dom.12154
- Flaten, G. E., Palac, Z., Engesland, A., Filipović-Grčić, J., Vanić, Ž., & Škalko-Basnet, N. (2015). In vitro skin models as a tool in optimization of drug formulation. *Eur J Pharm Sci*, 75, 10-24. doi:10.1016/j.ejps.2015.02.018
- Fleshner, M., & Crane, C. R. (2017). Exosomes, DAMPs and miRNA: Features of Stress Physiology and Immune Homeostasis. *Trends in Immunology*, 38(10), 768-776. doi:10.1016/j.it.2017.08.002
- Flexner, C., Owen, A., Siccardi, M., & Swindells, S. (2021). Long-acting drugs and formulations for the treatment and prevention of HIV infection. *International Journal of Antimicrobial Agents*, 57(1), 106220. doi:<https://doi.org/10.1016/j.ijantimicag.2020.106220>
- Foley, G. E., Lazarus, H., Farber, S., Uzman, B. G., Boone, B. A., & McCarthy, R. E. (1965). Continuous culture of human lymphoblasts from peripheral blood of a child with acute leukemia. *Cancer*, 18(4), 522-529. doi:[https://doi.org/10.1002/1097-0142\(196504\)18:4<522::AID-CNCR2820180418>3.0.CO;2-J](https://doi.org/10.1002/1097-0142(196504)18:4<522::AID-CNCR2820180418>3.0.CO;2-J)
- Geijtenbeek, T. B., Dunnen, J. d., & Gringhuis, S. I. (2009). Pathogen recognition by DC-SIGN shapes adaptive immunity. *Future Microbiology*, 4(7), 879-890. doi:10.2217/fmb.09.51
- Geijtenbeek, T. B. H., Krooshoop, D. J. E. B., Bleijs, D. A., van Vliet, S. J., van Duijnhoven, G. C. F., Grabovsky, V., . . . van Kooyk, Y. (2000). DC-SIGN–ICAM-2 interaction mediates dendritic cell trafficking. *Nature Immunology*, 1(4), 353-357. doi:10.1038/79815
- Geijtenbeek, T. B. H., Torensma, R., van Vliet, S. J., van Duijnhoven, G. C. F., Adema, G. J., van Kooyk, Y., & Figdor, C. G. (2000). Identification of DC-SIGN, a Novel Dendritic Cell-Specific ICAM-3 Receptor that Supports Primary Immune Responses. *Cell*, 100(5), 575-585. doi:10.1016/S0092-8674(00)80693-5

Giesbrecht, K., Eberle, M.-E., Wölfle, S. J., Sahin, D., Sähr, A., Oberhardt, V., . . . Hildebrand, D. (2017). IL-1 β As Mediator of Resolution That Reprograms Human Peripheral Monocytes toward a Suppressive Phenotype. *Frontiers in Immunology*, 8.

doi:10.3389/fimmu.2017.00899

Gilead, Sampson, M., & Younis, I. (2015). *FDA Clinical Pharmacology Review, Emtricitabine/tenofovir alafenamide (F/TAF or FTC/TAF), NDA 208215*. Retrieved from <https://www.fda.gov/media/98516/download>

Grande, F., Occhiuzzi, M. A., Rizzuti, B., Ioele, G., De Luca, M., Tucci, P., . . . Garofalo, A. (2019). CCR5/CXCR4 Dual Antagonism for the Improvement of HIV Infection Therapy. *Molecules*, 24(3). doi:10.3390/molecules24030550

Groell, F., Kalia, Y. N., Jordan, O., & Borchard, G. (2018). Hydrogels in three-dimensional dendritic cell (MUTZ-3) culture as a scaffold to mimic human immuno competent subcutaneous tissue. *Int J Pharm*, 544(1), 297-303. doi:10.1016/j.ijpharm.2018.04.050

Gstraunthaler, G. (2003). Alternatives to the use of fetal bovine serum: serum-free cell culture. *Altex*, 20(4), 275-281. doi:<https://doi.org/10.14573/altex.2003.4.257>

Guanggang, X., Diqiu, L., Jianzhong, Y., Jingmin, G., Huifeng, Z., Mingan, S., & Liming, T. (2013). Carbamate insecticide methomyl confers cytotoxicity through DNA damage induction. *Food and Chemical Toxicology*, 53, 352-358.

doi:<https://doi.org/10.1016/j.fct.2012.12.020>

Gunawardana, M., Remedios-Chan, M., Sanchez, D., Webster, S., Castonguay, A. E., Webster, P., . . . Baum, M. M. (2022). Fundamental aspects of long-acting tenofovir alafenamide delivery from subdermal implants for HIV prophylaxis. *Scientific Reports*, 12(1), 8224. doi:10.1038/s41598-022-11020-2

Guo, H., Callaway, J. B., & Ting, J. P. Y. (2015). Inflammasomes: mechanism of action, role in disease, and therapeutics. *Nature Medicine*, 21(7), 677-687. doi:10.1038/nm.3893

Gupta, R. K., Peppas, D., Hill, A. L., Gálvez, C., Salgado, M., Pace, M., . . . Olavarria, E. (2020). Evidence for HIV-1 cure after CCR5 Δ 32/ Δ 32 allogeneic haemopoietic stem-cell transplantation 30 months post analytical treatment interruption: a case report. *The Lancet HIV*, 7(5), e340-e347. doi:10.1016/S2352-3018(20)30069-2

Guzova, J. A., Primiano, M. J., Jiao, A., Stock, J., Lee, C., Winkler, A. R., & Hall, J. P. (2019). Optimized protocols for studying the NLRP3 inflammasome and assessment of potential targets of CP-453,773 in undifferentiated THP1 cells. *Journal of Immunological Methods*, 467, 19-28. doi:<https://doi.org/10.1016/j.jim.2019.02.002>

Haley, P. J. (2003). Species differences in the structure and function of the immune system. *Toxicology*, 188(1), 49-71. doi:[https://doi.org/10.1016/S0300-483X\(03\)00043-X](https://doi.org/10.1016/S0300-483X(03)00043-X)

Hamad, I., Hunter, A. C., Szebeni, J., & Moghimi, S. M. (2008). Poly(ethylene glycol)s generate complement activation products in human serum through increased alternative pathway turnover and a MASP-2-dependent process. *Mol Immunol*, 46(2), 225-232. doi:10.1016/j.molimm.2008.08.276

Heaton, B. J., Jensen, R. L., Line, J., David, C. A. W., Brain, D. E., Chadwick, A. E., & Liptrott, N. J. (2022). Exposure of human immune cells, to the antiretrovirals efavirenz and lopinavir, leads to lower glucose uptake and altered bioenergetic cell profiles through interactions with SLC2A1. *Biomed Pharmacother*, 150, 112999. doi:10.1016/j.biopha.2022.112999

Hennersdorf, F., Florian, S., Jakob, A., Baumgärtner, K., Sonneck, K., Nordheim, A., . . . BÜHring, H.-J. (2005). Identification of CD13, CD107a, and CD164 as novel basophil-activation markers and dissection of two response patterns in time kinetics of IgE-dependent upregulation. *Cell Research*, 15(5), 325-335. doi:10.1038/sj.cr.7290301

Hervé, C., Laupèze, B., Del Giudice, G., Didierlaurent, A. M., & Tavares Da Silva, F. (2019). The how's and what's of vaccine reactogenicity. *npj Vaccines*, 4(1), 39. doi:10.1038/s41541-019-0132-6

HIV Drug Interactions. (2016a, March 2016). Emtricitabine PK Fact Sheet *Pharmacokinetic Fact Sheets*. Retrieved from www.hiv-druginteractions.org/prescribing_resources/hiv-pk-emtricitabine

HIV Drug Interactions. (2016b, March 2016). Lamivudine PK Fact Sheet *Pharmacokinetic Fact Sheets*. Retrieved from www.hiv-druginteractions.org/prescribing_resources/hiv-pk-lamivudine

Hobson, J. J., Al-khouja, A., Curley, P., Meyers, D., Flexner, C., Siccardi, M., . . . Rannard, S. P. (2019). Semi-solid prodrug nanoparticles for long-acting delivery of water-soluble

antiretroviral drugs within combination HIV therapies. *Nature Communications*, 10(1), 1413. doi:10.1038/s41467-019-09354-z

Holec, A. D., Mandal, S., Prathipati, P. K., & Destache, C. J. (2017). Nucleotide Reverse Transcriptase Inhibitors: A Thorough Review, Present Status and Future Perspective as HIV Therapeutics. *Curr HIV Res*, 15(6), 411-421. doi:10.2174/1570162x15666171120110145

Hudson, K., Cross, N., Jordan-Mahy, N., & Leyland, R. (2020). The Extrinsic and Intrinsic Roles of PD-L1 and Its Receptor PD-1: Implications for Immunotherapy Treatment. *Frontiers in Immunology*, 11. doi:10.3389/fimmu.2020.568931

Jamjian, M. C., & McNicholl, I. R. (2004). Enfuvirtide: first fusion inhibitor for treatment of HIV infection. *Am J Health Syst Pharm*, 61(12), 1242-1247. doi:10.1093/ajhp/61.12.1242

Janeway CA Jr, T. P., Walport M, et al. (2001). *Immunobiology: The Immune System in Health and Disease*. (5th edition ed.).

Jardet, C., Pagès, E., Seeliger, F., Brandén, L., Braun, E., Ingelsten, M., & Descargues, P. (2018). LB1552 Evaluation of local inflammatory reactions following subcutaneous injection of a pro-inflammatory cocktail in a fully human ex vivo skin model. *Journal of Investigative Dermatology*, 138(9), B14.

Jensen, S. S., & Gad, M. (2010). Differential induction of inflammatory cytokines by dendritic cells treated with novel TLR-agonist and cytokine based cocktails: targeting dendritic cells in autoimmunity. *Journal of Inflammation*, 7(1), 37. doi:10.1186/1476-9255-7-37

Johnson, B. A. (2007). Naltrexone long-acting formulation in the treatment of alcohol dependence. *Ther Clin Risk Manag*, 3(5), 741-749.

Kabashima, K., Honda, T., Ginhoux, F., & Egawa, G. (2019). The immunological anatomy of the skin. *Nature Reviews Immunology*, 19(1), 19-30. doi:10.1038/s41577-018-0084-5

Kelley, N., Jeltema, D., Duan, Y., & He, Y. (2019). The NLRP3 Inflammasome: An Overview of Mechanisms of Activation and Regulation. *International journal of molecular sciences*, 20(13). doi:10.3390/ijms20133328

Kim, Y. J., Shin, Y. K., Sohn, D. S., & Lee, C. S. (2014). Menadione induces the formation of reactive oxygen species and depletion of GSH-mediated apoptosis and inhibits the FAK-

mediated cell invasion. *Naunyn-Schmiedeberg's Archives of Pharmacology*, 387(9), 799-809. doi:10.1007/s00210-014-0997-x

Koethe, J. R., Hulgan, T., & Niswender, K. (2013). Adipose Tissue and Immune Function: A Review of Evidence Relevant to HIV Infection. *The Journal of Infectious Diseases*, 208(8), 1194-1201. doi:10.1093/infdis/jit324

Kofanova, O., Henry, E., Quesada, R. A., Bulla, A., Linares, H. N., Lescuyer, P., . . . Betsou, F. (2018). IL8 and IL16 levels indicate serum and plasma quality. *Clinical Chemistry and Laboratory Medicine (CCLM)*, 56(7), 1054-1062. doi:doi:10.1515/cclm-2017-1047

Kolaczowska, E., & Kubes, P. (2013). Neutrophil recruitment and function in health and inflammation. *Nature Reviews Immunology*, 13(3), 159-175. doi:10.1038/nri3399

Kovarova, M., Benhabbour, S. R., Massud, I., Spagnuolo, R. A., Skinner, B., Baker, C. E., . . . Garcia, J. V. (2018). Ultra-long-acting removable drug delivery system for HIV treatment and prevention. *Nature Communications*, 9(1), 4156. doi:10.1038/s41467-018-06490-w

Kozma, G. T., Shimizu, T., Ishida, T., & Szebeni, J. (2020). Anti-PEG antibodies: Properties, formation, testing and role in adverse immune reactions to PEGylated nano-biopharmaceuticals. *Advanced Drug Delivery Reviews*, 154-155, 163-175. doi:<https://doi.org/10.1016/j.addr.2020.07.024>

Krawczyk, C. M., Holowka, T., Sun, J., Blagih, J., Amiel, E., DeBerardinis, R. J., . . . Pearce, E. J. (2010). Toll-like receptor-induced changes in glycolytic metabolism regulate dendritic cell activation. *Blood*, 115(23), 4742-4749. doi:10.1182/blood-2009-10-249540

La-Beck, N. M., Islam, M. R., & Markiewski, M. M. (2021). Nanoparticle-Induced Complement Activation: Implications for Cancer Nanomedicine. *Frontiers in Immunology*, 11. doi:10.3389/fimmu.2020.603039

LaRosa, D. F., & Orange, J. S. (2008). 1. Lymphocytes. *Journal of Allergy and Clinical Immunology*, 121(2), S364-S369. doi:10.1016/j.jaci.2007.06.016

Li, D., & Wu, M. (2021). Pattern recognition receptors in health and diseases. *Signal Transduction and Targeted Therapy*, 6(1), 291. doi:10.1038/s41392-021-00687-0

Li, G., Wang, Y., & De Clercq, E. (2022). Approved HIV reverse transcriptase inhibitors in the past decade. *Acta Pharmaceutica Sinica B*, *12*(4), 1567-1590.

doi:<https://doi.org/10.1016/j.apsb.2021.11.009>

Li, J., Hu, L., Liu, Y., Huang, L., Mu, Y., Cai, X., & Weng, C. (2015). DDX19A Senses Viral RNA and Mediates NLRP3-Dependent Inflammasome Activation. *J Immunol*, *195*(12), 5732-5749. doi:10.4049/jimmunol.1501606

Li, S., Yao, J.-C., Li, J. T., Schmidt, A. P., & Link, D. C. (2021). TLR7/8 agonist treatment induces an increase in bone marrow resident dendritic cells and hematopoietic progenitor expansion and mobilization. *Experimental Hematology*, *96*, 35-43.e37.

doi:<https://doi.org/10.1016/j.exphem.2021.02.001>

Li, Z., Ju, X., Silveira, P. A., Abadir, E., Hsu, W.-H., Hart, D. N. J., & Clark, G. J. (2019). CD83: Activation Marker for Antigen Presenting Cells and Its Therapeutic Potential. *Frontiers in Immunology*, *10*. doi:10.3389/fimmu.2019.01312

Lichtenstein, K., Balasubramanyam, A., Sekhar, R., & Freedland, E. (2007). HIV-associated adipose redistribution syndrome (HARS): definition, epidemiology and clinical impact. *AIDS Research and Therapy*, *4*(1), 16. doi:10.1186/1742-6405-4-16

Liptrott, N. J., Giardiello, M., McDonald, T. O., Rannard, S. P., & Owen, A. (2017). Lack of interaction of lopinavir solid drug nanoparticles with cells of the immune system.

Nanomedicine, *12*(17), 2043-2054. doi:10.2217/nnm-2017-0095

Liptrott, N. J., Giardiello, M., McDonald, T. O., Rannard, S. P., & Owen, A. (2018).

Assessment of interactions of efavirenz solid drug nanoparticles with human immunological and haematological systems. *Journal of nanobiotechnology*, *16*(1), 22-22.

doi:10.1186/s12951-018-0349-y

Liu, Y., Beyer, A., & Aebersold, R. (2016). On the Dependency of Cellular Protein Levels on mRNA Abundance. *Cell*, *165*(3), 535-550. doi:10.1016/j.cell.2016.03.014

Lombardi, V., Van Overtvelt, L., Horiot, S., & Moingeon, P. (2009). Human dendritic cells stimulated via TLR7 and/or TLR8 induce the sequential production of IL-10, IFN-gamma, and IL-17A by naive CD4+ T cells. *The Journal of Immunology*, *182*(6), 3372-3379.

doi:10.4049/jimmunol.0801969

- López-Cabrera, M., Santis, A. G., Fernández-Ruiz, E., Blacher, R., Esch, F., Sánchez-Mateos, P., & Sánchez-Madrid, F. (1993). Molecular cloning, expression, and chromosomal localization of the human earliest lymphocyte activation antigen AIM/CD69, a new member of the C-type animal lectin superfamily of signal-transmitting receptors. *Journal of Experimental Medicine*, *178*(2), 537-547. doi:10.1084/jem.178.2.537
- Lopez-Dee, Z., Pidcock, K., & Gutierrez, L. S. (2011). Thrombospondin-1: multiple paths to inflammation. *Mediators Inflamm*, *2011*, 296069. doi:10.1155/2011/296069
- Lv, Z., Chu, Y., & Wang, Y. (2015). HIV protease inhibitors: a review of molecular selectivity and toxicity. *HIV AIDS (Auckl)*, *7*, 95-104. doi:10.2147/hiv.S79956
- Ma, D. Y., & Clark, E. A. (2009). The role of CD40 and CD154/CD40L in dendritic cells. *Semin Immunol*, *21*(5), 265-272. doi:10.1016/j.smim.2009.05.010
- MacConmara, M., & Lederer, J. A. (2005). B cells. *Critical Care Medicine*, *33*(12), S514-S516. doi:10.1097/01.Ccm.0000190616.15952.4b
- Maedera, S., Mizuno, T., Ishiguro, H., Ito, T., Soga, T., & Kusuhara, H. (2019). GLUT6 is a lysosomal transporter that is regulated by inflammatory stimuli and modulates glycolysis in macrophages. *FEBS Letters*, *593*(2), 195-208. doi:<https://doi.org/10.1002/1873-3468.13298>
- Malik, A. F., Hoque, R., Ouyang, X., Ghani, A., Hong, E., Khan, K., . . . Mehal, W. Z. (2011). Inflammasome components Asc and caspase-1 mediate biomaterial-induced inflammation and foreign body response. *Proc Natl Acad Sci U S A*, *108*(50), 20095-20100. doi:10.1073/pnas.1105152108
- Mándi, Y., & Vécsei, L. (2012). The kynurenine system and immunoregulation. *Journal of Neural Transmission*, *119*(2), 197-209. doi:10.1007/s00702-011-0681-y
- Mapa, M. S. T., Araujo, M., Zhao, Y., Flynn, T., Sprando, J., Wiesenfeld, P., . . . Mossoba, M. E. (2020). A method to dissolve 3-MCPD mono- and di-esters in aqueous cell culture media. *MethodsX*, *7*, 100774. doi:<https://doi.org/10.1016/j.mex.2019.100774>
- Markiewski, M. M., & Lambris, J. D. (2007). The role of complement in inflammatory diseases from behind the scenes into the spotlight. *Am J Pathol*, *171*(3), 715-727. doi:10.2353/ajpath.2007.070166

Marsland, B. J., Bättig, P., Bauer, M., Ruedl, C., Lässig, U., Beerli, R. R., . . . Bachmann, M. F. (2005). CCL19 and CCL21 Induce a Potent Proinflammatory Differentiation Program in Licensed Dendritic Cells. *Immunity*, 22(4), 493-505.

doi:<https://doi.org/10.1016/j.immuni.2005.02.010>

Masterson, A. J., Sombroek, C. C., de Gruijl, T. D., Graus, Y. M. F., van der Vliet, H. J. J., Loughheed, S. a. M., . . . Scheper, R. J. (2002). MUTZ-3, a human cell line model for the cytokine-induced differentiation of dendritic cells from CD34+precursors. *Blood*, 100(2), 701-703. doi:10.1182/blood.V100.2.701

Maurer, M., & von Stebut, E. (2004). Macrophage inflammatory protein-1. *The International Journal of Biochemistry & Cell Biology*, 36(10), 1882-1886.

doi:<https://doi.org/10.1016/j.biocel.2003.10.019>

Merle, N. S., Church, S. E., Fremeaux-Bacchi, V., & Roumenina, L. T. (2015). Complement System Part I – Molecular Mechanisms of Activation and Regulation. *Frontiers in Immunology*, 6. doi:10.3389/fimmu.2015.00262

Mickaël Canouil, P. D., and, G. A. B., & Roderick C. Slieker, P. D. (2022, 31st May). NACHO: A NAnostring quality Control dasHbOard.

Miyake, K., & Karasuyama, H. (2017). Emerging roles of basophils in allergic inflammation. *Allergology International*, 66(3), 382-391. doi:<https://doi.org/10.1016/j.alit.2017.04.007>

Møller, S. H., Wang, L., & Ho, P.-C. (2022). Metabolic programming in dendritic cells tailors immune responses and homeostasis. *Cellular & Molecular Immunology*, 19(3), 370-383. doi:10.1038/s41423-021-00753-1

Morais, J. M., Papadimitrakopoulos, F., & Burgess, D. J. (2010). Biomaterials/tissue interactions: possible solutions to overcome foreign body response. *Aaps j*, 12(2), 188-196. doi:10.1208/s12248-010-9175-3

Mortensen, R. F. (2001). C-reactive protein, inflammation, and innate immunity. *Immunologic Research*, 24(2), 163-176. doi:10.1385/IR:24:2:163

Nachegea, J. B., Marconi, V. C., van Zyl, G. U., Gardner, E. M., Preiser, W., Hong, S. Y., . . . Gross, R. (2011). HIV treatment adherence, drug resistance, virologic failure: evolving concepts. *Infect Disord Drug Targets*, 11(2), 167-174. doi:10.2174/187152611795589663

- Nasrallah, H. A. (2007). The case for long-acting antipsychotic agents in the post-CATIE era. *Acta Psychiatr Scand*, 115(4), 260-267. doi:10.1111/j.1600-0447.2006.00982.x
- Neun, B. W., Ilinskaya, A. N., & Dobrovolskaia, M. A. (2018). Analysis of Complement Activation by Nanoparticles. In S. E. McNeil (Ed.), *Characterization of Nanoparticles Intended for Drug Delivery* (pp. 149-160). New York, NY: Springer New York.
- Nguyen, A. V., & Soulika, A. M. (2019). The Dynamics of the Skin's Immune System. *International journal of molecular sciences*, 20(8). doi:10.3390/ijms20081811
- Noris, M., & Remuzzi, G. (2013). Overview of Complement Activation and Regulation. *Seminars in Nephrology*, 33(6), 479-492.
doi:<https://doi.org/10.1016/j.semnephrol.2013.08.001>
- Pandey, K. K., & Grandgenett, D. P. (2008). HIV-1 Integrase Strand Transfer Inhibitors: Novel Insights into their Mechanism of Action. *Retrovirology (Auckl)*, 2, 11-16.
doi:10.4137/rrt.s1081
- Paszkiel, B. J., Spencer, V., Fein, J., Liu, C. Y., Dallas, M., Kumar, S., . . . Zmuda, J. (2017). *Development of an Improved Process for the Depletion of Exosomes from Fetal Bovine Serum*.
- Pau, A. K., & George, J. M. (2014). Antiretroviral therapy: current drugs. *Infect Dis Clin North Am*, 28(3), 371-402. doi:10.1016/j.idc.2014.06.001
- Phanuphak, N., & Gulick, R. M. (2020). HIV treatment and prevention 2019: current standards of care. *Current Opinion in HIV and AIDS*, 15(1), 4-12.
doi:10.1097/coh.0000000000000588
- Plant-Hatley, A. J., Eryilmaz, B., David, C. A. W., Brain, D. E., Heaton, B. J., Perrie, Y., & Liptrott, N. J. (2022). Exposure of the Basophilic Cell Line KU812 to Liposomes Reveals Activation Profiles Associated with Potential Anaphylactic Responses Linked to Physico-Chemical Characteristics. *Pharmaceutics*, 14(11). doi:10.3390/pharmaceutics14112470
- Rakkola, R., Matikainen, S., & Nyman, T. A. (2007). Proteome analysis of human macrophages reveals the upregulation of manganese-containing superoxide dismutase after toll-like receptor activation. *Proteomics*, 7(3), 378-384. doi:10.1002/pmic.200600582

- Ratner, B. D. (2002). Reducing capsular thickness and enhancing angiogenesis around implant drug release systems. *Journal of Controlled Release*, 78(1), 211-218.
doi:[https://doi.org/10.1016/S0168-3659\(01\)00502-8](https://doi.org/10.1016/S0168-3659(01)00502-8)
- Ravin, K. A., & Loy, M. (2016). The Eosinophil in Infection. *Clinical Reviews in Allergy & Immunology*, 50(2), 214-227. doi:10.1007/s12016-015-8525-4
- Reardon, S. (2023). Third patient free of HIV after receiving virus-resistant cells. *Nature*, 615(7950), 13-14. doi:10.1038/d41586-023-00479-2
- Rodrigues, M., Kosaric, N., Bonham, C. A., & Gurtner, G. C. (2019). Wound Healing: A Cellular Perspective. *Physiological Reviews*, 99(1), 665-706.
doi:10.1152/physrev.00067.2017
- Ruelas, D. S., & Greene, W. C. (2013). An integrated overview of HIV-1 latency. *Cell*, 155(3), 519-529. doi:10.1016/j.cell.2013.09.044
- Russo, E., Nitschké, M., & Halin, C. (2013). Dendritic cell interactions with lymphatic endothelium. *Lymphat Res Biol*, 11(3), 172-182. doi:10.1089/lrb.2013.0008
- Sanchez, V. C., Weston, P., Yan, A., Hurt, R. H., & Kane, A. B. (2011). A 3-dimensional in vitro model of epithelioid granulomas induced by high aspect ratio nanomaterials. *Particle and Fibre Toxicology*, 8(1), 17. doi:10.1186/1743-8977-8-17
- Sansom, D. M., Manzotti, C. N., & Zheng, Y. (2003). What's the difference between CD80 and CD86? *Trends in Immunology*, 24(6), 313-318. doi:[https://doi.org/10.1016/S1471-4906\(03\)00111-X](https://doi.org/10.1016/S1471-4906(03)00111-X)
- Shah, H., Eisenbarth, S., Tormey, C. A., & Siddon, A. J. (2021). Behind the scenes with basophils: an emerging therapeutic target. *Immunotherapy Advances*, 1(1).
doi:10.1093/immadv/ltab008
- Shahrabi-Farahani, S., Lerman, M. A., Noonan, V., Kabani, S., & Woo, S. B. (2014). Granulomatous foreign body reaction to dermal cosmetic fillers with intraoral migration. *Oral Surg Oral Med Oral Pathol Oral Radiol*, 117(1), 105-110.
doi:10.1016/j.oooo.2013.10.008
- Shakil, A., Hern, F. Y., Liu, C., Temburnikar, K., Chambon, P., Liptrott, N., . . . Rannard, S. P. (2022). Linear and branched polymer prodrugs of the water-soluble nucleoside reverse-

transcriptase inhibitor emtricitabine as structural materials for long-acting implants. *Journal of Materials Chemistry B*, 10(23), 4395-4404. doi:10.1039/D2TB00825D

Sichien, D., Lambrecht, B. N., Guilliams, M., & Scott, C. L. (2017). Development of conventional dendritic cells: from common bone marrow progenitors to multiple subsets in peripheral tissues. *Mucosal Immunology*, 10(4), 831-844. doi:10.1038/mi.2017.8

Sivin, I., Wan, L., Ranta, S., Alvarez, F., Brache, V., Mishell, D. R., Jr., . . . Schechter, J. (2001). Levonorgestrel concentrations during 7 years of continuous use of Jadelle contraceptive implants. *Contraception*, 64(1), 43-49. doi:10.1016/s0010-7824(01)00226-8

Skobe, M., & Detmar, M. (2000). Structure, Function, and Molecular Control of the Skin Lymphatic System. *Journal of Investigative Dermatology Symposium Proceedings*, 5(1), 14-19. doi:<https://doi.org/10.1046/j.1087-0024.2000.00001.x>

Soloneski, S., Kujawski, M., Scuto, A., & Larramendy, M. L. (2015). Carbamates: A study on genotoxic, cytotoxic, and apoptotic effects induced in Chinese hamster ovary (CHO-K1) cells. *Toxicology in Vitro*, 29(5), 834-844. doi:<https://doi.org/10.1016/j.tiv.2015.03.011>

Su, J. T., Simpson, S. M., Sung, S., Tfaily, E. B., Veazey, R., Marzinke, M., . . . Kiser, P. F. (2020). A Subcutaneous Implant of Tenofovir Alafenamide Fumarate Causes Local Inflammation and Tissue Necrosis in Rabbits and Macaques. *Antimicrobial Agents and Chemotherapy*, 64(3), e01893-01819. doi:doi:10.1128/AAC.01893-19

Szebeni, J. (2014). Complement activation-related pseudoallergy: A stress reaction in blood triggered by nanomedicines and biologicals. *Molecular Immunology*, 61(2), 163-173. doi:<https://doi.org/10.1016/j.molimm.2014.06.038>

Szebeni, J., Alving, C. R., Rosivall, L., Büniger, R., Baranyi, L., Bedöcs, P., . . . Barenholz, Y. (2007). Animal Models of Complement-Mediated Hypersensitivity Reactions to Liposomes and Other Lipid-Based Nanoparticles. *Journal of Liposome Research*, 17(2), 107-117. doi:10.1080/08982100701375118

Szebeni, J., & Bawa, R. (2020). Human Clinical Relevance of the Porcine Model of Pseudoallergic Infusion Reactions. *Biomedicines*, 8(4). doi:10.3390/biomedicines8040082

- Szebeni, J., Simberg, D., González-Fernández, Á., Barenholz, Y., & Dobrovolskaia, M. A. (2018). Roadmap and strategy for overcoming infusion reactions to nanomedicines. *Nature Nanotechnology*, *13*(12), 1100-1108. doi:10.1038/s41565-018-0273-1
- Tang, L., Jennings, T. A., & Eaton, J. W. (1998). Mast cells mediate acute inflammatory responses to implanted biomaterials. *Proc Natl Acad Sci U S A*, *95*(15), 8841-8846. doi:10.1073/pnas.95.15.8841
- Thevenot, P., Hu, W., & Tang, L. (2008). Surface chemistry influences implant biocompatibility. *Curr Top Med Chem*, *8*(4), 270-280. doi:10.2174/156802608783790901
- Thway, K., Strauss, D. C., Smith, M. J., & Fisher, C. (2015). Foreign body granulomas induced by intramuscular leuporelin acetate injection for prostate cancer: clinical mimics of soft tissue sarcoma. *Case Rep Oncol Med*, *2015*, 947040. doi:10.1155/2015/947040
- Tokunaga, R., Zhang, W., Naseem, M., Puccini, A., Berger, M. D., Soni, S., . . . Lenz, H. J. (2018). CXCL9, CXCL10, CXCL11/CXCR3 axis for immune activation - A target for novel cancer therapy. *Cancer Treat Rev*, *63*, 40-47. doi:10.1016/j.ctrv.2017.11.007
- Triantafilou, M., Hughes, T. R., Morgan, B. P., & Triantafilou, K. (2016). Complementing the inflammasome. *Immunology*, *147*(2), 152-164. doi:10.1111/imm.12556
- Tsuchiya, S., Yamabe, M., Yamaguchi, Y., Kobayashi, Y., Konno, T., & Tada, K. (1980). Establishment and characterization of a human acute monocytic leukemia cell line (THP-1). *Int J Cancer*, *26*(2), 171-176. doi:10.1002/ijc.2910260208
- van der Valk, J., Brunner, D., De Smet, K., Fex Svenningsen, A., Honegger, P., Knudsen, L. E., . . . Gstraunthaler, G. (2010). Optimization of chemically defined cell culture media--replacing fetal bovine serum in mammalian in vitro methods. *Toxicol In Vitro*, *24*(4), 1053-1063. doi:10.1016/j.tiv.2010.03.016
- van Meer, L., Moerland, M., Gallagher, J., van Doorn, M. B., Prens, E. P., Cohen, A. F., . . . Burggraaf, J. (2016). Injection site reactions after subcutaneous oligonucleotide therapy. *Br J Clin Pharmacol*, *82*(2), 340-351. doi:10.1111/bcp.12961
- Vandebriel, R. J., David, C. A. W., Vermeulen, J. P., & Liptrott, N. J. (2022). An inter-laboratory comparison of an NLRP3 inflammasome activation assay and dendritic cell maturation assay using a nanostructured lipid carrier and a polymeric nanomedicine, as

exemplars. *Drug Delivery and Translational Research*, 12(9), 2225-2242.

doi:10.1007/s13346-022-01206-6

Veisoh, O., Doloff, J. C., Ma, M., Vegas, A. J., Tam, H. H., Bader, Andrew R., . . . Anderson, D. G. (2015). Size- and shape-dependent foreign body immune response to materials implanted in rodents and non-human primates. *Nature Materials*, 14(6), 643-651.

doi:10.1038/nmat4290

Velnar, T., Bailey, T., & Smrkolj, V. (2009). The wound healing process: an overview of the cellular and molecular mechanisms. *J Int Med Res*, 37(5), 1528-1542.

doi:10.1177/147323000903700531

Venkatesan, P. (2022). Long-acting injectable ART for HIV: a (cautious) step forward. *The Lancet Microbe*, 3(2), e94. doi:10.1016/S2666-5247(22)00009-X

Verheijen, M., Lienhard, M., Schrooders, Y., Clayton, O., Nudischer, R., Boerno, S., . . . Caiment, F. (2019). DMSO induces drastic changes in human cellular processes and epigenetic landscape in vitro. *Scientific Reports*, 9(1), 4641. doi:10.1038/s41598-019-40660-0

Villeneuve, D. L., Landesmann, B., Allavena, P., Ashley, N., Bal-Price, A., Corsini, E., . . . Tschudi-Monnet, F. (2018). Representing the Process of Inflammation as Key Events in Adverse Outcome Pathways. *Toxicol Sci*, 163(2), 346-352. doi:10.1093/toxsci/kfy047

Wang, H., Horbinski, C., Wu, H., Liu, Y., Sheng, S., Liu, J., . . . Wang, C. (2016).

NanoStringDiff: a novel statistical method for differential expression analysis based on NanoString nCounter data. *Nucleic Acids Research*, 44(20), e151-e151.

doi:10.1093/nar/gkw677

Wanjalla, C. N., McDonnell, W. J., & Koethe, J. R. (2018). Adipose Tissue T Cells in HIV/SIV Infection. *Front Immunol*, 9, 2730. doi:10.3389/fimmu.2018.02730

Weinheimer-Haus, E. M., Mirza, R. E., & Koh, T. J. (2015). Nod-Like Receptor Protein-3 Inflammasome Plays an Important Role during Early Stages of Wound Healing. *PLOS ONE*, 10(3), e0119106. doi:10.1371/journal.pone.0119106

Weisberg, S. P., McCann, D., Desai, M., Rosenbaum, M., Leibel, R. L., & Ferrante, A. W., Jr. (2003). Obesity is associated with macrophage accumulation in adipose tissue. *J Clin Invest*, *112*(12), 1796-1808. doi:10.1172/jci19246

World Health Organisation. (2022). HIV data and statistics.

Yona, S., & Jung, S. (2010). Monocytes: subsets, origins, fates and functions. *Current Opinion in Hematology*, *17*(1), 53-59. doi:10.1097/MOH.0b013e3283324f80

Zamani, F., Zare Shahneh, F., Aghebati-Maleki, L., & Baradaran, B. (2013). Induction of CD14 Expression and Differentiation to Monocytes or Mature Macrophages in Promyelocytic Cell Lines: New Approach. *Adv Pharm Bull*, *3*(2), 329-332. doi:10.5681/apb.2013.053

Zheng, D., Liwinski, T., & Elinav, E. (2020). Inflammasome activation and regulation: toward a better understanding of complex mechanisms. *Cell Discovery*, *6*(1), 36. doi:10.1038/s41421-020-0167-x

Appendix

Chapter 3

A3.1 –MUTZ-3 and MoDC comparison

A3.1.1 Methods – MoDCs generation and marker expression assessment for MUTZ-3 comparison

This work was carried out by Dr Christopher David at the University of Liverpool and adapted from a previously published experiment analysis of DC maturation by nonmedicinal products (Vandebriel et al., 2022). PBMCs from three different donors were isolated from buffy coats from NHSBT, monocytes were then isolated from these PBMCs using CD14 beads and MACS columns. These monocytes were differentiated to immature DCs (MoDCs) in the presence of RPMI supplemented 10% with HyClone de-complemented fetal calf serum, 1% penicillin/streptomycin, 450 U/mL of GM-CSF, and 500 U/mL IL-4. The cells were then treated with LPS at 100 ng/mL for 48 hours. The cells were then stained with one of two panels of antibodies and ran on the MACSQuant Analyzer 9 using the markers, fluorescent dyes and channels illustrated in Table 3.2.

Table A3.1: Displays the cells lines, markers, fluorescent dyes and channels used for the marker analysis of the MoDCs.

Cell line/Panel	Marker	Fluorescent dye (Excitation (nm), Emission (nm))	MACSQuant Channel (Laser (nm), Filter (nm))
DC Panel 1	CD80	FITC (495, 520)	B1 (Blue 488, 525/50)
	CD14	PE (565, 578)	B2 (Blue 488, 585/40)
	CD274	APC (652, 660)	R1 (Red 635, 655-730)
	HLA-DR	Pacific Blue (405, 455)	V1 (Violet 405, 450/50)
DC Panel 2	CD83	FITC (495, 520)	B1 (Blue 488, 525/50)
	CD40	PE (565, 578)	B2 (Blue 488, 585/40)
	CD209	APC (652, 660)	R1 (Red 635, 655-730)

	CD86	Pacific Blue (405, 455)	V1 (Violet 405, 450/50)
--	------	-------------------------	-------------------------

The MFI for each of the three individual donor samples are displayed as mean (\pm standard deviation) in GraphPad Prism software 9.3.1.

A3.1.2 MoDCs and MUTZ-3 comparison

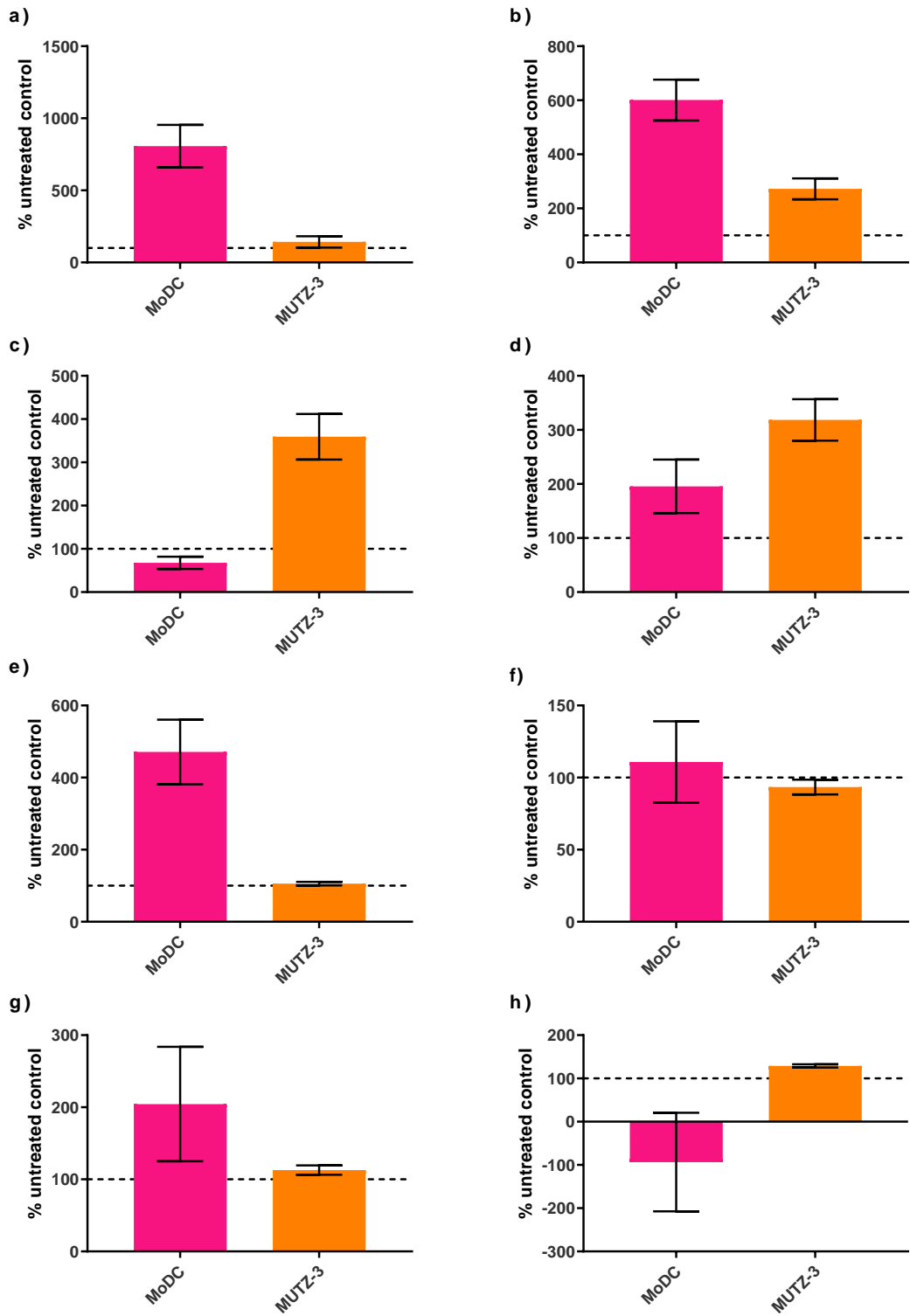


Figure A3.1: a) CD80 expression, b) CD86 expression, c) CD209 expression, d) CD40 expression, e) CD83 expression, f) HLA-DR expression, g) CD274 expression, and h) CD14 expression. MoDC data displayed as % untreated control n=3 (3 donors), mean (\pm standard

deviation). MUTZ-3 data displayed as n=3 technical replicates % untreated control n=2 experimental replicates, mean (\pm standard deviation).

A3.2 - Nano string quality control of data.

All the samples except for one were within the accepted limits for the general assay performance quality control metrics (Figure A3.2 a-d). Binding density looks at the image saturation to ensure that there are not lots of overlapping codes which could cause data loss. Field of view looks at the imaging performance of the assay. Positive control linearity is used to check the hybridisation reaction and is calculated from the six synthetic DNA control targets included in the assay. Limit of Detection is used to determine the ability to detect the second lowest positive control using the negative probes. Due to not meeting the limits for binding density and limit of detection, the sample 3TC and R848 repeat one was excluded from any further analysis (Figure 3.13).

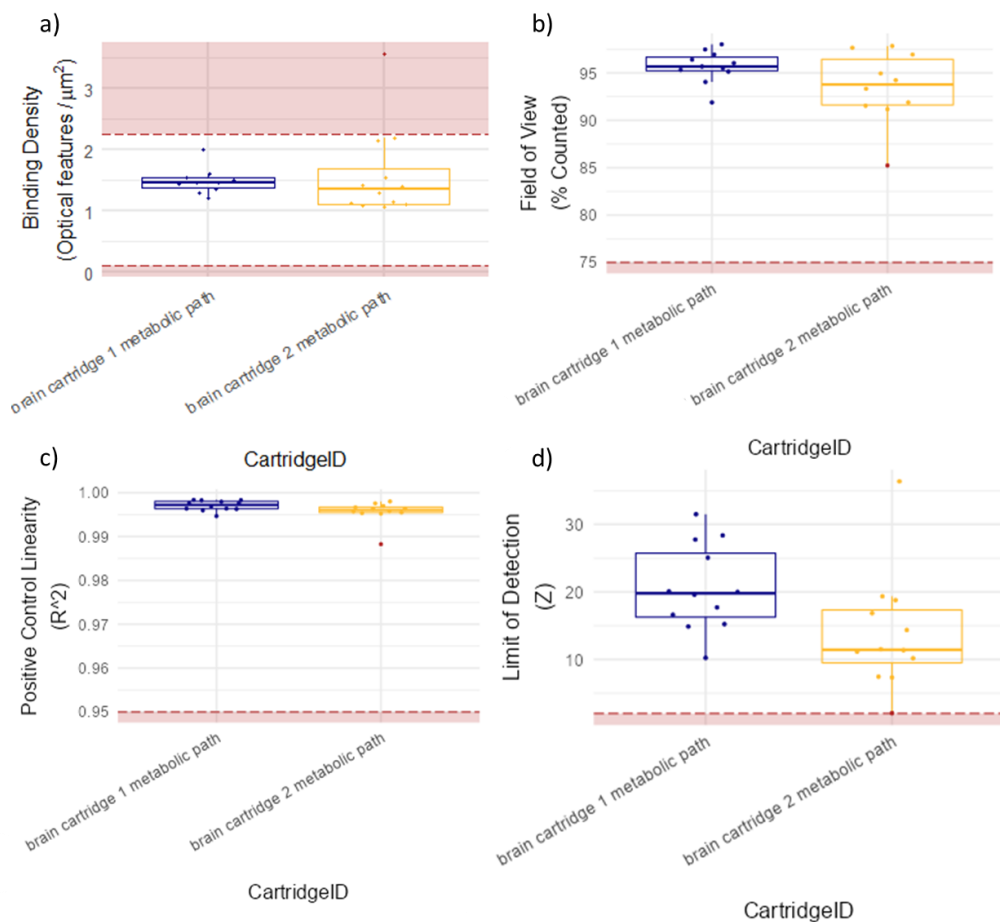


Figure A3.2: Quality control assessment of a) binding density, b) Field of View, c) Positive control linearity, and d) Limit of detection. Blue dots and box plot represents the data points

from cartridge 1 and the yellow dots and box plot represents the data points from cartridge 2. Red dots indicate outlier values.

The positive (figure A3.3a), negative (figure A3.3b) and the housekeeping (figure A3.3c) probes are visualised in Figure A3.3.

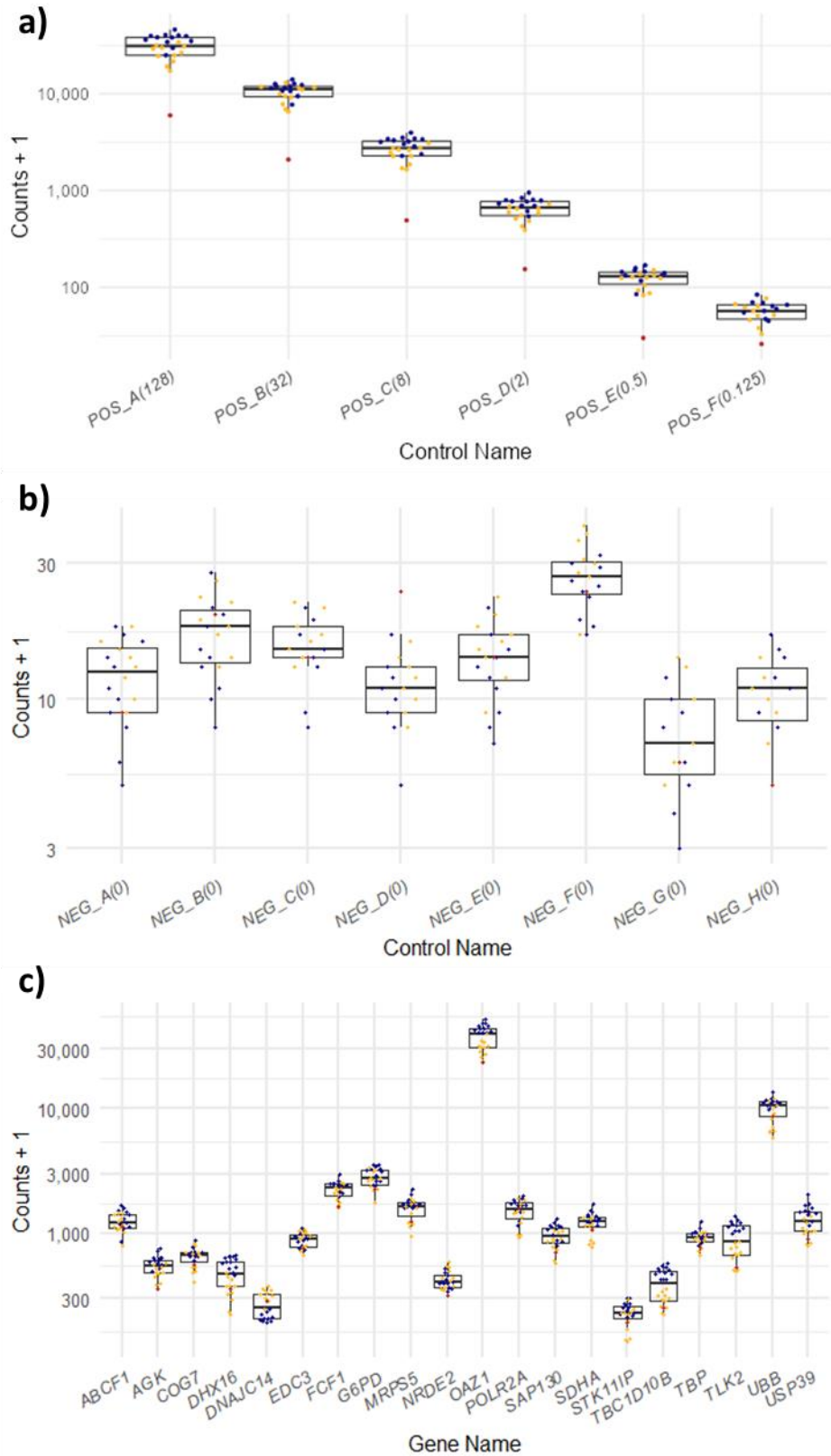


Figure A3.3: Quality control assessment of a) positive probes, b) negative probes, and c) housekeeping gene probes. Blue dots and box plot represents the data points from cartridge

1 and the yellow dots and box plot represents the data points from cartridge 2. Red dots indicate outlier values.